

**PYRROLOIMINOQUINONE METABOLITES FROM SOUTH
AFRICAN LATRUNCULID SPONGES**

**A thesis submitted in fulfillment of the requirements
for the degree of**

DOCTOR OF PHILOSOPHY

of

Rhodes University

by

Edith Martins Antunes

January 2003

ACKNOWLEDGEMENTS

A number of people have made valuable contributions to my work, for which I am truly grateful.

My supervisor, Professor M.T. Davies-Coleman, for introducing me to this field and for his patience, especially in the last two years of my PhD.

Dr. D.R. Beukes for his interest, encouragement and guidance on everything from NMR to HPLC.

Professor T. Nyokong for her expertise, support and constant willingness to help even though she is one of the busiest people in the department.

Drs. S.E and M.D. Maree for their guidance and input with the electrochemistry and especially the photochemistry.

Dr. G.M. Watkins for his help with the IR interpretation of the N-oximes and especially his constant encouragement.

Mr. A.W. Sonemann and Mr. A. Soper for their expert technical assistance.

Professors P.T. Kaye and D.E.A. Rivett who were always willing to lend a helping hand.

Drs. M. Kelly and T. Samaai for the identification of the latrunculid sponges.

Catherine Sincich (Scripps Institution of Oceanography), Katherine Marshall (University of Utah) and Catherine Arendse (University of Cape Town) for performing the various cytotoxicity assays.

Prof. L. Fourie of the Potchefstroomse Universiteit vir Christelike Hoër Onderwys for the prompt acquisition of the HRFABMS spectra.

Mrs. B. Tarr, Mrs. L. Berryman and Mrs. J. Sewry for their advice, their willingness to help and their support during some difficult times.

My lab mates, past and present: Dr. Kerry M^cPhail, Chris, Greg, Dr. Lynne Collett, Dave, Thomas, Andrew, Carole, Meke.

Rhodes University and the NRF (National Research Foundation) for their financial assistance.

My family.

For Matthew

TABLE OF CONTENTS:

ACKNOWLEDGEMENTS	ii
TABLE OF CONTENTS	iv
LIST OF FIGURES	viii
LIST OF SCHEMES	xiii
LIST OF TABLES	xv
LIST OF ABBREVIATIONS	xvii
ABSTRACT	xxi
Chapter 1: Introduction	1
1.1 Marine sponges: a prolific source of potential pharmaceuticals	1
1.2 Chemistry of pyrroloamino-<i>ortho</i>-quinone, pyrroloiminoquinone and bis-pyrroloiminoquinone alkaloids	5
1.2.1 <i>Damirones</i>	6
1.2.2 <i>Batzellines</i>	6
1.2.3 <i>Isobatzellines</i>	7
1.2.4 <i>Secobatzellines</i>	7
1.2.5 <i>Makaluvamines</i>	8
1.2.6 <i>Makaluvic acids</i>	10
1.2.7 <i>Discorhabdins</i>	10
1.2.8 <i>Prianosins</i>	15
1.2.9 <i>Epinardins</i>	16
1.2.10 <i>Tsitsikammamines, veitamine and wakayin</i>	17
1.3 Taxonomy of the Family Latrunculiidae	18
1.4 Biosynthesis of pyrroloamino-<i>ortho</i>-quinone and pyrroloiminoquinone alkaloids	24
1.5 Biological activity of pyrroloamino-<i>ortho</i>-quinone, pyrroloiminoquinone and bis-pyrroloiminoquinone alkaloids	26
1.6 Synthesis of pyrroloamino-<i>ortho</i>-quinone, pyrroloiminoquinone and bis-pyrroloiminoquinone metabolites	31
1.6.1 <i>Damirones</i>	31
1.6.2 <i>Batzellines and isobatzellines</i>	33
1.6.3 <i>Makaluvamines A - F</i>	34
1.6.4 <i>Discorhabdins</i>	39
1.6.5 <i>Related pyrroloiminoquinones</i>	42
1.7 Aim	42
Chapter 2: Pyrroloiminoquinone metabolites from <i>Tsitsikamma pedunculata</i>	44
2.1 Introduction	44
2.2 Results and Discussion	45

2.2.1	<i>The taxonomy of the sponge <u>Tsitsikamma pedunculata</u></i>	45
2.2.2	<i>Extraction and isolation of pyrroloiminoquinone metabolites from <u>T. pedunculata</u></i>	46
2.2.3	<i>Structure elucidation of pyrroloiminoquinone metabolites from <u>T. pedunculata</u></i>	48
a)	<i>14-bromo-disorhabdin C (1.51) and 14-bromo-3-dihydro-disorhabdin C (1.52)</i>	48
b)	<i>3-dihydro-disorhabdin C (1.53)</i>	51
c)	<i>7,8-dehydro-3-dihydro-disorhabdin C (2.1)</i>	52
d)	<i>14-bromo-7,8-dehydro-3-dihydro-disorhabdin C (2.2)</i>	54
e)	<i>Discorhabdin S (2.3)</i>	55
f)	<i>14-bromo-1-hydroxy-disorhabdin S (2.4)</i>	60
g)	<i>1-bromo-2-hydroxy-disorhabdin S (2.5)</i>	62
h)	<i>2,4-debromo-3-dihydro-disorhabdin C (2.6)</i>	66
 Chapter 3: Pyrroloiminoquinone metabolites from <i>Latrunculia lorii</i>		69
3.1 Introduction		69
3.2 Results and Discussion		70
3.2.1	<i>The taxonomy of the encrusting sponge <u>Latrunculia lorii</u></i>	70
3.2.2	<i>Extraction and isolation of pyrroloamino-ortho-quinone and pyrroloiminoquinone metabolites from <u>L. lorii</u></i>	70
3.2.3	<i>Structure elucidation of pyrroloamino-ortho-quinone and pyrroloiminoquinone metabolites from <u>L. lorii</u></i>	72
a)	<i>Makaluvamine C (1.33)</i>	72
b)	<i>Damirone B (1.20)</i>	73
c)	<i>Makaluvic acid A (1.47)</i>	73
d)	<i>Discorhabdin G* (3.1)</i>	74
e)	<i>Discorhabdin M (3.2)</i>	78
f)	<i>1-amino discorhabdin D (3.3)</i>	82
g)	<i>1-methoxy discorhabdin D (3.4)</i>	85
h)	<i>1-alanyl discorhabdin D (3.5)</i>	88
3.3 Summary and Conclusion		95
 Chapter 4: Pyrroloiminoquinone metabolites from <i>Tsitsikamma favus</i> and <i>Strongylodesma</i> sp.		96
4.1 Introduction		96
4.2 Results and Discussion		98
4.2.1	<i>The taxonomy of the sponge <u>Tsitsikamma favus</u></i>	98
4.2.2	<i>Extraction and isolation of pyrroloiminoquinone and bis-pyrroloiminoquinone metabolites from <u>T. favus</u></i>	99
4.2.3	<i>Structure elucidation of pyrroloiminoquinone and bis-pyrroloiminoquinone metabolites from <u>T. favus</u></i>	101
a)	<i>Tsitsikammamine A (1.71)</i>	101

b) <i>Tsitsikammamine B (1.72)</i>	103
c) <i>Tsitsikammamine A N-oxime (4.1)</i>	103
d) <i>Tsitsikammamine B N-oxime (4.2)</i>	109
e) <i>14-bromo-3-dihydro-disorhabdin C (1.52)</i>	113
f) <i>7,8-dehydro-3-dihydro-disorhabdin C (2.1)</i>	113
g) <i>14-bromo-1-hydroxy-disorhabdin S (2.4)</i>	113
h) <i>2,4-debromo-3-dihydro-disorhabdin C (2.6)</i>	113
4.3.1 <i>The taxonomy of the sponge <u>Strongyloidesma</u> sp..</i>	114
4.3.2 <i>Extraction and isolation of pyrroloiminoquinone metabolites from <u>Strongyloidesma</u> sp..</i>	114
4.3.3 <i>Structure elucidation of pyrroloiminoquinone metabolites from <u>Strongyloidesma</u> sp..</i>	115
i) <i>Discorhabdin A (1.57)</i>	115
j) <i>Discorhabdin D (1.61)</i>	117
k) <i>3-dihydro-disorhabdin C (1.53)</i>	118
l) <i>1-amino discorhabdin D (3.3)</i>	118
Chapter 5: Photochemistry	119
5.1 Introduction	119
5.2 Photochemistry	120
5.2.1 <i>Singlet Oxygen</i>	123
a) <i>Electronic structure and lifetime of singlet oxygen</i>	123
b) <i>Production of singlet oxygen</i>	124
c) <i>Detection and measurement of singlet oxygen</i>	125
d) <i>Reactions involving singlet oxygen</i>	126
e) <i>Quenching of singlet oxygen</i>	126
f) <i>Photodynamic therapy</i>	126
5.3 Photochemical techniques	127
5.3.1 <i>Singlet oxygen quantum yield determinations</i>	127
5.3.2 <i>Fluorescence quantum yield determinations</i>	128
5.4 Experimental	129
5.4.1 <i>Instrumentation and techniques for singlet oxygen determination</i>	129
5.4.2 <i>Instrumentation and techniques for fluorescence quantum yield determinations</i>	129
5.5 Results and Discussion	130
5.5.1 <i>Singlet oxygen quantum yield determinations</i>	130
5.5.2 <i>Fluorescence quantum yield determinations</i>	133
5.6 Conclusion	134
Chapter 6: Electrochemistry	136
6.1 Introduction	136
6.2 Electrochemical techniques	139

6.2.1	<i>Cyclic voltammetry</i>	139
a)	<i>Reversible processes</i>	141
b)	<i>Irreversible processes</i>	142
c)	<i>Quasi-reversible processes</i> ¹²⁹	143
6.2.2	<i>Osteryoung square – wave voltammetry</i>	143
6.3	Results and Discussion	145
6.3.1	<i>Voltammetric characterisation of pyrroloamino-ortho-quinone, pyrroloiminoquinone and bis-pyrroloiminoquinone metabolites</i>	145
a)	<i>Makaluvamine C (1.33) and Damirone B (1.20)</i>	148
b)	<i>Discorhabdin C type compounds</i>	149
c)	<i>Discorhabdin D / S type compounds</i>	151
d)	<i>Bis-pyrroloiminoquinones</i>	154
6.3.2	<i>Stability study</i>	156
6.4	Conclusion	159
Chapter 7:	Bioactivity	162
7.1	Human colon tumour (HCT-116), Oesophageal (WHC01) and ovarian (ME180) cytotoxicity assays	162
7.2	Topoisomerase I activity	164
7.3	Intercalation studies	167
7.4	Bioreductive activation as a basis for selective cytotoxicity?	169
7.5	Singlet oxygen production as a basis for selective cytotoxicity?	173
7.6	Conclusion	174
Chapter 8:	Experimental Section	175
8.1	General experimental section	175
8.2	Chapter 2: Experimental information	175
8.3	Chapter 3: Experimental information	177
8.4	Chapter 4: Experimental information	178
8.5	Chapter 5: Experimental information	181
8.6	Chapter 6: Experimental information	181
8.7	Chapter 7: Experimental information	182
References:		184

LIST OF FIGURES:

Chapter 1:

- Figure 1.1** The structures of discorhabdins H-O (from Urban *et al.*).²² The former names³⁹ are given in parentheses, together with any structural differences. 12

Chapter 2:

- Figure 2.1** Summary of the compounds isolated from *T. pedunculata*. 44
- Figure 2.2** An underwater photograph of *T. pedunculata*. 45
- Figure 2.3** The M + 1 ion isotopic cluster from the LC-MS spectrum of **1.51** clearly showing the presence of three bromine atoms. 49
- Figure 2.4** A three-dimensional model of 14-bromo-3-dihydro-discorhabdin C (**1.52**). (Spartan '02, Wavefunction, Inc., CA, USA. A semi-empirical force field was used to convert the 2D structures to 3D models). 50
- Figure 2.5** The M + 1 ion isotopic cluster in the LC-MS spectrum of **1.53** clearly showing the presence of two bromine atoms. 52
- Figure 2.6** The fully assigned ¹H NMR spectrum of **2.3** (400 MHz, DMSO-d₆) with the signals for the two NH protons offset. (Imp = impurity). 56
- Figure 2.7** A section (F1 = δ 15 – 80 ppm, F2 = δ 1.0 – 5.2 ppm) of the HMQC spectrum of compound **2.3** (400/100 MHz, DMSO-d₆). (Imp = impurity). 57
- Figure 2.8** A section (F1 = δ 10 – 100 ppm, F2 = δ 1.0 – 8.0 ppm) of the HMBC spectrum of compound **2.3** (400/100 MHz, DMSO-d₆). (Imp = impurity). 58
- Figure 2.9** A three dimensional model of **2.3** clearly showing a possible *quasi*-di-equatorial arrangement of the two H₂-1 protons relative to H-2. The 2S,* 6R* relative stereochemistry of discorhabdin D (**1.61**) is arbitrarily adopted. (Spartan '02, Wavefunction, Inc., CA, USA. A semi empirical forcefield was used to generate the 3D molecular structure). 59
- Figure 2.10** ¹H NMR spectra for **2.4** (400 MHz) obtained in a) CD₃OD/CDCl₃ mix and b) DMSO-d₆. 60
- Figure 2.11** A three dimensional model of **2.5** clearly showing that bromination is possible at both positions 1 and 2. (Spartan '02, Wavefunction, Inc., CA, USA. A semi empirical forcefield was used to generate the 3D molecular structure). 62
- Figure 2.12** ¹H NMR spectrum of **2.5** (400 MHz, DMSO-d₆) with the NH-9 and NH-13 protons offset. 63
- Figure 2.13** Comparison of the ¹³C NMR spectra (100 MHz, DMSO-d₆) of the structurally similar compounds **2.3** (a), **2.4** (b) and **2.5** (c). *Note the positions of the signals for carbons 1, 2, 3 and 17 (δ 40 – 90 ppm) in particular. 64
- Figure 2.14** ¹H NMR spectrum with the proton assignments for **2.6** (400 MHz, DMSO-d₆). A section (F1 = δ 15 – 140 ppm, F2 = δ 1.0 – 8.0 ppm) of the HMQC 66

Figure 2.15	spectrum of compound 2.6 (400/100 MHz, DMSO-d ₆). (Imp = impurity).	68
Chapter 3:		
Figure 3.1	Summary of the compounds obtained from <i>L. lorii</i> .	69
Figure 3.2	An underwater photograph of <i>L. lorii</i> .	70
Figure 3.3	¹ H NMR spectrum for 1.33 (400 MHz, DMSO-d ₆) with the signals for the three NH protons offset. Note: The water signal in the ¹ H NMR spectrum is quite small compared to the previous spectra obtained due to the higher concentration of the sample.	72
Figure 3.4	¹ H NMR spectrum for makaluvic acid A (1.47) (400 MHz, DMSO-d ₆) with the signals for the NH and OH protons offset.	74
Figure 3.5	¹ H NMR spectrum of discorhabdin G* (3.1) (400 MHz, DMSO-d ₆) with the signals for the three NH protons offset. (Imp = impurity).	76
Figure 3.6	¹³ C NMR spectrum of discorhabdin G* (3.1) (100 MHz, DMSO-d ₆).	76
Figure 3.7	Discorhabdin D (1.61) together with the energy minimised 3D models of its two possible C-8 epimers. (Spartan '02, Wavefunction, Inc., CA, USA. A semi-empirical minimization force field was used to generate the 3D model).	78
Figure 3.8	¹ H NMR Spectrum of 3.2 (400 MHz, DMSO-d ₆) with the signals for the two NH protons offset. (Imp = impurity).	79
Figure 3.9	¹³ C NMR spectrum of 3.2 (100 MHz, DMSO-d ₆).	80
Figure 3.10	Proposed structure and three dimensional model for discorhabdin M (3.2) with an arbitrarily assigned 1R,* 2S,* 6R,* 8S* configuration. (Spartan '02, Wavefunction, Inc., CA, USA. A semi-empirical minimization force field was used to generate the 3D model).	82
Figure 3.11	¹ H NMR spectrum of 1-amino discorhabdin D (3.3) (400 MHz, DMSO-d ₆) with the signals for the two NH protons offset. (Imp = impurity).	83
Figure 3.12	¹ H NMR spectrum for 3.4 (400 MHz, DMSO-d ₆) with the signals for the three NH protons offset. (Imp = impurity).	86
Figure 3.13	¹³ C NMR spectrum for 3.4 (100MHz, DMSO-d ₆) with the expansions for C-2, C-8 and C-1' offset.	87
Figure 3.14	A section (F1 = δ 15 – 130 ppm, F2 = δ 2.0 – 7.5 ppm) of the HMQC spectrum of compound 3.4 (400/100 MHz, DMSO-d ₆). (Imp = impurity).	87
Figure 3.15	¹ H NMR spectrum showing the absence and presence of exchangeable protons NH-9 and NH-13 in 3.5 (400 MHz) in a) CD ₃ OD and b) DMSO-d ₆ respectively. The NH-9 and NH-13 signals are offset. (Imp = impurity).	89
Figure 3.16	A section (F1 = δ 15 – 70 ppm, F2 = δ 2.0 – 7.5 ppm) of the HMBC spectrum of compound 3.5 (400/100 MHz, DMSO-d ₆). (Imp = impurity).	91
Figure 3.17	A section (F1 = δ 44 – 70 ppm, F2 = δ 2.5 – 4.6 ppm) of the HSQC-TOCSY spectrum of compound 3.5 (400/100 MHz, CD ₃ OD). (Imp = impurity).	92

Figure 3.18	A section (F1, F2 = δ 3.46 – 3.86 ppm) of the NOESY spectrum of compound 3.5 (400 MHz, CD ₃ OD).	93
Figure 3.19	Enhancements observed in the NOESY spectra of 3.5 (400 MHz, CD ₃ OD). For the sake of clarity, weak enhancements have been omitted (please see Table 3.6).	93
Chapter 4:		
Figure 4.1	Summary of the compounds isolated from <i>T. favus</i> .	96
Figure 4.2	Summary of the compounds isolated from <i>Strongyloidesma</i> sp..	98
Figure 4.3	An underwater photograph of <i>T. favus</i> .	98
Figure 4.4	¹ H NMR spectrum of tsitsikammamine A (1.71) (400 MHz, DMSO-d ₆) with NH-9 and NH-13 offset. (Imp = impurity).	101
Figure 4.5	¹ H NMR spectrum of tsitsikammamine A N-oxime (4.1) (400 MHz, DMSO-d ₆) with NH-9, NH-13 and OH-3 offset. (Imp = impurity).	104
Figure 4.6	¹³ C NMR spectrum (100 MHz, DMSO-d ₆) of a) tsitsikammamine A (1.71) and b) tsitsikammamine A N-oxime (4.1) with C-16 and C-17 offset. Please note the chemical shifts of C-17* and C-19* in particular. (Imp = impurity).	105
Figure 4.7	A section (F1, F2 = δ 2.0 – 8.5 ppm) of the COSY spectrum of compound 4.1 (400/100 MHz, DMSO-d ₆) showing the ³ J COSY coupling between N-18-OH and H ₂ -17.	105
Figure 4.8	Overlaid IR spectra (2000 – 400 cm ⁻¹) of a) tsitsikammamine A (1.71) and b) its N-oxime (4.1). The true N-oxide bands are indicated on the graph by means of an arrow while the bands which display the sensitivity typical of N-oxides and N-oximes are indicated by means of an asterisk (*).	106
Figure 4.9	A section (F1 = δ 10 – 50 ppm, F2 = δ 2.0 – 8.0 ppm) of the HMBC spectrum of compound 4.1 (400/100 MHz, DMSO-d ₆).	107
Figure 4.10	¹ H NMR of 4.2 (400 MHz, DMSO-d ₆) with NH-9, NH-13 and OH-3 offset. (Imp = impurity).	110
Figure 4.11	A section (F1, F2 = δ 2.0 – 8.5 ppm) of the COSY spectrum of compound 4.2 (400/100 MHz, DMSO-d ₆). (Imp = impurity).	110
Figure 4.12	An underwater photograph of <i>Strongyloidesma</i> sp..	114
Figure 4.13	¹ H NMR spectrum of discorhabdin A (1.57) (400 MHz, DMSO-d ₆) with NH-9 and NH-13 offset. (Imp = impurity).	116
Figure 4.14	The LC-MS spectrum of 1.57 showing the typical M + 1 1:1 doublet isotope ion cluster of a compound containing one bromine atom.	117
Figure 4.15	¹ H NMR spectrum of discorhabdin D (1.61) (400 MHz, DMSO-d ₆) with NH-9 and NH-13 offset. (Imp = impurity).	118
Chapter 5:		
Figure 5.1	Jablonski diagram. ¹¹⁷	121

Figure 5.2	Bonding in the diatomic oxygen molecule. ¹¹⁶	124
Figure 5.3	Jablonski diagram for an oxygen molecule. (Energy in kcal/mol). ¹¹²	124
Figure 5.4	A modified Jablonski diagram showing the relevant reactions for a Type II mechanism, emphasising the basis of PDT. (S = sensitiser).	125
Figure 5.5	Set-up for singlet oxygen quantum yield determinations.	129
Figure 5.6	A typical UV / Visible absorbance spectrum obtained during singlet oxygen production of compound 4.1 in the presence of the DPBF quencher.	130
Figure 5.7	Comparison of the singlet oxygen quantum yields and rate constants obtained for the pyrroloamino- <i>ortho</i> -quinone, pyrroloiminoquinones and <i>bis</i> -pyrroloiminoquinones.	130
Figure 5.8	The effects of deuterated, air saturated and 'nitrogen saturated' DMSO on the singlet oxygen (Φ_{Δ}) production of discorhabdin A. The difference between discorhabdin A (TFA salt) and its free base on Φ_{Δ} production is also shown.	132
Figure 5.9	Fluorescence quantum yield (Φ_F) data obtained for selected pyrroloiminoquinones (values given in the graph).	133
Figure 5.10	Fluorescence and absorbance spectra of 1.33 .	134
Chapter 6:		
Figure 6.1	Schematic representation of a) the basic setup for a cyclic and square wave voltammetric system and b) enlarged schematic of the reference electrode (Ag AgCl). (WFG = waveform generator, P = potentiostat, WE = working electrode, CE = counter electrode, RE = reference electrode). ¹²⁸	140
Figure 6.2	The current / potential (I / V) curves expected from an electroactive adsorbed species in a reversible redox reaction: $O_{ads} + ne^{-} \leftrightarrow R_{ads}$. E is the potential at which the maxima (E_a) and minima (E_c) in the current are observed. ¹²⁸	141
Figure 6.3	The current / potential (I / V) curves expected from an electroactive adsorbed species in an irreversible reaction.	143
Figure 6.4	Excitation signals observed in square wave voltammetry. ¹³⁰	144
Figure 6.5	The current <i>versus</i> potential (I / V) curves from a) an oxidised and b) a reduced electroactive adsorbed species in OSWV, which is often dependent on the scan direction.	144
Figure 6.6	Comparison of the $E_{1/2}$ values obtained for the pyrroloiminoquinone metabolites.	147
Figure 6.7	Cyclic voltammogram of 1.33 . Scan rate: 25 mV/s.	148
Figure 6.8	Proposed mechanism for the redox reaction of damirone B (1.20).	149
Figure 6.9	Proposed mechanism for the redox reaction of makaluvamine C (1.33).	149
Figure 6.10	A plot of the C-19 ¹³ C NMR shifts for the discorhabdin C type pyrroloiminoquinones.	151
Figure 6.11	Proposed mechanism for the redox reaction of 1.52 at pH 5.5 and 7.5.	151

Figure 6.12	Proposed mechanism for the redox reaction of 3.3 at both pH 5.5 and 7.5.	152
Figure 6.13	A plot of the C-19 ¹³ C NMR shifts for the discorhabdin C type pyrroloiminoquinones. Although the data points are few, this graph is intended to show the general trend for the tricyclic pyrroloiminoquinones (a), the discorhabdin D / S types (c) and the <i>bis</i> -pyrroloiminoquinone (d) classes in contrast to that obtained for the discorhabdin C types (b) (Figure 6.10).	153
Figure 6.14	Cyclic voltammogram of 1.72 . Scan rate: 25 mV/s.	154
Figure 6.15	Proposed mechanism for the redox reaction of 4.1 .	156
Figure 6.16	Plot of i_a versus the square root of the scan rate for 3.2 .	157
Figure 6.17	Comparison of the rate constants obtained for the pyrroloamino- <i>ortho</i> -quinone, pyrroloiminoquinone and bis-pyrroloiminoquinone metabolites.	158
 Chapter 7:		
Figure 7.1	DNA topoisomerase I – a unique target for anti-tumour drugs (reproduced with permission from Dr. Brad Carte).	164
Figure 7.2	DNA cleavage assayed by agarose gel electrophoresis. Electrophoresis was carried out in the presence of 9-amino-camptothecin (7.4). (Reproduced with permission from Katherine Marshall, University of Utah, USA). ¹⁴⁴ (r = relaxed, sc = supercoiled, n = nicked, top1 = topoisomerase I, 9AC = 9-amino-camptothecin, TA = tsitsikammamine A, TA-NO = tsitsikammamine A N-oxime, TB = tsitsikammamine B, TB-NO = tsitsikammamine B N-oxime).	167
Figure 7.3	Results obtained for the ethidium bromide displacement assay for the tsitsikammamines and their respective oximes (reproduced with permission from Katherine Marshall, University of Utah). ¹⁴⁴ EtBr displacement was determined by subtracting the amount of background EtBr fluorescence from all samples and then dividing by the amount of fluorescence in the DNA and EtBr control. 0 is complete displacement, >1 no displacement.	168
Figure 7.4	Plot of the $E_{1/2}$ (mV) reductive potentials at both pH 5.5 (a) and (c); and 7.5 (b) and (d) versus IC_{50} HCT-116 values obtained for a select group of nine pyrroloiminoquinone compounds. Plots a) and b) investigated the correlation between HCT-116 cytotoxicity and reduction potential of all nine compounds tested ($R^2 = 0.17$). Selective removal of discorhabdin A and three compounds with a discorhabdin C skeleton (1.51 , 1.52 and 1.53) suggested a possible correlation ($R^2 = 0.93$) between HCT-116 cytotoxicity and reduction potentials for the remaining six compounds.	172
Figure 7.5	Comparison of the singlet oxygen quantum yields (Φ_{Δ}) performed at $\lambda = 532$, nm versus the IC_{50} HCT-116 values obtained for a select group of thirteen pyrroloamino- <i>ortho</i> -quinone, pyrroloiminoquinone and bis-pyrroloiminoquinone metabolites. (SOQY = singlet oxygen quantum yield).	173

LIST OF SHEMES:

Chapter 1:

Scheme 1.1	A recently revised taxonomic relationship between the sponge families Latrunculiidae, Acarnidae, Podospongiidae and Mycalliidae. ^{55,58}	19
Scheme 1.2	Biogenesis of the discorhabdins as postulated by Munro <i>et al.</i> ⁵⁹	24
Scheme 1.3	Synthetic approach to damirones A and B. ⁷¹	32
Scheme 1.4	An alternative synthesis of 1.19 from 3,4-dimethoxyaniline. ⁷²	32
Scheme 1.5	Synthesis of batzelline C and isobatzelline C. ⁷³	33
Scheme 1.6	Total synthesis of isobatzelline B. ⁷⁴	34
Scheme 1.7	An alternative synthetic approach to makaluvamine C. ⁷⁶	34
Scheme 1.8	Preparation of makaluvamines A and K. ⁷⁷	35
Scheme 1.9	Preparation of makaluvamines D and I. ⁷⁷	35
Scheme 1.10	Total synthesis of makaluvamine D. ⁷⁸	36
Scheme 1.11	Synthetic approach to discorhabdin C and makaluvamine D. ⁷⁹	37
Scheme 1.12	Preparation of pyrroloquinoline nucleus for makaluvamine F. ⁸³	38
Scheme 1.13	Total synthesis of makaluvamine F. ^{83,84}	38
Scheme 1.14	Total synthesis of discorhabdin C. ⁸⁵⁻⁸⁷	39
Scheme 1.15	Total synthesis of discorhabdin C. ⁸⁸	40
Scheme 1.16	Total synthesis of discorhabdin A. ⁸⁹	41
Scheme 1.17	Total synthesis of veitamine. ⁹⁰	42

Chapter 2:

Scheme 2.1	Scheme for the extraction and isolation of pyrroloiminoquinone metabolites from <i>T. pedunculata</i> . The masses and yields (calculated relative to the dry mass of the sponge) of the <i>T. pedunculata</i> pyrroloiminoquinone metabolites are summarised below:	47
Scheme 2.2	Blunt <i>et al.</i> 's synthetic modification of the discorhabdin skeleton. ⁴⁴	51

Chapter 3:

Scheme 3.1	Scheme for the extraction and isolation of pyrroloamino- <i>ortho</i> -quinone and pyrroloiminoquinone metabolites from <i>L. lorii</i> . The masses and yields (calculated relative to the dry mass of the sponge) of the <i>L. lorii</i> pyrroloiminoquinone metabolites are summarised below:	71
-------------------	--	----

Chapter 4:

Scheme 4.1	Extraction and pyrroloiminoquinone isolation scheme for <i>T. favus</i> . The masses and yields (calculated relative to the dry mass of sponge) of the <i>T. favus</i> pyrroloiminoquinone metabolites are summarized below:	100
Scheme 4.2	Martínez <i>et al.</i> 's synthesis of the taxol intermediate 10-methylene-camphor. ¹⁰⁶	109

Scheme 4.3	Extraction and pyrroloiminoquinone isolation scheme for <i>Strongyloidesma sp.</i> . The masses and yields (calculated relative to the dry mass of sponge) of the <i>Strongyloidesma sp.</i> pyrroloiminoquinone metabolites are summarized below:	115
Chapter 6:		
Scheme 6.1	The two possible mechanisms for DNA Cleavage by tirapazamine (6.2). ¹²⁴	137
Chapter 7:		
Scheme 7.1	Bioreductive alkylation pathway for mitomycin C (6.1). ¹²⁴	170

LIST OF TABLES:

Chapter 1:

Table 1.1	Revision of the taxonomic assignments and phyletic distribution of the metabolites in the sponge families Latrunculiidae and Acarnidae.	22
Table 1.2	Summary of the biological activities reported for the pyrroloamino- <i>ortho</i> -quinone, pyrroloiminoquinone and <i>bis</i> -pyrroloiminoquinone metabolites.	30

Chapter 2:

Table 2.1	NMR (DMSO-d ₆ , 400 MHz for ¹ H and 100 MHz for ¹³ C) data for compound 2.1.	53
Table 2.2	NMR (DMSO-d ₆ , 400 MHz for ¹ H and 100 MHz for ¹³ C) data for compound 2.2.	55
Table 2.3	NMR (DMSO-d ₆ , 400 MHz for ¹ H and 100 MHz for ¹³ C) data for compound 2.3.	59
Table 2.4	NMR (DMSO-d ₆ , 400 MHz for ¹ H and 100 MHz for ¹³ C) data for compound 2.4.	61
Table 2.5	NMR (DMSO-d ₆ , 400 MHz for ¹ H and 100 MHz for ¹³ C) data for compound 2.5.	65
Table 2.6	NMR (DMSO-d ₆ , 400 MHz for ¹ H and 100 MHz for ¹³ C) data for compound 2.6.	67

Chapter 3:

Table 3.1	NMR (DMSO-d ₆ , 400 MHz for ¹ H and 100 MHz for ¹³ C) data for compound 3.1.	77
Table 3.2	NMR (DMSO-d ₆ , 400 MHz for ¹ H and 100 MHz for ¹³ C) data for compound 3.2.	81
Table 3.3	NMR (DMSO-d ₆ , 400 MHz for ¹ H and 100 MHz for ¹³ C) data for compound 3.3.	84
Table 3.4	NMR (DMSO-d ₆ , 400 MHz for ¹ H and 100 MHz for ¹³ C) data for compound 3.4.	88
Table 3.5	NMR (DMSO-d ₆ , 400 MHz for ¹ H and 100 MHz for ¹³ C) data for compound 3.5.	90
Table 3.6	NMR (CD ₃ OD, 400 MHz for ¹ H and 100 MHz for ¹³ C) data for compound 3.5.	94

Chapter 4:

Table 4.1	Substituent sensitivity of the planar ring modes in quinoline N-oxide compared to its homocyclic parent (naphthalene). ¹⁰⁰	107
Table 4.2	NMR (DMSO-d ₆ , 400 MHz for ¹ H and 100 MHz for ¹³ C) data for compound 4.1.	108

Table 4.3	NMR (DMSO-d ₆ , 400 MHz for ¹ H and 100 MHz for ¹³ C) data for compound 4.2.	111
 Chapter 5:		
Table 5.1	Singlet oxygen quantum yields (Φ_{Δ}), rate constants and R ² data obtained for the various pyrroloamino- <i>ortho</i> -quinone, pyrroloiminoquinone and <i>bis</i> -pyrroloiminoquinone metabolites in DMSO.	132
 Chapter 6:		
Table 6.1	The grouping of the sixteen pyrroloiminoquinone metabolites into four structural classes.	146
Table 6.2	Electrochemical CV data for the tricyclic pyrroloiminoquinones <i>versus</i> pH. Scan rate: 25 mV/s.	148
Table 6.3	Electrochemical CV data for discorhabdin C type pyrroloiminoquinones <i>versus</i> pH. Scan Rate: 25 mV/s.	150
Table 6.4	Electrochemical CV data for discorhabdin D type pyrroloiminoquinones <i>versus</i> pH. Scan Rate: 25 mV/s.	152
Table 6.5	Potential assignments (CV) of the <i>bis</i> -pyrroloiminoquinones <i>versus</i> pH. Scan Rate: 25 mV/s.	155
Table 6.6	Data (rate constants and R ² values) obtained for the plot of peak current (<i>i_a</i>) <i>versus</i> the square root of the scan rate at pH 5.5 and 7.5.	157
 Chapter 7:		
Table 7.1	Human colon tumour (HCT-116) cytotoxicity data for the pyrroloamino- <i>ortho</i> -quinone, pyrroloiminoquinone and <i>bis</i> -pyrroloiminoquinone metabolites.	163
Table 7.2	Oesophageal (WHC01) and ovarian (ME180) cancer inhibition of discorhabdin A and tsitsikammamine B.	163

LIST OF ABBREVIATIONS:

A	Area of electrode (cm ²)
A	Absorbance
A-549	Human non small cell lung cancer cells
ABTS	2,2'-Azinobis(3-ethylbenzothiazoline-6-sulfonic acid)
<i>m</i> -AMSA	4'-(9-Acridinylamino)-3'-methoxymethanesulfonanilide
APCI	Atmospheric pressure chemical ionisation
API	Atmospheric pressure ionization
Ara-C	Arabinosyl cytosine
amu	Atomic mass unit
B-16	Melanoma cells
(BOC) ₂ O	Di- <i>tert</i> -butyl dicarbonate
BR1	Breast cancer cells
br	Broad (used in conjunction with s)
C	Concentration (mol/cm ³)
CAN	Ceric ammonium nitrate
CaN	Calcineurin
CE	Counter electrode
CHO	Chinese hamster ovary cancer cells
COSY	¹ H - ¹ H homonuclear correlation spectroscopy
<i>m</i> -CPBA	<i>meta</i> -chloroperbenzoic acid
CPC	Coil planet centrifuge
CPP32	Caspase-3
CRRF	Coral Reef Research Foundation
CTAB	Cetyltrimethylammonium bromide
CV	Cyclic voltammetry
cm ⁻¹	Wavenumbers
D	Diffusion coefficient (cm ² /s)
DABCO	1,4-Diazobicyclo-[2,2,2]octane
DBU	1,8-Diazabicyclo[5.4.0]undec-7-ene
DCC	1,3 Dicyclohexylcarbodiimide
DCCC	Droplet counter current chromatography
DDQ	2,3-Dichloro-5,6-dicyano-1,4-benzoquinone
DEPT	Distortionless enhancement by polarisation transfer
DIBAH	Diisobutylaluminium hydride
DPBF	1,3-Diphenylisobenzofuran
DTT	Dithiothreitol
DQFCOSY	Double quantum filtered ¹ H - ¹ H homonuclear correlation spectroscopy
DX	Doxorubicin
dd	Double doublet
E	Potential
E ^o	Formal potential
E _a	Potential maxima (Anodic)

E_c	Potential minima (Cathodic)
$E_{p/2}$	Peak at half current
$E_{1/2}$	Half wave potential
ED ₅₀	Effective dose (50 %)
EM9	DNA repair deficient cells
EPR	Electron spin resonance
ESI	Electrospray ionization
ESIMS	Electrospray ionisation mass spectrometry
EtBr	Ethidium bromide
eV	Electron volt
F	Faraday's constant
GI	Growth inhibition
HCT-116	Human colon tumour cancer cells
HETCOR	Heteronuclear correlation
HREIMS	High resolution electron impact mass spectrometry
HRFABMS	High resolution fast atom bombardment mass spectrometry
HMBC	Heteronuclear multiple bond correlation
HMQC	Heteronuclear multiple quantum coherence
HOHAHA	Homonuclear Hartmann Hahn
HPLC	High performance liquid chromatography
HSQC-TOCSY	Heteronuclear single quantum coherence – Total correlation spectroscopy
HT-29	Human colon cancer cells
I	Current
IR	Infra-red
ISC	Intersystem crossing
ImdCO ₂	4-Imidazole carboxylic acid
i_a	Current (Anode)
i_c	Current (Cathode)
i_p	Peak current (amperes)
i_a / i_c	Unity
J	Coupling constant
KB	Human oral epidermoid cancer cells
kDa	Kilodaltons
L1210	Murine leukemia cells
L5178Y	Murine leukemia cells
LC	Liquid chromatography
LC ₅₀	Lethality concentration
LC-MS	Liquid chromatography – mass spectrometry
LiAlH ₄	Lithium aluminium hydride
LICA	Lithium <i>iso</i> -propylcyclohexylamide
LTB ₄	Leukotriene B ₄ receptor
lr	Long range
MCF-7	Human breast cancer cells
ME180	Ovarian cancer cells

MIC	Minimum inhibitory concentration
MOM	Methoxymethyl
MTT	3-(4,5-Dimethylthiazol-2-yl)-2,5-diphenyl-tetrazolium bromide
m	Multiplet
mmu	Millimass unit
mult	Multiplicity
<i>m/z</i>	Mass to charge ratio
NaBH ₄	Sodium borohydride
NaH	Sodium hydride
NBS	N-bromosuccinimide
NCI	National Cancer Institute
NCS	N-chlorosuccinimide
NIR	Near infra-red
NMR	Nuclear magnetic resonance
NOEDS	Nuclear Overhauser difference spectroscopy
NOESY	Nuclear Overhauser enhancement spectroscopy
n	Number of moles of electrons
O	Oxidised
ODS	Octadecylsilane
OSWV	Osteryoung square wave voltammetry
P	Potentiostat
P-388	Murine leukemia cells
PIFA	Phenyliodine(III) <i>bis</i> -(trifluoroacetate)
PDT	Photodynamic therapy
PIQ	Pyrroloiminoquinone
q	Quartet
R	Gas constant
R	Reduced
<i>R</i>	Resistance
RE	Reference electrode
ROESY	Rotating frame Overhauser enhancement spectroscopy
ROS	Reactive oxygen species
SCE	Standard calomel electrode
SCUBA	Self contained underwater breathing apparatus
SDS	Dodecyl sulfate, sodium salt
SOQY	Singlet oxygen quantum yield
SR	Sarcoplasmic reticulum
Std	Standard
SWV	Square wave voltammetry
s	Singlet
T	Temperature
T/C	Treated / control
TBAF	<i>tert</i> -Butylammonium fluoride
TBS	<i>tert</i> -Butyldimethylsilyl

TBSCI	<i>tert</i> -Butyldimethylsilyl chloride
TEAC	Trolox equivalent antioxidant activity
TEMP	2,2,6,6-Tetramethyl-4-piperidone
TFA	Trifluoroacetic acid
TIC	Total ion chromatogram
TLC	Thin layer chromatography
TMEDA	N,N,N',N'-Tetramethylethylenediamine
Tr	Triphenylmethyl
TrCl	Triphenylmethyl chloride
Ts	Toluene-4-sulfonyl
TsCl	Toluene-4-sulfonyl chloride
<i>p</i> -TsOH	<i>para</i> -Toluene sulfonic acid
t	Triplet
<i>t</i> -Bul	<i>tert</i> -butyliodide
<i>t</i> -BuOK	Potassium <i>tert</i> -butoxide
topo	Topoisomerase
top1	Topoisomerase I
top2	Topoisomerase II
V	Scan rate (V/s)
V	Potential
VLC	Vacuum liquid chromatography
$W_{1/2}$	Peak width at half height
WE	Working electrode
WFG	Waveform generator
WHC01	Oesophageal cancer cells
α	In plane bending vibration
f_T	Fraction of triplet state
Φ_Δ	Singlet oxygen quantum yield
Φ_F	Fluorescence quantum yield
Φ_T	Triplet yield
η	Refractive index
ν	Stretching vibration

ABSTRACT

An in depth chemical investigation of the major and minor pyrroloiminoquinone metabolites produced by four species of endemic South African Latrunculid sponges, collected from Algoa Bay and the Tsitsikamma Marine Reserve off the south eastern coast of South Africa, yielded eleven new and twelve known pyrroloiminoquinone metabolites. The structures of the new metabolites were determined using standard spectroscopic techniques.

Tsitsikamma pedunculata was shown to contain 7,8-dehydro-3-dihydro-disorhabdin C (**2.1**), 14-bromo-7,8-dehydro-3-dihydro-disorhabdin C (**2.2**), disorhabdin S (**2.3**), 14-bromo-1-hydroxy-disorhabdin S (**2.4**), 1-bromo-2-hydroxy-4-debromo-disorhabdin S (**2.5**), and 2,4-debromo-3-dihydro-disorhabdin C (**2.6**), together with the known compounds 14-bromo-disorhabdin C (**1.51**), 14-bromo-3-dihydro-disorhabdin C (**1.52**) and 3-dihydro-disorhabdin C. The metabolites from *T. pedunculata* were characterised by the presence of a reduced C-3 carbonyl and bromination at C-14.

Compounds isolated from a second Latrunculid sponge, *Latrunculia lorii*, ranged from a substituted bicyclic pyrrolecarboxylic acid, makaluvic acid A (**1.47**), to the simple tricyclic known pyrroloiminoquinones makaluvamine C (**1.33**) and damirone B (**1.20**) and the more complex disorhabdin D type metabolites, disorhabdin M (**3.2**), 1-amino disorhabdin D (**3.3**), 1-methoxy disorhabdin D (**3.4**) and 1-alanyl disorhabdin D (**3.5**). Disorhabdin G* (**3.1**) was also isolated and characterised. This is the first reported occurrence of the known compounds **1.20**, **1.33** and **1.47** in a *Latrunculia* sponge.

Disorhabdin and *bis*-pyrroloiminoquinone type compounds predominated in *Tsitsikamma favus*. Three known, tsitsikammamines A (**1.71**) and B (**1.72**), **1.52**, and five new pyrroloiminoquinones, tsitsikammamine N-oxime (**4.1**), tsitsikammamine B N-oxime (**4.2**), **2.1**, **2.4** and **2.6**, were isolated from this sponge. A fourth Latrunculid sponge (*Strongylodesma* sp.) yielded three known compounds, disorhabdins A (**1.57**), D (**1.61**) and **1.53**, and one new pyrroloiminoquinone **3.3**.

The dual role of these metabolites as cytotoxic agents and pigments resulted in an attempt to relate the photochemical properties of these metabolites to their cytotoxicity. The pyrroloiminoquinone metabolites studied exhibited moderate singlet oxygen quantum yields, while three compounds (**1.57**, **4.1** and **4.2**) were shown to be capable of producing radicals at a wavelength of 532 nm. The possibility of a correlation between the electrochemical properties and anti-cancer (HCT-116) activity of selected pyrroloiminoquinones was explored. A study of the oesophageal and ovarian cytotoxicities of two pyrroloiminoquinones (**1.57** and **1.72**), together with an investigation into the intercalation and topoisomerase I inhibitory activity of the *bis*-pyrroloiminoquinones (**1.71**, **1.72**, **4.1** and **4.2**), are presented.

Chapter 1: Introduction

1.1 Marine sponges: a prolific source of potential pharmaceuticals

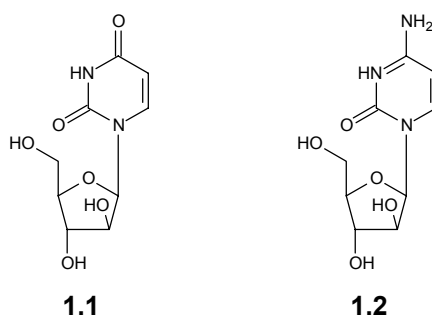
Natural products, the secondary metabolites produced by many organisms e.g. plants, microbes and marine invertebrates, have been utilised by people over the centuries as a source of food, medicine, insecticides, poison, dyes, and even cosmetics.¹ Terrestrial plants, which have formed the basis of many traditional herbal remedies, are still the major source of medicinally important natural products. Currently approximately one hundred and twenty products derived from ninety plant species can be considered as important drugs, and a 1993 analysis of prescription data from the United States revealed that over 50 % of the most frequently prescribed drugs either contained a plant natural product or were derived from a plant natural product.² The increased availability of SCUBA in the latter half of the twentieth century has made the marine environment far more accessible than before, and this, together with the knowledge that the marine environment diversity exceeds that of terrestrial organisms,³ has stimulated research into the vast marine natural products reservoir with the objective of discovering new pharmaceutical agents.^{3,4,5}

Marine sponges (Phylum Porifera) are the most prolific producers of biologically active marine natural products.^{3,6-10} Andersen and Williams report that 47 % of the natural products isolated from marine organisms in 1997 were sponge metabolites,⁵ and that sponges contributed 44 % of the total number of cytotoxic compounds identified from marine organisms up to 2000.⁵ Sponges, in common with other marine organisms, occupy very different habitats to terrestrial plants and are subjected to unique ecological, physiological and predatory challenges. Accordingly, it is not surprising that sponges have utilised unique biosynthetic pathways, or have adapted established pathways, to produce the plethora of novel marine natural products which abound in the literature.⁵⁻¹⁰ The role of these secondary metabolites in supporting the sponges' survival in the sea includes defence against predation, microbial infection and as chemical mediators in the competition for space in competitive marine reef ecosystems. It has been suggested that a significant number of sponge metabolites could be of microbial origin because of the large number of symbiotic microorganisms (bacteria and fungi) associated with the sponge. However this has only been proven in a few cases.¹¹

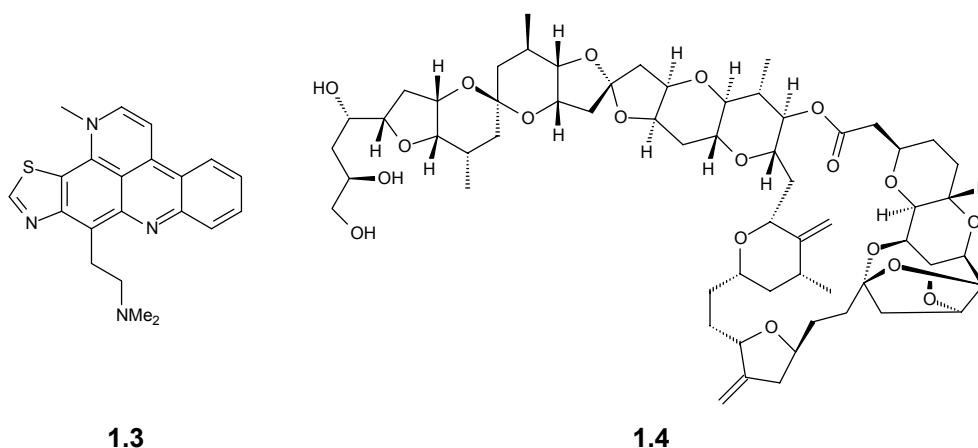
The ubiquitous Phylum Porifera which evolved more than 500 million years ago is found in a variety of habitats from intertidal zones to mid ocean trenches thousands of metres deep.¹ Sponges are the simplest of multicellular animals, sustaining a virtually protozoan independence for their constituent cells, which form no tissue layers or organs.¹ The location of a particular cell is dependent on the specialised functions performed by that cell and the life of a sponge revolves around the pumping of a large volume of water through the tissues. The sponge relies on the food and oxygen filtered out of the water column for survival. The bodies of sponges therefore consist of a system of pores, ostia, canals and chambers, which conduct water from the inhalant ostia on

the surface to the oscules, the exhalant apertures also on the surface. Sponges vary widely in colour, shape and size, from thin encrusting sponges to branched rope sponges and giant barrel sponges that are more than two metres in height.¹

The search for sponge marine natural products with pharmaceutical potential began during the 1950s with the work of Bergman and co-workers on the Caribbean sponge *Cryptotethia crypta*. The potent tumour inhibitor spongouridine (**1.1**) was isolated as a major metabolite, which led to the synthesis of a new class of arabinosyl nucleoside analogs such as arabinosyl cytosine (**1.2** ara-C). Ara-C is currently in clinical use for the treatment of acute myelocytic leukaemia and non-Hodgkin's lymphoma.^{1,3}

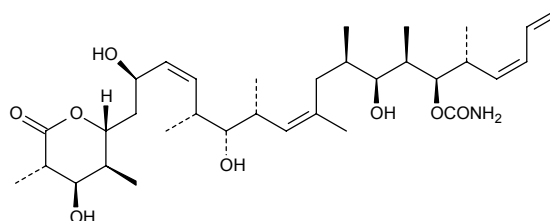


The following selection of compounds not only illustrates the potent pharmacological activity displayed by sponge metabolites but also their remarkable structural variety.



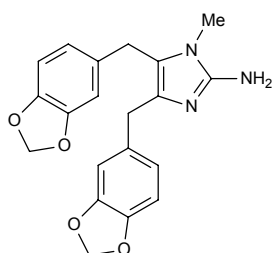
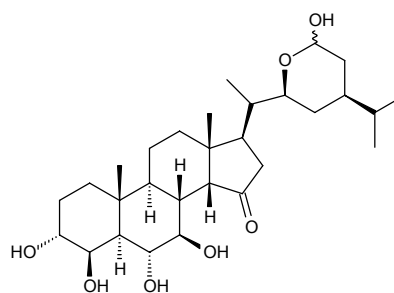
The novel aminoacridine alkaloid dercitin (**1.3**) was isolated from a Caribbean deep water sponge *Dercitus* sp..¹² Dercitin possesses *in vitro* cytotoxic activities in the low nanomolar concentration range, displaying activity against B-16 melanoma cells and small cell Lewis lung carcinoma. In animal studies, dercitin was found to prolong the life of mice bearing ascitic P-388 tumours (Treated / Control (T/C) 170, *i.e.* a 70 % increase in life span, at 5 mg/kg). Studies indicated that dercitin probably exerts its biological effects through DNA intercalation, which is also a mechanism of action for several clinically useful anticancer agents.¹²

The development of halichondrin B (**1.4**) from the sponge *Lissodendoryx* sp.¹³ as an anticancer agent is of interest as it highlights the problem of supply which hampers the success of many marine compounds in clinical trials. Originally isolated in small amounts from the Japanese sponge *Halichondria okadai*,¹⁴ Munro, Battershill and co-workers have successfully engineered the first sustainable supply of a sponge metabolite for clinical trials *via* aquaculture³ of the related *Lissodendoryx* sp..

**1.5**

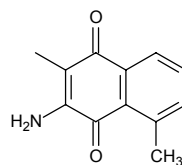
Another Caribbean sponge *Discodermia dissoluta* produced the potent immunosuppressant discodermolide (**1.5**), a polyhydroxylated lactone.¹⁵ While *in vitro* assays showed that the immunosuppressive activity of **1.5** is approximately equivalent to that of the clinically useful immunosuppressive agent cyclosporin A, the *in vivo* assays showed that **1.5** was 100 – 1000 times more powerful than cyclosporin A.

Leucettamine A (**1.6**), an imidazole alkaloid from the Palauan sponge *Leucetta microraphis*,¹⁶ displays anti-inflammatory activity by acting as a potent and selective antagonist for the leukotriene B4 (LTB4) receptor.

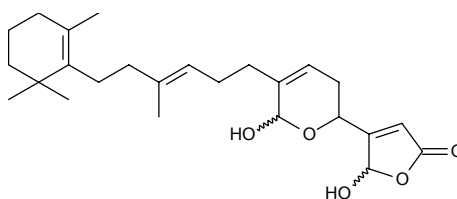
**1.6****1.7**

Another sponge metabolite with anti-inflammatory properties is contignasterol (**1.7**) isolated by Andersen and co-workers from the sponge *Petrosia contignata*.¹⁷ The Canadian pharmaceutical company Inflazyme has developed this compound and a more potent synthetic analogue IPL-576 as anti-asthma agents. The synthetic derivative was scheduled to enter clinical trials in 1999.¹⁸

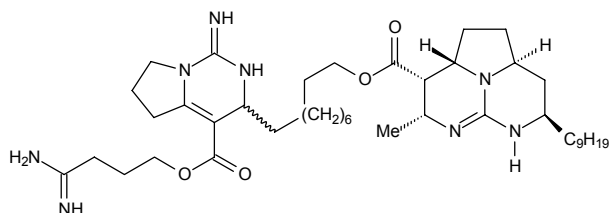
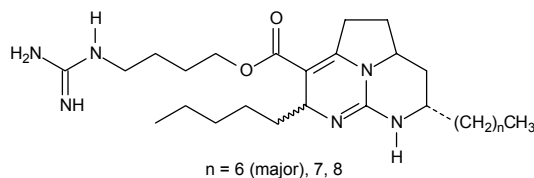
An Indian Ocean sponge collection yielded a series of cytotoxic quinones, such as cribrostatin 1 (**1.8**), isolated from the sponge *Cribrachalina* sp..¹⁹ Cribrostatin 1 (**1.8**) displayed selective activity against all nine melanoma cell lines in the NCI panel.

**1.8**

Manoalide (**1.9**), isolated from the sponge *Luffariella variables* by de Silva and Scheuer,²⁰ initially showed immense promise as an anti-inflammatory agent. Unfortunately the insolubility of this compound precluded its clinical development. Nonetheless this compound still finds application today as an important molecular probe in phospholipase A₂ inhibition.

**1.9**

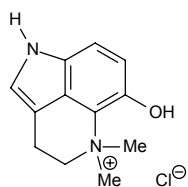
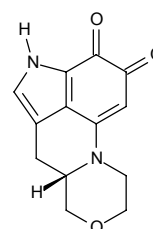
The polycyclic guanidine alkaloids batzelladines A (**1.10**) and C (**1.11**) isolated from the Caribbean sponge *Batzella* sp. have shown potential as anti-HIV agents, exhibiting potent inhibition of CD4/gp120 binding in various assays. The fact that HIV-1 cannot replicate autonomously, provided a target for AIDS therapeutic agents *i.e.* the binding site for the HIV-1 surface glycoprotein gp120 and CD4 receptors on T-cells.²¹

**1.10****1.11**

An important class of bioactive sponge metabolites are the pyrroloiminoquinone alkaloids confined to the sponge family Latrunculiidae. Wakayin (**1.73**), isolated from an ascidian (Phylum Ascidiacea) is the notable exception to this general trend (see pp. 17). As this thesis presents a comprehensive study of the pyrroloiminoquinone metabolites from four species of South African Latrunculid sponges, a review of this class of compounds is deemed necessary. This review limits its scope to a more thorough discussion of the isolation, identification, phyletic distribution, biosynthesis, bioactivity and synthesis of pyrroloiminoquinone and pyrroloamino-*ortho*-quinone alkaloids from the family Latrunculiidae than that presented in a recent review entitled "Bioactive Marine Alkaloids".²²

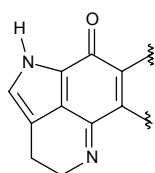
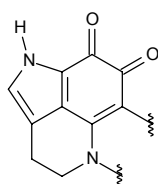
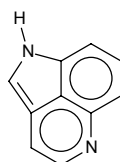
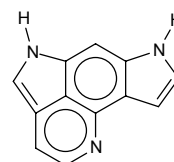
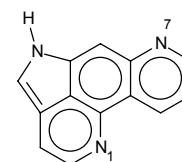
Pyrroloiminoquinones display significant biological properties, thus attracting both natural product and synthetic chemists alike, since almost all these alkaloids have been reported to exhibit significant cytotoxicity. The mechanism of this cytotoxicity includes inhibition of topoisomerase II, Ca^{2+} release activity and intercalation of DNA. For the natural products chemist these compounds provide challenging targets for structure elucidation studies given the paucity of resonances in their ^1H NMR spectra.

Interestingly pyrroloiminoquinones and pyrroloamino-*ortho*-quinone type compounds are not limited to the marine environment and two terrestrial sources of these compounds are known. The South American toad *Bufo marinus* was found to contain, as its principle indole constituent, dehyrobufotenine (**1.12**),²³ while a pyrroloquinoline pigment, haematopodin (**1.13**) was isolated from the fungus *Mycena haematopus*.²⁴

**1.12****1.13**

1.2 Chemistry of pyrroloamino-*ortho*-quinone, pyrroloiminoquinone and *bis*-pyrroloiminoquinone alkaloids

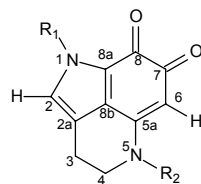
Over sixty alkaloids containing the characteristic pyrroloiminoquinone (**1.14**), and to a lesser extent the pyrroloamino-*ortho*-quinone (**1.15**) core structures have been isolated from the genera *Latrunculia*, *Zyzzya*, *Batzella*, *Prianos* and *Damiria*. Traditionally pyrroloiminoquinone and pyrroloamino-*ortho*-quinone metabolites have been further subdivided into three broad structure subclasses based on either a pyrroloquinoline (**1.16**), *bis*-pyrroloquinoline (**1.17**) or pyrrole-[1,7]-phenanthroline (**1.18**) skeleton.

**1.14****1.15****1.16****1.17****1.18**

Our review of the isolation and identification of pyrroloamino-*ortho*-quinone, pyrroloiminoquinone and *bis*-pyrroloiminoquinone metabolites from Latrunculid sponges has been subdivided according to the structural complexity of these compounds. The simpler, bicyclic and tricyclic

pyrroloquinoline metabolites precede the more complex pyrroloiminoquinones e.g. the tetracyclic makaluvamines and the penta-, hexa- and hepta-cyclic discorhabdins.

1.2.1 Damirones



1.19 $R_1 = \text{CH}_3$; $R_2 = \text{CH}_3$

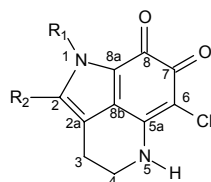
1.20 $R_1 = \text{H}$; $R_2 = \text{CH}_3$

1.21 $R_1 = \text{H}$; $R_2 = \text{H}$

The damirones, named after the original sponge source of these compounds, are characterised by an *ortho*-quinone moiety in addition to the pyrroloquinoline ring structure common to all the compounds discussed in this review. Damirones A (**1.19**) and B (**1.20**) were isolated by Stierle and Faulkner²⁵ from a Palauan sponge of the genus *Damiria*, which was subsequently reidentified²⁶ as *Zyzzya fuliginosa*. The dichloromethane partition fraction of the methanol extract of the sponge was subjected to Sephadex LH-20 chromatography using dichloromethane : methanol (1:1) as the eluant, followed by silica gel flash chromatography. The structures of **1.19** and **1.20** were based upon comparison with that of batzelline A (**1.22**) and corroborated with additional spectroscopic data such as nOe difference spectroscopy (NOEDS) experiments and UV data.²⁵

A third damirone, damirone C (**1.21**), was isolated by Schmidt *et al.*²⁶ along with several makaluvamines from a Pohnpeian sponge *Zyzzya fuliginosa*. Damirone C (**1.21**) lacks the N-methyl groups of **1.19** and **1.20** and the proposed structure was confirmed from one and two dimensional NMR data.²⁶

1.2.2 Batzellines



1.22 $R_1 = \text{CH}_3$; $R_2 = \text{SCH}_3$

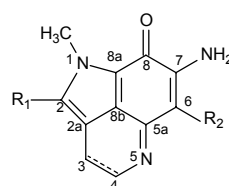
1.23 $R_1 = \text{H}$; $R_2 = \text{SCH}_3$

1.24 $R_1 = \text{CH}_3$; $R_2 = \text{H}$

The batzellines, also named after the sponge source, feature a chlorine substituent in addition to the pyrrolo-*ortho*-quinone structure seen in the damirones. The chlorine functionality in these

compounds, as well as the thiomethyl ether group in compounds **1.22** and **1.23**, are quite unusual and are rarely seen in marine natural products. Batzellines A-C (**1.22** - **1.24**) were obtained from a deep water collection of *Batzella* sp. from the Bahamas.²⁷ The methanol : chloroform extract of the sponge was extracted with ethyl acetate and the latter extract fractionated by counter current chromatography to give batzellines A to C. The structure of **1.22** was secured by a combination of NMR, HREIMS, UV absorption, chemical conversions and X-ray crystallographic analyses. The structures of **1.23** and **1.24** were established by comparison of their NMR data with those of **1.22** and through chemical interconversion.

1.2.3. Isobatzellines



1.25 R₁ = SCH₃; R₂ = Cl

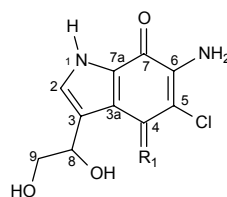
1.26 R₁ = SCH₃; R₂ = H

1.27 R₁ = H; R₂ = Cl

1.28 R₁ = SCH₃; R₂ = Cl; Δ³

An ongoing search for bioactive agents from *Batzella* sponges by the Sakemi and co-workers resulted in the isolation and characterisation of four additional alkaloids, the isobatzellines A-D (**1.25** – **1.28**), from the deep water Caribbean sponge *Batzella* sp..²⁸ The isobatzellines possess the same pyrroloquinoline ring system as the batzellines, but contain an iminoquinone moiety instead of the amino-*ortho*-quinone moiety found in the batzellines. The four structurally related isobatzellines were characterised by chemical interconversion and spectral comparison with **1.22**. Interestingly, auto-oxidation of **1.25** to **1.28** was observed on a thin layer chromatogram (TLC) containing **1.25** within a few hours or by treatment with 2,3-dichloro-5,6-dicyano-1,4-benzoquinone (DDQ), suggesting that oxidation of **1.25** is facile to give the more aromatic **1.28**. Isobatzelline A was converted to batzelline A by a diazotisation – substitution reaction in aqueous nitrous acid. Solvent partitioning of the chloroform : methanol extract and centrifugal counter current chromatography were used to purify compounds **1.25** – **1.28**.²⁸

1.2.4. Secobatzellines



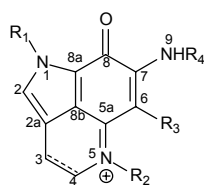
1.29 R₁ = NH

1.30 R₁ = O

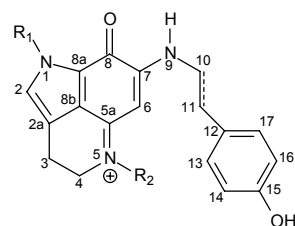
In a continuing search for new protein phosphatase inhibitors from marine organisms, two batzelline derivatives, the bicyclic secobatzellines A (**1.29**) and B (**1.30**) were isolated from a deep water Caribbean sponge of the genus *Batzella* sp..²⁹ The structures of secobatzellines A and B were determined by a combination of one and two dimensional NMR spectroscopy as well as chemical interconversion.²⁹ Secobatzelline A was found to possess the same basic pyrroloiminoquinone backbone reported for the structurally related isobatzellines A-D. Secobatzelline B was subsequently thought to be an isolation artefact.²² The ethanol extract of the *Batzella* sponge was partitioned between ethyl acetate and water and the former partition fraction subjected to silica gel chromatography using dichloromethane : methanol as the solvent and the fractions subsequently collected were monitored for inhibition of calcineurin (CaN). The CaN inhibitory fractions were then combined and purified using reversed phase HPLC.²⁹

1.2.5 Makaluvamines

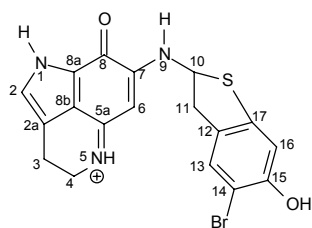
In 1993, as part of their ongoing search for potential antineoplastic agents from marine sources, Radisky *et al.*³⁰ were the first to present the isolation and characterisation of seven new pyrroloiminoquinones, makaluvamines A-F (**1.31** – **1.36**) and makaluvone (**1.37**), together with the known compounds discorhabdin A (**1.57**) and damirone B (**1.20**) from a Fijian sponge *Zyzzya cf. marsallis* (an incorrect spelling of *massalis* was later corrected and the sponge reidentified as *Zyzzya fuliginosa*²⁶) collected from Makaluva Island. Solvent partitioning of the methanol extract resulted in the cytotoxic activity being concentrated primarily in the chloroform layers. Routine silica gel flash chromatography followed by lipophilic Sephadex LH-20 chromatography yielded these pyrroloiminoquinones. Extensive two dimensional NMR data, together with comparison with the published data for a semisynthetic derivative of isobatzelline A (**1.25**) led to the initial structure of makaluvamine A. The structure of the *ortho*-quinone, makaluvone (**1.37**), established by comparison of the NMR data with isobatzelline C, followed the structure elucidation of the rest of the makaluvamine series.³⁰



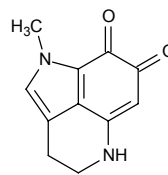
- 1.31** R₁ = CH₃; R₂ = H; R₃ = H; R₄ = H
1.32 R₁ = CH₃; R₂ = H; R₃ = H; R₄ = H; Δ³
1.33 R₁ = H; R₂ = CH₃; R₃ = H; R₄ = H
1.39 R₁ = CH₃; R₂ = CH₃; R₃ = H; R₄ = H
1.40 R₁ = H; R₂ = H; R₃ = H; R₄ = H
1.45 R₁ = H; R₂ = H; R₃ = Br; R₄ = H



- 1.34** R₁ = H; R₂ = H
1.35 R₁ = CH₃; R₂ = H; Δ¹⁰
1.38 R₁ = CH₃; R₂ = CH₃; Δ¹⁰
1.41 R₁ = H; R₂ = CH₃
1.42 R₁ = CH₃; R₂ = H
1.43 R₁ = H; R₂ = CH₃; Δ¹⁰
1.44 R₁ = H; R₂ = H; Δ¹⁰
1.46 R₁ = CH₃; R₂ = CH₃



1.36



1.37

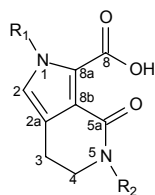
Other members of the makaluvamine group have subsequently been reported. Carney *et al.*³¹ isolated makaluvamine G (**1.38**) from a sponge collected from Indonesia of the genus *Histodermella* (later reidentified as *Zyzzya fuliginosa*²⁶). Solvent partitioning of the dichloromethane : 2-propanol (1:1) extract followed by Sephadex LH-20 chromatography yielded makaluvamine G as the major cytotoxic product. Makaluvamines A and C together with damirones A (**1.19**) and B (**1.20**) were also isolated from the sponge.³¹

Makaluvamines H-M (**1.39** - **1.44**) and damirone C (**1.21**) were isolated by Schmidt *et al.* from a Pohnpeian sponge, *Zyzzya fuliginosa*.²⁶ The methanol : dichloromethane extract of the sponge was partitioned between ethyl acetate and water and the water soluble material chromatographed on Sephadex LH-20 using methanol as the eluant. The known compounds makaluvamines C (**1.33**), D (**1.34**) and G (**1.38**) were also isolated. The new compounds were identified by recourse to extensive two dimensional NMR data and by comparison of their spectral data with those of the known members in these series.

Venables *et al.*³² reported the isolation of makaluvamine N (**1.45**), a pyrroloiminoquinone whose structure is reminiscent of the batzelline series. Makaluvamine N, which possesses a halogen at position 6 (uncommon for makaluvamines) was isolated from a Philippine sponge of the genus *Zyzzya fuliginosa* together with the known compounds makaluvamines A, C, D, E and I. The sponge was extracted with methanol and partitioned according to a modified Kupchan procedure. The methanol soluble material was purified on a reversed phase high performance liquid chromatography (HPLC) C₁₈ column followed by final purification on a Sephadex LH-20, while the chloroform soluble material was subjected to repeated Sephadex LH-20 chromatography.³²

In an ongoing search for cytotoxic marine metabolites, the sponge *Zyzzya fuliginosa* was collected off the Vanuatu Islands and yielded makaluvamine P (**1.46**), the last new makaluvamine reported to date.³³ The compound was identified by comparison of its spectral data with those of known compounds. The sponge was extracted with methanol and subsequently partitioned according to a modified Kupchan procedure. Fractionation of the bioactive chloroform soluble material was performed by droplet countercurrent chromatography (DCCC) followed by reversed phase HPLC on a C₁₈ column. Makaluvamine P was isolated together with makaluvamines G, J, K and L.³³

1.2.6 Makaluvic acids



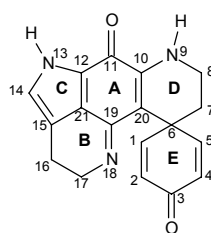
1.47 $R_1 = H$; $R_2 = CH_3$

1.48 $R_1 = CH_3$; $R_2 = H$

Due to the co-occurrence of the substituted pyrrole carboxylic acids, makaluvic acids A (**1.47**) and B (**1.48**), with makaluvamines although they are not strictly pyrroloquinoline metabolites they have been included in this section. Fu *et al.*³⁴ isolated makaluvic acids A and B from the sponge *Zyzya fuliginosus*. The known makaluvamines A, E and K, together with 4-hydroxybenzoic acid and 3,7-dimethylisoguanine were also found in the sponge. The sponge was extracted sequentially with methanol and methanol : dichloromethane (1:1) and the combined extracts subjected to Kupchan partitioning. The *n*-butanol and water fractions were found to exhibit significant cytotoxicity and contained the makaluvamine metabolites. 3,7-Dimethylisoguanine was obtained during the chromatography of the *n*-butanol partition fraction using a silica gel column and methanol : dichloromethane as the eluent. The makaluvic acids were obtained from silica gel chromatography using methanol : dichloromethane containing 1 % TFA as the eluent followed by reversed phase HPLC. The structure of makaluvic acid A was confirmed by X-ray analysis.³⁴

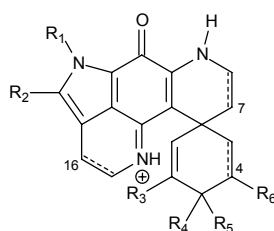
1.2.7 Discorhabdins

A basic discorhabdin skeleton together with the atom numbering used by the original authors³⁵ is given below:



The name discorhabdin is derived from the characteristic discorhabd spicules used to identify many Latrunculid sponges. Pyrroloiminoquinone discorhabdin metabolites isolated from marine sponges of the family Latrunculiidae have the following general structural features: the metabolites normally contain a pyrrolo-[1,7]-phenanthroline ring system together with a spiro cyclohexenone or spiro cyclohexadienone ring system. In addition, bromine is frequently incorporated into the skeleton, e.g. discorhabdin C (**1.49**), and some metabolites are also found to contain a tetrahydrothiophene bridge e.g. discorhabdin A (**1.57**).

Discorhabdin C was the first, and the simplest, of the discorhabdins to be isolated from a sponge of the genus *Latrunculia* du Bocage³⁵ and was discovered through wide scale screening of New Zealand's marine invertebrates for antiviral and antitumour activity. Discorhabdin C (**1.49**) thus represented a new class of potential antitumour agents.³⁵ The structure of the highly cytotoxic discorhabdin C was shown by single-crystal X-ray diffraction to contain a previously unknown tetracyclic pyrroloiminoquinone chromophore linked to a spiro 2,6-dibromocyclohexadienone ring. The NMR assignments of discorhabdin C were subsequently established by Perry *et al.*³⁶ Flash chromatography of the methanol : toluene extract followed by purification of the cytotoxic fractions by reversed phase LC afforded pure **1.49** which was characterised as its hydrochloride salt.³⁵



- 1.49** R₁ = H; R₂ = H; R₃ = Br; R₄ + R₅ = O; R₆ = Br; Δ⁴
1.50 R₁ = CH₃; R₂ = H; R₃ = Br; R₄ + R₅ = O; R₆ = Br; Δ⁴
1.51 R₁ = H; R₂ = Br; R₃ = Br; R₄ + R₅ = O; R₆ = Br; Δ⁴
1.52 R₁ = H; R₂ = Br; R₃ = Br; R₄ = OH; R₅ = H; R₆ = Br; Δ⁴
1.53 R₁ = H; R₂ = H; R₃ = Br; R₄ = OH; R₅ = H; R₆ = Br; Δ⁴
1.54 R₁ = H; R₂ = H; R₃ = Br; R₄ + R₅ = O; R₆ = H; Δ⁴
1.55 R₁ = H; R₂ = H; R₃ = Br; R₄ + R₅ = O; R₆ = H; Δ⁴, Δ¹⁶
1.56 R₁ = H; R₂ = H; R₃ = Br; R₄ + R₅ = O; R₆ = H; Δ⁷

The nomenclature of the discorhabdins has been unnecessarily complicated by the relative inaccessibility of the structures of discorhabdins H-O. Although the structures of discorhabdins E-M were presented by Munro *et al.*³⁷ at the New Zealand Institute of Chemistry Conference (7-10 December, 1993) and later at the 37th Annual Meeting of the American Society of Pharmacognosy (1996),³⁸ their spectral data has never been published. The uncertainty surrounding the structures of discorhabdins H-O has been relieved to some extent by the appearance of these structures in the recent review by Urban *et al.*²² (unfortunately again without spectral data). We were in a fortunate position to have access to both the structures and the ¹H NMR spectra of discorhabdins E-M³⁹ and were confused by the inconsistency between the structures of discorhabdin G and discorhabdin M we had in hand and those presented in the recent review (see Chapter 3, Section 3.2.3). In an attempt to clarify the structures of discorhabdins H-O we have presented these structures as *per* the Urban *et al.*²² review in Figure 1.1.

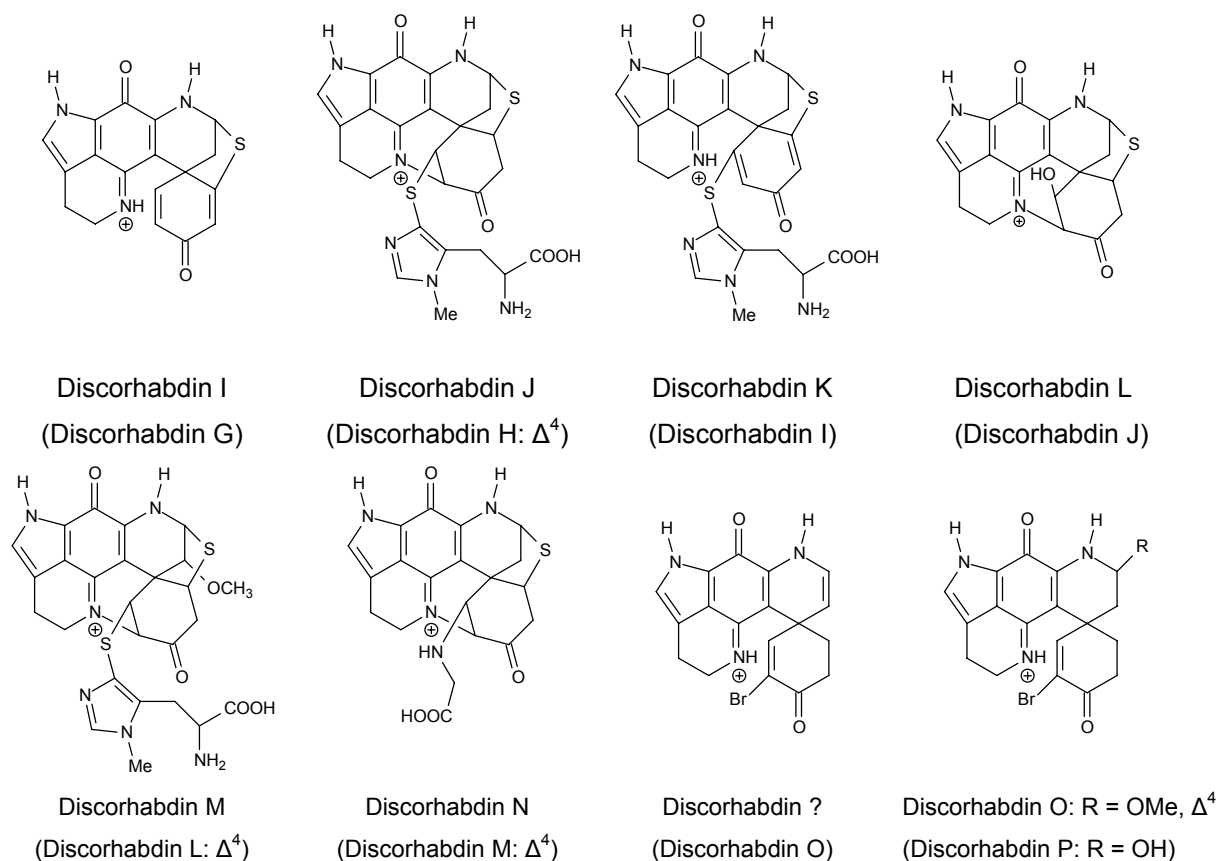


Figure 1.1 The structures of discorhabdins H-O (from Urban *et al.*).²² The former names³⁹ are given in parentheses, together with any structural differences.

Discorhabdin P (**1.50**), *i.e.* *N*-13-methyl discorhabdin C, was isolated from a deep water Caribbean sponge of the genus *Batzella* by Gunasekera *et al.*⁴⁰ in an ongoing search for new protein phosphatase inhibitors from marine organisms. The structure of discorhabdin P was solved using NMR spectroscopy and confirmed by X-ray diffraction analysis. The ethanol extract was partitioned between ethyl acetate and water and the ethyl acetate soluble material chromatographed over silica gel using gradient elution (methanol : dichloromethane) to afford discorhabdin P.⁴⁰

14-Bromo-discorhabdin C (**1.51**) and 14-bromo-3-dihydro-discorhabdin C (**1.52**) were isolated by Hooper *et al.* in 1996 from a South African marine sponge recently identified as *Tsitsikamma favus*. This was the first report of discorhabdin metabolites with a C-14 substituent. A combination of antibiotic assays and ¹H NMR spectroscopy was used to guide the extraction and the chromatographic procedures. Gradient elution on a C₁₈ Sep-Pak[®] cartridge was used to achieve the initial separation of the sponge extract partition fractions followed by exhaustive reversed phase HPLC. Extensive one and two dimensional NMR spectroscopy ultimately established the structures for **1.51** and **1.52**.⁴¹

In an ongoing search for cytotoxic metabolites from South African Latrunculid sponges, a third discorhabdin C analogue, 3-dihydrodiscorhabdin C (**1.53**) was isolated by Beukes⁴² as the second major metabolite from a sponge *Strongyloidesma coetzeei*. The structure was established by comparison of the spectral data with those of discorhabdin C and **1.52** together with further one and two dimensional NMR data. Solvent partitioning of the methanol : dichloromethane extract with ethyl acetate and water (containing 0.1 % TFA) followed by gradient elution on a C₁₈ Sep-Pak[®] and reversed phase HPLC (methanol : water, TFA pH 3) provided the pure compound **1.53**.⁴²

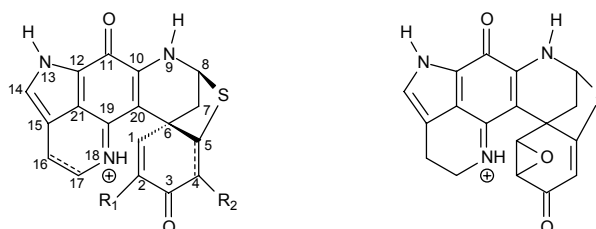
Discorhabdin E (**1.54**), a 4-debromo derivative of discorhabdin C (**1.49**) was isolated during a second investigation of the sponge *Latrunculia* du Bocage from New Zealand (*L. cf. bocagei*). The structure of discorhabdin E (**1.54**) was established based on comparison of the spectral data with those of discorhabdin C.⁴³ Blunt *et al.* reported the isolation of discorhabdin F (**1.55**) from a New Zealand Latrunculid sponge in a review of New Zealand marine natural products. However, no spectroscopic data were reported.⁴⁴

Discorhabdin G (**1.56**), isolated from the Antarctic sponge *Latrunculia apicalis* by Yang *et al.*,⁴⁵ was found to exhibit significant bioactivity, including antibiotic activity and activity influencing the feeding behaviour of sea stars. Discorhabdin G, characterised from extensive one and two dimensional NMR data as well as by comparison of the spectral data with those of discorhabdin C (**1.49**), differs from **1.49** in that the Δ^4 olefin is replaced with a Δ^7 double bond in **1.56**. In addition there is no bromine atom at C-4 in **1.56**. Sponges were subjected to solvent extraction of increasing polarity from hexane to 7 : 3 water : methanol, which resulted in the significant bioactivity residing in the chloroform and methanol partition fractions. The methanol extract was subjected to Sephadex LH-20 chromatography followed by repeated reversed phase HPLC (mobile phase contained 0.05 % TFA), to afford discorhabdins C and G.⁴⁵

Bioassay guided analyses of the sponge extracts from three different species of *Latrunculia* sponges led to the isolation of discorhabdins A (**1.57**) and B (**1.58**) together with discorhabdin C.³⁶ The sponges were collected as part of an ongoing search for antitumour and antiviral agents from marine invertebrates from New Zealand. The structures of discorhabdins A, and B, both of which contain an additional ring formed by a tetrahydrothiophene bridge between C-5 and C-8, were assigned by comparison of the spectral data of both compounds with the spectral data of discorhabdin C and extensive one and two dimensional NMR data, especially nOe difference spectroscopy, HETCOR and COSY NMR experiments. Both **1.57** and **1.58** lack a bromine substituent at C-4, while discorhabdin A lacks a Δ^4 double bond when compared with the structure of discorhabdin C. Following extraction of the sponge with methanol and dichloromethane, the methanol : dichloromethane extract was partitioned on a reversed phase column to give a number of cytotoxic fractions which were further purified using reversed phase LC to give **1.57**. The methanol : toluene sponge extract was partitioned on a reverse phase

column followed by preparative and semipreparative reversed phase LC (using 0.05 % TFA) to give **1.58**.³⁶

In an effort to identify new leads to antitumour agents from marine organisms, discorhabdin Q (**1.59**, 16, 17-dehydrodiscorhabdin B) was isolated from the sponge *Latrunculia purpurea* and interestingly, also from the sponges *Zyzya massalis*, *Z. fuliginosa* and an unidentified *Zyzya* spp..⁴⁶ Spectroanalytical techniques, such as one and two dimensional NMR, together with comparison of spectral data with known compounds were used to solve the structure of **1.59**. The ¹H NMR spectrum revealed that the usual pair of vicinally coupled methylene signals (H₂-16 and H₂-17) were replaced by a pair of mutually coupled olefinic methines. The methanol : dichloromethane extract was partitioned to give the cytotoxic chloroform and aqueous methanol partition fractions. Reversed phase gradient elution VLC of both these partition fractions followed by Sephadex LH-20 and VLC on silica gel afforded pure discorhabdin Q.⁴⁶



1.57 R₁ = Br; R₂ = H

1.58 R₁ = Br; R₂ = H; Δ⁴

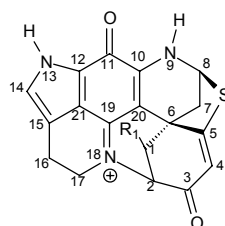
1.59 R₁ = Br; R₂ = H; Δ⁴; Δ¹⁶

1.60

The last discorhabdin reported thus far is discorhabdin R (**1.60**), a novel epoxy discorhabdin isolated from a southern Australian *Negombata* sp. and an Antarctic *Latrunculia* sp.. The structure was assigned from spectroscopic data including one and two dimensional NMR data and upon comparison of the spectral data with those of discorhabdin B (**1.58**). Discorhabdin R lacks a bromine substituent at C-2 and a Δ¹ olefin, containing instead two mutually coupled epoxy methine signals in the ¹H NMR spectrum. The ethanol extracts of both the *Latrunculia* and *Negombata* species were subjected to reversed phase partitioning (with TFA) to give the TFA salts of **1.58** and **1.60**. Although the authors were unable to assign the stereochemistry of the epoxide using nOe difference or NOESY experiments, they assigned the configurations of the remaining chiral centres of the molecule *via* spectroscopic comparisons with discorhabdin B (**1.58**).⁴⁷

The third class of discorhabdin alkaloids contains an additional ring formed by formation of a bond between N-18 and C-2. Discorhabdin D (**1.61**), a quaternary iminium salt, and discorhabdin A were isolated from two New Zealand sponges (*Latrunculia brevis* and *Prianos* sp.).⁴⁸ The structure of **1.61** was established from spectral data (one and two dimensional NMR) and comparison of this spectral data with known discorhabdins. The heptacyclic discorhabdin D contains two more heterocyclic rings than discorhabdin C. The additional rings are formed

through a C-5 to C-8 tetrahydrothiophene bridge and a bond between N-18 and one of the spiro ring atoms (C-2). The methanol and methanol : toluene (for *L. brevis*) or acetone (*Prianos* sp.) sponge extracts were partitioned on a reversed phase column or with ethyl acetate, respectively. The methanol : toluene extract was subjected to further reversed phase chromatography using a sequence of preparative LC gave pure **1.61**. The ethyl acetate partition fraction was, on the other hand separated by centrifugal counter current chromatography using chloroform : methanol : water. Selected fractions were further purified on silica gel (chloroform : methanol) to give pure discorhabdin D.⁴⁸



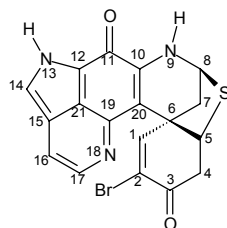
1.61 $R_1 = H$

1.62

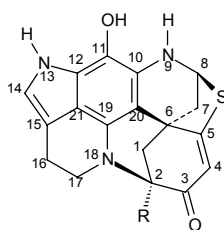
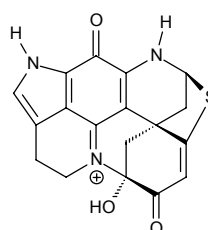
The most complex of the discorhabdin D series is discorhabdin H (**1.62**), previously isolated by Munro *et al.* (Figure 1.1).^{22,37-39} Discorhabdin H (**1.62**), was however isolated and characterised as its TFA salt by Beukes⁴² from three South African Latrunculid sponges *i.e.* from *Strongyloidesma coetzeei*, *Latrunculia gibbonsi* and *Latrunculia lúnaviridis*. The structure was established by extensive one and two dimensional NMR data as well as through the use of ozonolysis followed by chiral GC-MS to establish the stereochemistry of the histidine residue at C-1. The relative stereochemistry of the rest of the molecule was established using a combination of a ROESY NMR experiment and molecular modelling. The methanol : dichloromethane sponge extract was subjected to solvent partitioning between aqueous methanol and dichloromethane or ethyl acetate followed by gradient elution on a C₁₈ Sep-Pak[®] cartridge and exhaustive reversed phase HPLC (TFA pH 3) of the dichloromethane / ethyl acetate partition fraction.⁴²

1.2.8 Prianosins

Bioassay guided fractionation of the methanol : toluene extract of a tropical green Okinawan sponge (*Prianos melanos*) yielded the cytotoxic pigment prianosin A (**1.57**).⁴⁹ The structure of **1.57** which was found to be identical to discorhabdin A (**1.57**), isolated from a New Zealand sponge (*Latrunculia brevis*).³⁶ The structure of prianosin A was determined by spectral comparisons of the NMR data of this compound with those of discorhabdin C, while the absolute stereochemistry of **1.57** was defined by X-ray crystallography. The methanol : toluene extract was initially partitioned between toluene and water and the chloroform soluble material from further partitioning of the aqueous phase was subjected to silica gel chromatography followed by LH-20 and further silica gel chromatography to give prianosin A.⁴⁹

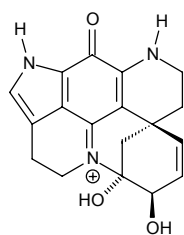
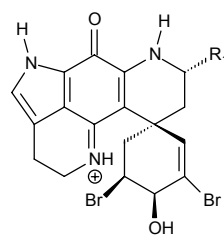
**1.63**

Prianosin B (**1.63**), the 16, 17-dehydro derivative of discorhabdin A, was isolated from a second investigation of *Prianos melanos* by Cheng *et al.*⁵⁰ in a continuing effort to isolate the bioactive compounds of this sponge. Prianosin B was isolated together with prianosins A, C (**1.64**) and D (**1.65**), all of which possess a C-5 to C-8 tetrahydrothiophene bridge. HMBC correlations were essential in establishing the structures of the prianosins (due to the paucity of protons and the abundance of heteroatoms present in the molecule). Bioassay guided fractionation in a manner similar to that described for the isolation of prianosin A was once again employed. The structures of **1.64** and **1.65**, which contain the novel aminophenol moieties, were characterised as their acetate derivatives and were subsequently shown to be artefacts of the acetylation procedure.⁵¹ The structures of **1.64** and **1.65** were thus revised to 2-hydroxy-discorhabdin D (**1.66**) and discorhabdin D (**1.61**), respectively.⁵¹

**1.64** R = OH**1.65** R = H**1.66**

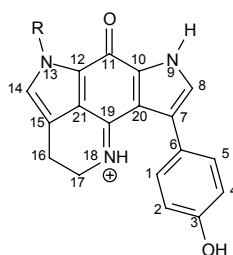
1.2.9 Epinardins

D' Ambrosio *et al.*⁵² isolated epinardins A -D (**1.67** - **1.70**) from two undescribed South Indian ocean sponges. The epinardins are characterised by the presence of a cyclohexanol spiro ring instead of the typical cyclohexanone ring described in previous discorhabdins. The structures of the epinardins were determined using standard one and two dimensional NMR experiments including NOESY experiments. The ethanol sponge extract was subjected to gradient elution reversed phase flash chromatography, followed by further purification by TLC where necessary, to give **1.67** - **1.70**.⁵²

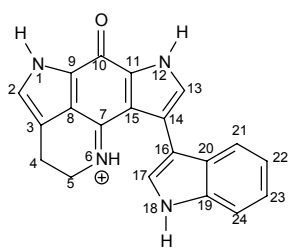
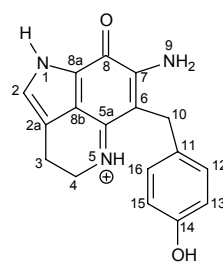
**1.67****1.68** R₁ = H**1.69** R₁ = H, Δ⁷**1.70** R₁ = OCH₃

1.2.10 *Tsitsikammamines, veitamine and wakayin*

Two *bis*-pyrroloiminoquinone alkaloids, *tsitsikammamine* A (**1.71**) and B (**1.72**) were isolated from the South African *Latrunculid* sponge of the new genus *Tsitsikamma* along with 14-bromo-discorhabdin C (**1.51**) and 14-bromo-3-dihydro-discorhabdin C (**1.52**), described previously. The structures of **1.71** and **1.72** were proposed from extensive NMR data.⁴¹

**1.71** R = H**1.72** R = CH₃

A unique, related *bis*-pyrroloiminoquinone alkaloid, *wakayin* (**1.73**), was isolated from a Fijian ascidian of the genus *Clavelina*.⁵³ Pyrroloiminoquinones have only previously been isolated from the phylum Porifera, suggesting that these compounds may be produced by symbiotic micro-organisms. The structure of *wakayin* was obtained by interpretation of DQFCOSY, HMBC and HMQC NMR spectra. *Wakayin* (**1.73**), which has an ostensible structural affinity with the *tsitsikammamines* (**1.71**, **1.72**), requires an additional tryptophan molecule in the biogenesis of this alkaloid.⁵³

**1.73****1.74**

The isolation and characterisation of veitamine (**1.74**) from a Fijian sponge of the genus *Zyzya fuliginosa* was reported by Venables *et al.*⁵⁴ The structure of veitamine, suggestive of the makaluvamines, was the first reported pyrroloiminoquinone with a *para*-hydroxy benzyl substituent at position 6. The structure of **1.74** was established using standard one and two dimensional NMR experiments. Following partition of the methanol extract according to a modified Kupchan procedure, the chloroform and aqueous methanol soluble material were subjected to Sephadex LH-20, and silica gel (using TFA) together with LH-20 chromatography, respectively. A variety of makaluvamines (**1.31** - **1.36**), makaluvone (**1.37**), damirone B (**1.20**) and discorhabdin A (**1.57**) were obtained from the chloroform partition fraction, while the aqueous methanol partition fraction yielded veitamine (**1.74**) and additional quantities of makaluvamines (**1.31**, **1.33** - **1.35**).⁵⁴

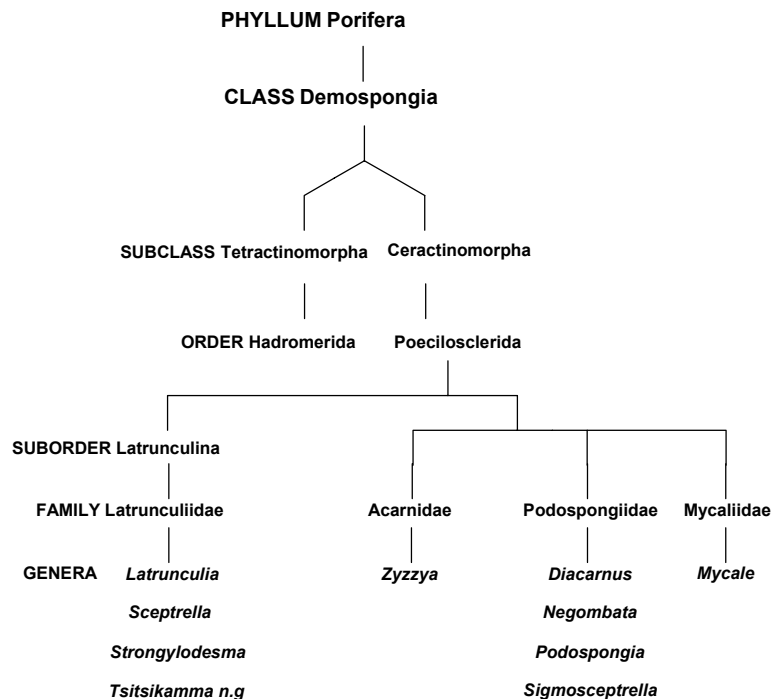
1.3 Taxonomy of the Family Latrunculiidae

Sponges of the family Latrunculiidae are massive, encrusting, hemispherical, spherical or pedunculate with areolate porefields. Kelly and Samaai⁵⁵ have described the texture of these sponges as leathery and is generally “brownish black with forest-green or blue tinges, liquorice brown, as fawn or forest green” in colour as observed with the sponges *Latrunculia*, *Strongyloidesma* and *Tsitsikamma* or pale beige to white as seen with sponges of *Sceptrella* sp..⁵⁵

The sponge distribution is shallow sublittoral to bathybentic, while the geographic distribution is from polar to warm temperate regions. The *Latrunculia* and *Tsitsikamma* sponges are concentrated mainly at a depth of 30 m on a hard, rocky substrate in the temperate regions of the southern hemisphere, while sponges of the genus *Strongyloidesma* are located also on hard, rocky substrates in the warm temperate regions or on dead coral rubble in sandy lagoon environments in the tropical regions of both the southern and northern hemisphere.⁵⁵ Sponges of the genus *Sceptrella* are predominantly deep water (down to a depth of 2460 m) and are located in the northern temperate regions of the Atlantic Ocean.⁵⁵ Sponges of the genus *Tsitsikamma* are exclusively located in sheltered coastal rocky reefs at depth of 25 - 40 m off the southeast coast of South Africa (Chapters 2 and 4).

Taxonomy is crucially important in any marine natural products study. Many marine organisms, producing bioactive metabolites, either remain undescribed, are described only to genus level or are identified incorrectly.⁵⁶ van Soest and Braekman⁵⁷ aptly predicted that taxonomic uncertainties amongst the porifera would ultimately lead to a “babylonian confusion of sponge sources of interesting chemistry”. The sponge family Latrunculiidae (Topsent) first described in 1922 produces the vast majority of pyrroloamino-*ortho*-quinone and pyrroloiminoquinone alkaloids described in the preceding section. Since its inception eight decades ago, generations of sponge taxonomists have juggled this family between two Orders *viz* Poeciloscleridae and Hadromerida.⁵⁵ In an attempt to resolve this taxonomic dilemma Kelly and Samaai⁵⁵ have recently placed the

family Latrunculiidae within a new monophyletic suborder Latrunculina residing in the Order Poecilosclerida (Scheme 1.1).



Scheme 1.1 A recently revised taxonomic relationship between the sponge families Latrunculiidae, Acarnidae, Podospongiidae and Mycalliidae.^{55,58}

Kelly and Samaai's reassignment of the family Latrunculiidae to its own suborder and their taxonomic reasons for confining membership of this family to four genera, *Latrunculia*, *Sceptrella*, *Strongylodesma* and the new South African genus *Tsitsikamma* were, as follows: the presence of similar microrhabd microscleres together with the arrangement of these microscleres in a dense layer in the outer ectosome and areolate porefield and distinctive short fistular oscules (exhalant pores).⁵⁵ Tentative supporting evidence for this taxonomic revision was provided by the presence of related pyrroloiminoquinone chemotaxonomic markers.

A major problem complicating the use of chemotaxonomic markers for sponge classification is their lack of consistency. No marker appears to be ideal, due either to a report of its occurrence outside the group for which it is supposed to be a marker, or because the marked groups partially overlap. To be useful for classification, chemotaxonomic markers should either include or exclude taxonomic groups completely. For example, discorhabdins have been isolated from sponges of the genera *Latrunculia*, *Strongylodesma*, and *Zyzzya*. The genus *Zyzzya* is placed in the family Acarnidae. Although the families Latrunculiidae and Acarnidae possess enough morphological similarities to place them in the same Order they are sufficiently different to warrant splitting into separate families.⁵⁸ Possible reasons for inconsistent distribution of chemical markers may include:

- 1) Parallel biosynthetic pathways. Secondary metabolites are generated from primary metabolic precursors and parallel evolution of biosynthetic pathways may allow for the biosynthesis of structurally related compounds.
- 2) Microsymbiotic involvement. Although the evidence for the involvement of microsymbionts is largely circumstantial, several studies have established that compounds suspected to be of microsymbiont origin were indeed produced by bacteria and fungi isolated from sponges.¹¹ Perry *et al.*³⁶ have suggested that microsymbionts may be involved in the production of the pyrroloiminoquinone alkaloids, though this has been shown to be unlikely by Munro *et al.*⁵⁹
- 3) Collection of sponge specimens. Field collections of sponges do not always follow a set protocol. Overgrowing algae and the epizootic invertebrates are often not removed from specimens and may be sources for compounds reported to be produced by the sponge. Mix-ups involving labelling and or sorting of samples can result in much confusion.⁶⁰
- 4) Some sponge groups are extremely difficult to identify to family or genus level and considerable taxonomic expertise is needed.

Currently the degree of chemical marker inconsistency is such that direct use of chemical data to solve classification problems, or to erect new higher taxa, is tenuous. Large scale re-examination of voucher specimens, in collaboration with microbiologists and organic chemists, are necessary to demonstrate whether or not chemical marker compounds are true indicators of sponge systematics. Therefore in an attempt to establish the validity of using pyrroloamino-*ortho*-quinone and pyrroloiminoquinone metabolites as chemotaxonomic markers for the families Latrunculiidae and Acarnidae, Samaai⁵⁸ has re-examined the taxonomy of many of the sponge voucher specimens used in the original natural products investigations described in Section 1.2. This is an important clarification of our knowledge of the distribution of pyrroloamino-*ortho*-quinone and pyrroloiminoquinone metabolites across the two families and the results of Samaai's⁵⁸ investigation is summarised in Table 1.1.

General trends evident from Table 1.1 are as follows. The simplest of the pyrroloquinoline alkaloids, the batzellines A-C, isobatzellines A-D and secobatzellines A and B were isolated from a deep water Caribbean sponge of the genus *Batzella* (renamed *Strongylodesma* n.sp1-2). The related damirones A-B from Palau, the makaluvamines A-G from Fiji and Indonesia, and makaluvamines H-M and damirone C from Pohnpei, have been isolated from sponges taxonomically assigned to the genus *Zyzya* (Acarnidae). The related complex alkaloids, exemplified by discorhabdin C were originally reported from sponges of the genus *Latrunculia*. Interestingly, a recent comprehensive study of *Latrunculia brevis* collected from around the coast of New Zealand revealed that the two colour morphs of this sponge contained different profiles of discorhabdin metabolites (discorhabdin B and C predominate in brown and green *L. brevis* sponges respectively).⁵⁶ Since then, the isolation of discorhabdins A-P and R from South Pacific sponges of the genera *Latrunculia* and *Negombata*, the South African *Tsitsikamma* and *Strongylodesma* sp. and the Japanese sponge of the genus *Prianos* (renamed *Strongylodesma*

sp.) indicated the ubiquitous occurrence of these metabolites. Epinardins were isolated from a deep water undescribed spinach-green sponge (~200 m) and the authors therefore surmised that the discorhabdins and epinardins could not be of cyanobacterial origin since a sponge emerging from the dark at a depth of 200 m in pre-Antarctic waters could be assumed to be free of cyanobacterial symbionts. Significantly, the isolation of discorhabdin A from *Zyzzya fuliginosa*, discorhabdin P from a *Batzella* sp. (reassigned to the genus *Zyzzya*) and discorhabdin Q from sponges of the genera *Zyzzya* sp., *Zyzzya massalis* and *Zyzzya fuliginosa* precludes the use of discorhabdins as a Latrunculiidae specific chemotaxonomic marker.

The new genus *Tsitsikamma* (see Chapters 2 and 4) also produces discorhabdin type compounds. The internal morphology (in terms of choanosomal skeletal arrangement) of *Tsitsikamma* sponges has been taxonomically interpreted as being a mixture of both the internal morphology of *Zyzzya* and *Latrunculia* sponges.⁴¹

The discovery of the unusual *bis*-pyrroloiminoquinones, tsitsikammamines A and B, in the *T. favus* extract was initially thought to have major chemotaxonomic significance, due to the intermediacy of the tsitsikammamine structures between those of the makaluvamines and discorhabdins. However, the absence of the tsitsikammamines in the *T. pedunculata* extracts (see Chapter 2) together with the obvious structural similarities between the tsitsikammamines and wakayin (**1.73** previously isolated from an ascidian) tentatively suggests the intriguing possibility of a symbiotic source for these compounds.

A notable omission from Table 1.1 is the absence of any reports describing the discovery of pyrroloiminoquinone metabolites or any other metabolites in the genus *Sceptrella*.⁶¹ A possible reason for this absence may be that the extreme depths at which *Sceptrella* occurs (ca. 2 kms) making this sponge inaccessible to the majority of marine natural product chemists.

While sponges in the families Latrunculiidae and Acarnidae are linked by their common pyrroloiminoquinone metabolites these two families are clearly chemically distinct from the Podospongiidae and Mycalliidae. The macrocyclic compound latrunculin A (**1.75**)⁶² and cyclic peroxides (**1.76**)⁶³ are characteristic of the types of compound found in the latter two families.

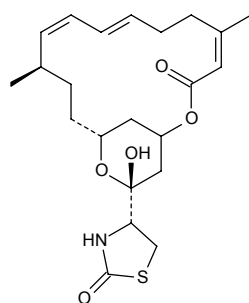
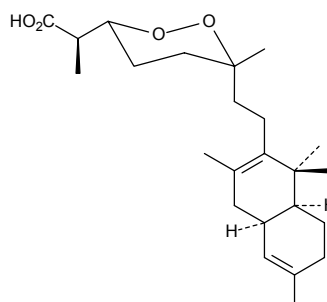
**1.75****1.76**

Table 1.1 Revision of the taxonomic assignments and phyletic distribution of the metabolites in the sponge families Latrunculiidae and Acarnidae.

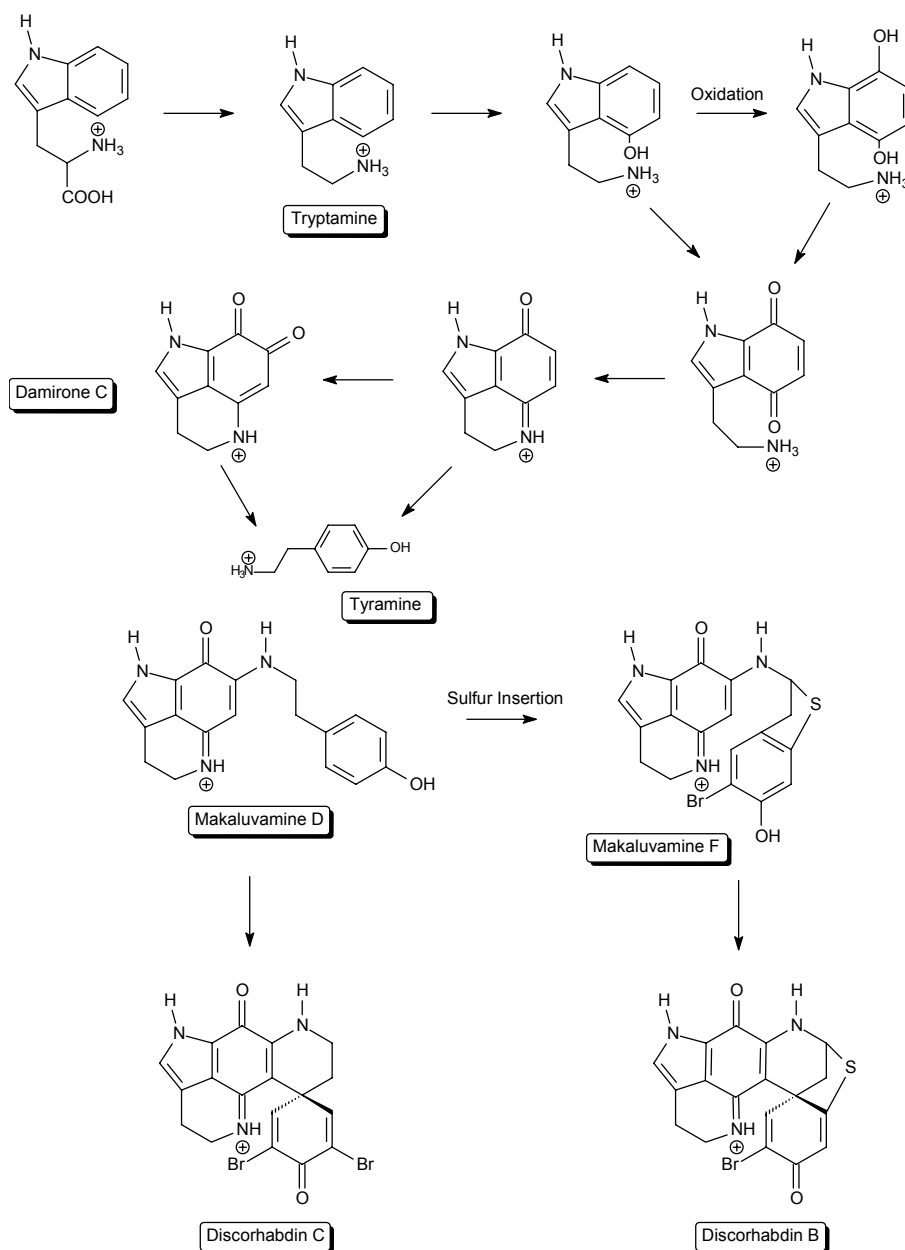
Compounds	Sponge ID (original)	Sponge ID (reassigned) ^{26,55,58}	Locality	Co-occurring Compounds	Ref.
<i>Damirones</i>					
1.19	<i>Damiria</i> sp. Keller	<i>Zyzzya fuliginosa</i>	-20 m, Ngemelis drop off, Palau Makaluva Island and Mbengga harbour, Fiji Islands	-	25
1.20	<i>Damiria</i> sp. Keller	<i>Zyzzya fuliginosa</i>	- 20m, Ngemelis drop off, Palau Makaluva Island and Mbengga harbour, Fiji Islands	-	25 30
1.21	<i>Zyzzya fuliginosa</i>	-	-13 m, Nahpali Island, Pohnpei, Micronesia	1.33, 1.34, 1.38, 1.39 - 1.44	26
<i>Batzellines</i>					
1.22 - 1.24	<i>Batzella</i> sp.	<i>Strongyloidesma</i> n.sp1	-120 m, Freeport and West End, Grand Bahama Islands	-	27
<i>Iso-batzellines</i>					
1.25 - 1.27	<i>Batzella</i> sp.	<i>Strongyloidesma</i> n.sp1	-120 m, Freeport and West End, Grand Bahama Islands	-	28
		<i>Strongyloidesma</i> n.sp2	-141 m, Great Bahama Bank, Bahamas		28
1.28	<i>Batzella</i> sp.	<i>Strongyloidesma</i> n.sp1	-120 m, Freeport and West End, Grand Bahama Islands	-	28
<i>Seco-batzellines</i>					
1.29 - 1.30	<i>Batzella</i> sp.	<i>Strongyloidesma</i> sp.	-152 m , Great Bahama Bank, Bahamas and -138 m, North Bimini, Bahamas	- 1.50	29
<i>Makaluvamines</i>					
1.31 - 1.36	<i>Zyzzya marsailis</i>	<i>Zyzzya fuliginosa</i>	Makaluva Island and Mbengga harbour, Fiji Islands	1.20, 1.57	30
<i>Makaluvone</i>					
1.37	<i>Zyzzya marsailis</i>	<i>Zyzzya fuliginosa</i>	Makaluva Island and Mbengga harbour, Fiji Islands	1.20, 1.31 - 1.36, 1.57	30
1.38	Undescribed <i>Histodermella</i>	<i>Zyzzya fuliginosa</i>	7 – 40 m, Manado Bay, Sulawesi, Indonesia	1.31, 1.33, 1.19, 1.20	31
1.39 - 1.44	<i>Zyzzya fuliginosa</i>	-	-13 m, Nahpali Island, Pohnpei, Micronesia	1.33, 1.34, 1.38	26
1.45	<i>Zyzzya fuliginosa</i>	-	Cape S. Idefonso, The Philippines	1.31, 1.33 - 1.35, 1.40	32
1.46	<i>Zyzzya fuliginosa</i>	-	Vanuatu Islands	1.38, 1.41 - 1.43	33
<i>Makaluvic Acids</i>					
1.47, 1.48	<i>Zyzzya fuliginosus</i> (Carter)		Chuuk State -20 m, Federated states of Micronesia	1.31, 1.35, 1.42 , 3,7-dimethyl- isoguanine, 4-hydroxybenzoic acid.	34
<i>Discorhabdins</i>					
1.49	<i>Latrunculia du Bocage</i>	<i>Latrunculia</i> spp.	New Zealand	-	35

Compounds	Sponge ID (original)	Sponge ID (reassigned) ^{31,54,57}	Locality	Co-occurring Compounds	Ref.
1.50	<i>Batzella</i> sp.	<i>Zyzzya</i> sp.	-141 m, Great Bahama Bank, Bahamas	-	40
1.51	<i>Tsitsikamma</i> n.g	<i>Tsitsikamma favus</i>	Tsitsikamma Marine Reserve, South Africa	1.52, 1.71, 1.72	41
1.52	<i>Tsitsikamma</i> n.g	<i>Tsitsikamma favus</i>	Tsitsikamma Marine Reserve, South Africa	1.51, 1.71, 1.72	41
1.53	<i>Strongyloidesma</i> sp.	<i>Strongyloidesma coetzei</i>	-15 m, Port Elizabeth, South Africa	1.57, 1.61, 1.62	42
1.54	<i>Latrunculia</i> du Bocage	<i>Latrunculia</i> spp.	New Zealand	1.61	43
1.55	<i>Latrunculia apicalis</i> (Ridley and Dendy)	<i>Latrunculia biformis</i>	-6 to -40 m, Hut Point, Danger Slopes, and Cape Evans on Ross Island, Antarctica	1.49	45
1.57	<i>L. brevis</i> (Ridley & Dendy)	-	- 110 to -145 m, Otago Peninsula	1.49, 1.58	36
1.57	<i>Prianos Melanos</i> , <i>Prianos</i>	<i>Strongyloidesma</i> sp.	2-3 m, Motobu Peninsula Okinawa Is.	-	49
1.58	Undescribed <i>Latrunculia</i>	<i>Latrunculia</i> spp.	-25 m, Kaikoura Peninsula	1.49, 1.57	36
1.59	<i>Zyzzya</i> sp.	-	Assail Bank, North Island & Wallab group, Australia		46
	<i>Zyzzya massalis</i>	<i>Zyzzya fuliginosa</i>	Sphinx Head Wessel Island, Australia		
	<i>Zyzzya fuliginosa</i>	-	Bega Lagoon Fiji		
	<i>Latrunculia purpurea</i>	-	Horseshoe Reef Australia		
1.60	<i>Negombata</i> sp.*	-	Port Campbell, Victoria, Australia	1.58	47
	<i>Latrunculia</i>	-	Prydz channel, Prydz Bay, Antarctica		
1.61	<i>Latrunculia brevis</i> ⁴⁸	-	-30 m Sugar Loaf Islands, New Zealand	1.57	48
1.62	<i>Strongyloidesma</i> sp.,	<i>Strongyloidesma coetzei</i>	-15 m, Port Elizabeth, South Africa	1.57, 1.61	42
	Undescribed Latrunculid	<i>Latrunculia lūnaviridis</i>	-17 - 20 m, Cape Town, South Africa	1.57	42
	Undescribed Latrunculid	<i>Latrunculia gibbonsi</i>	-28 m, Tsitsikamma Marine Reserve, South Africa		
1.63 – 1.66	<i>Prianos melanos</i>	<i>Strongyloidesma</i> sp.	-2-3 m, Okinawa Island, Motobu Peninsula	1.57	51
<i>Epinardins</i>					
1.67-1.70	Undescribed sponge		-200 m, Apotres, Iles Crozet, South Indian Ocean	-	52
<i>Tsitsikammamines</i> / <i>wakayin</i> / <i>veiutamine</i>					
1.71, 1.72	<i>Tsitsikamma</i> n.g	<i>Tsitsikamma favus</i>	-20 m, Tsitsikamma Marine Reserve, South Africa	1.51, 1.52	41
1.73	<i>Clavelina</i> sp. (ascidian)	-	Fiji	-	53
1.74	<i>Zyzzya Fuliginosa</i>		Fiji Islands	1.20, 1.31 - 1.37, 1.57	54

* The voucher of this species was not taxonomically re-examined.

1.4 Biosynthesis of pyrroloamino-*ortho*-quinone and pyrroloiminoquinone alkaloids

Biosynthetic studies of metabolites from marine sponges is complicated by slow sponge growth rates, low incorporation rates as well as the presence of symbiotic micro-organisms. The makaluvamines (such as makaluvamines D (**1.34**) and F (**1.36**)) and the discorhabdins are structurally related, which prompted Munro *et al.*⁵⁹ to propose a biosynthetic pathway linking these compounds (Scheme 1.2).

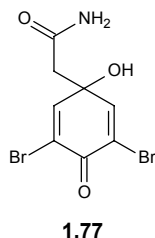


Scheme 1.2 Biogenesis of the discorhabdins as postulated by Munro *et al.*⁵⁹

The co-occurrence of discorhabdin A with makaluvamines A - F (**1.31** - **1.36**), damirone B (**1.20**) and makaluvone (**1.37**) in the sponge of the genus *Zyzya marsailis* (reassigned *massalis*²⁶),

together with the co-occurrence of makaluvamines D (**1.34**) and F (**1.36**) with makaluvamine G (**1.38**) from *Latrunculia apicalis*, provided compelling support for Munro's proposed biosynthetic pathway. The amino acids tryptamine and phenylalanine are considered to be the precursors of the discorhabdin skeleton. Functionalisation and oxidation of tryptamine forms the backbone of the pyrroloiminoquinone core of the makaluvamines, damirones and discorhabdin skeletons. The incorporation of a tyramine residue in damirone C (**1.21**) would lead to makaluvamine D (**1.34**) and further cyclisation and elaboration would lead to the more complex discorhabdins. Some uncertainty exists as to how the hypothetical biosynthetic pathway proceeds. Munro *et al.*⁵⁹ investigated the production of discorhabdin metabolites *in vivo* by examining preparations of the marine sponge *Latrunculia* sp. B, where sponge tissue slices had been incubated with {U – ¹⁴C}-L-phenylalanine. Results indicated that ¹⁴C from the {U – ¹⁴C}-L-phenylalanine was incorporated into discorhabdin B (**1.58**). Tissue slices of *Latrunculia* sp. B were presoaked in a broad spectrum antibiotic mixture before the addition of {U – ¹⁴C}-L-phenylalanine to determine whether discorhabdin B was produced by sponge cells or symbiotic micro-organisms. The unchanged ¹⁴C incorporation from {U – ¹⁴C}-L-phenylalanine into discorhabdin B indicated that discorhabdin B biosynthesis is a function of sponge cells. L-phenylalanine (the decarboxylated analogue of tyrosine the precursor of tyramine) was thus also established as a possible precursor of the discorhabdin skeleton.⁵⁹

The 2,6-dibromocyclohexadienone portion of discorhabdin C (**1.49**) is duplicated in compound **1.77**, which was isolated from the sponge *Aplysina fistularis* (Family Aplysinidae, order Verongida).^{64,65} The compound, a product of tyrosine metabolism, has both cytotoxic and antimicrobial properties. Discorhabdins have been suggested to play defensive roles in sponges, and sponges that contain antimicrobial metabolites are rarely observed to be overgrown, and no evidence of predation or of epibionts have been associated with Latrunculid sponges.³⁶ Previous workers have suggested that batzellines²⁷ and this sponge metabolite (**1.77**) may be the biosynthetic precursors of discorhabdins. In turn, the secobatzellines A (**1.29**) and B (**1.30**) are thought to be probable precursors of the simpler pyrroloiminoquinone alkaloids.²⁹



Interestingly, makaluvamine A (**1.31**) has also been isolated from a terrestrial myxomycete, *Didymium bahiense*.⁶⁶ Authors also showed previously that a cultured myxomycete *D. squamulosum* produced clionasterol,⁶⁷ which was previously isolated from marine sponges such as *Cliona celata* and *Hymeniacion perleve*⁶⁸ and marine microalgae such as *Nitella flexilis* and *Chara vulgaris*.⁶⁹

The batzellines, isobatzellines or makaluvamines are thought to give rise to the makaluvic acids (**1.47**, **1.48**) through standard biosynthetic oxidation processes. Interestingly, 4-hydroxybenzoic acid, which is an oxidation product of the tyramine-derived portion of makaluvamine E and K, was found to co-occur in the sponge of the genus *Zyzzya fuliginosus* (Carter).³⁴

1.5 Biological activity of pyrroloamino-ortho-quinone, pyrroloiminoquinone and bis-pyrroloiminoquinone alkaloids

Pyrroloiminoquinone compounds, such as the discorhabdins and isobatzellines, display potent *in vitro* toxicity to the P-388 murine leukaemia cell line, while no such activity is reported for compounds which lack the iminoquinone moiety, such as the batzellines or damirones. The pyrroloiminoquinone moiety may therefore be responsible for the cytotoxicity generally observed in Latrunculid sponge metabolites.^{30,70} Isobatzellines (**1.25** - **1.28**) were also found to exhibit moderate antifungal activity against *Candida albicans*. It is interesting to note that it is the isobatzellines, and not the batzellines, that are moderately antifungal.²⁸ Secobatzellines were found to inhibit calcineurin (CaN) and secobatzelline A (**1.29**) shows some inhibition towards the peptidase activity of CPP32 (IC₅₀ 0.02 µg/mL).²⁹

CaN or Calcineurin – threonine protein phosphatase is involved in signal transduction and is recognised as one of the principal signalling molecules that regulates the immune response. Caspase *e.g.* CPP32, involves a group of at least ten cysteine proteases which play a major role in apoptosis. Inhibitors of caspase-3 (CPP32) have been shown to prevent apoptotic mediated cell death in cell lines and various tissues. CPP32 has also been shown to be involved in the stimulation of IL-8 secretion of synviocytes in rheumatoid arthritis, which serves to increase joint inflammation and the progress of the disease.^{29,40}

Makaluvamines D (**1.34**), G (**1.38**), H (**1.39**) and J-M (**1.41** - **1.44**) were shown to be inactive against topoisomerase in an assay that employed three genetically engineered yeast strains. One of the strains was insensitive to DNA damaging agents, another strain was hypersensitive to these agents and possessed a deleted DNA repair gene, while the third strain had neither topoisomerase I nor a DNA repair gene.²⁶ Makaluvamines were, however, found to be cytotoxic against HCT-116 *in vitro*. In a semi quantitative assay, makaluvamines I (**1.40**) and L (**1.43**) were an order of magnitude more active than makaluvamines C (**1.33**), G, H and K (**1.42**), while makaluvamines D and M were found to be the least active.²⁶

Makaluvamine G (**1.38**) was only moderately cytotoxic toward several cell lines and displayed no antifungal activity against *Aspergillus oryzae*, *C. albicans*, *Penicillium notatum*, *Saccharomyces cerevisiae* or antiviral activity to *Herpes simplex* 1 and 2 and polio viruses. However, moderate inhibition of RNA (IC₅₀ = 15 µM), DNA (15 µM) and protein (21 µM) synthesis was shown. In contrast to makaluvamines A (**1.31**), C, E (**1.35**), F (**1.36**), makaluvamine G showed no significant

inhibition of topoisomerase II and only moderate inhibition of topoisomerase I.³¹ Makaluvamine N (**1.45**) exhibited a greater than 90 % inhibition of topoisomerase II unwinding of pBR322 at concentrations of 5 µg/mL.³²

Antioxidant activity was displayed by makaluvamine P (**1.46**) in the two different spectrophotometric analyses used. Makaluvamine P showed high inhibition of xanthine oxidase ($IC_{50} = i.e. 16.5 \mu M$), an important biological source of superoxide radicals involved in oxidative stress in an organism. In the ABTS radical cation decolouration assay makaluvamine P showed moderate activity (TEAC = 0.341), where the standard employed is Trolox and the results are quoted as Trolox equivalent antioxidant activity (TEAC).³³

Discorhabdins C (**1.49**), A (**1.57**) and B (**1.58**) were found by Perry *et al.*³⁶ to be highly active in *in vitro* P-388 assays, with respective ED_{50} values of 0.03, 0.05 and 0.1 µg/mL. However, *in vivo* testing in the P-388 leukaemia system in mice showed no increase in lifespan with either discorhabdins C or A, where they were found to be toxic to mice at about 2 mg per kg of body weight. Discorhabdin B did show some antitumour effect with a T/C of 117 % at a dose of 0.25 mg/kg, without achieving the significance level of 120 %. In addition, the discorhabdins were shown to possess antimicrobial activity. In a disk assay, with 30 µg/disk, discorhabdins C and A were active against *Escherichia coli*, *B. subtilis* and *C. albicans*, but not against *Pseudomonas aeruginosa*. Discorhabdin B was active against *E. coli* and *B. subtilis*, but not against *P. aeruginosa* or *C. albicans*.³⁶ Discorhabdins A, B and C are powerful cytotoxins in the *in vitro* P-388 cell line but in the *in vivo* P-388 model these compounds were found to be inactive (T/C <120 %). Discorhabdin D (**1.61**), on the other hand, had a more potent *in vivo* activity (T/C 132 % at 20 mg/kg). Structural modification studies to ascertain the mode of action were underway to establish the site of biological activity for this compound, but fourteen years later no results have been reported.³⁶

Discorhabdin C (**1.49**) was found to be toxic toward L1210 tumour cells at very low levels ($ED_{50} < 100 \text{ ng/mL}$),³⁵ while the *in vitro* IC_{50} cytotoxic activity of discorhabdin A was 37 and 14 ng/mL against L1210 and L5178Y murine leukaemia cells respectively.³⁶ Discorhabdin A also induced Ca^{2+} release from sarcoplasmic reticulum and was found to be ten times more potent than caffeine in this assay.⁴⁹ Similarly, prianosin D (**1.61**) also induced Ca^{2+} release from sarcoplasmic reticulum, at the same potency as discorhabdin A. Interestingly, prianosins B (**1.63**) and C (**1.66**) showed no activity in this assay.⁵⁰

Discorhabdins G (**1.56**) and C (**1.49**) showed similar activities against both Gram-positive and Gram-negative bacteria. In addition, discorhabdin G was shown to occupy a central position in the chemical ecology of *Latrunculia apicalis* by causing feeding deterrence behaviour in the major Antarctic sponge predator *Perknaster fuscus* as well as inhibiting in the growth of two common water column microorganisms isolated from the surrounding water.⁴⁵

Discorhabdin P (**1.50**) inhibited CaN and CPP32 with IC₅₀ values of 0.55 and 0.37 µg/mL, respectively. Positive controls for calcineurin and CPP32 assays consisted of the addition of both substrate and enzyme in the absence of test compounds. These levels of inhibition are highly significant as there are presently only a handful of compounds in the literature that demonstrate nM potency for inhibition of either calcineurin or CPP32 and calcineurin enzyme activity. Interestingly, the parent compound discorhabdin C indicated no activity against CPP32 and calcineurin enzymes at the highest dose of 5.0 µg/mL.⁴⁰

In the NCI 60 cell line antitumour screen, discorhabdin Q (**1.59**) exhibited moderate, generalised cytotoxicity (mean panel GI₅₀ = 0.5 µg/mL), but no real differential cytotoxicity profile. The authors proposed that full aromatisation of the pyrroloiminoquinone system confers reduced cytotoxicity relative to the Δ^{16} saturated members of the family, but this remains to be confirmed.⁴⁶

Ethanol extracts of the Antarctic *Latrunculia* sp. and the southern Australian *Negombata* sp. demonstrated antibacterial activity against Gram positive (*Staphylococcus aureus*, *Micrococcus luteus*) and Gram negative (*Serratia marcescens*, *E. coli*) bacteria. Discorhabdins R (**1.60**) and B were found to be the antibacterial agents in the sponge extract.⁴⁷

Tsitsikammamines A (**1.71**) and B (**1.72**), together with 14-bromo-3-dihydro-discorhabdin C (**1.52**) and 14-bromo-discorhabdin C (**1.51**) exhibited antibacterial activity against *B. subtilis*.⁴¹ Initial studies indicated that the tsitsikammamines showed topoisomerase II inhibition comparable to that of wakayin (**1.73**). Wakayin was found to have a diverse array of bioactivities including murine cell line cytotoxicities, antifungal activity and topoisomerase II inhibition.⁵³

Epinardins A (**1.67**) and C (**1.69**) were assayed against L1210 and doxorubicin-resistant L1210/DX murine lymphocytic leukaemia cells *in vitro*.⁵² Epinardin C proved to be clearly active, though with a poor resistant index. Since the dienone parent compound discorhabdin C was more cytotoxic than the corresponding dienol form by one order of magnitude, the authors unsuccessfully attempted the selective C-3 oxidation of epinardin C with a variety of reagents. The biological assays indicated that the raw extract showed antibacterial activity against the Gram-negative wall-defective bacteria *E. coli* and *Proteus vulgaris* as well as the Gram-positive bacteria *Xanthomonas vesicatoria* and *Sarcina lutea*. The extract also demonstrated some antifungal activity against the human epidermal pathogen *Trichophyton mentagrophytes* and the rice pathogen *Piricularia oryzae*. The assays were, however, not carried out on the pure compounds. The epinardins were instead assayed for *in vitro* cytotoxicity against both the L1210 murine lymphocytic leukaemia cell lines and on the subline resistant to doxorubicin (L1210/Dx). The results were compared with those of doxorubicin itself. The IC₅₀ values obtained for epinardins A and C were 6.8 µg/mL and 0.358 µg/mL, while doxorubicin was active at 0.711 µg/mL for the L1210/Dx cell line and 0.0297 µg/mL for the L1210 cell line.⁵²

Wakayin (**1.73**) was shown by the authors to inhibit the topoisomerase II enzyme at 250 μM as well as a 3-fold differential toxicity toward the CHO cell line EM9 (a strain which is sensitive to DNA-damaging genotoxic agents) versus BR1 (resistant to BCNU), suggesting that wakayin exhibits its cytotoxicity by interfering with or damaging DNA. Wakayin also showed some antimicrobial activity against *B. subtilis* ($\text{MIC} \approx 0.3 \mu\text{g/mL}$).⁵³

Veiutamine (**1.74**) was found to be a potent *in vitro* cytotoxin. In a 25 cell line panel it exhibited a mean IC_{50} of 0.12 $\mu\text{g/mL}$ with some selectivity against solid leukaemia tumours. Veiutamine was also shown to be 7 times more active than makaluvamine D (**1.34**, IC_{50} 2.0 $\mu\text{g/mL}$) against the human colon tumour cell line HCT-116.⁵⁴ The bioactivities of the pyrroloamino-*ortho*-quinone, pyrroloiminoquinone and *bis*-pyrroloiminoquinone alkaloids are summarised in Table 1.2.

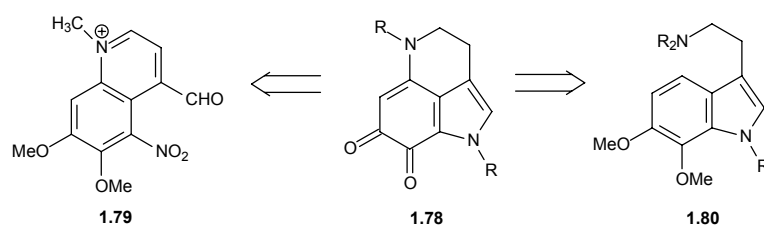
Table 1.2 Summary of the biological activities reported for the pyrroloiminoquinones.

Compound	HCT-116	L1210	L5178Y	KB	P-388	A-549	HT-29	MCF-7	Topo I	Topo II	CaN	xrs - 6	Decat inhib ⁿ	Red. Cleav.	DNA K _s	Ref.
1.20	> 50											> 50 μ M	>500 μ M	>1000 μ M	1.07 mM	30
1.29					0.06	0.04					0.55					29
1.30					1.22	2.86					2.21					29
1.31	1.3 μ M											0.41 μ M	41 μ M	2.1 μ M	0.022 mM	30
1.32	> 50											13.49 μ M	> 500 μ M	181 μ M	0.070 mM	30
1.33	36.2 μ M											5.4 μ M	420 μ M	1.2 μ M	0.013 mM	30
1.34	17.1 μ M											14.0 μ M	320 μ M	52 μ M	0.024 mM	30
1.35	1.2 μ M											1.12 μ M	310 μ M ³⁰	15 μ M ³⁰	0.0046 mM	30
1.36	0.17 μ M											0.08 μ M	25 μ M	1.1 μ M	0.021 mM	30
1.37	> 50											> 50 μ M	>500 μ M	>1000 μ M	1.16 mM	30
1.38	-			0.35	0.50	0.50	0.50	0.50	3.0 μ M							31
1.45	0.6 ⁱ															32
1.46	3.2															33
1.49		< 0.1*			0.03*											36
1.50					0.025	0.41					0.55					40
1.57	0.08	0.037	0.014		0.05*							0.02	>500 μ M	33 μ M	0.085 mM	30, 36, 49
1.58					0.1*											36
1.61		0.18	0.048	0.46	6.0											48, 50
1.63		2.0	1.8	>5.0												50
1.66		0.15	0.024	0.57												50
1.67		1.7														52
1.69		0.324														52
1.73	0.5									250 μ M						53, 91
1.74	0.3															54

Values are all IC ₅₀ (µg/mL), except where indicated.	KB	human oral epidermoid carcinoma
No values for 1.19 and 1.20	P-388	murine leukaemia
# value is for 64% inhibition of cell growth.	A-549	human non-small cell lung cancer
[†] LC ₅₀ value	HT-29	human colon cancer
*ED ₅₀ values	MCF-7	human breast cancer
K _s Measure of DNA intercalation (1.57 considered to be a poor intercalator)	Topo	topoisomerase I and or II
CaN calcineurin - threonine protein phosphates involved in signal transduction	CPP32	Caspase, cysteine proteases which play a major role in apoptosis.

1.6 Synthesis

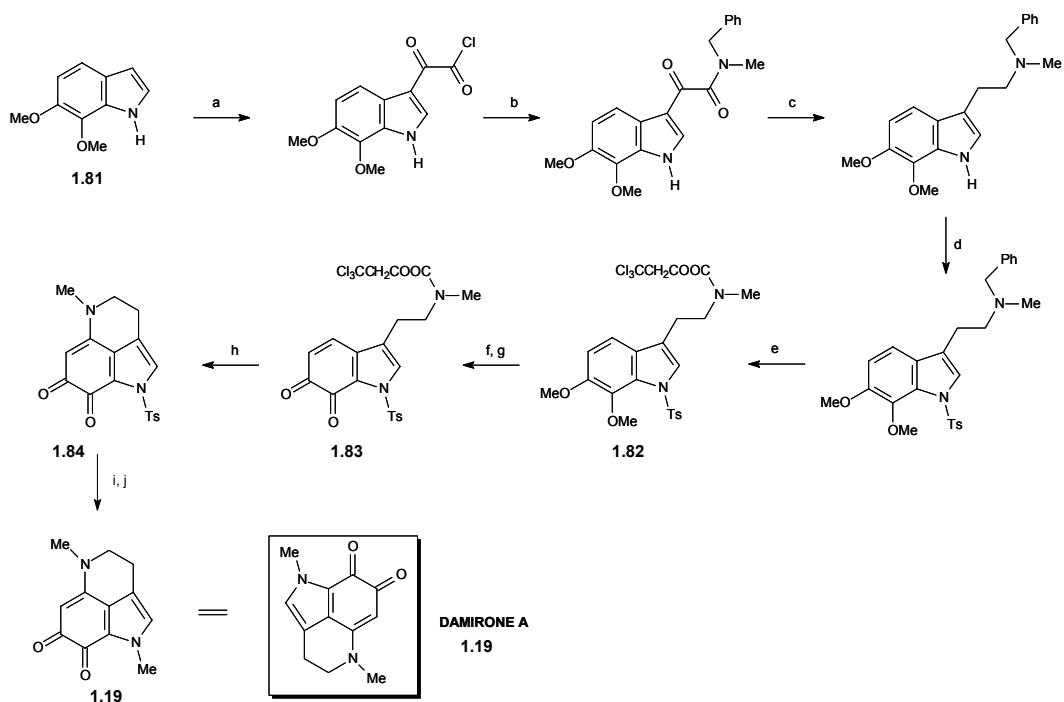
Numerous total syntheses have been reported of pyrroloamino-*ortho*-quinone and pyrroloiminoquinone metabolites. A key synthetic intermediate in the majority of the published syntheses is the tricyclic pyrroloamino-*ortho*-quinone heterocycle (**1.78**). The synthesis of this key intermediate has been generally tackled from two directions, from either a suitably substituted quinoline (e.g. **1.79**) or an indole (e.g. **1.80**).



In the following Section selected syntheses of damirones, batzellines, isobatzellines, makaluvamines and discorhabdins are presented. These syntheses incorporate the key intermediate **1.78** and illustrate the dual approach to its construction.

1.6.1 Damirones

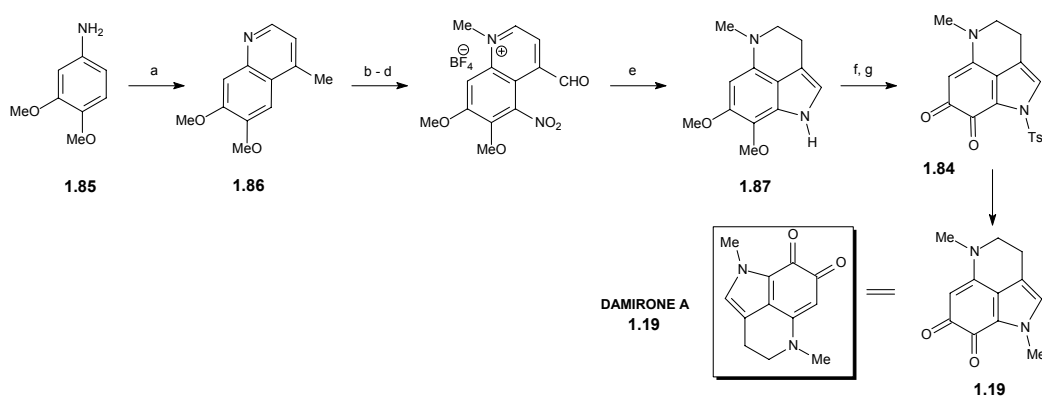
The structures of damirone B (**1.20**) and its congener, damirone A (**1.19**), were confirmed by synthesis from 6,7-dimethoxyindole (**1.81**) via a tryptamine derivative (**1.82**), obtained by the conventional route illustrated in Scheme 1.3. De-O-methylation of **1.82**, followed by oxidation yielded **1.83**. Following deprotection of the side chain nitrogen, **1.83** was cyclised to give the desired pyrroloamino-*ortho*-quinone core skeleton (**1.84**). Removal of the tosyl protecting group and subsequent methylation led to damirone A.⁷¹



Scheme 1.3 Synthetic approach to damirone A and B.⁷¹

a) $(\text{COCl})_2$, Et_2O , $0\text{ }^\circ\text{C}$, 1 hr, 94 %; b) $\text{PhCH}_2\text{NHCH}_3$, H_2O , $25\text{ }^\circ\text{C}$, 3 hr, 96 %; c) LiAlH_4 , $\text{THF} + \text{Et}_2\text{O}$, reflux, 4 hr, 96 %; d) TsCl , NaOH , CH_2Cl_2 , CTAB , $25\text{ }^\circ\text{C}$, 12 hr, 90 %; e) $\text{Cl}_3\text{CCH}_2\text{COOC}$, MeCN , $0\text{ }^\circ\text{C}$, 30 min, 76 %; f) BBr_3 , CH_2Cl_2 , 0 to $25\text{ }^\circ\text{C}$, 12 hr, 90 %; g) CAN , CH_3CN , $0\text{ }^\circ\text{C}$, 10 min, 86 %; h) dithienyl ditelluride, THF , NaBH_4 , H_2O , NaOH , $67\text{ }^\circ\text{C}$, 6 hr, 36 %; i) 10 % NaOH , MeOH , $25\text{ }^\circ\text{C}$, 30 min, 76 %; j) K_2CO_3 , MeI , MeOH , $25\text{ }^\circ\text{C}$, 86 %.⁷¹

The key synthetic precursor (**1.87**, Scheme 1.4) of damirone A and B was also synthesised *via* a quinoline intermediate (**1.86**) by Joule *et al.*⁷² from 3,4-dimethoxyaniline (**1.85**). The exposure of **1.86** to trimethyloxonium tetrafluoroborate ($\text{Me}_3\text{O}^+\text{F}_4\text{B}^-$) followed by reduction produced the indole **1.87**. Chemical transformations involving protection of the indole nitrogen of **1.87** followed by oxidation gave **1.84**.⁷²

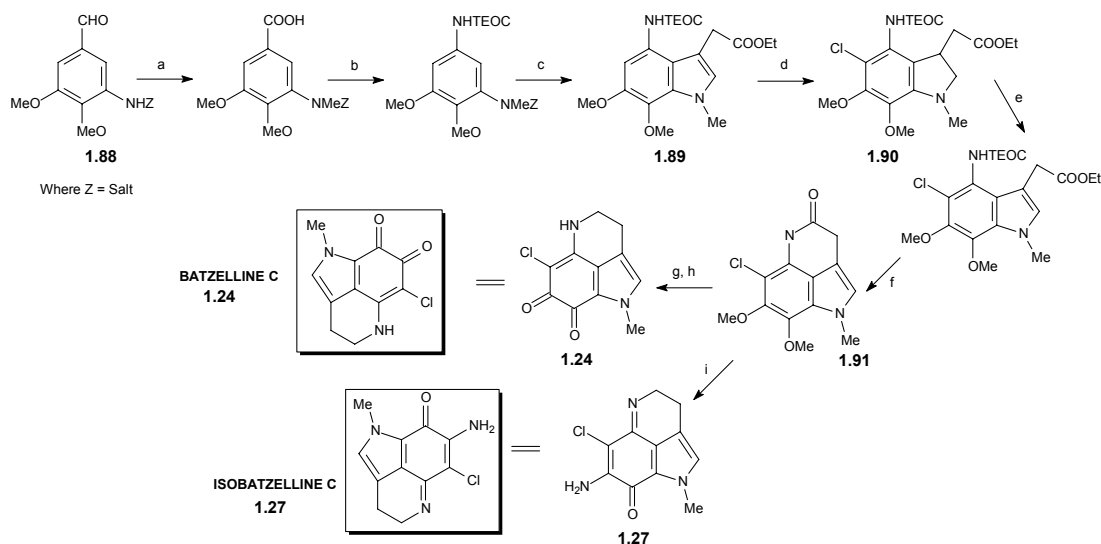


Scheme 1.4 An alternative synthesis of **1.19** from 3,4-dimethoxyaniline.⁷²

a) $\text{CH}_2=\text{CHCO.Me}$, FeCl_3 , AcOH , reflux, 66 %; b) HNO_3 , -50 to $-40\text{ }^\circ\text{C}$, 64 %; c) I_2 , $t\text{-BuI}$, FeCl_2 , TFA , DMSO , $80\text{ }^\circ\text{C}$, 73 %; d) $\text{Me}_3\text{O}^+\text{F}_4\text{B}^-$, $20\text{ }^\circ\text{C}$; e) NaBH_4 , $\text{NiCl}_2 \cdot 6\text{H}_2\text{O}$, MeOH , $20\text{ }^\circ\text{C}$; f) TsCl , NaOH , CH_2Cl_2 , $\text{Bu}_4\text{N}^+\text{HSO}_4^-$, $20\text{ }^\circ\text{C}$, 14 %; g) BBr_3 , CH_2Cl_2 , -78 to $-20\text{ }^\circ\text{C}$, 37 %.⁷²

1.6.2 Batzellines and isobatzellines

In 1994, Tao *et al.*⁷³ presented a full account of the syntheses of discorhabdin C (**1.49**), batzelline C (**1.24**) and isobatzelline C (**1.27**) together with an evaluation of the cytotoxic activities of the synthetic intermediates. The synthesis of batzelline and isobatzelline C were carried out using a protected aromatic aldehyde (**1.88**) as the starting material (Scheme 1.5). The synthetic sequence involved the introduction of a carbamate functionality using a modified Curtius reaction followed by the formation of the indole **1.89**. Since regiospecific chlorination could not be achieved cleanly, **1.89** was first reduced and subsequently reacted with *N*-chlorosuccinimide (NCS) to give the chloro intermediate **1.90**. The double bond was then reintroduced by reaction with 2,3-dichloro-5,6-dicyano-1,4-benzoquinone (DDQ). Batzelline C was obtained following deprotection, cyclisation, reduction, de-*O*-methylation and oxidation of the subsequent indole derivatives, whereas oxidation of **1.91** with ceric ammonium nitrate (CAN) followed by reaction with ammonium chloride yielded isobatzelline C.⁷³

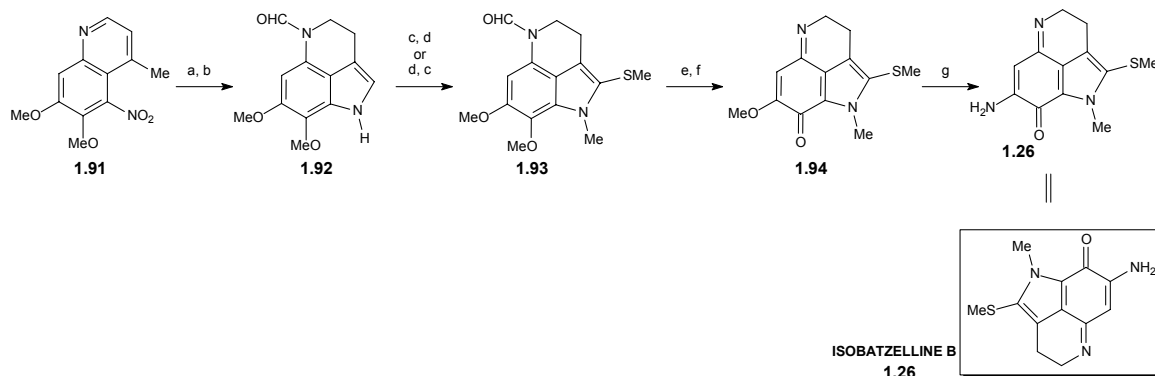


Scheme 1.5 Synthesis of batzelline C and isobatzelline C.⁷³

a) i) MeI, NaH, 66 %, ii) Jones oxidation, 89 %; b) i) Imd₂CO, ii) NaN₃, heat, iii) trimethylsilylethanol, 86 %; c) i) H₂, 10 % Pd/C, 100 %, ii) ethyl 4-acetoacetate, 87 %; d) NaBH₃CN, 80 %, ii) NCS, 69 % (**1.89**); e) DDQ, 66 %; f) i) 60 % HClO₄, ii) NaOH, iii) DCC, 58 %; g) BH₃SMe₂, 80 %; h) BBr₃, 78 %; i) i) CAN, 64 %, ii) NH₄Cl, 64 %.⁷³

Joule and co-workers⁷⁴ described the first preparation (Scheme 1.6) of a pyrroloquinoline nucleus containing a methylthioether substituent from a tetrahydroquinoline precursor (**1.92**). The synthetic approach initially involved the low temperature, regioselective mononitration of 6,7-dimethoxy-4-methylquinoline. Reduction of the nitro quinoline (**1.91**) followed by oxidation of the C-4 methyl group, facile cyclisation of the C-5 amino and C-4 aldehyde moieties and finally reduction of the quinoline ring and formylation of the resultant piperidine nitrogen yielded **1.92**. The key step in the synthesis was the formation of **1.93** by the regioselective introduction of the methylthioether group, using MeSCl, at the pyrrole α -position. Hydrolysis followed by oxidation

gave the iminoquinone **1.94** and replacement of the methoxyl group with an amino group was achieved smoothly with ammonium chloride to give isobatzelline B (**1.26**).⁷⁴



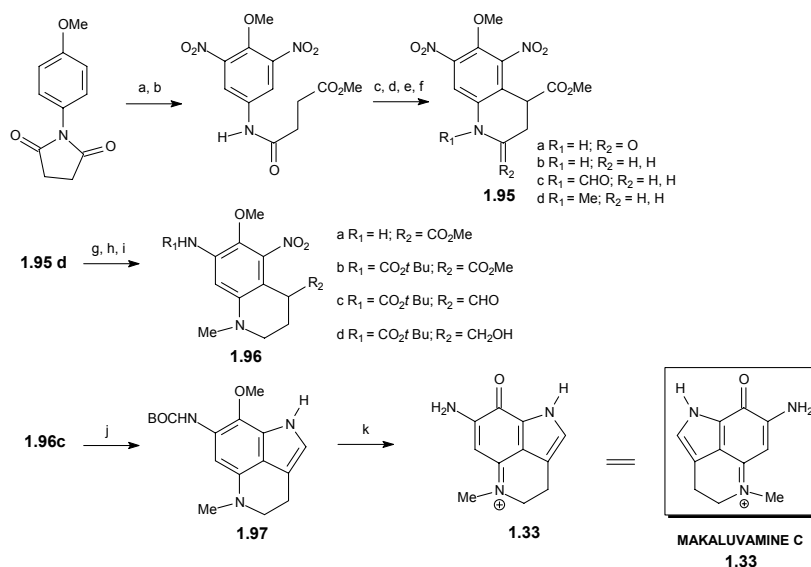
Scheme 1.6 Total synthesis of isobatzelline B.⁷⁴

a) NaBH₄, NiCl₂·6H₂O, MeOH, rt, 55 %; b) HCO₂H, Ac₂O, rt, 18 %; c) MeSSMe, SO₂Cl₂, CH₂Cl₂, 0 °C to rt, 35 %; d) NaH, MeI, THF, rt, 88 %; e) 2.5 M aq. NaOH, reflux; f) CAN, MeCN, H₂O, rt, 29 %; g) NH₄Cl, MeOH, 50 °C, sealed tube, 98 %.⁷⁴

A similar, alternative approach to the total syntheses of batzelline A, batzelline B, isobatzelline A and isobatzelline B was reported by Alvarez *et al.*⁷⁵ The tricyclic rings were again prepared from a quinoline derivative, with batzelline B synthesised from the pyrroloquinoline in two steps.⁷⁵

1.6.3 Makaluvamines A - F

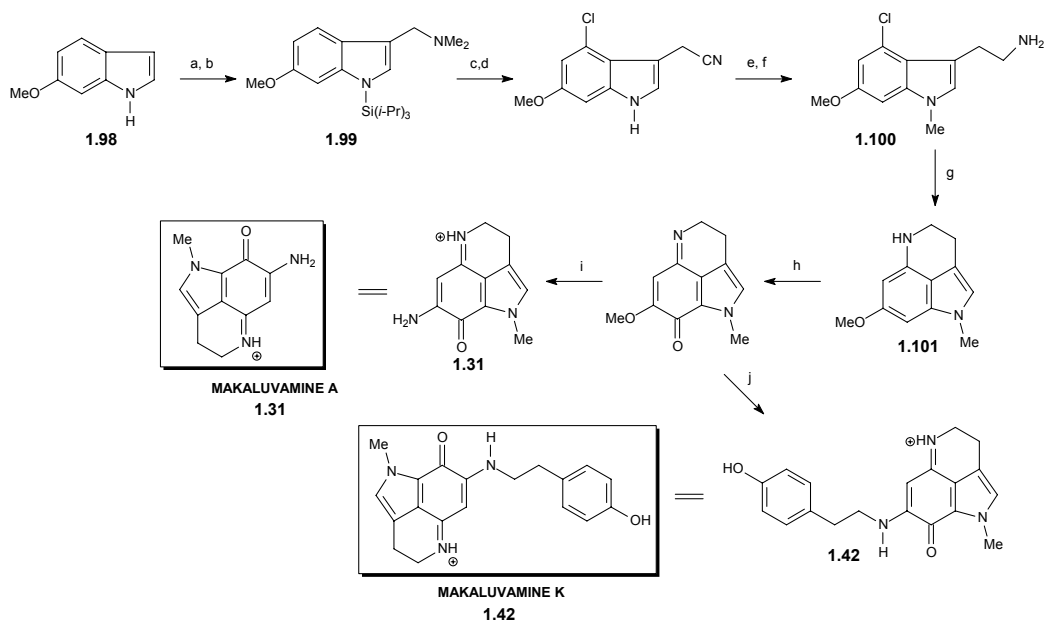
Makaluvamine C was synthesised by Kraus and Selvakumar from an alternate route using a *p*-anisidine derivative (Scheme 1.7).⁷⁶



Scheme 1.7 An alternative synthetic approach to makaluvamine C.⁷⁶

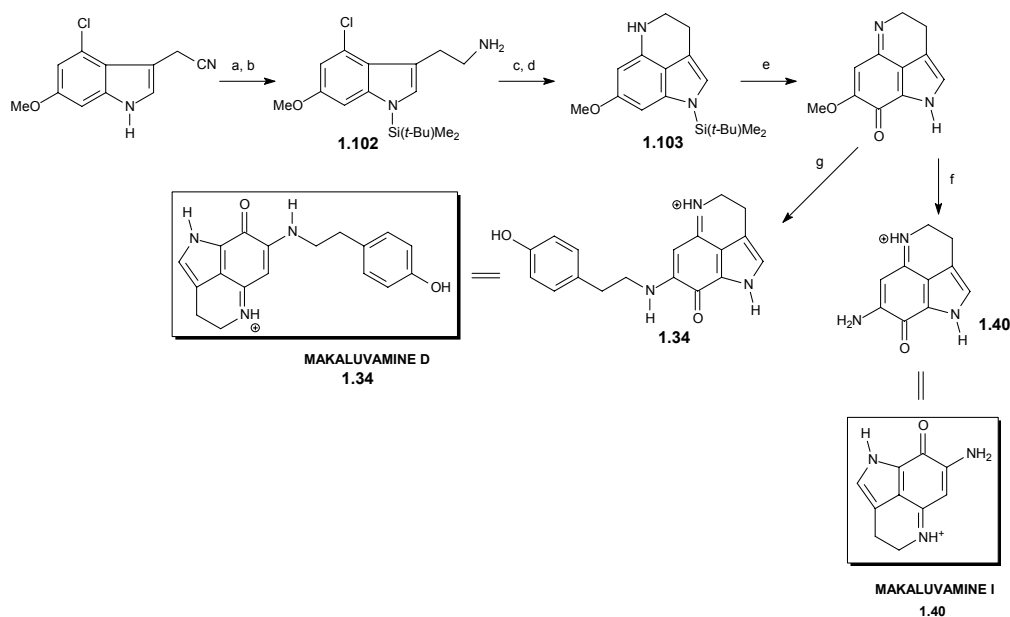
a) HNO₃, H₂SO₄; b) MeONa; c) *t*-BuOK, CAN; d) BH₃; e) AcOCHO; f) BH₃; g) H₂, Pd/C; h) BOC₂O; i) DIBAL; j) H₂, Pd/C; k) TMSCl, NaI, Fremy's salt.⁷⁶

An intramolecular nucleophilic aromatic substitution reaction mediated by potassium *tert*-butoxide gave the quinoline precursor **1.95**; selective reduction of **1.95** using catalytic hydrogenation; and the use of Fremy's salt (transformation of **1.97** to **1.33**) to synthesise an iminoquinone from an amino phenol, formed the key steps in this synthetic sequence.⁷⁶



Scheme 1.8 Preparation of makaluvamines A and K.⁹⁷

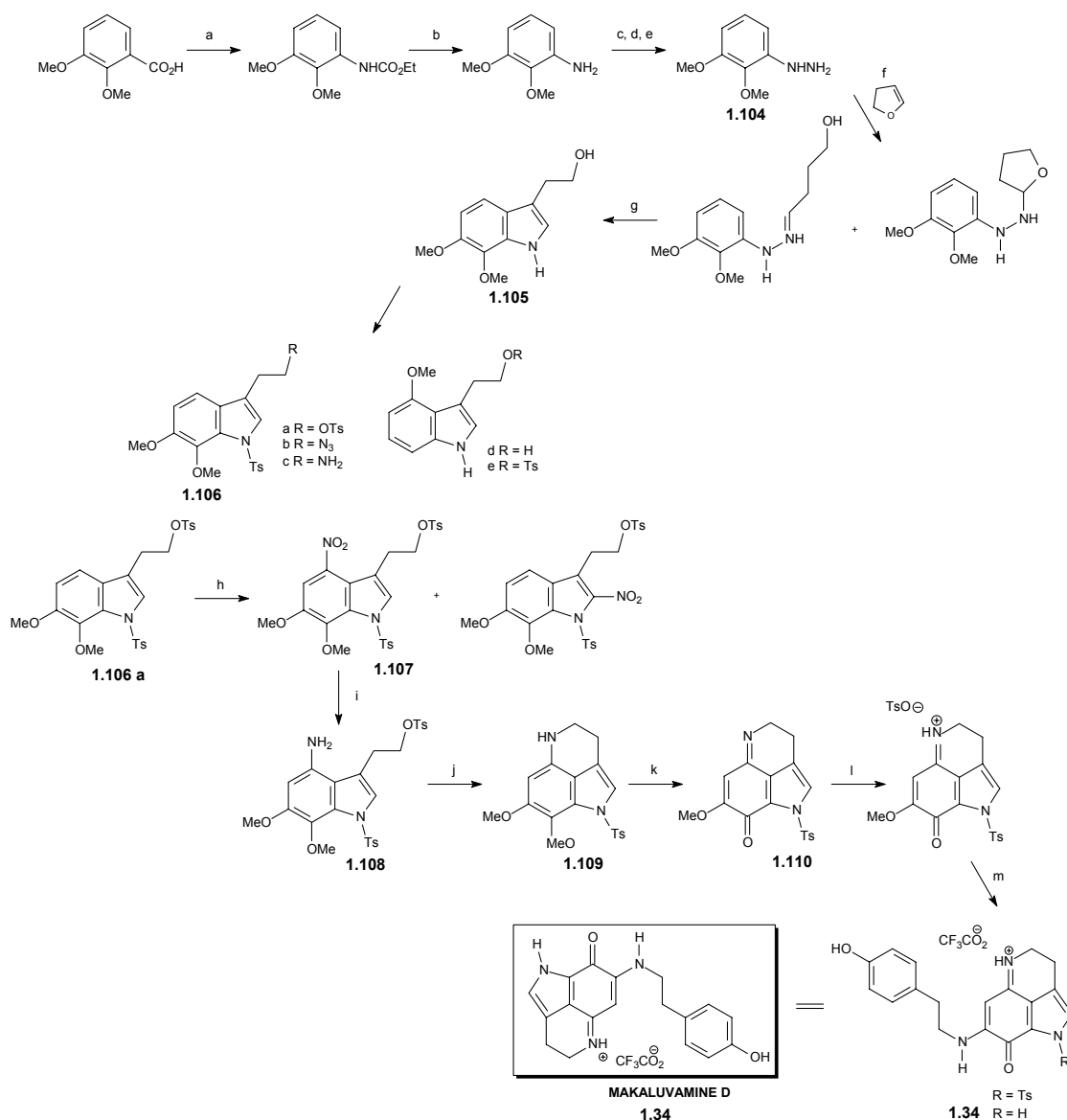
a) HCHO, HNMe₂, AcOH, 98 %; b) i) NaH, THF, ii) (*i*-Pr)₃SiCl, 97 %; c) i) *t*-BuLi, Et₂O, 0 °C, 1hr, ii) Cl₃CCl₃, 90 %; d) i) MeI, ii) Me₃SiCN, TBAF, 87 %; e) i) NaH, THF, ii) MeI, 99 %; f) BH₃.THF, 52 % or LiAlH₄, benzene-Et₂O, 92 %; g) LICA, THF, 0 °C, 1 hr, 78 %; h) O₂, Salcomine; i) NH₄Cl, MeOH, 40 % from **1.101**; j) tyramine hydrochloride, MeOH, 44 % from **1.101**.⁹⁷



Scheme 1.9 Preparation of makaluvamines D and I.⁷⁷

a) NaH, THF, ii) *t*-BuMe₂SiCl, 91 %; b) BH₃.THF, 88% or LiAlH₄, Et₂O-benzene, 90 %; c) LICA, THF, 0 °C, 1 hr, 75 %; d) TBAF, 95 %; e) Fremy's salt, pH 7 phosphate buffer, MeOH, 0 °C, 5 min, 41 %; f) NH₄Cl, MeOH, 67 %; g) tyramine hydrochloride, MeOH, 78 %.⁷⁷

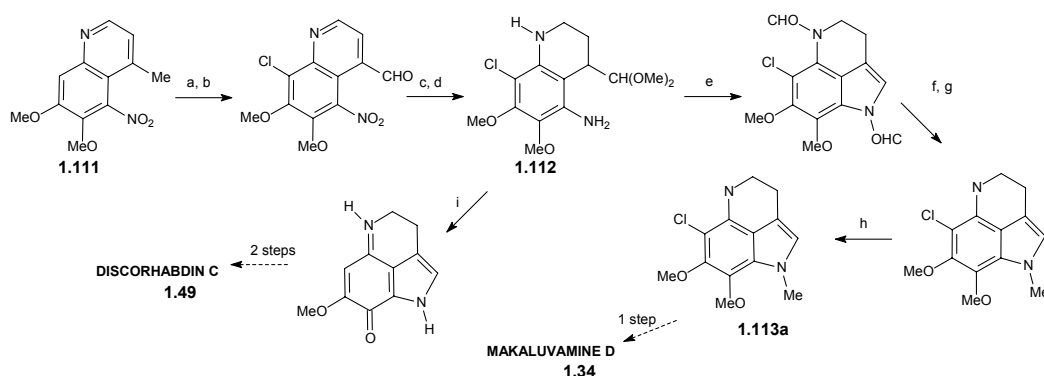
Iwao *et al.*⁷⁷ accomplished the total synthesis of makaluvamines A, D, I and K (Scheme 1.8 and 1.9) *via* a new entry into the makaluvamine nucleus using 6-methoxyindole (**1.98**, Scheme 1.8) as the starting material. The key intermediates **1.101** (Scheme 1.8) and **1.103** (Scheme 1.9) were prepared by aryne-mediated cyclisation of the tryptamine derivatives **1.100** and **1.102**, respectively. The required substituents at positions 3 and 4 on the indole ring were introduced by consecutive directed lithiation and fluoride ion-induced elimination-addition reactions of the methiodide of **1.99**.⁷⁷



Scheme 1.10 Total synthesis of makaluvamine D.⁷⁸

a) (PhO)₂PON₃, EtOH, Et₃N; b) KOH, EtOH; c) NaNO₂, HCl; d) SnCl₂, HCl; e) NaOH; f) HCl; g) ZnCl₂, HOCH₂CH₂OH; h) AcONO₂, Ac₂O; i) H₂, PtO₂, EtOH; j) (*i*-Pr)₂Et; k) CAN, MeCN, H₂O; l) *p*-TsOH; m) i) tyramine, EtOH, heat, ii) TFA.⁷⁸

A novel approach to the synthesis of the pyrroloquinoline system was developed by White *et al.* and is illustrated (Scheme 1.10) by the total synthesis of makaluvamine D. The approach involved a Fischer indole synthesis using hydrazine (**1.104**) and dihydrofuran, which led to tryptophol (**1.105**).⁷⁸ The tryptophol, protected as its ditosylate (**1.106a**), was then subjected to nitration at the C-4 position on the indole ring to give compound **1.107**. Reduction to the amine (**1.108**) followed by deprotection, oxidation and cyclisation gave **1.109**, while selective demethylation and oxidation with CAN provided the iminoquinone core (**1.110**). Replacement of the methoxy group with an amine functionality followed by treatment with tyramine and TFA successfully yielded the natural product (**1.34**).⁷⁸



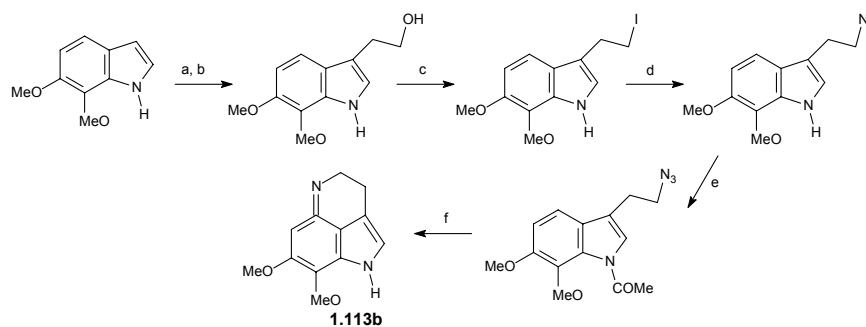
Scheme 1.11 Synthetic approach to discorhabdin C and makaluvamine D.⁷⁹

a) NCS, DMF, 60 °C, 55 %; b) I₂, *t*-BuI, FeCl₂, TFA, DMSO, 80 °C, 78 %; c) MeOH, HCl, reflux, 90 %; d) NaBH₄, NiCl₂·6H₂O, MeOH, 0 °C, 90 %; e) HCO₂H, Ac₂O, rt, 50 %; f) aq. NaOH, MeOH, CH₂Cl₂, rt, 82 %; g) MeI, NaH, THF, rt, 56 %; h) aq. 2N NaOH, reflux, 95 %; i) aq. 1N HCl, THF, 40 °C.⁷⁹

Roberts *et al.* employed 6,7-dimethoxy-4-methyl-5-nitroquinoline (**1.111**, Scheme 1.11) to give the key intermediate **1.113a** which led to makaluvamine D. Following treatment of the amine-acetal **1.112** with hydrochloric acid, the iminoquinone precursor of discorhabdin C was produced (Scheme 1.11).⁷⁹ These intermediates had been shown in previous reports to lead to the total synthesis of makaluvamine D⁸⁰ and discorhabdin C.⁸¹

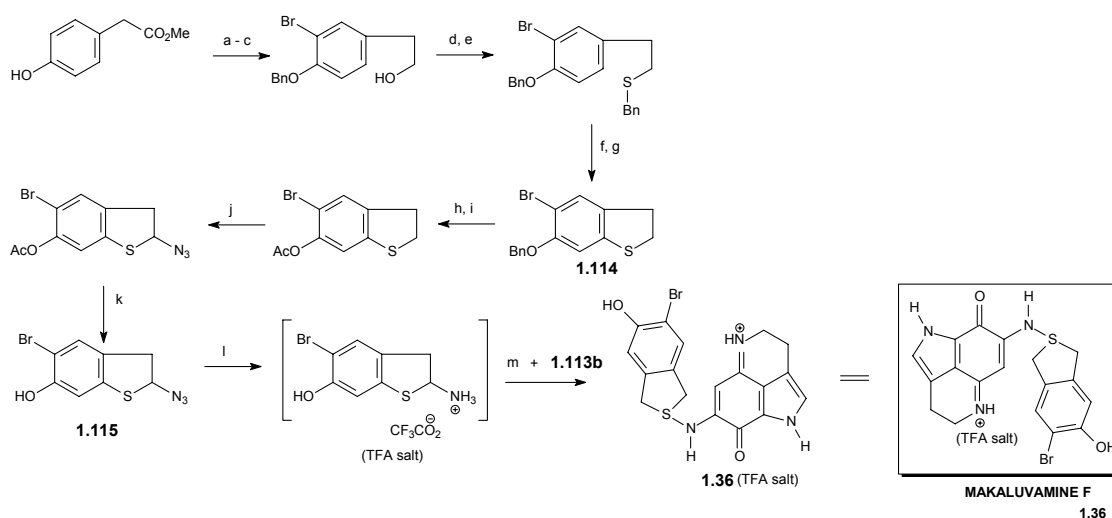
Lown *et al.* prepared a lexitropsin derivative of makaluvamine A, and the tricyclic systems were constructed from indole precursors.⁸²

Kita *et al.*⁸³ accomplished the first total synthesis of makaluvamine F (**1.36**) in 1999. Key steps in this synthetic sequence included the formation of the pyrroloquinoline nucleus (**1.113b**, Scheme 1.12), the formation of the dihydrobenzothiophene ring (**1.114**, Scheme 1.13) and the preparation of the α -azidodihydrobenzothiophene ring by hypervalent iodine (III) induced reactions (**1.115**, Scheme 1.13).⁸³



Scheme 1.12 Preparation of pyrroloquinoline nucleus for makaluvamine F.⁸³

a) $(\text{COCl})_2$, Et_2O , EtOH , 94 %; b) LiAlH_4 , THF (quant); c) I_2 , imidazole, PPh_3 , toluene, 68 %; d) AcCl , $t\text{-BuOK}$, THF, 91 %; e) PIFA- Me_3SiOTf , $(\text{CF}_3)_2\text{CHOH-H}_2\text{O}$ (50:1).⁸³



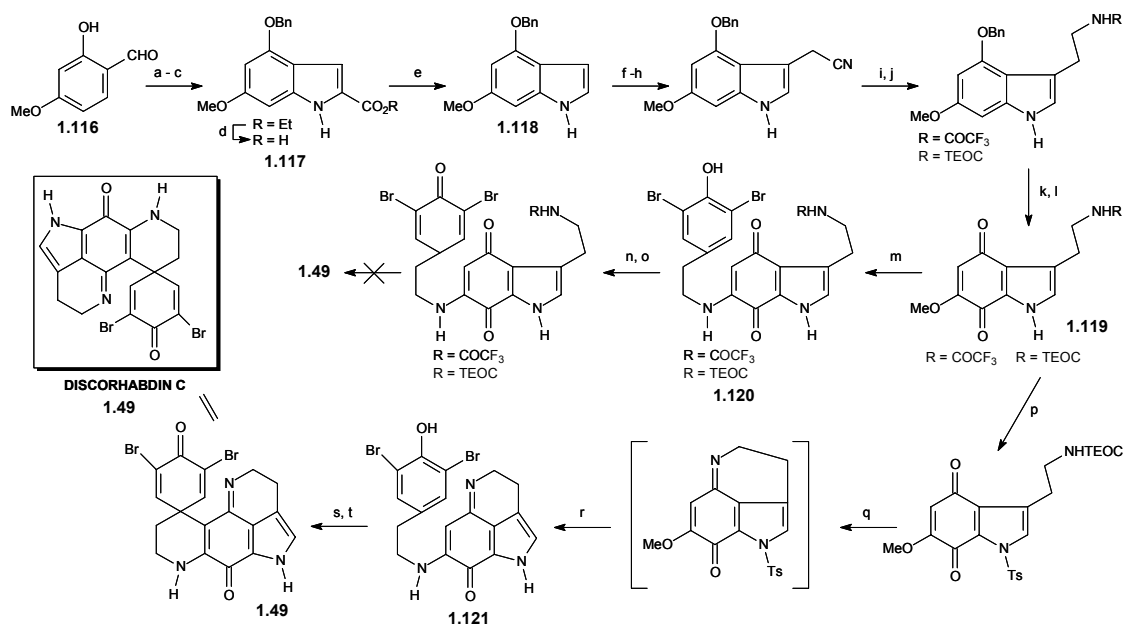
Scheme 1.13 Total synthesis of makaluvamine F.^{83,84}

a) Br_2 , AcOH ; b) BnBr , K_2CO_3 , EtOH ; c) LiAlH_4 , THF, 71 %; d) I_2 , PPh_3 , imidazole, PhMe , 65 %; e) AcSBn , NaOH , MeOH , 98 %; f) PIFA- $\text{BF}_3\cdot\text{OEt}_2$; g) aq. MeNH_2 , 66 %; h) $\text{BF}_3\cdot\text{OEt}_2$, EtSH ; i) Ac_2O , NaOAc , aq. NaOH , 83 %; j) $\text{PhI=O-Me}_3\text{SiN}_3$, MeCN , -40 to -25 °C, 46 %; k) 5 % NaOH , MeOH , 90 %; l) H_2 , 10 % Pd/C , EtOH-TFA , 100 %; m) MeOH , rt, 86 %.^{83,84}

In order to construct the N,S-acetal moiety (Scheme 1.13) the authors^{83,84} designed a dihydrobenzothiophene system bearing a hydroxy group. Various dihydrobenzothiophene ring systems were therefore prepared from phenol ethers bearing an alkyl sulfide sidechain *via* an intramolecular cyclisation using phenyliodine(III) *bis*-(trifluoroacetate) (PIFA- $\text{BF}_3\cdot\text{Et}_2\text{O}$) followed by treatment with aqueous methylamine which gave the 6-benzyloxy-5-bromo-dihydrobenzothiophene intermediate (**1.114**). Azidation of **1.114** was carried out after debenzoylation followed by acetylation of **1.114** to give the corresponding α -azido compound. After hydrolytic deprotection of the 6-acetoxy group, the 2-azido-5-bromo-6-hydroxy-dihydrobenzothiophene intermediate (**1.115**) was obtained. Catalytic hydrogenation of **1.115** in the presence of TFA followed by a final coupling reaction with **1.113b** in methanol gave the TFA salt of **1.36**.

1.6.4 Discorhabdins

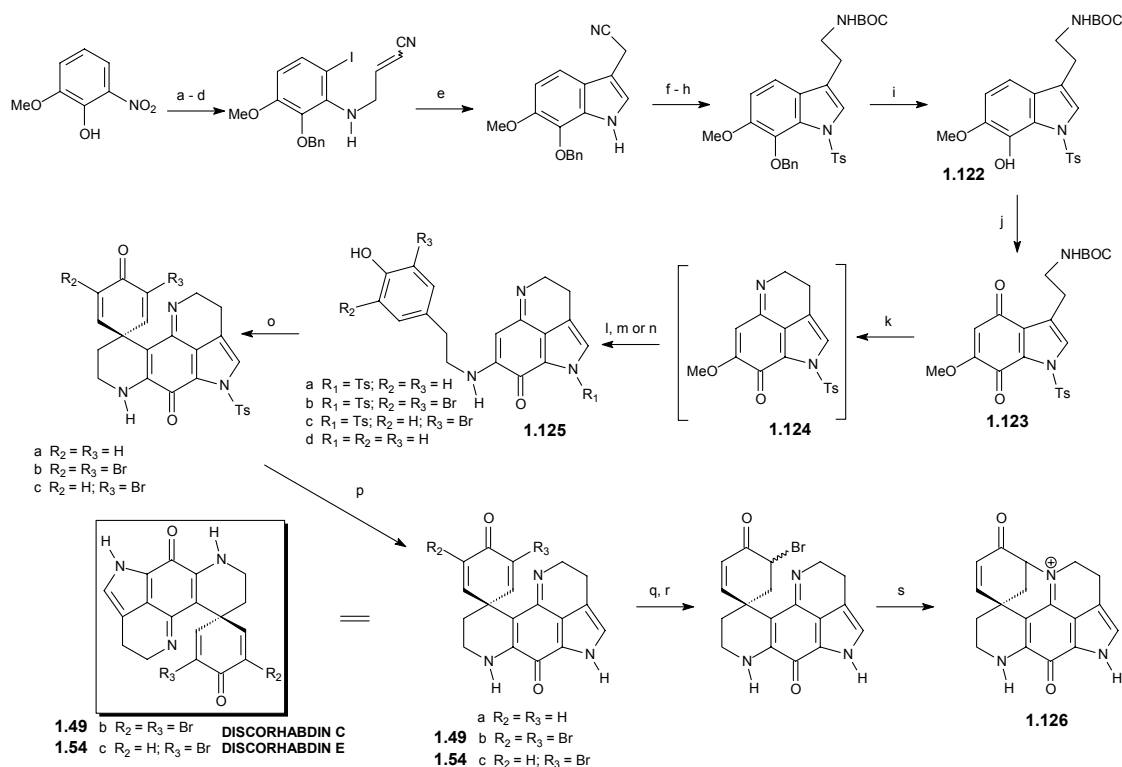
To generate the spirodienone ring system common in the discorhabdins, the coupling reactions have involved hypervalent iodine (III) reagents,⁸⁵⁻⁸⁷ electrochemical oxidations^{73,81} and an intramolecular Michael addition followed by copper (II) catalysed re-oxidation of the resultant amino phenol derivatives.⁸⁸



Scheme 1.14 Total synthesis of discorhabdin C.⁸⁵⁻⁸⁷

a) $C_6H_5CH_2Br$, K_2CO_3 , EtOH, reflux; b) $N_3CH_2CO_2Et$, NaOEt, EtOH, $-15\text{ }^\circ\text{C}$; c) Xylene, reflux, 73 %; d) KOH, EtOH, reflux; e) Copper chromite, quinoline, $215\text{ }^\circ\text{C}$, 68 %; f) $CH_2=N^+Me_2^-$, CH_2Cl_2 , rt; g) MeI, $0\text{ }^\circ\text{C}$; h) NaCN, H_2O , $80\text{ }^\circ\text{C}$, 36 %; i) H_2 , Raney Ni, NH_3 , EtOH, 3.3 atm; j) CF_3COSEt , NaOMe, MeOH; *p*- $O_2NC_6H_4OCO_2(CH_2)_2SiMe_3$, NaOEt, EtOH, $0\text{ }^\circ\text{C}$, 78 – 89 %; k) H_2 , 10 % Pd/C, EtOH, 3.3 atm; l) Fremy's salt, KH_2PO_4 , acetone- H_2O 56 – 59 %; m) 3,5-dibromotyramine HBr, Et_3N , EtOH, reflux, 55 – 58 %; n) $MeCH=C(OMe)(OSiMe_3)$, CH_2Cl_2 , rt; o) $PhI(OCOCF_3)_2$ (PIFA), CF_3CH_2OH , rt, 58 – 62 %; p) TsCl, *t*-BuOK, THF, 92 %; q) Anhydrous TsOH, MeCN; r) 3,5-dibromotyramine HBr, $NaHCO_3$, EtOH, reflux, 51 %; s) $MeCH=C(OMe)(OSiMe_3)$, CH_2Cl_2 , rt; t) $PhI(OCOCF_3)_2$ (PIFA), CF_3CH_2OH , rt, 42 %.⁸⁵⁻⁸⁷

Kita *et al.* accomplished a total synthesis of discorhabdin C (1.49) in 1992.⁸⁵⁻⁸⁷ A general route to the spirocyclic quinones by an oxidative coupling reaction of various O-silylated aminoquinones using phenyliodine(III) *bis*-(trifluoroacetate)(PIFA) was described and this method was applied to a general synthesis of azacarbocyclic spirodienone systems.⁸⁵⁻⁸⁷ Benzoylation of 1.116 (Scheme 1.14) followed by condensation with ethyl azidoacetate gave the vinyl azide which, upon decomposition gave the indole 1.117. Hydrolysis followed by decarboxylation gave the disubstituted indole 1.118. Following protection, hydrogenation and subsequent benzoylation and oxidation, the quinone 1.119 was obtained. Protection of the indoloquinone to form the imine followed by coupling with 3,5 dibromotyramine hydrobromide afforded the phenol derivative 1.121. Protection followed by oxidation afforded discorhabdin C.

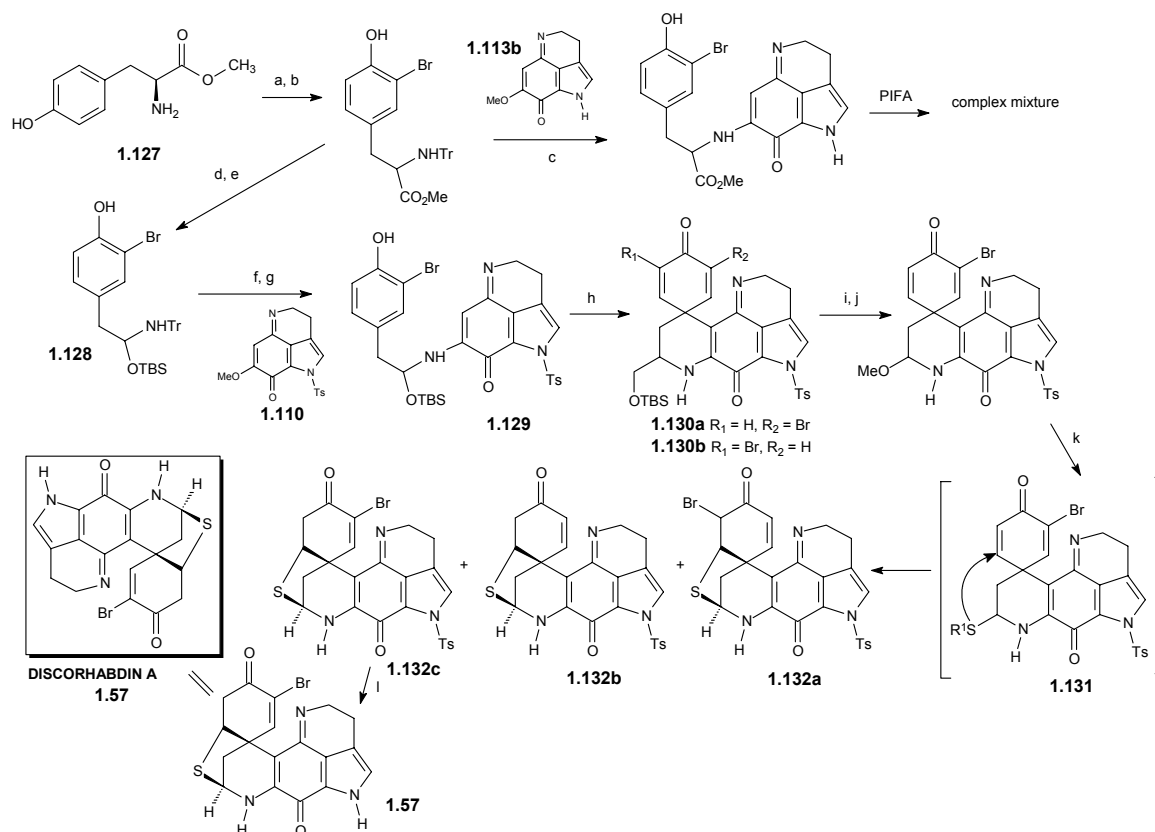


Scheme 1.15 Total synthesis of discorhabdin C.⁸⁸

a) BnBr , K_2CO_3 , DMF; b) Fe , HCl , H_2O ; c) ICl , Et_2O , H_2O , Na_2CO_3 ; d) $\text{BrCH}_2\text{CH}=\text{CHCN}$, NaHCO_3 , acetone, H_2O , 59 %; e) 5 mol % $\text{Pd}(\text{OAc})_2$, $(o\text{-MeC}_6\text{H}_4)_3\text{P}$, Et_3N , MeCN, reflux, 3 hr, 89 %; f) LiAlH_4 , Et_2O ; g) $(\text{BOC})_2\text{O}$, CH_2Cl_2 ; h) Ts_2O , NaH , DMF, 60 %; i) H_2 , Pd/C, MeOH, 100 %; j) Fremy's salt, acetone- H_2O , 82 %; k) TFA, CH_2Cl_2 ; l) NaHCO_3 , EtOH, tyramine HCl; m) NaHCO_3 , EtOH, bromotyramine HCl; n) NaHCO_3 , EtOH, dibromotyramine HCl, 46 – 62 %; o) 3 eq. CuCl_2 , Et_3N , O_2 , MeCN, 81 – 90 %; p) NaOMe, MeOH 67 – 80 %; q) H_2 , Pd/C, MeOH, 69 %; r) $\text{PhMe}_3\text{N}^+\text{Br}^-$, CHCl_3 , TFA, s) basic alumina, 73 %.⁸⁸

Alternatively, Heathcock and Aubart showed, following the preparation and the oxidation of a suitably substituted indole **1.122**, that the iminoquinone **1.124** was able to undergo a nucleophilic amination with a suitably substituted tyramine to give **1.125**. Oxidative cyclisation of **1.125** in the presence of excess copper dichloride followed by deprotection gave discorhabdin C and E. Further reaction with hydrogen over palladium of the debromo analogue, followed by regioselective bromination gave a bromoenone mixture which on contact with basic alumina afforded dethiadiscorhabdin D (**1.126**). Formation of the C-2-N-18 bond was achieved by nucleophilic displacement of the C-2 bromide by N-18. The authors thus showed a possible biomimetic approach to the synthesis of discorhabdins C and E. Discorhabdin C type structures indicate that the tryptamine substructure is incorporated in the iminoquinone moiety, while the rest of the molecule may be constructed from a tyrosine unit implicating the possibility that analogues of **1.120** (Scheme 1.14) act as intermediates in the biosynthetic pathway.⁸⁸ However, on separate occasions, Kita⁸⁵⁻⁸⁷ and Heathcock⁸⁸ in particular, both demonstrated through their attempts to synthesise discorhabdin C that this intermediate could not undergo the crucial iminoquinone cyclisation, thus negating analogues of **1.120** as possible biosynthetic intermediates. The key cyclisation step did, however, take place with the **1.121** (Scheme 1.14) and **1.125** intermediates

(Scheme 1.15). Heathcock also showed that a possible precursor to the pyrroloquinoline nucleus is likely to be analogous to **1.123**, whereas an unsubstituted **1.123** (*i.e.* lacking the methoxy substituent) did not give rise to the pyrroloquinoline core **1.124** as reported previously by Kita and co-workers.⁸⁸



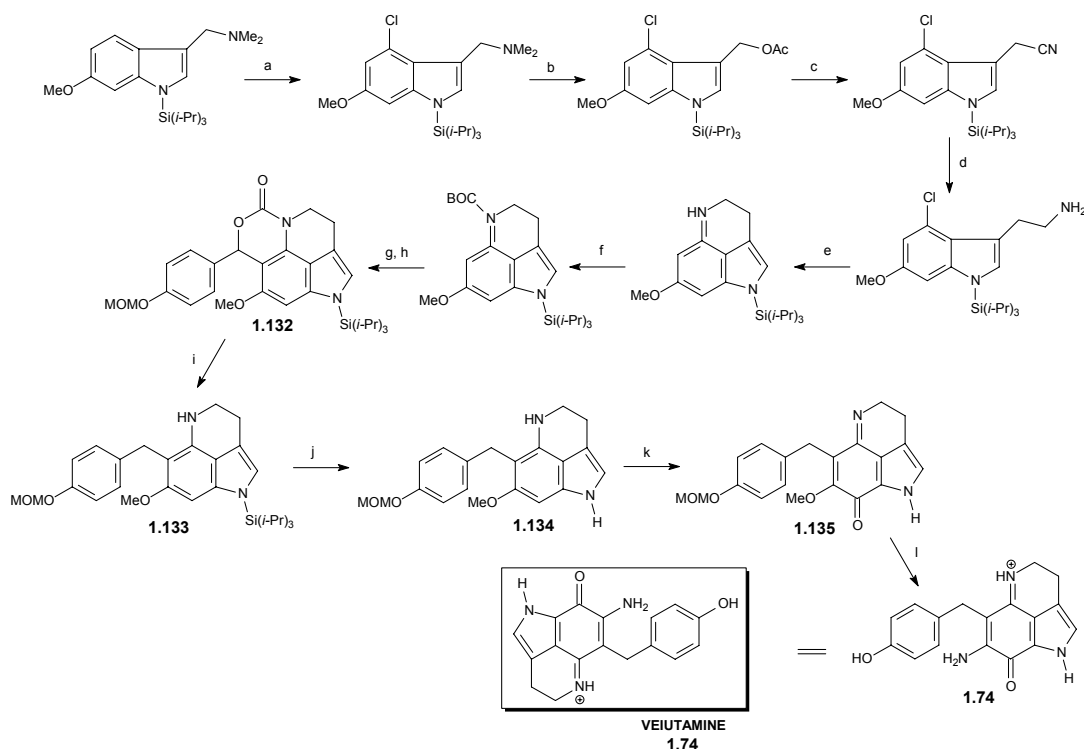
Scheme 1.16 Total synthesis of discorhabdin A.⁸⁹

a) TrCl, Et₃N, DMF, quant.; b) NBS, DMF, 65 %; c) 0.1 N HCl, MeOH, then **1.113**, MeOH, 20 hr, 46 %; d) DIBAH, CH₂Cl₂, -78 °C to rt., 5 hr, 96 %; e) TBSCl, DBU, CH₂Cl₂, 0 °C, 1.5 hr, 87 %; f) TBAF, THF, 0 °C, 0.5 hr, quant.; g) 0.1 NH₄Cl, MeOH, then **1.110**, MeOH, 16 hr, 54 %; h) PIFA-MK10, CF₃CH₂OH, 0.5 hr, 45 %; i) BF₃·Et₂O, CH₂Cl₂, 0 °C to rt., 7 hr, 90 %; j) Pb(OAc)₄, CH₂Cl₂-MeOH (2:1), 0 °C, 1.5 hr, 88 %; k) R¹SH (where R¹ = *p*-MeOC₆H₄CH₂), 30 % HBr-AcOH, CH₂Cl₂, -78 to 4 °C, 15 hr, 13 % for **1.132a**, 19 % for **1.132b**, 22 % for **1.132c**; l) NaOMe, THF-MeOH, 0 °C, 1 hr, 65 %.⁸⁹

Kita *et al.* described the first total synthesis of discorhabdin A (Scheme 1.16) in 2002.⁸⁹ Key elements of the synthetic strategy, which employed L-tyrosine methyl ester (**1.127**) as the starting material, included the use of the iodine (III)-induced oxidative spirocyclisation to form **1.130** and in one of the final steps, and the introduction of the sulfur group (**1.131**) which led to the cross-linked core of **1.132a** - **1.132c**.⁸⁹ Tritylation of **1.127** followed by monobromination, reduction, and silylation gave the bisilylated intermediate **1.128**. Selective desilylation of **1.128** followed by a coupling reaction with **1.110** yielded **1.129**. Spirodienone formation using phenyliodine (III) *bis*-(trifluoroacetate) (PIFA) gave a mixture of two diastereomers (**1.130a** and **1.130b**), which were subjected to desilylation, oxidative dealkylation. Introduction of a *p*-methoxybenzylthiol group gave **1.131** which on treatment with aqueous methylamine and detosylation afforded **1.57**.⁸⁹

1.6.5 Related pyrroloiminoquinones

Moro-oka *et al.* completed the first total synthesis of veitamine in 1999⁹⁰ (Scheme 1.17). The key steps in this synthesis involved the regioselective functionalisation at the C-6 position of the pyrroloquinoline nucleus (**1.132** to **1.135**) which was accomplished through directed lithiation procedures and the use of *p*-MOMO-C₆H₄-CH(OH) as an electrophile to generate the cyclic carbamate **1.132**. Following hydrolysis, decarboxylation and deprotection, **1.134** was oxidised to the iminoquinone **1.135** and treated with ammonium chloride to give **1.74**.⁹⁰



Scheme 1.17 Total synthesis of veitamine.⁹⁰

a) i) *t*-BuLi (1.2 equiv.), Et₂O, 0 °C, 1 hr, ii) Cl₂CCl₃, 90 %; b) Ac₂O (3 equiv.), toluene, 0 °C, 15 hr, 78 %; c) Et₂AlCN (2 equiv.) toluene, 0 °C, 20 min, 80 %; d) LiAlH₄ (5 equiv.) benzene-Et₂O, reflux, 0.5 hr, 96 %; e) LICA (5 equiv.), THF, 0 °C, 15 min, 70 %; f) BOC₂O (3 equiv.) reflux, 8 hr, 96 %; g) i) *s*-BuLi (1.5 equiv.), TMEDA, ether, -78 °C, 1 hr, ii) *p*-MOM-C₆H₄-CHO, 72 %; h) NaH (1.5 equiv.), THF, 0 °C, 20 min, 86 %; i) H₂, Pd(OH)₂/C, MeOH-AcOEt, rt, 6 hr; j) TBAF (1.2 equiv.), THF, rt, 15 min, 99 %; k) (KSO₃)₂NO (2 equiv.), pH 7 MeOH : phosphate buffer, 0 °C, 10 min, 33 %; l) i) NH₄Cl (10 equiv.), MeOH, rt, 36 hr, ii) cat. HCl, reflux, 1 hr, iii) NaHCO₃, iv) TFA, 89 %.⁹⁰

1.7 Aim

As described in Section 1.3 the taxonomy of the sponge family Latrunculiidae is presently the subject of some debate. For non-taxonomists it is especially difficult to keep track of all the changes. In an attempt to contribute to this debate we present in this thesis an in depth study of the major and minor pyrroloamino-*ortho*-quinone and pyrroloiminoquinone metabolites produced by four species of endemic South African Latrunculid sponges belonging to three genera *Tsitsikamma*, *Latrunculia* and *Strongylodesma*. The sponges were collected in our two main study

sites namely Algoa Bay and the Tsitsikamma Marine Reserve. Both these study sites are situated on the temperate south eastern coast of South Africa. The isolation and structure elucidation of eleven new and twelve known pyrroloamino-*ortho*-quinones and pyrroloiminoquinones are presented in Chapters 2 – 4. The dual role of these metabolites as both cytotoxic chemical agents and pigments piqued our interest in attempting to relate their photochemical properties to their cytotoxicity (Chapter 5). Pyrroloamino-*ortho*-quinones and pyrroloiminoquinone metabolites have been shown to exhibit interesting electrochemical behaviour³⁰ which in certain instances may be related directly to the anti-cancer activity of these compounds. Our possession of a unique suite of twenty three pyrroloamino-*ortho*-quinones and pyrroloiminoquinone metabolites therefore put us in an excellent position to attempt to explore the correlation between the electrochemical properties and anti-cancer (HCT-116) activity of these compounds (Chapters 6 and 7). A later report on the topoisomerase I inhibitory activity (in contrast to that reported by Copp *et al.*⁵⁴) of the *bis*-pyrroloiminoquinone wakayin (**1.73**)⁹¹ necessitated a similar investigation of topoisomerase I activity in the *bis*-pyrroloiminoquinones isolated from *T. favus*.

Chapter 2: Pyrroloiminoquinone metabolites from *Tsitsikamma pedunculata*

2.1 Introduction

The “golf ball shaped” laticrucid sponge *Tsitsikamma pedunculata* (Figure 2.2) was collected from Algoa Bay in 1999 and contained mainly discorhabdin-type pyrroloiminoquinone compounds. The very polar discorhabdins are difficult to purify giving broad peaks, even under optimised reversed phase HPLC conditions. As a result signals from small amounts of impurities are frequently observed in the NMR spectra of these compounds. Once recognised, however, these impurities do not impede the structure elucidation of the pyrroloiminoquinone metabolites. We have developed a standard isolation protocol which allowed us to minimise the amount of impurities present in the purified extracts. Thus, a methanolic extract of *T. pedunculata* was subjected to a sequence of solvent partitioning, solid phase extraction and high performance liquid chromatography to yield three known (**1.51** – **1.53**) together with six new discorhabdins (**2.1** – **2.6**, Figure 2.1). Purified samples were subjected to direct injection low resolution LC-MS, which, from the isotope pattern of the *pseudo*-molecular ion, enabled the determination of the number of bromine atoms (if any) incorporated into the discorhabdin skeleton (e.g. Figure 2.3, p. 49).

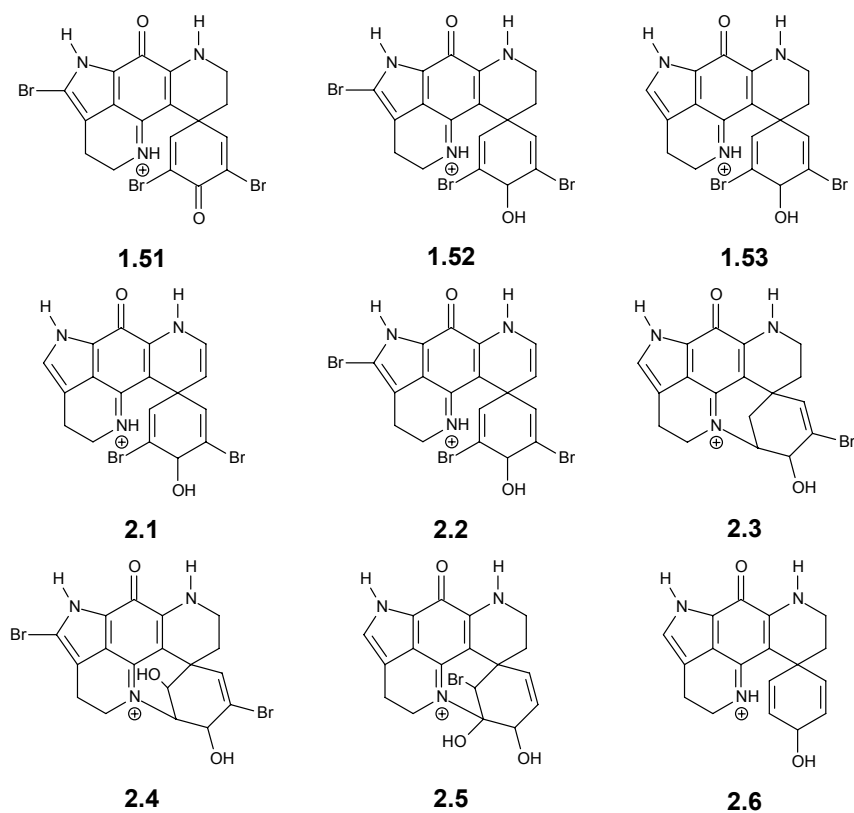


Figure 2.1 Summary of the compounds isolated from *T. pedunculata*.

The pyrroloiminoquinone structures were established using standard spectroanalytical techniques as well as by comparison of their spectroscopic data with those of known compounds in the series. Given the paucity of hydrogen atoms in pyrroloiminoquinone metabolites the structure elucidation is not trivial. To maximise the information available from exchangeable protons, the deuterated solvent DMSO- d_6 was preferred over CD₃OD (see Figure 2.10, p. 60). Unfortunately, many of the minor impurities alluded to above are also very soluble in DMSO- d_6 . The new compounds (**2.1** – **2.6**) are the minor metabolites in *T. pedunculata* and were obtained in small quantities (ca. 1 - 8 mg). The metabolites from *T. pedunculata* (OCDN 6451-V) are characterised by a) a reduced C-3 carbonyl; b) bromination at C-14; c) a discorhabdin C and a dethia-discorhabdin D (discorhabdin S) type skeleton, i.e. a N-18 to C-2 bond; and d) a Δ^7 olefin.

2.2 Results and Discussion

2.2.1 The taxonomy of the sponge *Tsitsikamma pedunculata*



Figure 2.2 An underwater photograph of *T. pedunculata*.

The “golf ball shaped” Latrunculid sponge, *T. pedunculata* (OCDN 6451-V) was collected by SCUBA from a depth of 38 – 40 m off Thunderbolt reef (34 03.14S and 25 41.35E), Algoa Bay, South Africa in 1999. Samaai *et al.*⁹² described the sponge as follows: “In life the sponge is pedunculate, up to 7 cm high and 3 cm wide. The surface is smooth, leathery with circular areolate porefields and raised volcano-shaped oscula. The texture is extremely tough, firm and leathery. The colour in life is salmon pink and between the oscula and areolate porefields it’s dark pink. Colour in preservative is dark brown. The choanosomal skeleton consists of a confused, ill-formed, irregular reticulation of anisostyles, meandering vertically and horizontally within the choanosome (70 – 110 μ m), with no distinction between the primary and secondary tracts.

Discorhabds are also found abundantly throughout the choanosomal tissue. The ectosome is composed of a thick dark, dense feltwork of tangential and paratangential oriented anisostyles approximately 1300 µm thick. A single layer of erect discorhabds (29 µm thick) lines the surface of the ectosome. Megascleres are anisostyles. Microscleres are isodiscorhabds with two whorls of cylindrical, conical tubercles. Free end of conically rounded spines is acanthose." The sponge is the second species to be described in the new genus *Tsitsikamma* within the Family Latrunculiidae.

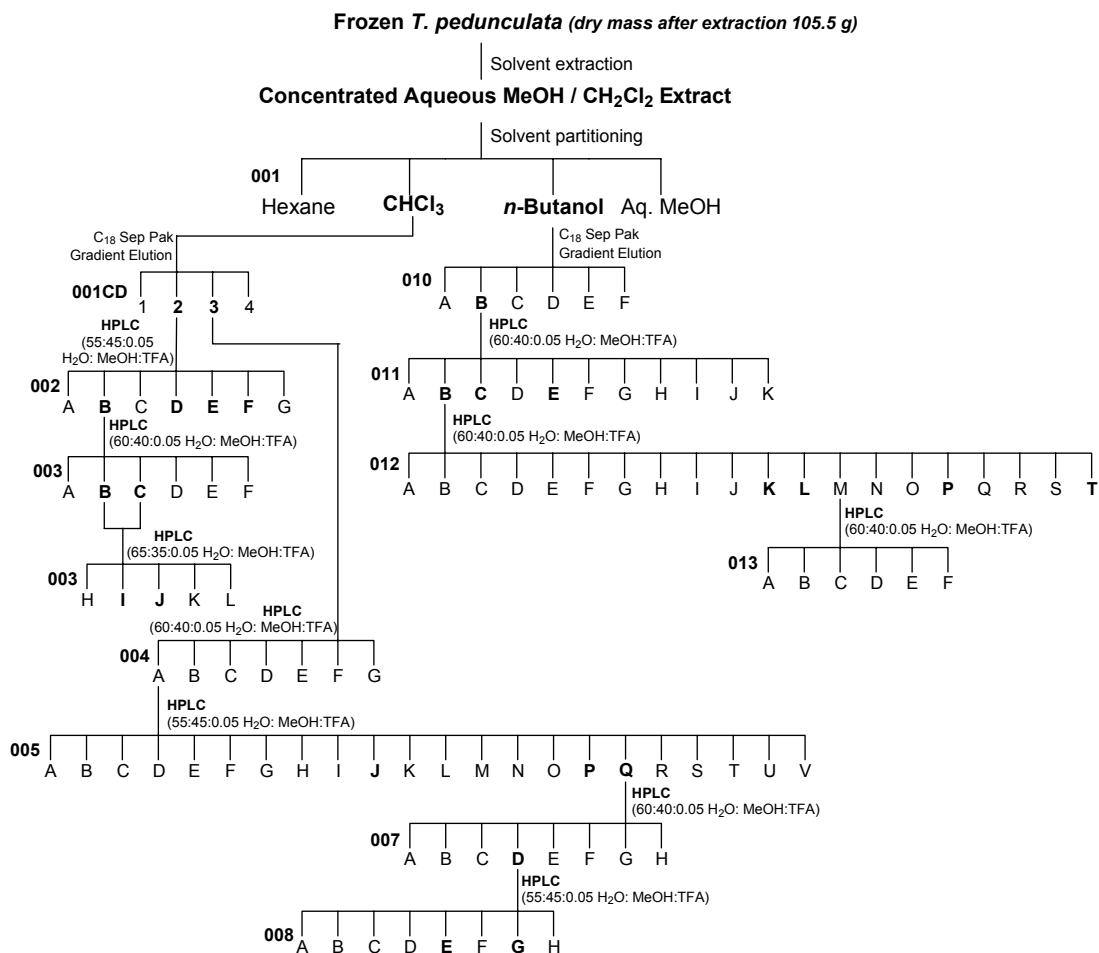
2.2.2 Extraction and isolation of pyrroloiminoquinone metabolites from *T. pedunculata*

The frozen sponge was extracted with methanol and the aqueous methanol extract concentrated and partitioned according to a modified Kupchan procedure (Scheme 2.1). The known compounds 14-bromo-discorhabdin C (**1.51**),⁴¹ 14-bromo-3-dihydro-discorhabdin C (**1.52**)⁴¹ and 3-dihydro-discorhabdin C (**1.53**);^{42,44} together with five new compounds; 7,8-dehydro-3-dihydro-discorhabdin C (**2.1**), 14-bromo-7,8-dehydro-3-dihydro-discorhabdin C (**2.2**), discorhabdin S (**2.3**), 14-bromo-1-hydroxy-discorhabdin S (**2.4**), 1-bromo-2-hydroxy-4-debromo-discorhabdin S (**2.5**), and 2,4-debromo-3-dihydro-discorhabdin C (**2.6**), were isolated from *T. pedunculata*.

Several methods are routinely used to work up frozen marine invertebrate material. The most common is lyophilisation followed by extraction with a polar solvent e.g. methanol of the frozen marine organism. One of the advantages of this approach is that it provides the dry mass of the marine organism prior to extraction which in turn is routinely used to calculate the yield of natural products isolated from the marine organism. The significance of this dry mass is, however, debatable given the prodigious and variable amounts of seawater-derived sodium chloride present in any filter feeding marine organism. The National Cancer Institute's (NCI) protocol for extracting marine invertebrate and algal material is of interest. McCloud *et al.*⁹³ have shown that initial lyophilisation of the frozen marine organism is not a prerequisite requirement for extracting bioactive marine metabolites. The NCI procedure which involves an initial aqueous extraction (grinding of the frozen material with dry ice, addition of water and subsequent centrifugation) has a number of advantages. The most important advantage to emerge from this procedure has been the discovery of many bioactive marine proteins which would have been denatured in an initial solvent extraction. The organic residue after centrifugation is lyophilised and extracted with a solvent combination of 1:1 dichloromethane : methanol.

Previous investigations^{41,42} of the natural product chemistry of South African Latrunculid sponges used the former method of sponge extraction *viz* lyophilisation followed by solvent extraction. Unfortunately, this approach apparently did not provide access to minor pyrroloiminoquinone metabolites which increasingly became the focus of our research. A defunct freeze drier at the start of our investigations fortuitously forced us to soak the frozen Latrunculid sponges in methanol or a 1:1 dichloromethane : methanol solvent mixture. Although the concentration of the

initial aqueous methanol extracts on a rotary evaporator was laborious we were rewarded as the subsequent chromatographic separations resulted in the discovery of many minor metabolites in reasonable yield. Solid phase extractions on C₁₈ Sep Paks[®], as the first stage in the chromatographic sequence, proved effective in removing the problem of the ever-present sodium chloride. The sponge was air dried after extraction to provide its dry mass. It can be argued that the removal of most of the sodium chloride during the aqueous methanol : dichloromethane extraction process makes this dry mass of the sponge possibly more relevant than that from prior lyophilisation.



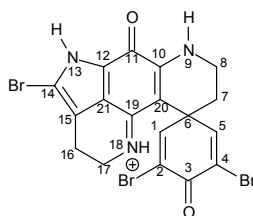
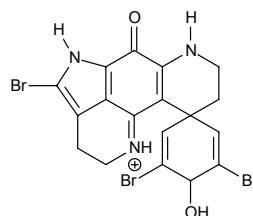
Scheme 2.1 Scheme for the extraction and isolation of pyrroloiminoquinone metabolites from *T. pedunculata*. The masses and yields (calculated relative to the dry mass of the sponge) of the *T. pedunculata* pyrroloiminoquinone metabolites are summarised below:

003I	1.51	22.7 mg	0.02 %
002D; 011E	1.52	18.7 mg	0.02 %
003J; 011C	1.53	90.4 mg	0.09 %
002E	2.1	1.2 mg	0.001 %
002F	2.2	7.7 mg	0.007 %
012L	2.3	4.4 mg	0.004 %
012P	2.4	4.2 mg	0.004 %
012K	2.5	2.6 mg	0.003 %
012T	2.6	1.2 mg	0.001 %

Compounds **1.51** - **1.53**, **2.1** and **2.2** were isolated from the chloroform partition fraction of the sponge extract, while **1.52**, **1.53** and **2.3** – **2.6** were obtained from the butanol partition fraction. The structures of compounds **2.1** – **2.6** reported here, are based on spectral comparisons with known discorhabdins. Compared to the ring system found in dihydro-discorhabdin C, the structures of **2.3** – **2.5** possess a further heterocyclic ring to give six interlocking rings (four heterocyclic and one spiro) which forms the basis of a discorhabdin D type skeleton.

2.2.3 Structure elucidation of pyrroloiminoquinone metabolites from *T. pedunculata*

a) 14-bromo-discorhabdin C (**1.51**) and 14-bromo-3-dihydro-discorhabdin C (**1.52**)

**1.51****1.52**

HRFABMS analyses of the TFA salts of **1.51** (22.7 mg, 0.02% yield) and **1.52** (18.7 mg, 0.02% yield) provided molecular formulae of $C_{18}H_{14}N_3O_2^{79}Br_3$ and $C_{18}H_{16}N_3O_2^{79}Br_3$, respectively.⁴¹ The basic skeleton of discorhabdin C was evident from the 1H and ^{13}C NMR data for both **1.51** and **1.52**,⁴¹ and the proton and carbon resonances were found to be consistent with those values published by Hooper *et al.*⁴¹ The 1H NMR spectrum of **1.51** is deceptively simple, showing only four methylene signals, one olefinic methine signal representing two protons, in addition to the three exchangeable NH protons. The absence of the H-14 signal in the 1H NMR spectrum, usually present at around δ 7 ppm (e.g. **1.53**), together with the ^{13}C shift obtained for C-14 (δ_C 112.4), placed the third bromine atom at C-14. The ^{13}C NMR data for **1.51** showed the characteristic presence of two α,β -unsaturated ketone carbonyls corresponding to C-3 (δ 171.2) and C-11 (δ 164.3).

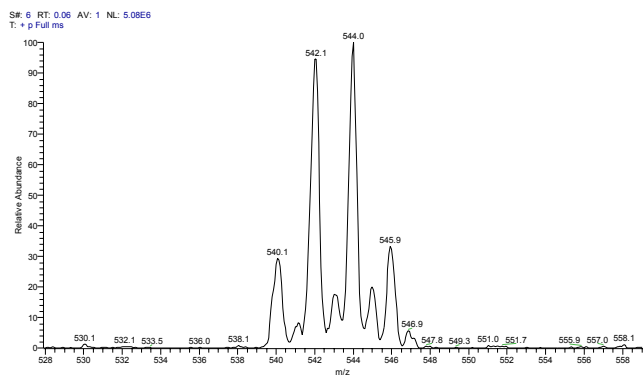


Figure 2.3 The $M + 1$ ion isotopic cluster from the LC-MS spectrum of **1.51** clearly showing the presence of three bromine atoms.

LC-MS is an ideal, quick and an exceptionally powerful analytical method because of this technique's ability to achieve extremely low detection limits and to discriminate between peaks that co-elute during HPLC. LC-MS is therefore used extensively in the pharmaceutical industry for drug identification, metabolite profiling and identification, screening and quantitation.⁹⁴ Many drugs contain basic nitrogen atoms which may be manipulated by protonation in the electrospray process and are therefore easily detected. An added advantage of LC-MS is that detailed structural information can also be obtained using MS-MS techniques. The atmospheric ionisation (API) sources that may be used include Atmospheric Pressure Chemical Ionisation (APCI) and Electrospray Chemical Ionisation (ESI) sources. Both sources utilise a "soft" ionisation technique which means that the molecular ion of a particular sample (unless the compound is extremely unstable) will remain intact. The isotopic ion cluster of the intact molecular ion in multi-halogenated compounds e.g. the pyrroloiminoquinone metabolites from *Latrunculid* sponges, is particularly useful in providing initial information about the degree and type of halogenation in the molecule. The isotopic ion cluster for the $M+1$ ion of the tribrominated **1.51** is reproduced in Figure 2.3.

A Finnigan Mat LCQ system fitted with an ion trap analyser was used to obtain the low resolution molecular ion data in this thesis research. Although ionisation of the pyrroloiminoquinones was easily achieved with both sources, the ESI source was chosen over APCI because of the general absence of background noise (APCI sources employ a vaporiser which from experience often leads to the deposition of carbon based material in the source and consequently background noise). During the isolation of the discorhabdins, TFA was used in the HPLC mobile phase to improve the resolution of the peaks obtained during chromatography. Unfortunately, the presence of TFA in the mobile phase unexpectedly proved problematic during LC-MS analyses. The TFA was observed to produce multiply charged ion clusters from approximately 500 to 1200 amu which, although this does not normally interfere with the molecular ions typically observed for halogenated pyrroloiminoquinones, leads to a large amount of background noise and the total ion

chromatograms (TIC) thus obtained were therefore often disappointing. Not surprisingly, the manufacturers (Finnigan Mat) do not recommend the use of TFA in the LCQ system.⁹⁵ Consequently, to avoid problems associated with TFA in the HPLC mobile phase, the HPLC separations of the pyrroloiminoquinone metabolites were performed independently. The TFA containing HPLC eluent was removed from the HPLC fractions and the purified metabolites reconstituted in methanol to provide solutions with concentrations of approximately 100 $\mu\text{g/mL}$. Aliquots (20 μL) of each solution were introduced into the LC-MS source by standard direct injections techniques. After exhaustive attempts to optimise the ESI conditions the following settings were employed to record the mass spectra to give maximum sensitivity for pyrroloiminoquinone metabolites (after tuning); positive ion mode, capillary temperature 200 $^{\circ}\text{C}$, capillary voltage 7.0 V, discharge voltage 4.5 kV, tube lens offset -60.0 V, discharge current 50 μA , octapole 1 offset -5.8 V, octapole 2 offset -7.5 V, interoctapole lens -58.0 V, with the sheath and auxiliary gases set to 30 and 0 arbitrary units.

The ^1H NMR spectrum of **1.52** also revealed the absence of the H-14 signal, while an extra oxymethine singlet signal (H-3, δ 4.68) was observed. The ^{13}C NMR data for **1.52** once again indicated that a bromine atom resided at C-14 (δ 112.1) and a signal corresponding to δ 70.8 for C-3 (which implicates a hydroxyl group functionality on C-3) was observed. The analogous chemical shift for C-3 in **1.51** is δ 171.2. Not unexpectedly an energy minimised three-dimensional model of compound **1.52** shows that the spiro ring lies perpendicular to the plane of the rest of the molecule (Figure 2.4).

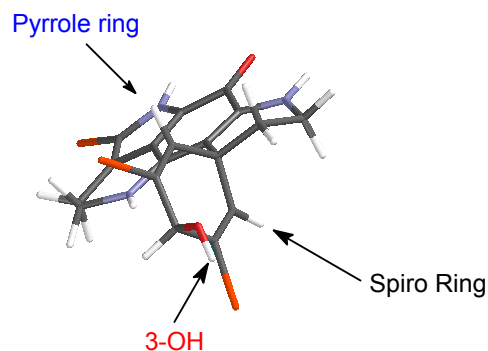
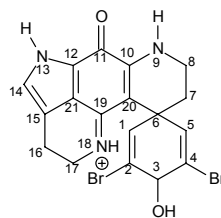
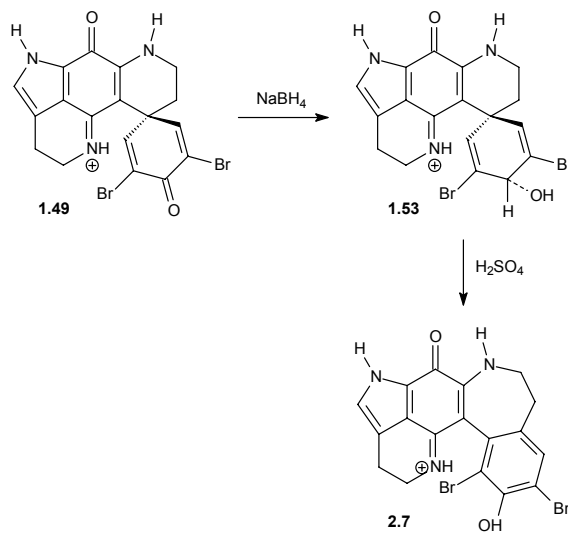


Figure 2.4 A three-dimensional model of 14-bromo-3-dihydro-disorhabdin C (**1.52**). (Spartan '02, Wavefunction, Inc., CA, USA. A semi-empirical force field was used to convert the 2D structures to 3D models).

b) 3-dihydro-discorhabdin C (**1.53**)**1.53**

The known compound **1.53** was previously isolated and characterised from another Alga Bay Latrunculid sponge (*Strongyloidesma coetzei*).⁴² Interestingly, Blunt *et al.*⁴⁴ synthesised **1.53** from discorhabdin C (**1.49**) *via* reduction with NaBH₄ as part of a synthetic programme to gain access to 1H-azepine analogues of discorhabdin C (**2.7**).⁴⁴ Compounds **1.53** and **2.7** were far less active *in vitro* against the P-388 murine leukaemia cell line (IC₅₀ 530 and 3050 ng/mL) than **1.49** (IC₅₀ 40 ng/mL). Our data for **1.53** matched those reported by Beukes⁴² and Blunt *et al.*⁴⁴

**Scheme 2.2** Blunt *et al.*'s synthetic modification of the discorhabdin skeleton.⁴⁴

Compound **1.53** (90.4 mg, 0.09 % yield) showed a molecular ion peak at m/z 464.9688 ($M+1$: Δ +0.1 mmu) in the HRFABMS analyses corresponding to a molecular formula of C₁₈H₁₇N₃O₂⁷⁹Br₂. The ¹H and ¹³C NMR spectra also indicated a basic discorhabdin C type skeleton with the proton NMR spectra showing eight non-exchangeable and four exchangeable sets of protons. The ¹³C NMR spectrum showed resonances corresponding to all eighteen carbons and a DEPT experiment confirmed that the eleven non-exchangeable protons were attached to carbons. Deshielded proton signals corresponding to H-3 (δ 4.60) and H-14 (δ 7.40) were observed in the ¹H NMR spectrum, with the oxymethine and vinylic ¹³C carbon chemical shifts at δ 69.2 and 127.4

in agreement with the presence of a hydroxyl group at C-3 and the absence of a bromine at C-14 (compared to the analogous chemical shifts obtained for **1.51** and **1.52**). The NMR data obtained for this compound is consistent with the literature values.^{42,44} Figure 2.5 shows the M + 1 isotope ion cluster in the LC-MS spectrum of **1.53** indicative of a compound containing two bromine atoms.

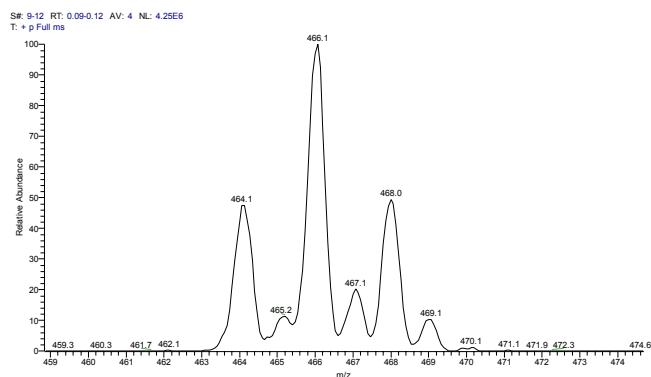
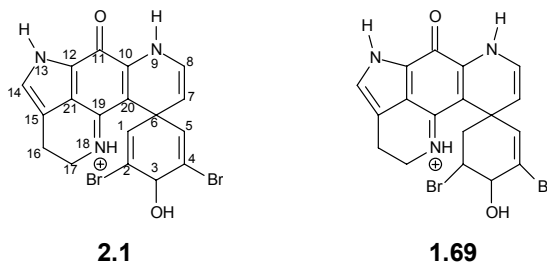


Figure 2.5 The M + 1 ion isotopic cluster in the LC-MS spectrum of **1.53** clearly showing the presence of two bromine atoms.

c) *7,8-dehydro-3-dihydro-discorhabdin C (2.1)*



To establish the structure of **2.1** (1.2 mg, 0.001 % yield), the available NMR data was compared to that of **1.53**. The molecular formula $C_{18}H_{15}N_3O_2^{79}Br_2$ for **2.1** was determined by HRFABMS (m/z 462.9532, M+1; Δ -0.1 mmu). The 1H NMR spectrum showed seven non-exchangeable and four exchangeable sets of protons, and was relatively simple showing three deshielded sp^2 methine signals at δ 7.37 (s, H-14), 6.64 (s, H-1 and H-5), and 6.33 (dd, J = 4.3, 7.6 Hz, H-8), another deshielded vinylic resonance δ 4.72 (d, J = 7.6 Hz, H-7) and an oxymethine resonance at δ 4.55 (s, H-3). Three of the four exchangeable protons at δ 13.23 (br s), 10.59 (br s) and 8.31 (br s) were assigned as NH-13, NH-9 and NH-18 respectively, by analogy with the 1H NMR data of known compounds e.g. **1.51**,⁴¹ **1.52**,⁴¹ **1.53**,⁴² and **1.69**.⁵² The ^{13}C NMR spectrum revealed fourteen carbon signals and a DEPT experiment confirmed the presence of eight protonated carbons as shown in Table 2.1. The quaternary carbon chemical shifts for C-2, C-4, C-6, C-10, C-11, C-12, C-14, C-15, C-19, C-20 and C-21 were assigned initially by analogy to related

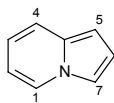
compounds.^{42,52} The characteristic ^{13}C shift of C-16, together with the COSY and HMBC correlations obtained for **2.1**, enabled C-16 and C-17 and their methylene protons to be assigned. The two and three bond HMBC correlations from H₂-16 and H₂-17 to their surrounding carbon atoms confirmed the chemical shifts of the quaternary carbons C-14, C-15, C-19 and C-21. An HMQC experiment linked the two sp² methine protons at δ 4.72 (H-7) and 6.33 (H-8) to carbons δ 112.5 and 122.2, respectively, implying the presence of a double bond between C-7 and C-8. The position of the olefin was confirmed by the $J_{7,8}$ coupling constant (7.6 Hz) and the COSY correlations from H-8 to H-7 and NH-9. The third sp² methine proton (δ 7.37), which showed a COSY correlation to NH-13, was thus assigned to H-14, in accordance with published values.^{42,52} Epinardin C⁵² (**1.69**) differs from the structure proposed for **2.1**, in that it lacks a Δ^1 olefin. This difference probably accounts for the differences in the C-7 chemical shifts observed for **2.1** (δ 112.5) and (**1.69**) (δ 105.5). The fully assigned NMR spectral data for **2.1** is presented in Table 2.1.

Table 2.1 NMR (DMSO-d₆, 400 MHz for ^1H and 100 MHz for ^{13}C) data for compound **2.1**.

Atom No.	δ_{C}	δ_{H} (mult, J, Hz)	COSY	HMBC
C1	132.1 (d)	6.64 (s), 1H	H-8 (5J)	C2, C3, C4, C5, C6
C2	122.2 (s)			
C3	68.7 (d)	4.55 (s), 1H	-	C1, C2, C4, C5
C4	122.2 (s)			
C5	132.1 (d)	6.64 (s), 1H	H-8 (5J)	C2, C3, C4, C5, C6
C6	45.4 (s)			
C7	112.5 (d)	4.72 (d), 1H, 7.6 Hz	H-8	-
C8	122.2 (d)	6.33 (dd), 1H, 4.3, 7.6 Hz	H1/H5 (5J), H-7, NH-9	-
NH-9	-	10.59 (br s), 1H	H-8	-
C10	-			
C11	-			
C12	122.5 (s)			
NH-13		13.23 (br s), 1H	H-14	-
C14	126.2 (d)	7.37 (s), 1H	NH-13	C12/C21
C15	119.5 (s)			
C16	17.7 (t)	2.88 (t), 2H, 7.6 Hz	H-17	C15, C17
C17	44.0 (t)	3.82 (t), 2H, 7.6 Hz	H-16, NH-18	C15, C16, C19
NH-18	-	8.31 (br s), 1H		-
C19	158.0 (s)			
C20	-			
C21	-			

⁵J = five bond long range COSY coupling.

Of interest to note in Table 2.1 are the long range (5J) COSY couplings which are common in discorhabdins. Long range proton proton couplings ($^5J \leq 1\text{Hz}$) are particularly prevalent when the coupling path contains one or more sp² carbons e.g. indolazine (**2.8**).⁹⁶

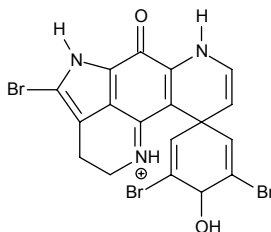
**2.8**

$J_{1-3} = 1.1 \text{ Hz}$

$J_{1-4} = 1.2 \text{ Hz}$

$J_{1-5} = 0.9 \text{ Hz}$

$J_{4-7} = 0.7 \text{ Hz}$

d) 14-bromo-7,8-dehydro-3-dihydro-discorhabdin C (**2.2**)**2.2**

Compound **2.2** (7.7 mg, 0.007 % yield) gave a molecular ion at m/z 540.8635 ($\Delta +0.1$ mmu) in its HRFABMS spectrum, which is consistent with the molecular formula $C_{18}H_{14}N_3O_2^{79}Br_3$. The 1H NMR spectrum of **2.2** was relatively simple and, upon comparison with the proton spectrum of compound **2.1**, the only difference noted was the disappearance of the H-14 proton signal at around δ 7.3 again implying the presence of a bromine atom at C-14. Bromination at C-14 was confirmed by the carbon chemical shift of C-14 (δ 111.6). Two olefinic sp^2 methine signals at δ 6.52 (s, H-1 and H-5) and 6.25 (dd, $J = 4.8, 7.3$ Hz, H-8) and another two deshielded methine signals at δ 4.82 (d, $J = 7.3$ Hz, H-7) and 4.59 (s, H-3) were observed in the 1H NMR spectrum of **2.2**. The 1H NMR spectrum also showed three exchangeable protons at δ 14.13 (br s), 10.64 (br s) and 8.62 (br s) that correspond to NH-13, NH-9 and NH-18 respectively. Data obtained from a DEPT experiment indicated the presence of two methylene groups (δ 44.3 and 17.3), three sp^2 methine groups at δ 133.9 (overlapped), 122.5 and 114.6, one sp^3 methine group at δ 71.0. The HMQC data established that the deshielded methine signals at δ 4.82 and 4.59 resided on carbons resonating at δ 114.6 (C-7) and 71.0 (C-3) respectively, while the vinylic methine protons were attached to carbons at δ 133.9 (C-1 / C-5) and 122.5 (C-8). Consequently, the presence of a double bond between C-7 and C-8 was again suggested and confirmed through the observation of COSY correlations between H-8 and H-7 and between H-8 and NH-9. Even though apparently adequate amounts of **2.2** were obtained (7.7 mg) for NMR analyses, four of the eleven quaternary (and one sp^2 methine carbon signal) carbons were not observed in the ^{13}C NMR spectrum. In order to compensate for the possible longer T_1 relaxation times of these missing quaternary carbons, the relevant NMR delay time (d1) parameter was varied (1.0 and 1.5 s) and numerous scans acquired (18 000 - 31 000). Frustratingly, the four quaternary carbons remained undetected and we therefore elected to exploit the sensitivity of more sensitive inverse detection techniques, such as HMBC correlations, to yield the missing carbon data. After assigning the nearby protons *via* COSY and / or HMQC correlations, the protons were used to identify the surrounding quaternary carbon chemical shifts e.g. HMBC correlations from H-1, H-5 and H-8 were used to

identify the carbon chemical shift of C-6 (δ 44.7). Likewise, the HMBC correlations from the H-8, NH-9 and H₂-16 protons were used to identify the carbon chemical shifts of C-10 (δ 144.2), C-20 (δ 97.3) and C-14 (δ 111.6). (The HMQC data provided the carbon chemical shift for C-7 at δ 114.6).

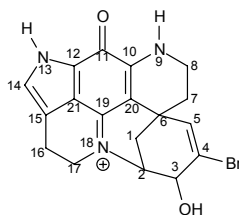
Table 2.2 NMR (DMSO-d₆, 400 MHz for ¹H and 100 MHz for ¹³C) data for compound **2.2**.

Atom No.	δ_c	δ_H (mult, J, Hz)	COSY	HMBC
C1	133.9 (d)	6.52 (s), 2H	H-7 (⁴ J)	C2, C3, C4, C5, C6,* C20*
C2	124.5 (s)			
C3	71.0 (d)	4.59 (s), 1H	-	C1, C2, C4, C5
C4	124.5 (s)			
C5	133.9 (d)	6.52 (s), 2H	H-7 (⁴ J)	C1, C2, C3, C4, C6,* C20*
C6	44.7* (s)			
C7	114.6* (d)	4.82 (d), 1H, 7.3 Hz	H-8	-
C8	122.5 (d)	6.25 (dd), 1H, 4.8, 7.3 Hz	H-7, NH-9	C6,* C10*
NH-9	-	10.64 (s), 1H	H-8	C20,* C11
C10	144.2* (s)			
C11	165.2 (s)			
C12	122.4 (s)			
NH-13		14.13 (br s), 1H	-	-
C14	111.6* (s)			
C15	119.1 (s)			
C16	17.3 (t)	2.78 (t), 2H, 7.6 Hz	H-17	C14,* C15, C17, C21
C17	44.3* (t)	3.90 (t), 2H, 7.6 Hz	H-16, NH-18	C15, C16, C19
NH-18	-	8.62 (s), 1H	H-17	C21
C19	156.4 (s)			
C20	97.3* (s)			
C21	122.6 (s)			

*Note: Chemical shifts of ¹³C resonances obtained from HMQC or HMBC data.

⁴J = four bond long range COSY correlation.

e) *Discorhabdin S* (**2.3**)



2.3

High resolution FABMS established a molecular formula of $C_{18}H_{18}N_3O_2^{79}Br$ (m/z 387.0582; $M+1$; Δ -0.1 mmu) for **2.3** (4.4 mg, 0.004 % yield). The 1H NMR spectrum (Figure 2.6) indicated thirteen non-exchangeable and two exchangeable sets of protons. Well-resolved resonances for seventeen carbons were observed in the ^{13}C NMR spectrum. The DEPT NMR experiment disclosed the presence of five methylene signals (δ 19.2, 29.1, 34.6, 37.7 and 52.7), two sp^3 methines (δ 60.6 and 70.5), two sp^2 methines (δ 126.5 and 136.6), seven sp^2 quaternary carbons (δ 96.6, 118.0, 122.6, 122.8, 126.4, 146.4 and 150.0), together with an α,β -unsaturated ketone (δ 166.7), accounting for all, except one, of the carbons of **2.3**. Despite varying the ^{13}C NMR acquisition parameters as described previously, the quaternary spiro C-6 signal was not observed. Unfortunately, a relative paucity of HMBC data prevented the assignment of the C-6 chemical shift *via* correlations from surrounding protons.

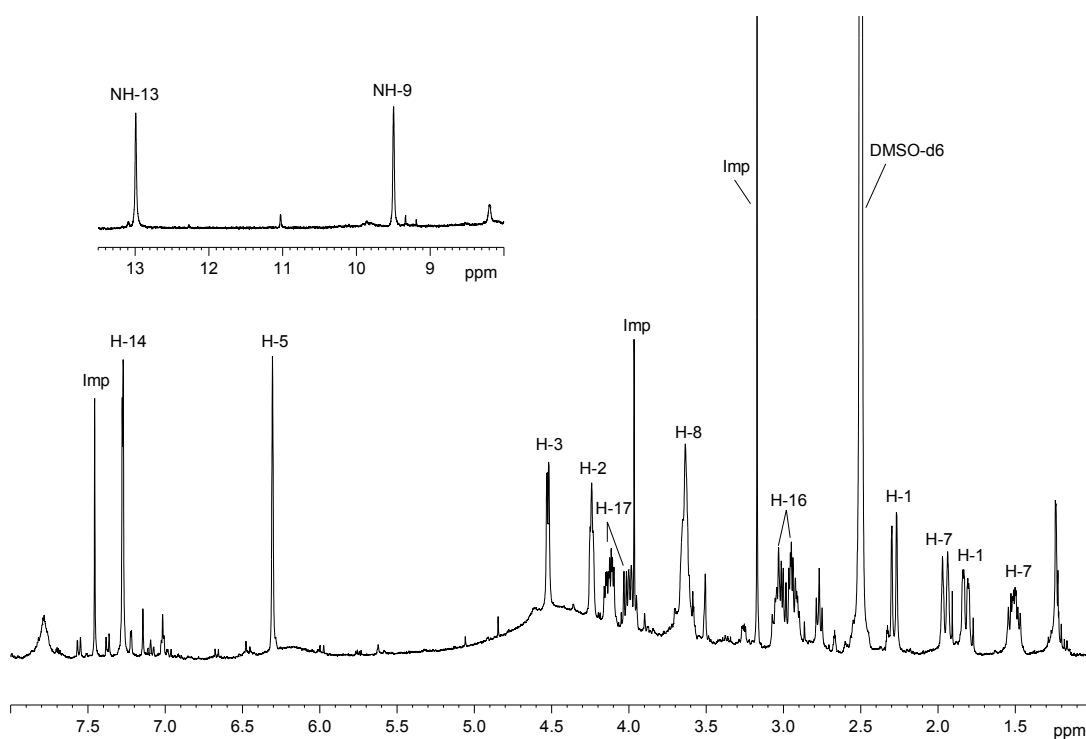


Figure 2.6 The fully assigned 1H NMR spectrum of **2.3** (400 MHz, $DMSO-d_6$) with the signals for the two NH protons offset. (Imp = impurity).

The olefinic proton at δ 7.28 (d, J = 2.5 Hz, H-14) was shown by an HMQC experiment (Figure 2.7) to reside on a carbon at δ 126.5 and displayed strong HMBC correlations to C-15 and C-21. The two pairs of diastereotopic methylene protons at δ 3.03 (m, H-16b) and 2.93 (m, H-16a), and δ 4.14 (m, H-17b) and 3.99 (m, H-17a) were attached to carbons at δ 19.2 and δ 52.7, respectively. The H_{2-16} and H_{2-17} methylene protons were also shown to be vicinally coupled in a COSY experiment. Typical HMBC correlations were observed from H_{2-16} and H_{2-17} to two groups of carbon atoms δ 118.0 (C-15), 52.7 (C-17) and 122.6 (C-21) and 118.0 (C-15), 19.2 (C-

16) and 150.0 (C-19), respectively. An HMQC experiment also established that the methylene protons at δ 3.64 ppm (m, H₂-8) were attached to the carbon at δ 37.7; the pair of diastereotopic methylene protons at δ 1.95 (d, J = 13.4 Hz, H-7b) and 1.51 (m, H-7a) resided on a carbon at δ 29.1; and that the olefinic proton at δ 6.31 (s, H-5) was attached to the carbon at δ 136.6. A COSY experiment established that the H₂-8 methylene group was vicinally coupled to the H₂-7 methylene protons.

The HMQC experiment also positioned the diastereotopic methylene protons at δ 2.28 (d, J = 13.1 Hz, H-1b) and δ 1.82 (dd, J = 2.3, 13.1 Hz, H-1a) on C-1 (δ 34.6), and revealed that the methine protons at δ 4.24 (dd, J = 3.8, 5.3 Hz, H-2) and 4.53 (d, J = 5.3 Hz, H-3) resided on carbons at δ 60.6 (C-2) and δ 70.5 (C-3), respectively. The COSY experiment confirmed that the sp³ methine proton H-2 was coupled to the methylene protons H₂-1. The HMBC data (Table 2.3) showed that H₂-7 correlated to the carbons at δ 136.6 (C-5), 37.7 (C-8) and 96.6 (C-20) and that H₂-1 correlated to carbons at δ 60.6 (C-2), 70.5 (C-3), 136.6 (C-5) and 96.5 (C-20). The carbon resonance at δ 70.5 was assigned as C-3 on the basis of the COSY and HMBC correlations from H-2. HMBC correlations from H₂-1 and H-5 to C-2, C-3, C-5, C-20 and C-1, C-3, C-4, C-7 respectively confirmed the structure of the spiro ring and confirmed that H₂-1 and H-5 reside on opposite sides of the ring. Additional HMBC correlations (Figure 2.8) from H-2 to C-1, C-3, C-4 and especially to C-17 implied the basic structure of a discorhabdin D (**1.61**) type skeleton.

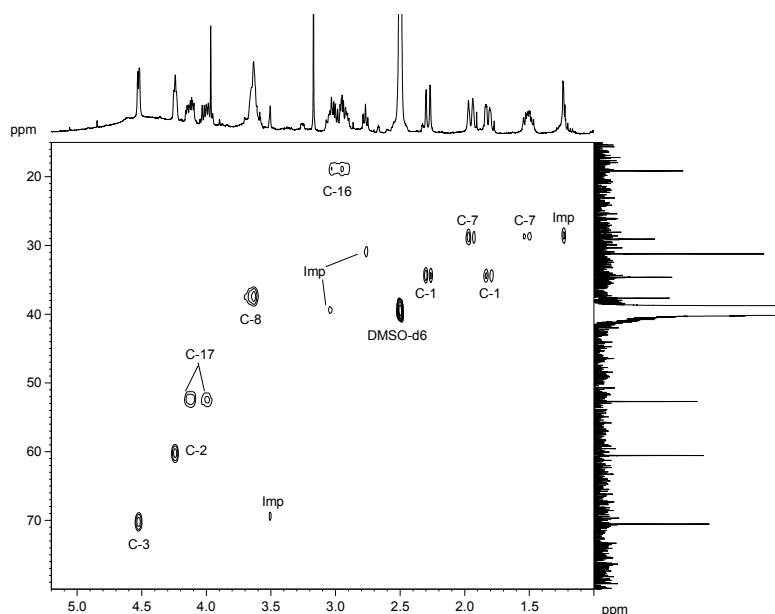


Figure 2.7 A section (F1 = δ 15 – 80 ppm, F2 = δ 1.0 – 5.2 ppm) of the HMQC spectrum of compound **2.3** (400/100 MHz, DMSO-d₆). (Imp = impurity).

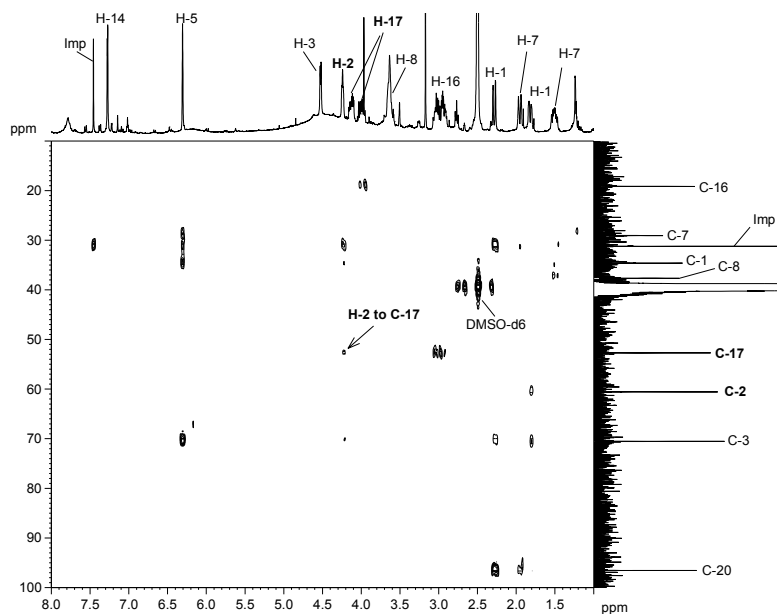
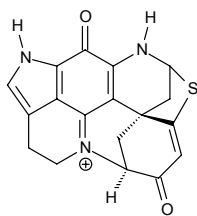
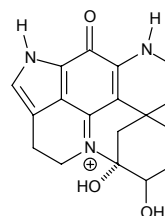


Figure 2.8 A section ($F1 = \delta 10 - 100$ ppm, $F2 = \delta 1.0 - 8.0$ ppm) of the HMBC spectrum of compound **2.3** (400/100 MHz, DMSO- d_6). (Imp = impurity).



1.61



1.67

Initial evidence for a discorhabdin D (**1.61**) type heptacyclic structure followed from the absence of the NH-18 signal in the ^1H NMR spectrum of **2.3**. This resonance is conspicuous in the ^1H NMR spectra of compounds **1.51** – **1.53**, **2.1** and **2.2** occurring between $\delta 7.8 - 8.5$ and is easily identifiable from a COSY correlation with the methylene protons (H_2 -17). Conclusive evidence for the bond between N-18 and C-2 was provided firstly by the approximate 10 ppm downfield shift of the C-17 resonance (*cf.* compounds **1.51** – **1.53**, **2.1** and **2.2**) and the three bond HMBC correlation between H-2 and C-17 (Figure 2.8).

A model proved (Figure 2.9) to be particularly helpful in assessing the possible stereochemistry at C-3, assuming a similar relative stereochemistry to discorhabdin D⁴⁸ (**1.61**) and epinardin A (**1.67**).⁵² A geminal coupling constant of 13.1 Hz was observed for the protons at position 1 while the vicinal coupling between the H-2 and H-3 protons ($J_{2,3} = 5.3$ Hz) was consistent with a possible axial-equatorial arrangement of these two protons. From the modified Karplus equation, if both H-1a and H-1b are *quasi*-equatorial relative to H-2 (*i.e.* have the same bond angle $\sim 60^\circ$) the resultant coupling will be very small (~ 1 Hz).

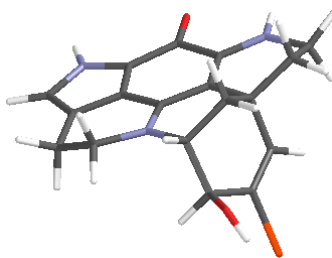


Figure 2.9 A three dimensional model of **2.3** clearly showing a possible *quasi*-diequatorial arrangement of the two H₂-1 protons relative to H-2. The 2S,* 6R* relative stereochemistry of discorhabdin D (**1.61**) is arbitrarily adopted. (Spartan '02, Wavefunction, Inc., CA, USA. A semi empirical forcefield was used to generate the 3D molecular structure).

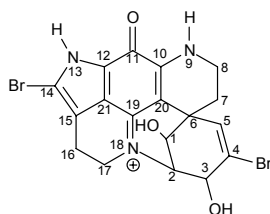
Table 2.3 NMR (DMSO-d₆, 400 MHz for ¹H and 100 MHz for ¹³C) data for compound **2.3**.

Atom No.	δ_c	δ_H (mult, J, Hz)	COSY	HMBC
C1	34.6 (t)	1.82 (dd), 1H, 2.3, 13.1 Hz 2.28 (d), 1H, 13.1 Hz	H-1	C2, C3, C5 C3, C20
C2	60.6 (d)	4.24 (dd), 1H, 3.8, 5.3 Hz	H-1	C1, C3, C4, C17
C3	70.5 (d)	4.53 (d), 1H, 5.3 Hz	H-5	C4, C5
C4	126.4 (s)	-	-	-
C5	136.6 (d)	6.31 (s), 1H	H-3, H-1b	C1, C3, C4, C7
C6	-*			
C7	29.1 (t)	1.51 (m), 1H 1.95 (d), 1H, 13.4 Hz	H-7, H-8	C5, C20, C8 C5, C8
C8	37.7 (t)	3.64 (m), 1H	H-7	-
NH-9	-	9.50 (s), 1H	H-8	-
C10	146.4 (s)			
C11	166.7 (s)			
C12	122.8 (s)			
NH-13	-	12.99 (s), 1H	H-14	C14, C15
C14	126.5 (d)	7.28 (d), 1H, 2.5 Hz	NH-13	C15, C21
C15	118.0 (s)		-	-
C16	19.2 (t)	2.93 (m), 1H 3.03 (m), 1H	H-17	C15, C17, C21 C15, C17
C17	52.7 (t)	3.99 (m), 1H 4.14 (m), 1H	H-16 H-16	C15, C16, C19 C15, C16, C19
NH-18	-	-	-	-
C19	150.0 (s)		-	-
C20	96.6 (s)		-	-
C21	122.6 (s)		-	-

* ³C resonance not seen in ¹³C and HMBC data.

Although compound **2.3** could possibly be referred to as 3-dihydro-4-bromo-dethiadiscorhabdin D, in accordance with the general trends in discorhabdin nomenclature compound **2.3** is sufficiently different to discorhabdin D to warrant its own name and was accordingly given the next available alphabetical letter in the discorhabdin series and named discorhabdin S.

f) 14-bromo-1-hydroxy-discorhabdin S (**2.4**)



2.4

Based on the NMR data, compound **2.4** (4.2 mg, 0.004% yield) was proposed as having a similar structure to that of **2.3** differing only in the addition of a hydroxyl group at C-1 and a bromine atom at C-14. Compound **2.4** gave a M+1 ion at m/z 480.9638 ($\Delta +0.1$ mmu) by HRFABMS analysis, consistent with the molecular formula $C_{18}H_{17}N_3O_3^{79}Br_2$.

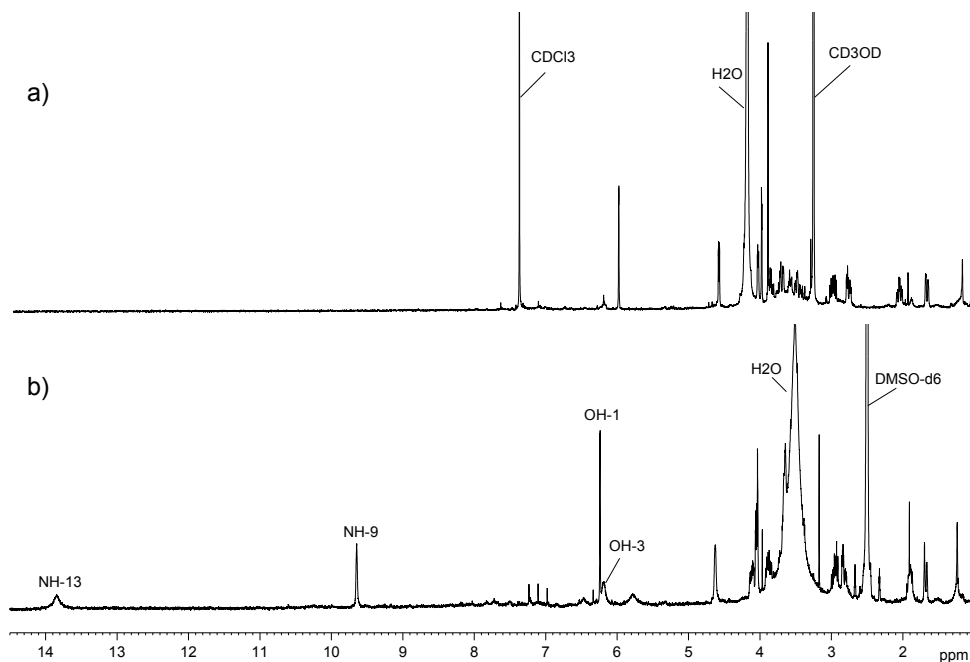


Figure 2.10 1H NMR spectra for **2.4** (400 MHz) obtained in a) $CD_3OD/CDCl_3$ mix and b) $DMSO-d_6$.

The proton NMR spectra (Figure 2.10) indicated twelve non-exchangeable and four exchangeable protons. Well-resolved resonances for sixteen of the eighteen carbon signals were observed in the ^{13}C NMR spectrum. Unfortunately, the ^{13}C resonances for the two adjacent quaternary carbons C-12 and C-21 were not seen in the ^{13}C NMR spectrum of **2.4** and could not be resolved indirectly through HMBC correlations from surrounding protons. The DEPT data revealed the presence of four methylene signals (δ 18.7, 23.9, 37.8 and 53.0), three sp^3 methines (δ 65.4, 66.5 and 70.5), one sp^2 methine (δ 134.8); and one sp^3 (δ 36.8) and six sp^2 quaternary carbons (δ 94.0, 118.1, 123.1, 126.2, 148.3 and 148.9), and an α,β -unsaturated ketone (δ 165.5), thus accounting for sixteen of the carbon resonances observed in the ^{13}C NMR spectrum of **2.4**.

Table 2.4 NMR (DMSO- d_6 , 400 MHz for ^1H and 100 MHz for ^{13}C) data for compound **2.4**.

Atom No.	δ_c	δ_H (mult, J, Hz)	COSY	HMBC
C1	65.4 (d)	4.04 (m), 1H	-	C20
C2	66.5 (d)	4.05 (m), 1H	H-3	C1, C3, C4, C17, C19
C3	70.5 (d)	4.63 (s), 1H	H-2, H-5	-
C4	126.2 (s)	-	-	-
C5	134.8 (d)	6.24 (s), 1H	H-3	C1, C3, C4, C6, C7
C6	36.8 (s)	-	-	-
C7	23.9 (t)	1.68 (d), 1H, 13.4 Hz	H-8	C6
		1.90 (m), 1H	H-8	C5, C8
C8	37.8 (t)	3.65 (m), 2H	H-7, NH-9	-
NH-9	-	9.65 (s), 1H	H-8	-
C10	148.3 (s)			
C11	165.5 (s)			
C12	-*			
NH-13	-	13.85 (s), 1H	-	C14, C15
C14	118.1 (s)			
C15	123.1 (s)			
C16	18.7 (t)	2.81 (m), 1H	H-17	C14, C17
		2.95 (m), 1H	H-17	C14, C17
C17	53.0 (t)	3.88 (m), 1H	H-16	-
		4.11 (m), 1H	H-16	-
NH-18	-	-	-	-
C19	148.9 (s)			
C20	94.0 (s)			
C21	-*			
OH-1		6.184 (br s), 1H	-	-
OH-3		5.78 (s), 1H	-	-

*Signals for C-12 and C-21 could not be resolved from the HMBC spectrum.

†Overlapping signals of H-1 and H-2 made it difficult to unequivocally determine the HMBC correlations.

HMQC experiments established that the methine protons at δ 4.05 (m, H-2) were attached to the carbon at δ 66.5, while the two remaining sp^3 methine protons, at δ 4.04 (m, H-1) and 4.63 (s, H-3), resided on the carbons at δ 65.4 and 70.5 respectively. COSY correlations were observed between H-2 and H-3 and the ^{13}C chemical shifts observed for C-2 and C-3 were similar to those observed in **2.3**, while the downfield shift of C-1 from δ 34.6 to 65.4 indicated the possible presence of a hydroxyl group at this carbon. The substitution of a secondary alcohol functionality at C-1 was also consistent with the requirements of the molecular formula. Again, the signal corresponding to NH-18 in the 1H NMR spectrum of **2.4** was absent, while the C-17 signal, observed to be approximately 10 ppm further downfield (when compared to the known compounds **1.51** – **1.53**), confirmed that **2.3** and **2.4** shared the same basic skeleton. In accordance with the NMR data of **2.3**, the chemical shifts of C-2, C-3, C-4 and C-17 (Table 2.4) confirmed the structure of the spiro ring and allowed the formation of the additional ring through a bond between N-18 and C-2. Further confirmation of the hexacyclic structure of **2.4** came from the HMBC correlation between H-2 and C-17. No COSY correlations were observed between NH-13 and H-14 suggesting, together with the carbon chemical shift observed for C-14 (δ 118.1) (*cf.* C-14 in **1.51** has a carbon shift of δ 112.4), that a bromine atom was attached at C-14. HMBC correlations between H-5 and C-1, C-3, C-4, C-6 and C-7, and between H-2 and C-1, C-3, C-4, C-17 and C-19 contributed significantly to the structure proposed for **2.4**.

g) *1-bromo-2-hydroxy-disorhabdin S (2.5)*

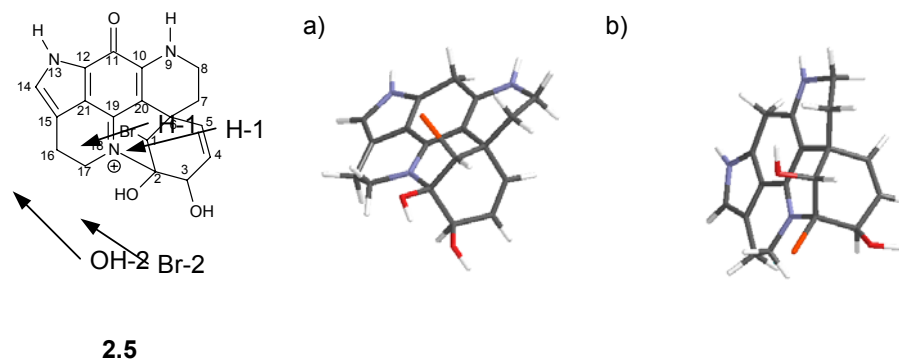


Figure 2.11 A three dimensional model of **2.5** clearly showing that bromination is possible at both positions 1 and 2. (Spartan '02, Wavefunction, Inc., CA, USA. A semi empirical forcefield was used to generate the 3D molecular structure).

The molecular formula $C_{18}H_{18}N_3O_3^{79}Br$ for compound **2.5** (2.6 mg, 0.003 % yield) was determined by HRFABMS (m/z 403.0532, $M + 1$). Compound **2.5** (Figure 2.11) is structurally similar to compounds **2.3** and **2.4** from the available NMR data. The proton NMR spectra (Figure 2.12) showed eleven non-exchangeable and four exchangeable sets of protons. Once again, a proton chemical shift normally attributed to NH-18 was absent. The ^{13}C NMR spectrum (Figure 2.13)

showed seventeen well resolved carbon signals with a DEPT experiment confirming the presence of nine protonated carbons. The DEPT data also revealed four methylene signals (δ 19.4, 27.8, 37.7 and 42.7), two sp^3 methines (δ 59.5 and 66.8), three sp^2 methine signals (δ 124.9, 126.9, 131.4); and one sp^3 (δ 87.8) and six sp^2 quaternary carbons (δ 94.7, 118.6, 122.4, 123.0, 148.3 and 148.7), and an α,β -unsaturated ketone (δ 166.0), thus accounting for the seventeen carbons observed in the ^{13}C NMR spectrum of **2.5**. The ^{13}C signal of the spiro carbon C-6 was again not observed. The ^1H and ^{13}C signals for compound **2.5** were assigned from COSY, HMQC and HMBC correlations in the usual manner. The quaternary carbon chemical shifts of the pyrroloiminoquinone skeleton for C-10, C-11, C-12, C-19, C-20, C-21 (δ 148.3, 166.0, 123.0, 148.7, 94.7 and 122.4, respectively) were tentatively assigned by analogy to the respective carbon chemical shifts of related compounds (e.g. **1.53**, **1.61**, **2.3**) and confirmed where possible using 2D NMR data (Table 2.5). The chemical shift of H-14, initially assigned from its characteristic ^1H chemical shift (δ 7.29) and later confirmed by HMBC correlations to C-15, C-12/C-21 (the close proximity of the C-12 and C-21 signals made an unequivocal assignment impossible), was assigned to the carbon signal resonating at δ 126.9 from HMQC data. Two of the four methylene carbon signals assigned to C-16 and C-17 (Table 2.5) were initially assigned using the characteristic C-16 chemical shift (δ 19.4) and later confirmed by a combination of COSY and HMQC correlations. The absence of an NH-18 exchangeable proton ($\sim \delta$ 8 ppm) in the ^1H NMR spectrum suggested that **2.5** possessed the same hexacyclic structure as **2.3** and **2.4**.

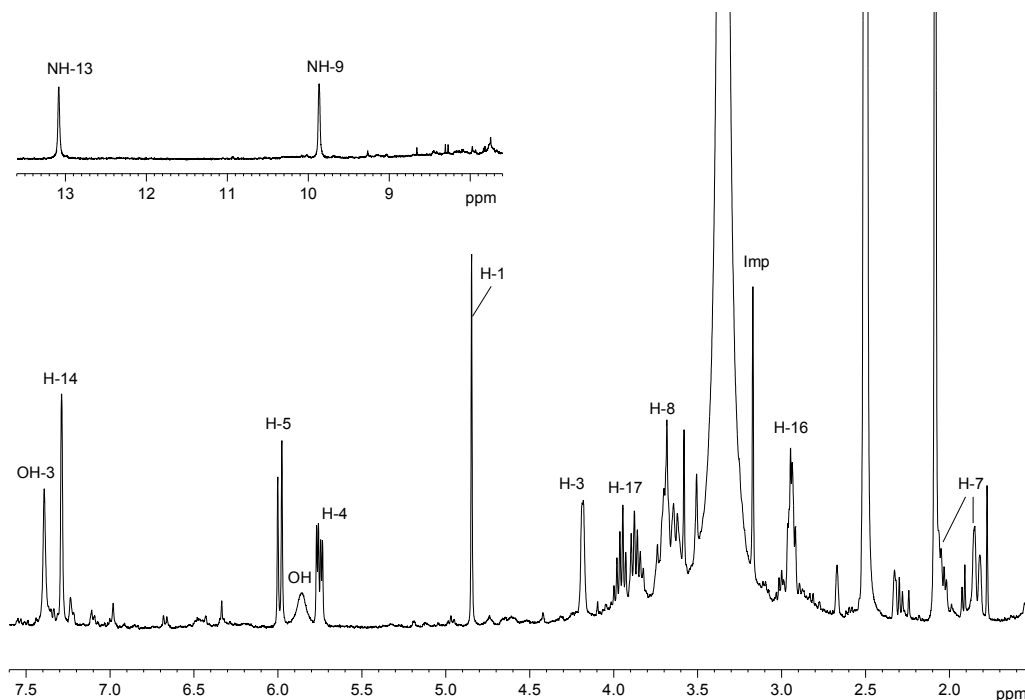


Figure 2.12 ^1H NMR spectrum of **2.5** (400 MHz, DMSO-d_6) with the NH-9 and NH-13 protons offset.

The deshielded carbon chemical shift at δ 66.8 was assigned to C-3, and is consistent with an hydroxyl functionality attached to this carbon. HMQC data placed the oxymethine proton on C-3 (δ_{H} 4.18, δ_{C} 66.8), with the H-3 proton subsequently showing COSY correlations to H-4 and H-5. The fact that the C-3 signal was shifted slightly further upfield than usual (Figure 2.13) indicated the possible presence of a strong electron withdrawing group on a neighbouring carbon *i.e.* either C-2 or C-4. Since C-4 was clearly an sp^2 methine signal, the upfield shift was attributed to the substituent present on C-2 (an sp^3 quaternary carbon). COSY correlations between two of the sp^2 methine signals at δ 5.75 and 5.99 and their subsequent attachment to the carbon signals resonating at δ 124.9 and 131.4 from HMQC data, resulted in the assignment of these signals as C-4 and C-5.

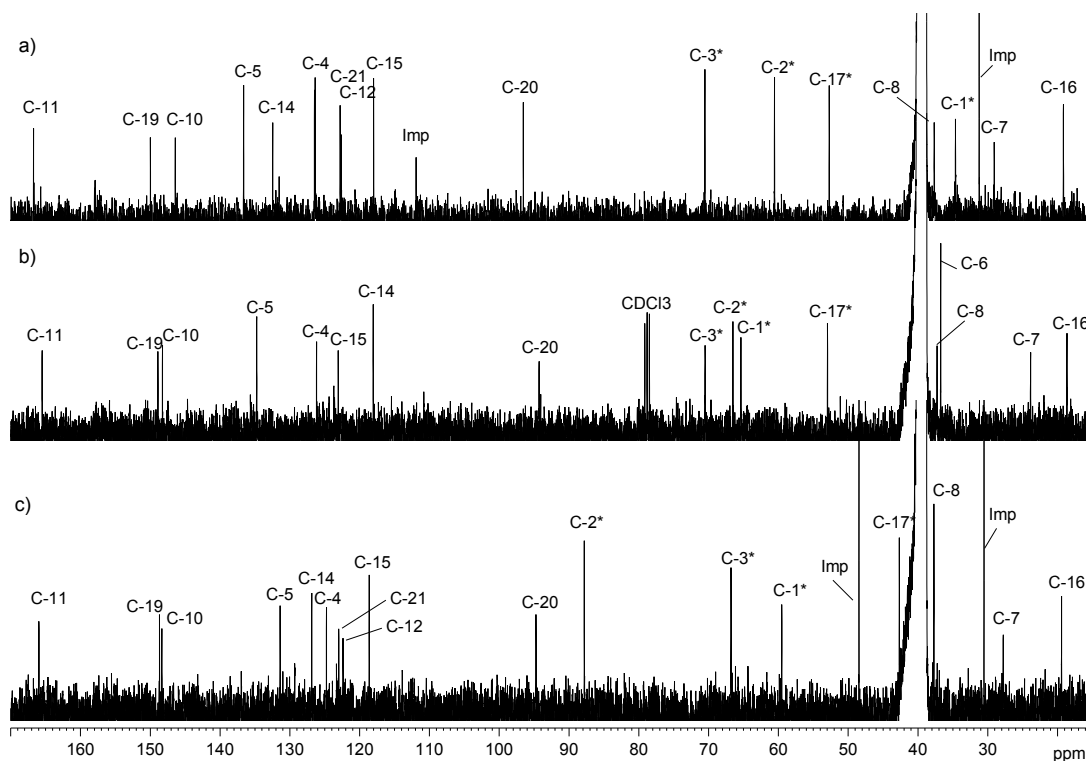
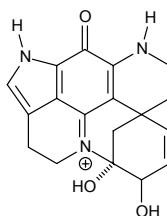


Figure 2.13 Comparison of the ^{13}C NMR spectra (100 MHz, DMSO-d_6) of the structurally similar compounds **2.3** (a), **2.4** (b) and **2.5** (c). *Note the positions of the signals for carbons 1, 2, 3 and 17 (δ 40 – 90 ppm) in particular.

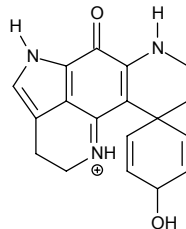
According to the molecular formula, two substituents (a hydroxyl group and a bromine atom) remained to be assigned and could therefore only reside on either C-1 or C-2. C-1 is an sp^3 methine signal and was assigned to the carbon resonance at δ 59.5 (following HMBC correlations observed between H-1 and C-2, C-7, C-8 and C-20, as well as between H-5 and C-1), while C-2 was assigned as an sp^3 quaternary carbon resonating at δ 87.8 (also following HMBC correlations from H-1). Since the carbon shift for C-3 is further upfield than usual, the stronger electron

withdrawing substituent, *i.e.* the hydroxyl group, is tentatively assigned to C-2. This is in agreement with the chemical shift of C-1 at δ 59.5 which implicates a substituent such as bromine at this carbon. In support of this rather unusual structure, d' Ambrosio *et al.* isolated epinardin A⁸ (**1.67**) from an unidentified deep water Antarctic sponge reported the resonance of the C-1 and C-2 signals at δ 44.8 and 89.0 respectively, which may support our C-1 and C-2 assignments for **2.5**.

**1.67****Table 2.5** NMR (DMSO-d₆, 400 MHz for ¹H and 100 MHz for ¹³C) data for compound **2.5**.

Atom No.	δ_c	δ_H (mult, J, Hz)	COSY	HMBC
C1	59.5 (d)	4.85 (s), 1H	-	C2, C7, C8, C20
C2	87.8 (s)			
C3	66.8 (d)	4.18 (d), 1H, 3.0 Hz	H4, H5	-
C4	124.9 (d)	5.75 (dd), 1H, 14.2 Hz	H3, H5	C2, C5, C8
C5	131.4 (d)	5.99 (d), 1H, 9.9 Hz	H3, H4	C1, C3, C7, C8
C6	-*			
C7	27.8 (t)	1.84 (d), 1H, 12.9 Hz	H8	C5, C8
		2.04 (m), 1H	H8	C5, C8
C8	37.7 (t)	3.68 (m), 2H	H7	-
NH-9		9.87 (s), 1H	-	-
C10	148.3 (s)			
C11	166.0 (s)			
C12	123.0 (s)			
NH-13		13.08 (s), 1H	-	-
C14	126.9 (d)	7.29 (s), 1H	-	C15, C12/C21
C15	118.6 (s)			
C16	19.4 (t)	2.94 (m), 2H	H17	C15, C17
C17	42.7 (t)	3.87 (m), 1H	H16	C15, C16, C19
		3.96 (m), 1H	H16	
NH-18		-	-	
C19	148.7 (s)			
C20	94.7 (s)			
C21	122.4 (s)			
OH -1/2		5.86 (s), 1H	-	
OH-3		7.39 (s), 1H	-	

*Signal assumed to be under the DMSO-d₆ solvent peak.

h) 2,4-debromo-3-dihydro-discorhabdin C (**2.6**)**2.6**

Mass spectral analysis of the salt **2.6** (1.2 mg, 0.001 % yield) provided a molecular formula for $C_{18}H_{18}N_3O_2$ (M^+ , m/z 308.1400, Δ +0.1). The proton NMR spectra (Figure 2.14) revealed eight non-exchangeable and four exchangeable sets of protons. A well-resolved ^{13}C NMR spectrum of only a milligram of sample material did not unexpectedly prove difficult to obtain even after 65 000 scans (fortunately, recourse to HMQC and HMBC data provided sufficient information to assign the ^{13}C data) and the structure is thus assigned by comparison with literature values^{42,52} and the available 2D NMR data.

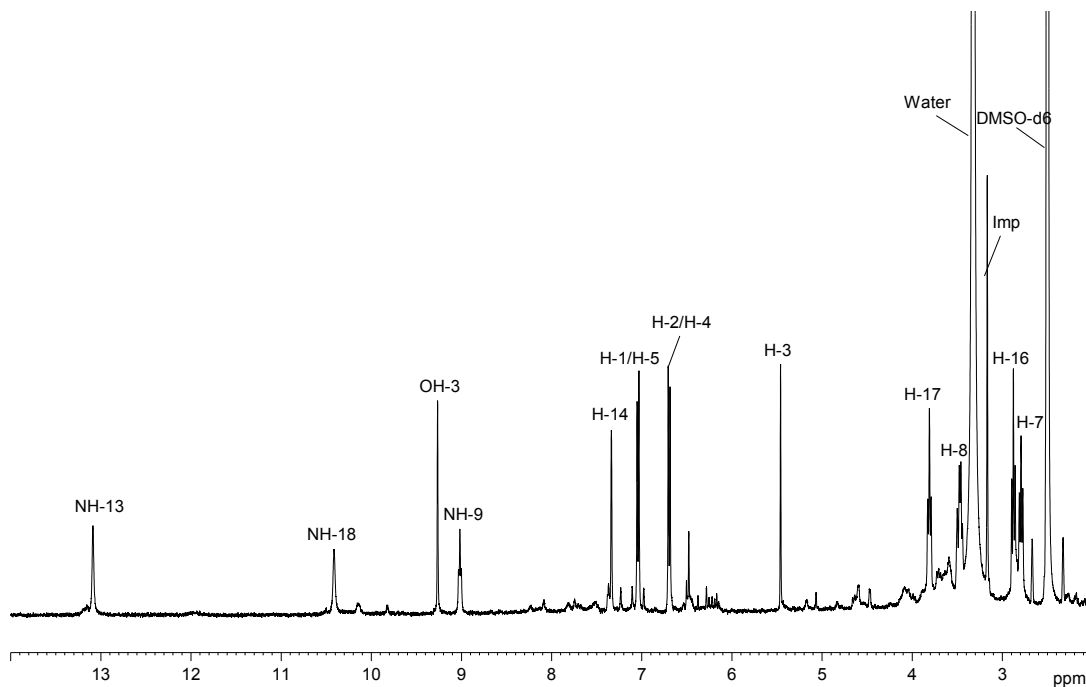


Figure 2.14 1H NMR spectrum with the proton assignments for **2.6** (400 MHz, $DMSO-d_6$).

HMQC correlations provided the characteristic carbon assignment for C-16 (δ 18.1). Following the establishment of the C-16 and H_2 -16 assignments, COSY correlations showed H_2 -16 to be coupled to H_2 -17, which in turn were attached to a carbon at δ 42.3. Following the observation of

a long range COSY correlation from H₂-16 to H-14 (δ 7.34), HMQC data (Figure 2.15) subsequently provided the ¹³C chemical shift of C-14 (δ 127.2). HMBC correlations from H-14 to carbons resonating at δ 118.7 and 123.3 resulted in the assignment of C-15 and C-12 or C-21 (the latter two carbons often resonate close to each other). However, because H₂-16 also exhibited an HMBC correlation to the signal at δ 123.3, this resonance was assigned as C-21. A COSY correlation between H₂-17 and one of the exchangeable protons provided the assignment of NH-18 (δ 10.41), which is shifted further downfield than expected (*cf.* compounds **1.51** – **1.53**). HMBC correlations from H₂-17 to carbons resonating at approximately δ 118.7 and 157.0 yielded the chemical shifts for C-15 and C-19 respectively.

Table 2.6 NMR (DMSO-d₆, 400 MHz for ¹H and 100 MHz for ¹³C) data for compound **2.6**.

Atom No.	δ_c	δ_H (mult, J, Hz)	COSY	HMBC
C1	129.8 (d)	7.04 (d), 2H, 8.1 Hz	H-2/H-4	C5, C7, C10
C2	115.5 (d)	6.70 (d), 2H, 8.1 Hz	H-1/H-5	C1/C5, C4, C10
C3	84.1 (d)	5.46 (s), 1H		C-21
C4	115.5 (d)	6.70 (d), 2H, 8.1 Hz		C1/C5, C2, C10
C5	129.8 (d)	7.04 (d), 2H, 8.1 Hz		C1, C7, C10
C6	-	-		
C7	32.6 (t)	2.79 (t), 2H, 16.0 Hz	H-8	C1/C5, C8
C8	45.2 (t)	3.47 (q), 2H, $J_{7,8}$ 16.0 Hz $J_{8,NH9}$ 7.2 Hz	H-7, NH-9	C1/C5, C10/C20
NH-9		9.02 (t), 1H, 7.2 Hz	H-8	
C10	155.9 (s)			
C11	-	-		
C12	-	-		
NH-13		13.09 (s), 1H	H-14	
C14	127.2 (d)	7.34 (s), 1H	NH-13, H-16	C15, C21
C15	118.7 (s)	-		
C16	18.1 (t)	2.88 (t), 2H, 7.6 Hz	H-14 (lr), H-17	C14, C15, C17, C21
C17	42.3 (t)	3.81 (t), 2H, 7.6 Hz	H-16, NH-18	C16, C15, C19
NH-18		10.41 (s), 1H	H-17	
C19	157.0 (s)	-		
C20	-	-		
C21	123.3 (s)	-		
OH	-	9.27 (s), 1H		C2/C4, C10

COSY correlations between H₂-8 and H₂-7, and also to the exchangeable proton NH-9 (δ 9.02), established the proton chemical shifts as δ 3.47 (q, J = 16.0, 7.2 Hz), 2.79 (t, J = 16.0 Hz) and 9.01 (t, J = 7.2 Hz), respectively. HMQC data revealed that H₂-8 and H₂-7 resided on carbons resonating at δ 45.2 and 32.6 respectively, while the methylene spin system at δ 7.04 (d, 2H, J = 8.1 Hz) was positioned on a carbon at δ 129.8 (C-1), which was in turn (from the COSY data)

coupled to a spin system at δ 6.70 (d, 2H, $J = 8.1$ Hz) attached to a carbon at δ 115.5 (C-2). The olefinic ^1H NMR resonances for the spiro ring (δ 6.70 and 7.04) integrated to two protons each suggesting that they were overlapping signals in a symmetrical magnetically equivalent environment. Only two protons remained to be assigned. The proton residing at δ 5.46 (s, 1H) was shown *via* the HMQC experiment to be attached to a carbon resonating at δ 84.1, which implied that the substituent attached to this carbon is a strong electron withdrawing group *e.g.* a hydroxyl functionality. The molecular formula allowed for an additional hydroxyl group and this is in agreement with the ^{13}C shift observed. Therefore, despite the absence of ^{13}C NMR data, the relative simplicity of this very minor metabolite and the adequate HMQC/HMBC data enabled the structure of this compound to be tentatively proposed as a 2,4-debrominated analogue of 3-dihydrodiscorhabdin C (**1.53**).

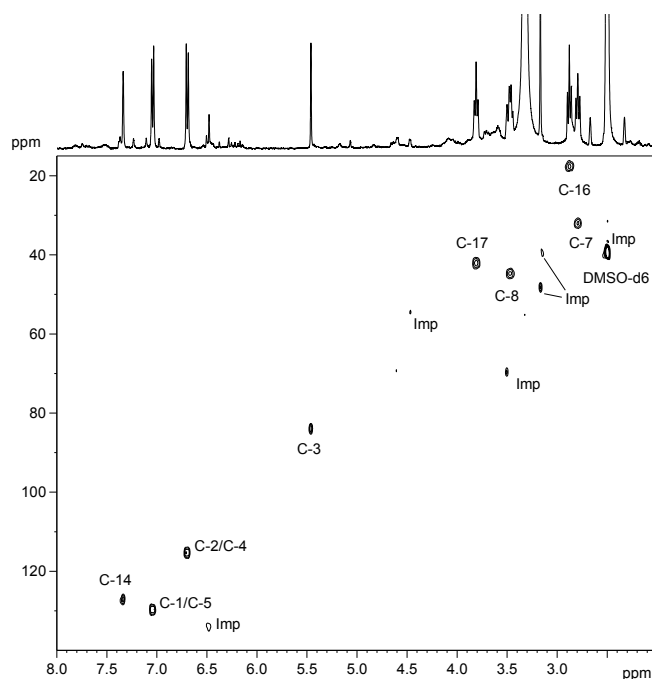


Figure 2.15 A section (F1 = δ 15 – 140 ppm, F2 = δ 1.0 – 8.0 ppm) of the HMQC spectrum of compound **2.6** (400/100 MHz, DMSO- d_6). (Imp = impurity).

Chapter 3: Pyrroloiminoquinone metabolites from *Latrunculia lorii*

3.1 Introduction

A second latrunculid sponge was collected off Riy Banks in Algoa Bay during the summer of 1999. The sponge was collected as part of a collaborative research programme between Rhodes University, the NCI and the Coral Reef Research Foundation (CRRF).

The ^1H NMR spectrum of the crude methanol extract of *Latrunculia lorii* showed typical discorhabdin signals. The crude extract was fractionated by a sequence of solvent-solvent partitioning, preparative C_{18} chromatography, semi-preparative reversed phase high performance liquid chromatography and molecular exclusion (LH-20) chromatography. Five known compounds; makaluvamine C,³⁰ damirone B,²⁵ makaluvic acid A,³⁴ discorhabdin G*,³⁷⁻³⁹ and discorhabdin M³⁷⁻³⁹ (**1.33**, **1.20**, **1.47**, **3.1**, **3.2**), and three new pyrroloiminoquinones; 1-amino discorhabdin D (**3.3**), 1-methoxy discorhabdin D (**3.4**) and 1-alanyl discorhabdin D (**3.5**) were subsequently isolated, and characterised, from *L. lorii* (Figure 3.1). Although compounds **3.1** and **3.2** are known, their data as yet remains unpublished and will be presented in this Chapter. In addition, since there have been two structures assigned the trivial name discorhabdin G, the discorhabdin isolated from this sponge refers to the compound isolated by Munro *et al.*³⁷⁻³⁹ and will be referred to as discorhabdin G*.

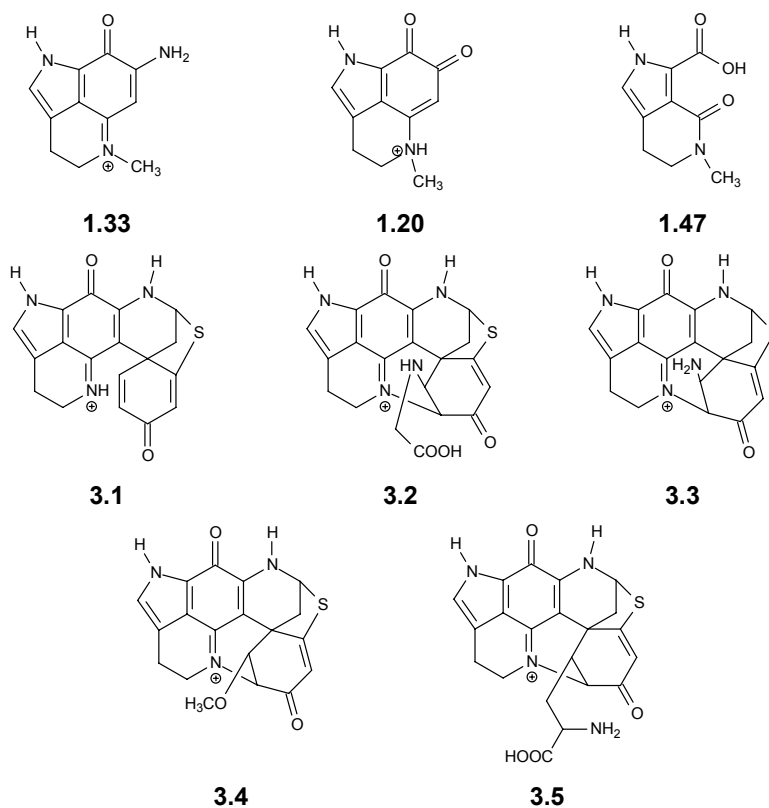


Figure 3.1 Summary of the compounds obtained from *L. lorii*.

The range of compounds isolated from the *L. lorii* sponge is characterised by simple tricyclic pyrroloiminoquinones, a substituted bicyclic pyrrolecarboxylic acid and five discorhabdin type metabolites, all of which, with the exception of discorhabdin G* (**3.1**), contain a discorhabdin D basic skeleton.

3.2 Results and Discussion

3.2.1 *The taxonomy of the encrusting sponge Latrunculia lorii*

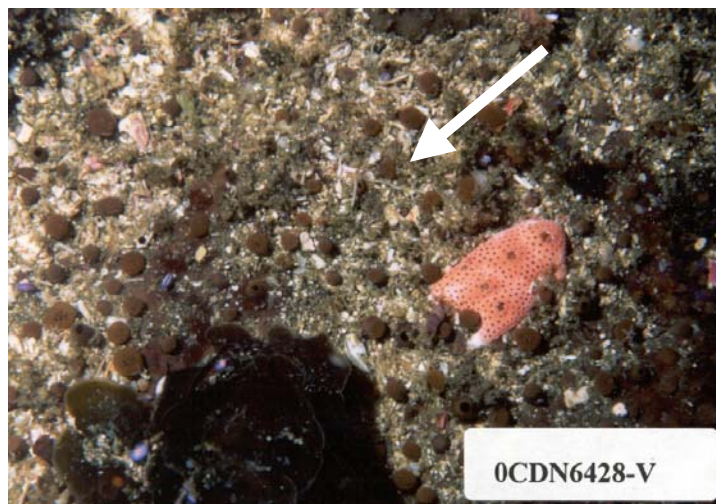


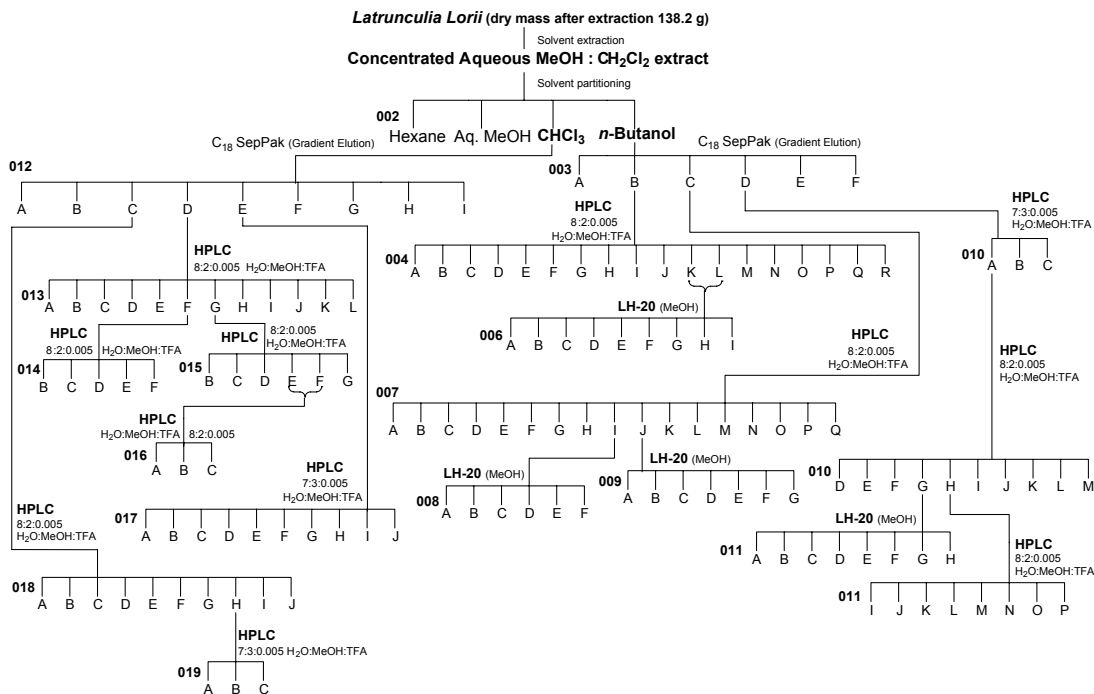
Figure 3.2 An underwater photograph of *L. lorii*.

A taxonomic description of *L. lorii* (OCDN 6428-V) by Kelly and Samaai⁵⁵ follows: “The sponge was collected at -24 m on Riy Banks, Algoa Bay, South Africa, on 23 February 1999, and is encrusting, 10 mm thick in life, growing in 50 cm square patches, with only spherical areolate porefields and conical oscules visible through a dense covering of algal epiphytes and sand. The texture is compressible and fleshy, the colour in life olive to very dark emerald green. The sponge is an undescribed species of *Latrunculia* (Order Poecilosclerida: Family Latrunculiidae), similar to recently described *Latrunculia oxydiscorhabda* Alvarez, Bergquist & Battershill, 2002 from New Zealand, but lacks oxydiscorhabd spicules present in *L. oxydiscorhabda*.” The sponge has been named *Latrunculia lorii* and a taxonomic description of this new sponge is in preparation. Voucher specimens are held at CRRF, NIWA, Rhodes University and the Smithsonian Institution.

3.2.2 *Extraction and isolation of pyrroloamino-ortho-quinone and pyrroloiminoquinone metabolites from L. lorii*

The frozen latrunculid sponge was thawed and extracted three times with methanol and then once with methanol : dichloromethane (1:1). The combined extracts were concentrated and

subjected to a modified Kupchan partition procedure to give hexane, chloroform, *n*-butanol and aqueous methanol partition fractions (Scheme 3.1).



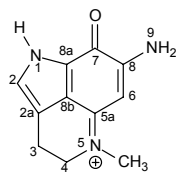
Scheme 3.1 Scheme for the extraction and isolation of pyrroloamino-*ortho*-quinone pyrroloiminoquinone metabolites from *L. lorii*. The masses and yields (calculated relative to the dry mass of the sponge) of the *L. lorii* pyrroloiminoquinone metabolites are summarised below:

006C, 008D, 018E	1.33	22.6 mg	0.02 %
004P, 007M, 014B	1.20	70.2 mg	0.05 %
017G	1.47	2.7 mg	0.002 %
010J, 013H	3.1	18.2 mg	0.01 %
007K, 018F	3.2	35.1 mg	0.03 %
007L, 013D	3.3	56.9 mg	0.04 %
013I	3.4	4.1 mg	0.003 %
007P	3.5	16.3 mg	0.01 %

The chloroform and *n*-butanol partition fractions were adjudged from their ^1H NMR spectra to contain discorhabdin-type compounds and therefore selected for further purification. Following solid phase extraction, reversed phase HPLC and LH-20 chromatography, the *n*-butanol fraction was found to contain the more complex discorhabdins (**3.1** – **3.3** and **3.5**) together with the simpler pyrroloiminoquinones (**1.20** and **1.47**), while the chloroform fraction afforded the compounds **1.33**, **1.20**, **1.47**, **3.1** - **3.4**.

3.2.3 Structure elucidation of pyrroloamino-ortho-quinone and pyrroloiminoquinone metabolites from *L. lorii*

a) Makaluvamine C (**1.33**)



1.33

The known compound makaluvamine C (**1.33**) (22.6 mg, 0.02 % yield) showed a molecular ion at m/z 202.0980 by HRFABMS analysis, in agreement with the molecular formula $C_{11}H_{12}N_3O$.

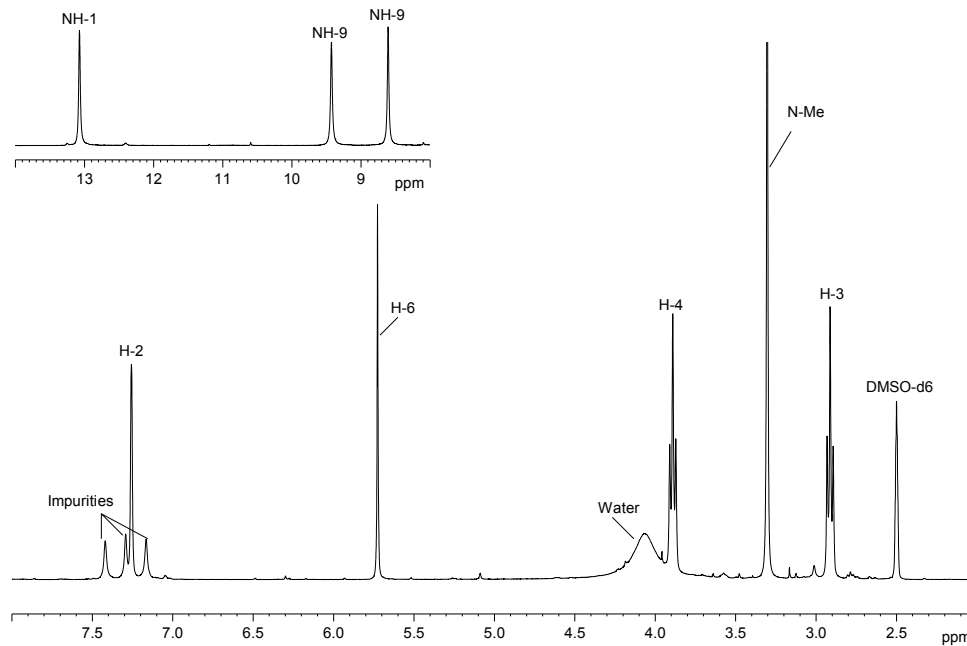
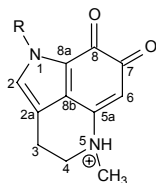


Figure 3.3 ^1H NMR spectrum for **1.33** (400 MHz, DMSO-d_6) with the signals for the three NH protons offset. Note: The water signal in the ^1H NMR spectrum is quite small compared to the previous spectra obtained due to the higher concentration of the sample.

The ^{13}C NMR spectrum revealed eleven well resolved resonances comprising two sp^2 methine signals (δ 126.5 and 85.4), four sp^2 quaternary signals (δ 156.5, 123.3, 123.2 and 117.7), two methylene sp^3 signals (δ 18.8 and 52.5), one methyl signal at δ 38.9, as well as the characteristic pyrroloiminoquinone core carbon resonances at δ 155.6 (C-5a), 156.5 (C-7), 167.3 (C-8). Characteristic pyrroloiminoquinone resonances in the ^1H NMR spectrum of **1.33** (Figure 3.3) included mutually coupled methylene signals at δ 2.91 (t, $J = 7.6$ Hz, H-3) and 3.89 (t, $J = 7.6$ Hz,

H-4), a pyrrole H-2 proton at δ 7.26, an olefinic proton resonance at δ 5.73 (H-6), an N-Me signal at δ 3.31, together with the exchangeable proton signals at δ 8.61 (1H, s, NH-9a), 9.43 (1H, s, NH-9b) and 13.07 (1H, s, NH-1). Upon comparison of the ^1H NMR data of **1.33** with the published values for makaluvamine C, the methyl group was placed on N-5, in accordance with the NH-1 and the N-Me proton chemical shifts (δ_{H} 13.10 and 3.31) reported for makaluvamine C (**1.33**).¹

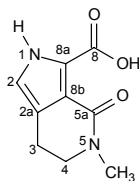
b) *Damirone B (1.20)*



1.19 R = Me **1.20** R = H

HRFABMS established the molecular formula $\text{C}_{11}\text{H}_{11}\text{N}_2\text{O}_2$ (m/z 203.0821) for compound **1.20** (70.2 mg, 0.05 % yield). The ^1H NMR spectrum was relatively simple and revealed five sets of non-exchangeable protons, including an indole proton at δ 7.06 (d), an sp^2 methine at 5.20 (s), two mutually coupled sp^3 methylene signals at δ 3.61 (t, $J = 6.6$ Hz, H-4) and 2.81 (t, $J = 6.6$ Hz, H-3) and a methyl signal at 3.05 (s). Two exchangeable protons corresponding to NH-1 (δ 12.42) and NH-5 (δ 6.66) were also observed. The ^{13}C NMR spectrum (CD_3OD) contained two α,β -unsaturated carbonyl signals at δ 177.5 (s) and 170.2 (s) together with six pyrroloiminoquinone core olefinic signals at δ 153.8 (s), 124.7 (s), 124.2 (s), 124.0 (d), 116.4 (s) and 92.6 (d), two sp^3 methylene signals at δ 51.3 and 19.6 and, finally, a methyl signal at δ 37.8. Placement of the methyl on position N-5 was based on comparison of the NMR data of **1.20** with known compounds damirone A (**1.19**) and B (**1.20**).²⁵ The N₅-methyl signal in the ^{13}C NMR spectrum of for damirone B resonated at δ 38.6, compared to δ 39.8 for **1.19**, while the N-1-methyl carbon chemical shift for **1.19** occurred at δ 35.9 (360/90 MHz, CD_3OD).²⁵

c) *Makaluvic acid A (1.47)*



1.47

The known pyrrolocarboxylic acid, makaluvic acid A (**1.47**) (2.7 mg, 0.002 % yield) was identified by comparison of its MS, ^1H and ^{13}C NMR data with published values.³⁴ A protonated molecular formula of $\text{C}_9\text{H}_{11}\text{N}_2\text{O}_3$ was established for **1.47** by HRFABMS (m/z 195.0760, $\Delta -1.0$ mmu) and supported by ^{13}C NMR data. The ^{13}C NMR spectrum revealed the presence of one sp^2 methine at δ 118.2 (d) and three sp^2 quaternary carbons at δ 123.2, 122.1 and 115.1. ^{13}C NMR signals at 165.0 (s) and 159.8 (s) indicated the presence of carboxylic acid and amide functionalities when

compared with the spectra of the makaluvic acids. Inspection of the ^1H NMR spectrum (Figure 3.4) revealed four non-exchangeable and two exchangeable sets of protons at δ 12.29 (1H, br s, NH-1) and 16.05 (1H, s, OH-8). As expected, the position of the COOH ^1H NMR signal was found to be dependent on both the solvent, the concentration of the sample solution and the presence of other exchangeable protons. Very broad signals are induced by intermediate rates of proton exchange (*i.e.* neither fast nor slow), resulting in the signals occasionally not being detected.⁹⁷ For example, the COOH signal observed in the ^1H NMR spectrum of **1.47** (Figure 3.4) was a sharp singlet, while the proton signals corresponding to hydroxyl group functionalities for compound **4.1** (Figure 4.5) are broad. Two mutually coupled sp^3 methylene signals at δ 2.81 (2H, t, $J = 7.1$ Hz, H-3) and 3.63 (2H, t, $J = 7.1$ Hz, H-4), together with a methyl singlet (δ 3.06) and a doublet at 6.89 (1H, $J = 2.8$ Hz, H-2) led to structure **1.47** for makaluvic acid A. The ^{13}C and ^1H NMR data for **1.47** is in accordance with the literature values for makaluvic acid A.³⁴

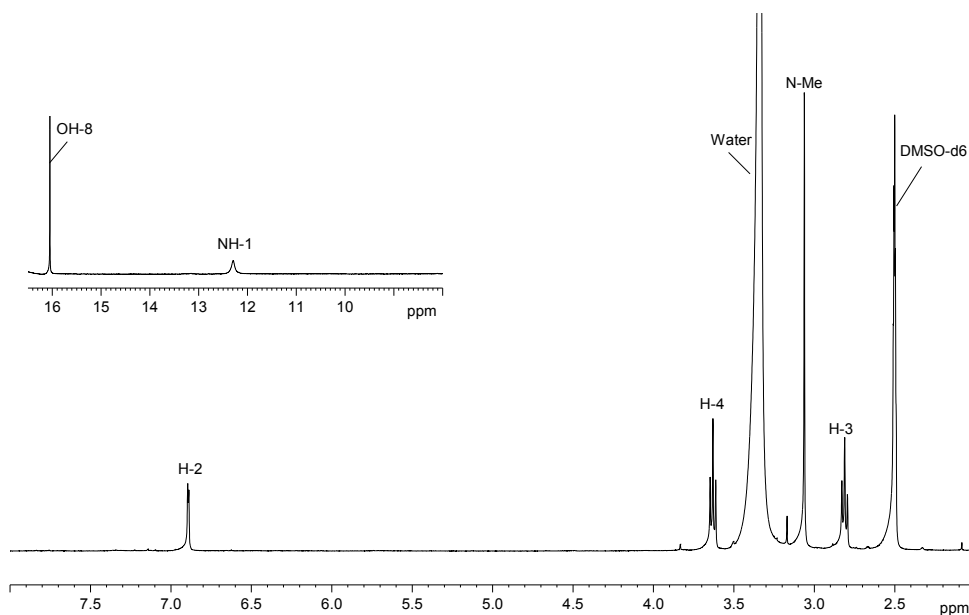
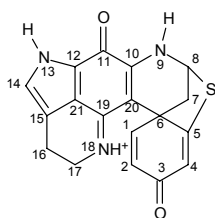
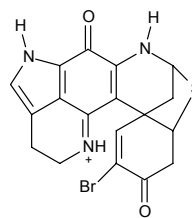


Figure 3.4 ^1H NMR spectrum for makaluvic acid A (**1.47**) (400 MHz, DMSO-d_6) with the signals for the NH and OH protons offset.

d) *Discorhabdin G** (**3.1**)



3.1



1.57

The ^1H NMR spectrum of compound **3.1** was found to be consistent with that of discorhabdin G first proposed by Munro *et al.*³⁷⁻³⁹ Unfortunately the relative inaccessibility of Munro *et al.*'s fully assigned spectral data necessitated a complete assignment of the NMR data for **3.1** from careful analysis of both 1D and 2D NMR data (described below and presented in Table 3.1). As discussed in Chapter One, the inaccessibility of the data for Munro *et al.*'s discorhabdins E-M in the mainstream chemical literature has led to a number of inconsistencies in the naming of discorhabdins in the A–Z sequence. Yang *et al.*'s published structure for a compound they named discorhabdin G (**1.56**) from the Antarctic sponge *Latrunculia apicalis*⁴⁵ reflects the confusion that abounds in the literature. To avoid confusion with Yang *et al.*'s structure for discorhabdin G, compound **3.1** is referred to as discorhabdin G*. Even though Munro's discorhabdin G has been renamed discorhabdin I in a subsequent review,²² we have retained the former name for the sake of simplicity and clarity.

A molecular ion at m/z 336.0807 was established by HRFABMS for compound **3.1** (18.2 mg, 0.01 % yield) suggesting a molecular formula of $\text{C}_{18}\text{H}_{14}\text{N}_3\text{SO}_2$ for this compound. Thirteen signals were observed in the ^1H NMR spectrum (Figure 3.5) of **3.1**, which, at first glance, appeared quite complicated for the ^1H NMR spectrum for a typical a discorhabdin skeleton. These signals included an indole proton at δ 7.38 (s), two coupled olefinic doublets at δ 7.31 (d) and δ 6.53 (dd), a sharp vinylic doublet at δ 6.18, a thiomethine doublet at δ 5.69, methylene multiplets at δ 3.89 and 3.75, and a multiplet at approximately δ 2.80, as well as an sp^3 methylene doublet signals at δ 2.73 and 2.33 (dd). The H-8 methine signal (δ 5.69), which resonates at δ 5.37 and 5.60 in discorhabdin A and D, respectively, suggested a thioether functionality. The presence of sulfur in **3.1** was confirmed from the HRFABMS data.

The ^{13}C NMR (Figure 3.6) spectrum of **3.1** showed the expected eighteen well resolved signals, with no indication of any overlapped signals. The pyrroloiminoquinone structure followed from characteristic carbon signals at δ_{C} 165.1, 154.1, 151.0 and 97.1 corresponding to C-11, C-19, C-10 and C-20. The ^{13}C NMR spectrum indicated two α,β -unsaturated carbonyls at δ 181.0 and 165.1 corresponding to C-3 and C-11 upon comparison with the published data for discorhabdin A (**1.57**). All the protonated carbon signals were assigned from HMQC data. The proton signal at δ 5.69, attached to a carbon resonating at δ 60.3, confirmed the thioether functionality implied by the molecular formula. Analysis of the COSY spectrum indicated that H-8 (d, $J = 3.5$ Hz) was coupled to two diastereotopic methylene protons at δ 2.73 (d, $J = 11.6$ Hz) and 2.33 (dd, $J = 3.5, 11.6$ Hz) which in turn resided on a single carbon resonating at δ 41.9. The methylene proton spin system was thus assigned as H-7.

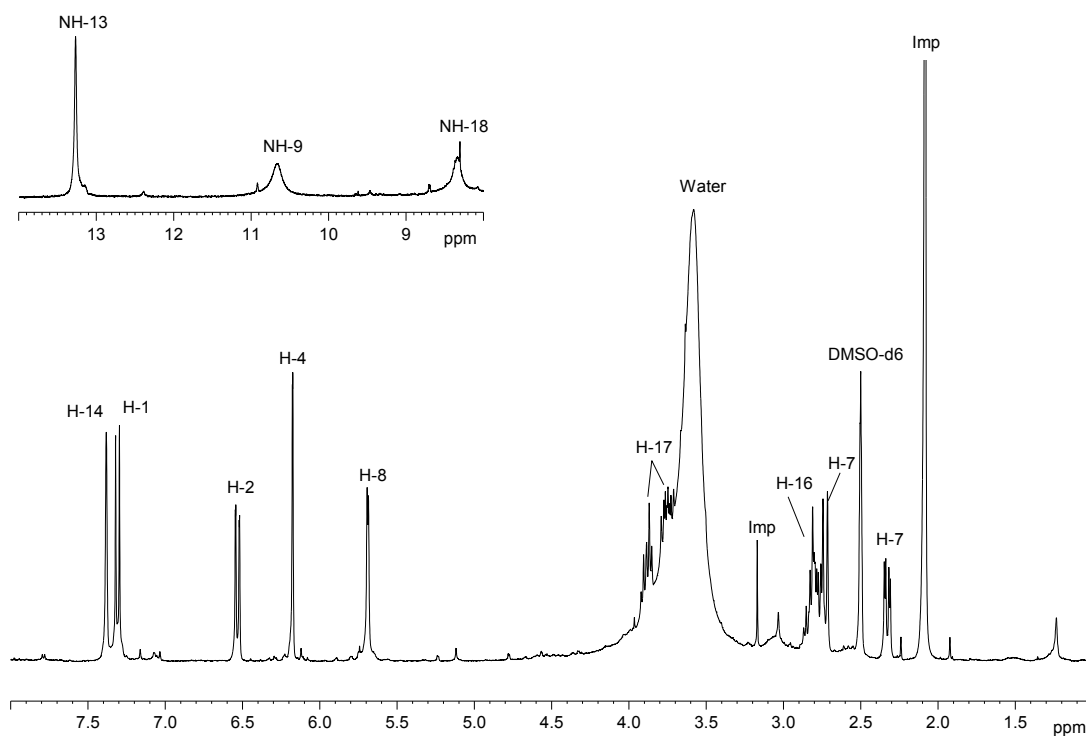


Figure 3.5 ^1H NMR spectrum of discorhabdin G* (3.1) (400 MHz, DMSO-d_6) with the signals for the three NH protons offset. (Imp = impurity).

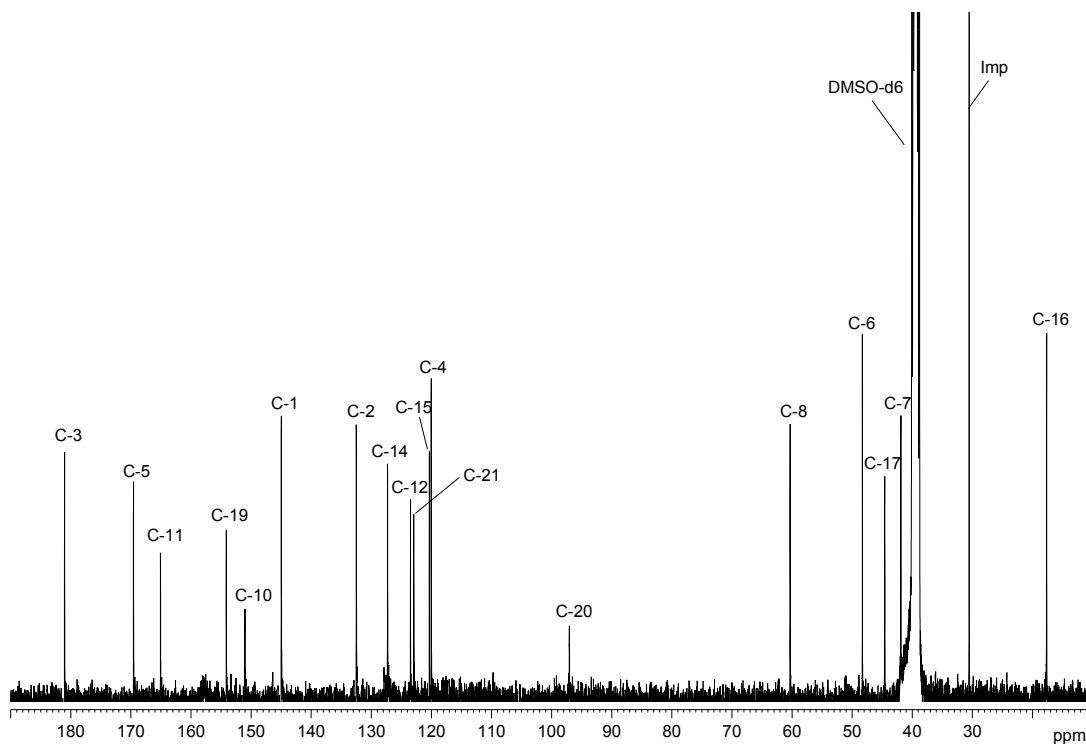


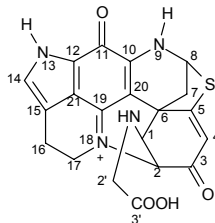
Figure 3.6 ^{13}C NMR spectrum of discorhabdin G* (3.1) (100 MHz, DMSO-d_6).

The HMQC data showed that the two proton multiplet at δ_{H} 2.80 (H₂-16) resided on the carbon at δ 17.6 enabling the subsequent assignment of the mutually coupled H₂-16 and H₂-17 spin systems from the COSY data. A three bond HMBC correlation showed H₂-16 to be correlated to an sp² methine carbon resonating at δ 127.3 (C-14), which in turn was coupled to NH-13 in the COSY experiment. HMBC correlations from H-14, H₂-16 and H₂-17 provided the assignments of C-12, C-15, C-19 and C-21. The COSY experiment also showed the sp² methine signals at δ 7.31 (d, $J = 9.9$ Hz) and 6.53 (dd, $J = 9.9$ Hz, 1.3 Hz) were coupled and could be assigned as H-1 and H-2 respectively. The signal for H-2 appears as a double doublet reflecting the vicinal coupling with H-1 ($^3J_{1,2} = 9.9$ Hz) and long range W coupling with the H-4 proton ($^4J_{2,4} = 1.3$ Hz). Further support for the discorhabdin A (**1.57**) basic skeleton for **3.1** was established from analysis of the HMBC data (Table 3.1). The presence of the spiro cyclohexadienone moiety was confirmed by the HMBC correlations from the doublet at δ 7.31 (H-1) to carbons at δ_{C} 41.9 (C-7), 48.3 (C-6), 97.1 (C-20), 169.6 (C-5) and 181.0 (C-3), and from δ 6.53 (H-2) to C-6, C-4 (δ 120.0) and C-3, thus completing the structural assignment of **3.1**.

Table 3.1 NMR (DMSO-d₆, 400 MHz for ¹H and 100 MHz for ¹³C) data for compound **3.1**.

Atom				
No.	δ_{C}	δ_{H} (mult, J , Hz)	COSY	HMBC
C1	145.0 (d)	7.31 (d), 1H, $J = 9.9$ Hz	H-2	C3, C5, C6, C7, C20
C2	132.5 (d)	6.53 (dd), 1H, $J = 9.9$ Hz, 1.3 Hz	H-1, H-4 (4J)	C3, C4, C6
C3	181.0 (s)	-	-	-
C4	120.0 (d)	6.18 (d), 1H, $J = 1.3$ Hz	H-2 (4J)	C2, C5, C6
C5	169.6 (s)	-	-	-
C6	48.3 (s)	-	-	-
C7	41.9 (t)	2.73 (d), 1H, $J = 11.6$ Hz 2.33 (dd), 1H, $J = 3.5$ Hz, 11.6 Hz	H-7b, H-8 H-7a, H-8	C1, C5, C6, C8, C20 C5, C6, C8, C20
C8	60.3 (d)	5.69 (d), 1H, $J = 3.5$ Hz	H-7a, H-7b	C5, C6, C7, C10
NH-9	-	10.65 (br s), 1H	-	-
C10	151.0 (s)	-	-	-
C11	165.1 (s)	-	-	-
C12	123.5 (s)	-	-	-
NH-13	-	13.27 (s), 1H	H-14	-
C14	127.3 (d)	7.38 (s), 1H	NH-13, H-16	C12, C15
C15	120.3 (s)	-	-	-
C16	17.6 (t)	2.80 (m), 2H	H-17	C15, C17, C21
C17	44.6 (t)	3.89 (m), 1H 3.75 (m), 1H	H-16, NH-18 H-16, NH-18	C15, C16, C19 C15, C16, C19
NH-18	-	8.34 (br s), 1H	H-17	-
C19	154.1 (s)	-	-	-
C20	97.1 (s)	-	-	-
C21	122.9 (s)	-	-	-

⁴ J = four bond long range COSY coupling.

e) *Discorhabdin M* (**3.2**)**3.2**

The next four structures all possess a basic discorhabdin D skeleton *i.e.* containing an additional ring formed by a bond from N-18 to C-2 on the spiro ring. Discorhabdin D (**1.61**, Figure 3.7) was first isolated from a New Zealand latrunculid sponge *L. brevis* (Ridley and Dendy) and was found to co-occur with discorhabdin A (**1.57**).⁴⁸

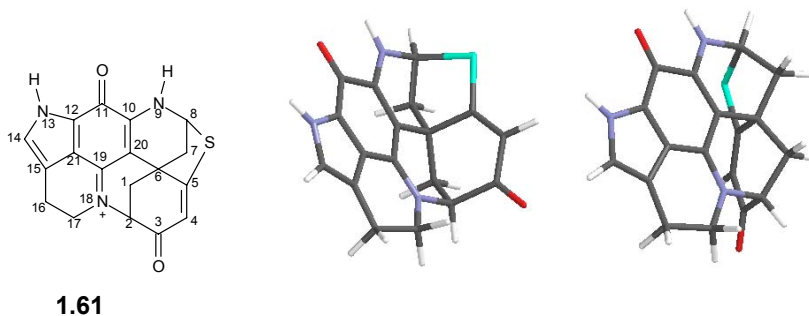
**1.61**

Figure 3.7 Discorhabdin D (**1.61**) together with the energy minimised 3D models of its two possible C-8 epimers. (Spartan '02, Wavefunction, Inc., CA, USA. A semi-empirical minimization force field was used to generate the 3D model).

A molecular formula of $C_{20}H_{17}N_4SO_4$ was inferred from the molecular ion at m/z 409.0971 for compound **3.2** (35.1 mg, 0.03 % yield) in the high resolution FABMS spectrum. The 1H NMR spectrum of **3.2** in $DMSO-d_6$ (Figure 3.8) showed two olefinic methine signals (δ 7.28 and 6.17) and another two deshielded methine resonances at δ 5.68 (d, $J = 2.3$ Hz, H-8) and 4.34 (d, $J = 2.8$ Hz, H-2). Only two exchangeable protons at δ 13.15 (NH-13, s) and 10.75 (NH-9, br s), were observed in the 1H NMR spectrum of **3.2**, with NH-18 (usually resonating at approximately δ_H 8.0) conspicuously absent.

The ^{13}C (Figure 3.9) and DEPT-135 NMR data revealed all twenty well resolved signals including four methylene carbons, five methine carbons and eleven quaternary carbons. Two α,β -unsaturated ketone carbonyls were evident from the carbon signals at δ 182.9 and 173.4, while the iminoquinone moiety was discernible from the signals at δ 166.3, 147.4 and 146.2. A thioether functionality was again suggested by the presence of carbon chemical shifts at δ 168.6 (C-5) and a carbon resonance at δ 62.2 (C-8). COSY correlations from H-8 (δ 5.68) to H_2 -7 (δ 3.10 and

~2.50) were observed and these assisted the assignment of the carbon chemical shifts for these protons *via* an HMQC experiment (Table 3.2).

The mutually coupled methylene protons H₂-16 and H₂-17 (assigned *via* the COSY experiment) as well as the indole proton (δ 7.28, s, H-14) were used to assign, and in some cases confirm, the carbon resonances of C-11, C-12, C-15, C-19 and C-21 (Table 3.2). The absence of the NH-18 signal in the ¹H NMR spectrum, the lack of a COSY correlation between H₂-17 and NH-18 as well as HMBC correlations from H-2 to C-17, suggested the formation of an additional ring by a bond between N-18 and C-2, as typically found with discorhabdin D skeletons.⁴⁸ Further evidence in support of this basic structure was provided by the presence of a carbon chemical shift at δ 63.8 (C-2), which certainly complies with the discorhabdin D type skeleton.⁴⁸ The H-2 (δ 4.34, d, J = 2.8 Hz) and H-1 (δ 3.63, d, J = 2.8 Hz) methine signals were shown to be coupled in a COSY experiment, while their HMBC correlations confirmed their placement as well as the presence of the spiro cyclohexadienone moiety.

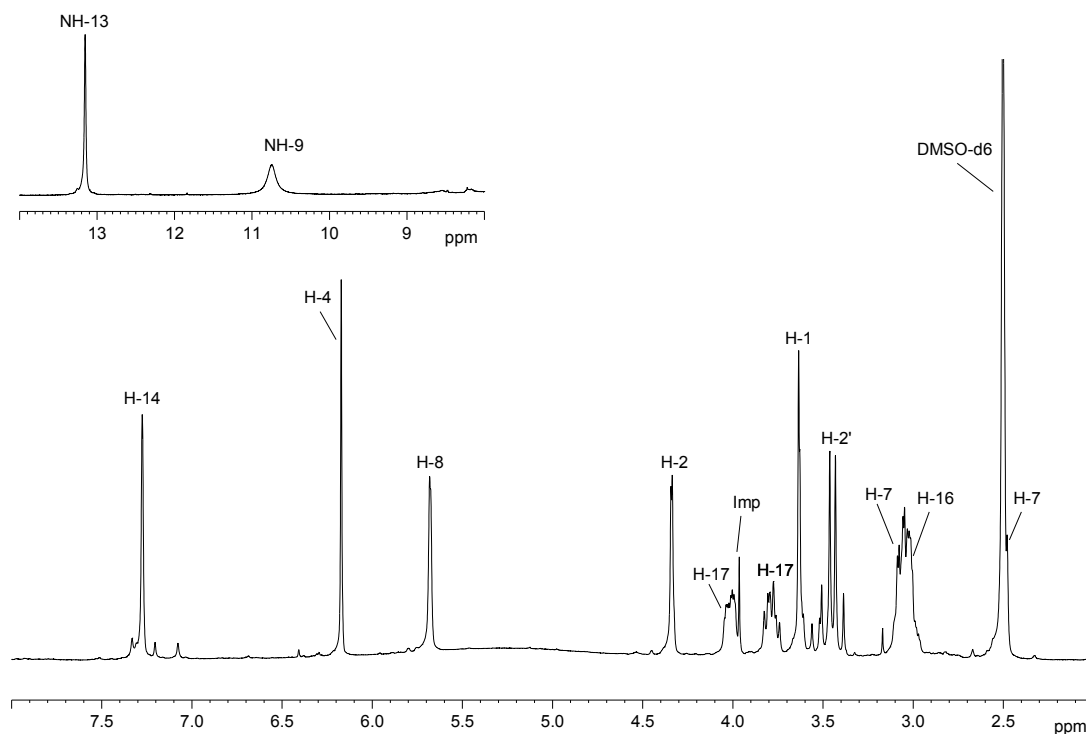


Figure 3.8 ¹H NMR Spectrum of **3.2** (400 MHz, DMSO-d₆) with the signals for the two NH protons offset. (Imp = impurity).

All that remained was the assignment and the elucidation of the substituent at position 1. Mutual HMBC correlations between H-1 and the sp³ methylene H-2' signal at δ 47.8 (C-2'), resulted in the tentative establishment of a -X₁-CH₂-X₂ fragment (where X₁ is a heteroatom and X₂ is the remainder of the side chain) at position 1.

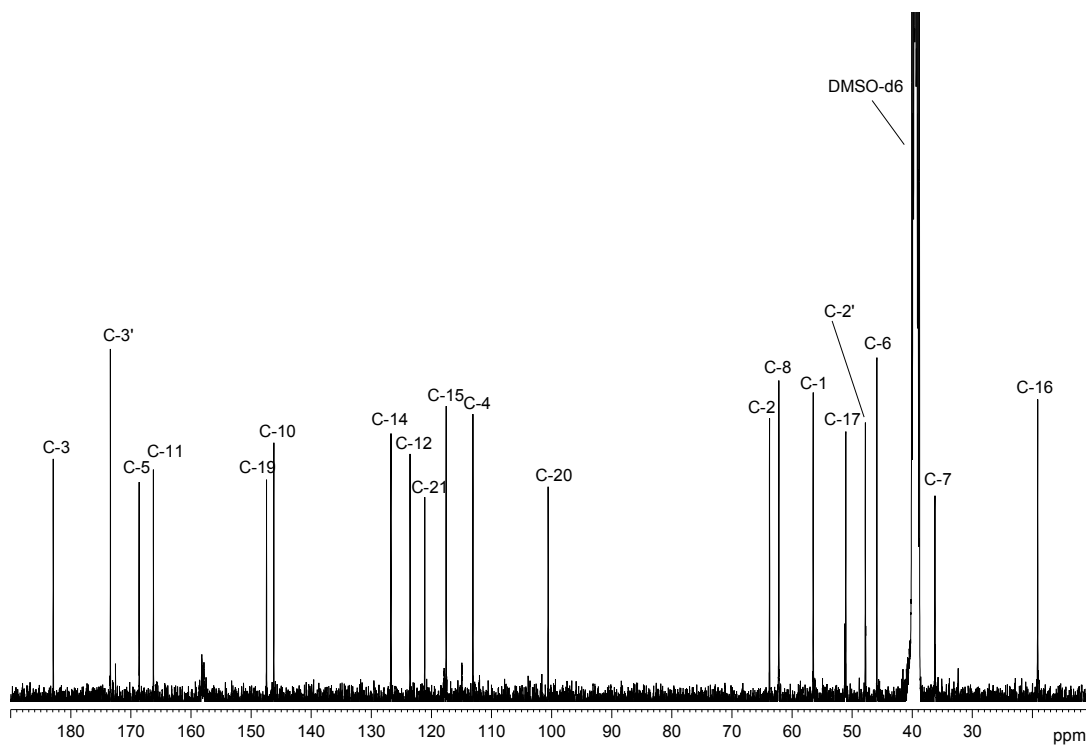
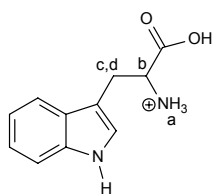
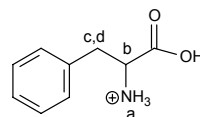


Figure 3.9 ^{13}C NMR spectrum of **3.2** (100 MHz, DMSO-d_6).



3.6

δ_{H} (TFA)	J (Hz)
a = 7.05	$^3J_{bc} = 4.0$
b = 4.71	$^3J_{bd} = 8.0$
c = 3.79	$^2J_{cd} = -15.5$
d = 3.57	



3.7

δ_{H} (TFA)	J (Hz)
a = 7.33	$^3J_{bc} = 8.5$
b = 4.68	$^3J_{bd} = 4.5$
c = 3.37	$^2J_{cd} = -14.5$
d = 3.64	

Interestingly, a large coupling constant was observed for the $\text{H}_2\text{-2}'$ protons ($J = 17.9$ Hz). Such large coupling constants have been typically observed where the vicinal conformations are fixed ($^3J_{\text{HH}} \approx 0 - 18$ Hz), whereas with systems where the conformation is not fixed, the geminal coupling constants tend to be $^3J_{\text{HH}} \approx 7$ Hz.⁹⁷ Similar large geminal couplings of methylene protons (where the conformation is fixed) have been observed in the amino acids tryptophan (**3.6**) and phenylalanine (**3.7**).⁹⁷

Table 3.2 NMR (DMSO- d_6 , 400 MHz for ^1H and 100 MHz for ^{13}C) data for compound **3.2**.

Atom				
No.	δ_{C}	δ_{H} (mult, J , Hz)	COSY	HMBC
C1	56.5 (d)	3.63 (d), 1H, $J = 2.8$ Hz	H-2	C2, C2', C3, C5, C20
C2	63.8 (d)	4.34 (d), 1H, $J = 2.8$ Hz	H-1, H-4	C1, C3, C4, C6, C17, C19
C3	182.9 (s)	-		
C4	113.1 (d)	6.17 (s), 1H	H-2, H-7 (lr), H-8 (lr)	C2, C5, C6, C20
C5	168.6 (s)	-		
C6	45.9 (s)	-		
C7	36.2 (t)	3.10 (m), 1H 2.50 (m), 1H	H-7b, H-8 H-4 (lr), H-7a, H-8	C5, C6, C8, C20 C5, C6, C8, C20
C8	62.2 (d)	5.68 (d), 1H, $J = 2.3$ Hz	H-4 (lr), H-7a, H-7b	C5, C6, C10
NH-9	-	10.75 (br s), 1H	-	
C10	146.2 (s)	-		
C11	166.3 (s)	-		
C12	123.6 (s)	-		
NH-13	-	13.15 (s), 1H	H-14	C12, C15, C21
C14	126.7 (d)	7.28 (s), 1H	NH-13	C11, C12, C15, C19, C21
C15	117.5 (s)	-		
C16	19.1 (t)	3.00 (m), 2H	-	C14, C15, C17, C21
C17	51.1 (t)	4.02 (m), 1H 3.79 (m), 1H	H-16, H-17b H-16, H-17a	C15, C16, C19 C15, C16, C19
C19	147.4 (s)	-		
C20	100.6 (s)	-		
C21	121.1 (s)	-		
C2'	47.8 (t)	3.52 (dd), 2H, $J = 17.9, 31.6$ Hz	-	C1, C3'
C3'	173.4 (s)	-		
NH-1'	-	5.30 (br s)*	-	

* Note: extremely broad singlet, which may be due to an intermediate rate of exchange with other protons. The ^1H NMR signal for COOH was not observed and is also likely to be due to an intermediate rate of exchange with other protons (Section 3.2.3, c) as well as the presence of other exchangeable protons (*i.e.* NH-9 and NH-13).⁹⁷

A deshielded carbon resonance at δ_{C} 173.4 remained to be assigned and because only the H-2' proton showed a correlation to the carbon at δ_{C} 173.4 in the HMBC experiment, the fragment was thus altered to $-\text{X}_1-\text{CH}_2-\text{COOH}$. The carbon chemical shift for a carboxylic acid carbonyl may be accommodated at δ 173.4 (C-3') and the molecular formula does indeed show an additional two oxygen atoms (as opposed to the usual two for discorhabdins) that need to be accounted for. The molecular formula required an additional amino group at position 1. The chemical shift at δ 56.5 (C-1) supported the assignment of an NH substituent at C-1 and confirmed the structure of the substituent as $-\text{NH}-\text{CH}_2-\text{COOH}$. The structure obtained for compound **3.2** is thus identical to that obtained by Munro *et al.* and compared favourably to the ^1H NMR data (kindly supplied to us by

Professor Munro).³⁹ This compound, named initially discorhabdin M,³⁷⁻³⁹ was later referred to as discorhabdin N in a subsequent publication by Urban *et al.*,²² but the compound lacked a Δ^4 olefin, which is inconsistent with the original ^1H NMR spectra supplied by Munro and unfortunately contributes to the confusion surrounding the nomenclature of the discorhabdins. We have thus retained the former name here.

The 3D model of one of the isomers of **3.2** is shown in Figure 3.10 to give an indication of the complexity of the heptacyclic discorhabdin M structure. The stereochemistry at the four chiral carbon atoms (C-1, C-2, C-6 and C-8) remains unassigned.

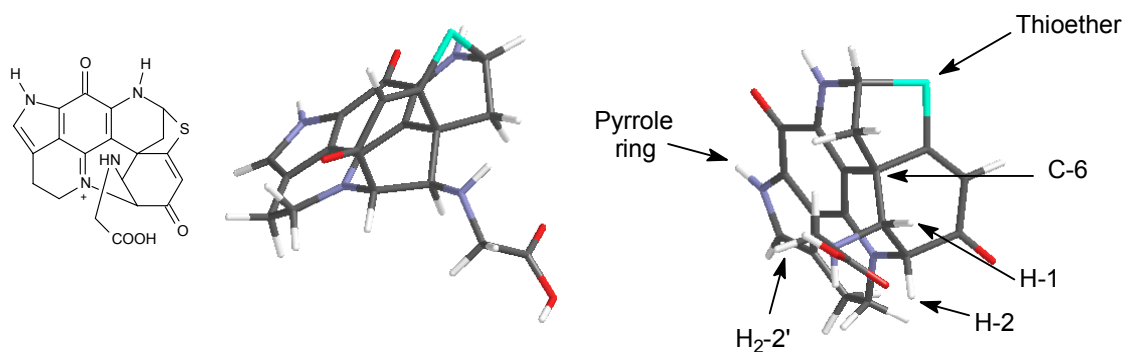
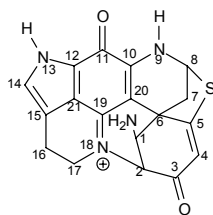


Figure 3.10 Proposed structure and three dimensional model for discorhabdin M (**3.2**) with an arbitrarily assigned 1R,* 2S,* 6R,* 8S* configuration. (Spartan '02, Wavefunction, Inc., CA, USA. A semi-empirical minimization force field was used to generate the 3D model).

f) *1-amino discorhabdin D (3.3)*



3.3

The new compound 1-amino discorhabdin D (**3.3**) (56.9 mg, 0.04 % yield) was identified by comparison of its MS and ^1H (Figure 3.11) and ^{13}C NMR data with **3.2**. A molecular formula of $\text{C}_{18}\text{H}_{15}\text{N}_4\text{SO}_2$ was established for **3.3** by HRFABMS (M^+ , m/z 352.0995 (Δ +0.1 mmu)) and supported by ^{13}C NMR data.

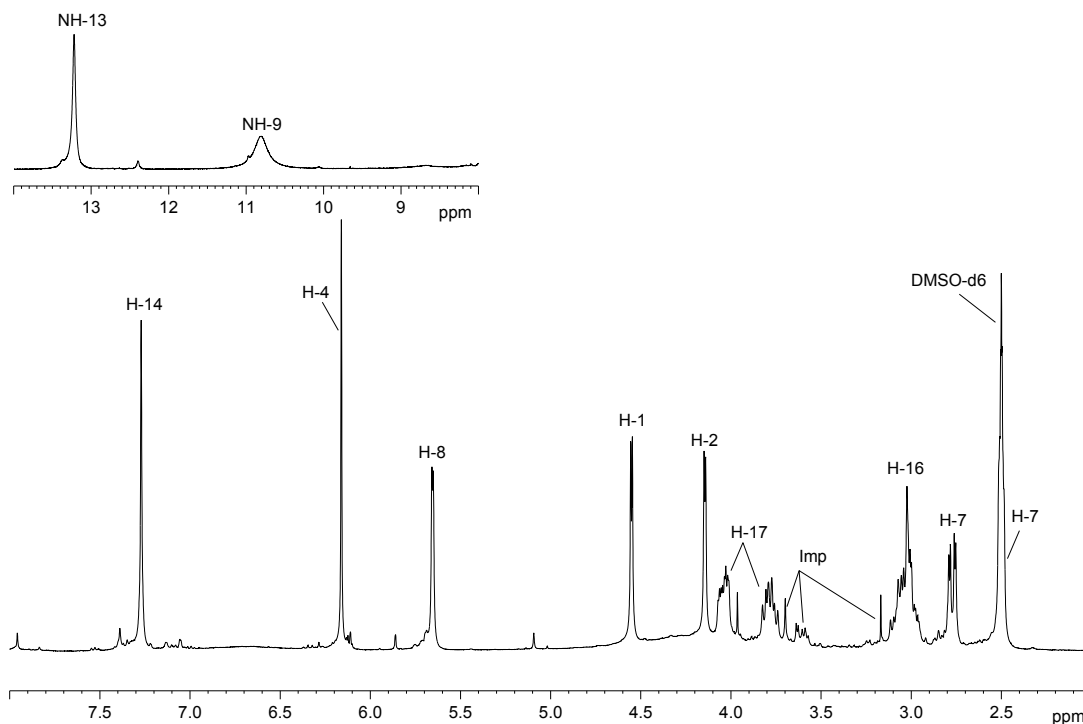


Figure 3.11 ^1H NMR spectrum of 1-amino discorhabdin D (**3.3**) (400 MHz, DMSO-d_6) with the signals for the two NH protons offset. (Imp = impurity).

The ^{13}C and DEPT 135 NMR spectrum revealed the presence of eighteen well resolved carbon signals with two sp^2 methine signals at δ 126.8 and 112.7, three sp^3 methine signals at δ 66.6, 65.7 and 62.3, only three sp^3 methylene signals at δ 50.9, 35.9 and 19.1, one sp^3 quaternary at δ 46.8, eight sp^2 quaternary carbons as well as an α,β -unsaturated carbonyl at δ 182.5 (Table 3.3). Inspection of the ^1H NMR spectrum (Figure 3.11) revealed nine non-exchangeable and only two clearly exchangeable protons at δ 13.20 (1H, s) and 10.81 (1H, br s). Once again, the absence of an NH-18 proton signal, together with a methine doublet at δ 5.66 (d, $J = 2.5$ Hz, H-8) and the presence of only three methylene groups (from the DEPT 135 data) suggested the presence of a discorhabdin D skeleton with its thioether functionality. A COSY experiment established the contiguous coupling sequence between H-8 and NH-9 and the two protons at δ 2.77 (1H, dd, $J = 3.5$ Hz, 12.1 Hz, H-7b) and possibly at δ 2.50 (m, H-7a). The HMQC experiment showed that H-8 was attached to a carbon at δ 62.3, which is in accordance with the expected ^{13}C chemical shift of C-8 in a discorhabdin D skeleton, and that the protons at δ 2.77 (H-7b) and 2.50 (H-7a) resided on the same carbon at δ 35.9 (C-7).

H-1 (δ 4.55) and H-2 (δ 4.15) were shown to be mutually coupled by a COSY experiment and the difficulty in the structure determination of **3.3** lay in assigning the carbon chemical shifts at δ 66.6 and 65.7 to either C-1 or C-2. HMBC correlations from H-4 and H-7 to carbon resonances at δ 65.7 (C-2) and 66.6 (C-1) respectively, were noted. Based on previous observations e.g. **3.1** and

3.2 that H-4 displays HMBC correlations to C-2 and similarly H-7 to C-1, enabled a tentative assignment of C-1 and C-2. The molecular formula requires an additional amino group and as C-1 is a methine carbon resonating at δ 66.6, a primary amine functionality is thus assigned to C-1. The possibility of a hydroxyl functional group was eliminated on the basis of the requirements of the molecular formula, as well as the carbon chemical shift obtained for **3.3**.

Table 3.3 NMR (DMSO- d_6 , 400 MHz for ^1H and 100 MHz for ^{13}C) data for compound **3.3**.

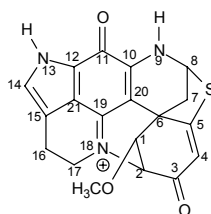
Atom No.	δ_{C}	δ_{H} (mult, J, Hz)	COSY	HMBC
C1	66.6 (d)	4.55 (d), 1H, J = 3.5 Hz	H-2	
C2	65.7 (d)	4.15 (d), 1H, J = 3.5 Hz	H-1	
C3	182.5 (s)	-		
C4	112.7 (d)	6.16 (s), 1H	H-7b (lr)	C2, C5, C6
C5	169.0 (s)	-		
C6	46.8 (s)	-		
C7	35.9 (t)	2.77 (dd), 1H, J = 3.5 Hz, 12.1 Hz 2.50 (m)	H-7b, H-8 H-4 (lr), H-7a, H-8	C1, C5, C6, C17 C1, C5, C6, C17
C8	62.3 (d)	5.66 (d), 1H, J = 2.5 Hz	H-7a, H-7b	C5, C6
NH-9	-	10.81 (br s), 1H	-	
C10	146.7 (s)	-		
C11	166.2 (s)	-		
C12	123.6 (s)	-		
NH-13	-	13.20 (s), 1H	H-14	
C14	126.8 (d)	7.27 (s), 1H	NH-13	C15
C15	117.6 (s)	-		
C16	19.1 (t)	3.01 (m), 2H	-	
C17	50.9 (t)	4.04 (m), 1H 3.78 (m), 1H	H-16, H-17b H-16, H-17a	C5
C19	147.5 (s)	-		
C20	99.9 (s)	-		
C21	121.1 (s)	-		
NH-1'	-	4.10 (br s)	-	

The signals for the amine protons were not observed in the ^1H NMR spectrum of **3.3**. Because of the rapid intermolecular exchange of amine protons, the coupling of amine protons with vicinal hydrogen atoms is usually not seen in aliphatic amines.⁹⁷ Where the exchange rate is slower, however, coupling with neighbouring hydrogen atoms is usually detected (splitting is often observed), for example with aromatic amines, amides and enamines. In addition, the signals belonging to NH protons are often broad (Figure 3.11, for example NH-9) due to intermediate exchange rates. The amino and especially ammonium proton signals are broadened further due to the ^{14}N - ^1H coupling which is only partly eliminated by the quadrupole relaxation of ^{14}N (spin quantum number, $I = 1$; natural abundance, 99.6 %; $^1J_{\text{NH}} \approx 60$). Sharp multiplets are, however, still

observed for neighbouring H atoms, as this line broadening has no effect on the vicinal H-C-N-H coupling.⁹⁷

The HMBC correlations established by the remaining mutually coupled sp^3 methylene signals at δ 3.01 (2H, m, H-16) and 4.04 (1H, m, H-17b) and 3.78 (1H, m, H-17a), together with the indole proton at δ 7.27 (which showed a COSY correlation to NH-13 and was thus assigned as H-14) enabled, through HMBC correlations, the carbon chemical shift assignments for the pyrroloiminoquinone core structure of **3.3** (Table 3.3).

g) *1-methoxy discorhabdin D (3.4)*



3.4

1-Methoxy discorhabdin D (**3.4**) (4.1 mg, 0.003 % yield) exhibited a molecular ion peak at m/z 366.0912 (Δ -0.1 mmu) in the HRFABMS spectrum corresponding to a molecular formula of $C_{19}H_{16}N_3SO_3$. The 1H NMR spectrum in DMSO- d_6 (Figure 3.12) showed eleven non-exchangeable and, once again, only two exchangeable protons corresponding to NH-9 and NH-13 at δ 10.84 and 13.16 respectively.

The non-exchangeable signals appeared as two sp^2 methine signals at δ 7.30 (d, J = 2.3 Hz, H-14) and 6.19 (s, H-4), three sp^3 methylene signals at δ 2.74 (d, J = 3.5 Hz, 12.1 Hz, H-7b) and 2.59 (d, J = 12.1 Hz, H-7a), 3.05 (m, H₂-16) together with δ 4.05 (m, H-17b) and 3.83 (m, H-17a), three sp^3 methine signals at δ 4.30 (d, J = 3.3 Hz, H-1), 4.57 (d, J = 3.3 Hz, H-2) and at 5.65 (d, J = 2.3 Hz, H-8). A methyl signal at δ 3.50 (s, H-1') suggested the presence of a methoxy substituent. The ^{13}C NMR spectrum (Figure 3.13) showed eighteen well resolved signals with typical quaternary pyrroloiminoquinone carbons resonating at δ 166.1 (C-11), 146.7 (C-10), 123.6 (C-12), 147.4 (C-19), 99.3 (C-20), and 121.0 (C-21). An α,β -unsaturated carbonyl signal (C-3) resonating at δ 182.5 was again observed and the above assignments were later confirmed through the use of 2D NMR experiments. A DEPT 135 experiment revealed the presence of four methine signals at δ 75.8, 62.1, 112.81 and 126.9 and, upon comparison with the ^{13}C NMR data of **3.3**, the latter two were assigned as C-4 and C-14 respectively and confirmed through 2D NMR experiments. In addition, three sp^3 methylene signals at δ 35.6 (C-7), 19.1 (C-16) and 51.0 (C-17) as well as a methyl carbon at δ 58.3 (C-1') were observed. In accordance with the methoxy singlet observed in the 1H NMR spectrum, the carbon chemical shift at δ 58.3 confirmed a methoxy type substituent.

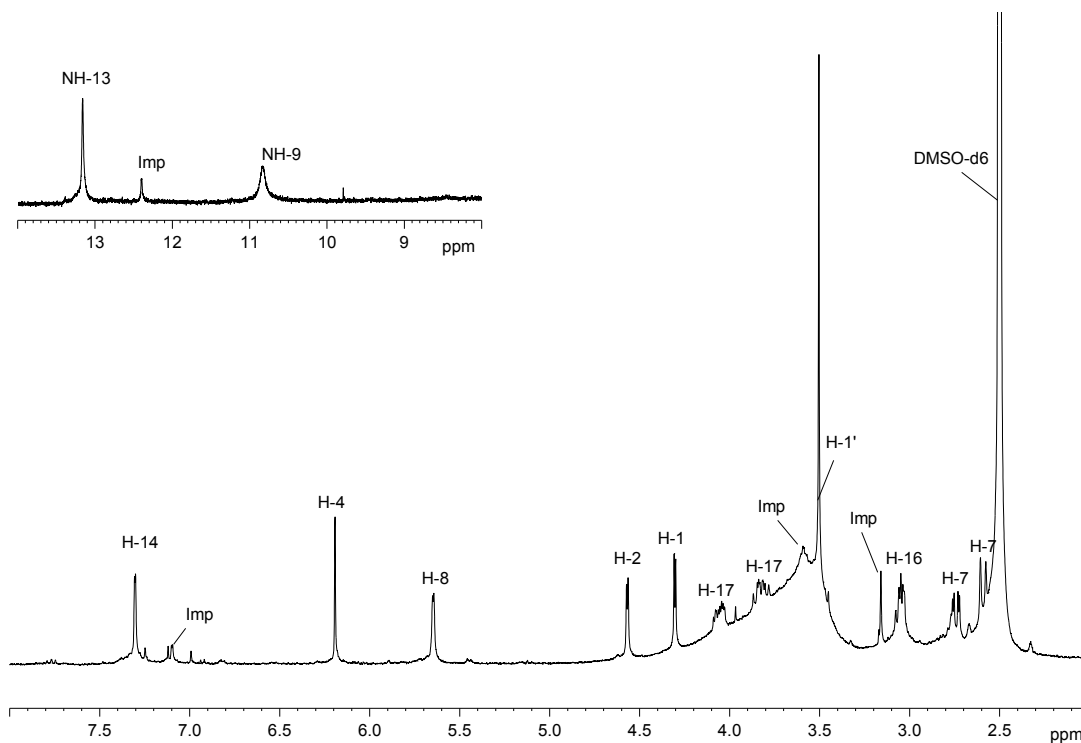


Figure 3.12 ¹H NMR spectrum for **3.4** (400 MHz, DMSO-d₆) with the signals for the three NH protons offset. (Imp = impurity).

Various COSY and HMQC correlations once again established the assignments of C-7 and C-8 as well as C-16 and C-17, with the spin system at δ_{H} 5.65 (H-8) and δ_{C} 62.1 (C-8) implying a thioether functionality as obtained with the previous compounds. A discorhabdin D type skeleton was evident from the absence of a NH-18 proton signal, the lack of a COSY correlation and the long range HMBC correlation from an sp^3 methine proton resonating at δ 4.57 to C-17, which also resulted in the assignment of the proton as H-2. The ¹³C NMR spectrum of **3.7** (Figure 3.13) only showed eighteen of the expected nineteen carbon resonances. The HMQC data revealed that H-2 was shown to be attached to the same carbon at δ 62.1 as H-8 (Figure 3.14). An enlargement of the carbon signals at δ 62 ppm showed the carbon signal to be slightly broader than the carbon signal corresponding to C-1' (see offset resonances in Figure 3.13) suggesting that C-2 and C-8 were overlapped. A COSY correlation showed that H-2 was coupled to H-1 (δ 4.30, d, 1H) whereas an HMQC experiment showed H-1 to be attached to a carbon resonating at δ 75.8, implicating a strong electron withdrawing group residing on C-1, which therefore supported the placement of the methoxy substituent at position 1. This was confirmed through an HMBC correlation (Table 3.5) between H-1 and C-1' (OMe).

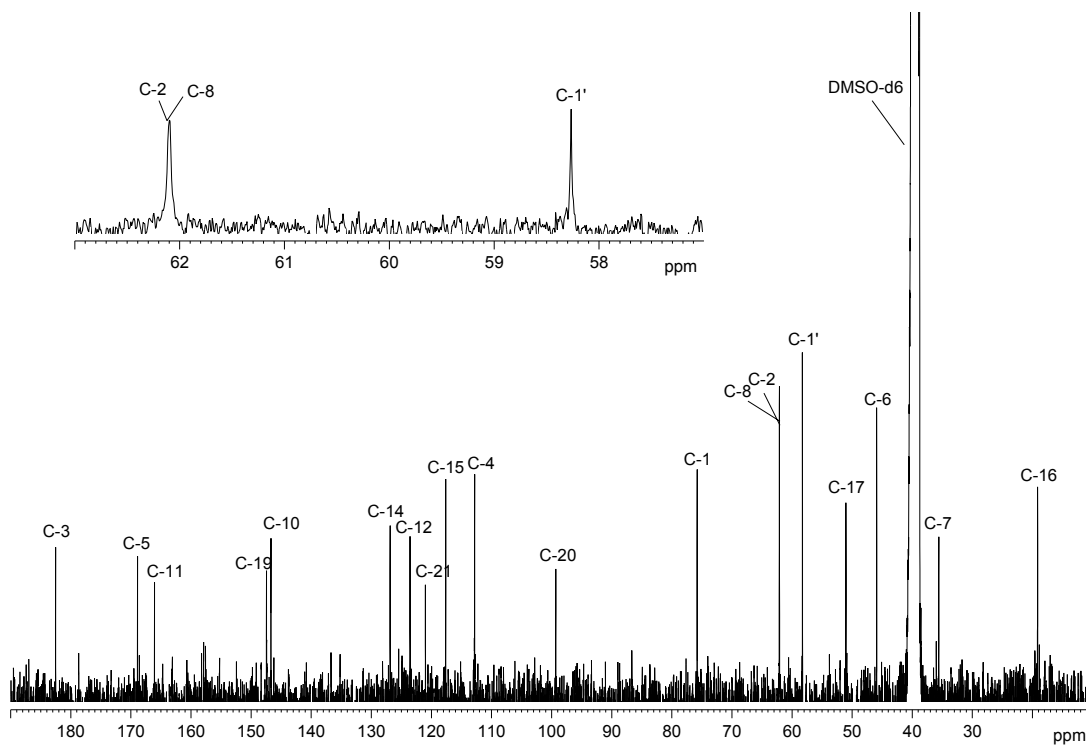


Figure 3.13 ^{13}C NMR spectrum for **3.4** (100MHz, DMSO-d_6) with the expansions for C-2, C-8 and C-1' offset.

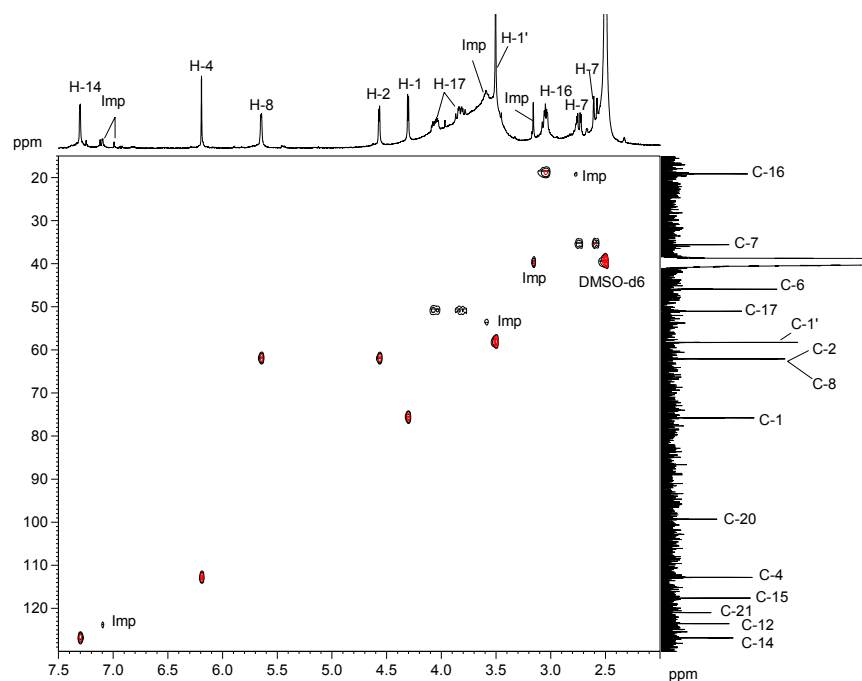


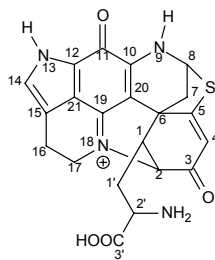
Figure 3.14 A section ($F1 = \delta 15 - 130$ ppm, $F2 = \delta 2.0 - 7.5$ ppm) of the HMQC spectrum of compound **3.4** (400/100 MHz, DMSO-d_6). (Imp = impurity).

The final quaternary carbon resonating at δ 168.9 was initially assigned by a process of elimination, and later confirmed, as C-5 from comparison with the ^{13}C NMR data of compounds **3.1** and **3.2** and discorhabdin D (**1.61**). Methoxy substituents have not been reported in the discorhabdins and this may suggest that compound **3.4** is an artefact.

Table 3.4 NMR (DMSO- d_6 , 400 MHz for ^1H and 100 MHz for ^{13}C) data for compound **3.4**.

Atom				
No.	δ_{C}	δ_{H} (mult, J , Hz)	COSY	HMBC
C1	75.8 (d)	4.30 (d), 1H, $J = 3.3$ Hz	H-2	C3, C5, C1'
C2	62.1 (d)	4.57 (d), 1H, $J = 3.3$ Hz	H-1, H-4	C1, C3, C6, C17, C19
C3	182.5 (s)	-		
C4	112.8 (d)	6.19 (s), 1H	H-2, H-7 (lr)	C2 / C8, C5, C6
C5	168.9 (s)	-		
C6	45.9 (s)	-		
C7	35.6 (t)	2.74 (d), 1H, $J = 3.5$ Hz, 12.1 Hz 2.59 (d), 1H, $J = 12.1$ Hz	H-7b, H-8 H-7a, H-8, H-4 (lr)	C5, C6, C20 C5, C6, C2 / C8, C20
C8	62.1 (d)	5.65 (d), 1H, 2.3 Hz	H-7a, H-7b, NH-9	C5, C6, C10
NH-9	-	10.84 (br s), 1H	H-8	
C10	146.7 (s)	-		
C11	166.1 (s)	-		
C12	123.6 (s)	-		
NH-13	-	13.16 (s), 1H	H-14	
C14	126.9 (d)	7.30 (d), 1H, $J = 2.3$ Hz	NH-13, H-16	C15, C12, C21
C15	117.6 (s)	-		
C16	19.1 (t)	3.05 (m), 2H	H-14, H-17	C14, C15, C17, C21
C17	51.0 (t)	4.05 (m), 1H 3.83 (m), 1H	H-16, H-17b H-16, H-17a	C15, C16, C19 C16, C19
C19	147.4 (s)	-		
C20	99.3 (s)	-		
C21	121.0 (s)	-		
C1'	58.3 (q)	3.50 (s), 3H	-	C1

h) *1-alanyl discorhabdin D (3.5)*



3.5

The structure of **3.5** (16.3 mg, 0.01 % yield) was in part established from comparison of the NMR data for compounds **3.2**, **3.3** and **3.4** with the data obtained for **3.5** and supported by careful analysis of the 2D NMR data. Analysis of the HRFABMS spectrum gave an M^+ peak at m/z 423.1127 corresponding to a molecular formula of $C_{21}H_{19}N_4SO_4$ for **3.5**.

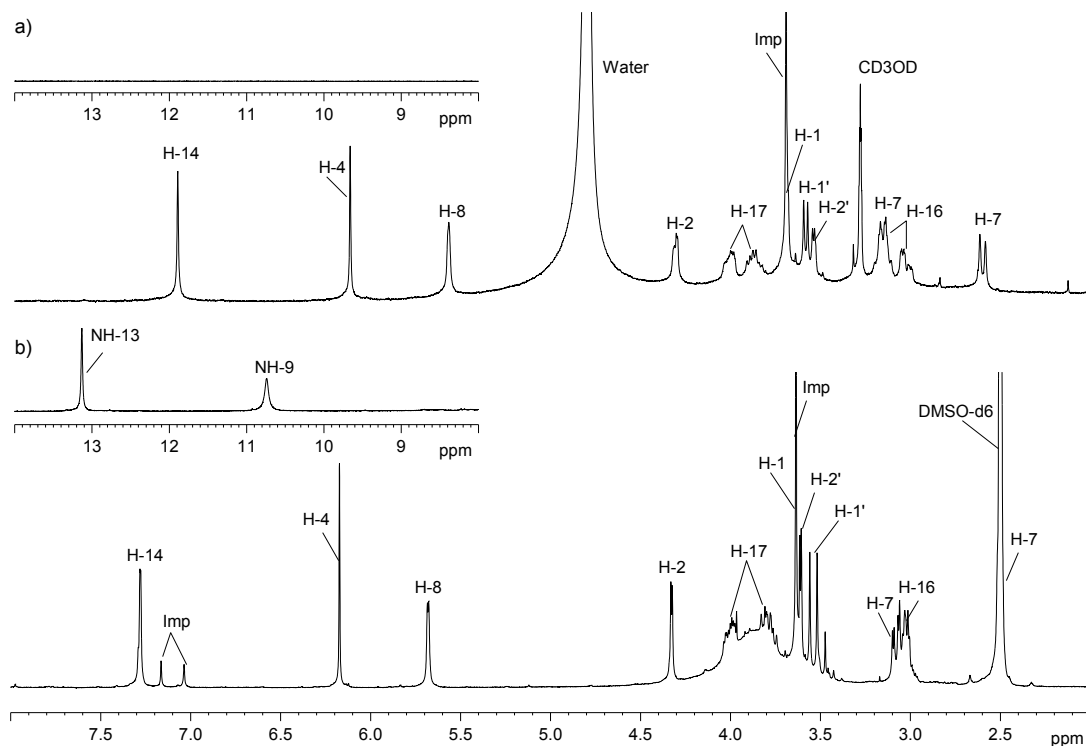


Figure 3.15 1H NMR spectrum showing the absence and presence of exchangeable protons NH-9 and NH-13 in **3.5** (400 MHz) in a) CD_3OD and b) $DMSO-d_6$ respectively. The NH-9 and NH-13 signals are offset. (Imp = impurity).

The 1H NMR spectrum of **3.5** (Figure 3.15) revealed a number of overlapped non-exchangeable signals as well as the now familiar two exchangeable protons (corresponding to NH-9 and NH-13). Inspection of the ^{13}C and DEPT 135 NMR data revealed twenty one well resolved carbon signals with two α,β -unsaturated carbonyl resonances at δ 182.9 (C-3), 166.2 (C-11) and 172.5 (C-3'), in addition to two sp^2 methines at δ 113.1 and 126.7 (initially assigned and eventually confirmed as C-4 and C-14 respectively (on comparison with the NMR data of compounds **3.2**, **3.3** and **3.4**), and four sp^3 methine signals at δ 63.7, 62.1, 56.4, and 51.2, four sp^3 methylene resonances at δ 51.0, 47.7, 36.1 and 19.1. The quaternary carbon resonances for the pyrroloiminoquinone core structure were also clearly evident at δ 146.2 (C-10), 166.2 (C-11), 123.5 (C-12), 117.5 (C-15), 147.4 (C-19), 100.6 (C-20) and 121.1 (C-21), while an sp^3 quaternary carbon at δ 45.8 was initially assigned and later confirmed as C-6 from the HMBC data. The HMQC data verified that the proton resonating at δ 5.68 (d, H-8) was attached to a carbon resonating at δ 62.1 implying a thioether functionality, while a carbon signal at δ 168.5 (C-5)

supported the thioether assignment. HMBC correlations from a proton at δ 6.17 (H-4) to C-2, C-5, C-6 and C-20 positioned C-4 as well as providing the initial assignment of C-2, while the HMQC experiment showed that H-2 (δ 4.33, d, 1H) was attached to C-2 (δ 63.7). COSY correlations between H-2 and H-1 (δ 3.64, s, 1H), in conjunction with HMQC data, led to the assignment of C-1 (δ 51.2). All that remained to be assigned was the substituent at position 1.

Table 3.5 NMR (DMSO- d_6 , 400 MHz for ^1H and 100 MHz for ^{13}C) data for compound **3.5**.

Atom No.	δ_c	δ_H (mult, J, Hz)	COSY	HMBC
C1	51.2 (d)	3.64 (m), 1H	H-2	C4'
C2	63.7 (d)	4.33 (d), 1H, $J = 3.2$ Hz	H-1, H-4, H-7 (5J)	C1, C3, C4, C6, C3' , C19
C3	182.9 (s)	-		
C4	113.1 (d)	6.17 (s), 1H	H-2, H-7	C2, C5, C6, C20 (lr)
C5	168.5 (s)	-		
C6	45.8 (s)	-		
C7	36.1 (t)	3.08 (dd), 1H, $J = 3.3$ Hz, 12.4 Hz 2.50 (m), 1H	H-7b, H-8 H-4, H-7a, H-8	C1, C5, C6, C8, C20, C21 C1, C5, C6, C8, C20
C8	62.1 (d)	5.68 (d), 1H, $J = 2.8$ Hz	H-7a, H-7b, NH-9	C5, C6, C7, C10
NH-9	-	10.74 (br s), 1H	H-8	
C10	146.2 (s)	-		
C11	166.2 (s)	-		
C12	123.5 (s)	-		
NH-13	-	13.13 (s), 1H	H-14	C12, C15, C21
C14	126.7 (d)	7.28 (d), 1H, $J = 1.8$ Hz	NH-13, H-16	C11, C12, C15, C21
C15	117.5 (s)	-		
C16	19.1 (t)	3.02 (m), 1H	H-14, H-17	C14, C15, C17, C21
C17	51.0 (t)	4.00 (m), 1H 3.79 (m), 1H	H-16, H-17b H-16, H-17a	C5, C15, C16, C19 C5, C15, C16, C19
C19	147.4 (s)	-		
C20	100.6 (s)	-		
C21	121.1 (s)	-		
C1'	47.7 (t)	3.54 (q), 2H, $J = 17.9, 34.4$ Hz	-	C1, C2', C3'
C2'	56.4 (d)	3.61 (d), 1H, $J = 3.3$ Hz	-	C2, C3, C5, C6, C20
C3'	172.5 (s)	-		
NH ₂ -2'	-	-*	-	

⁵J = five bond long range COSY coupling.

*Note: Proton chemical shift not observed for NH₂-2'. The ^1H NMR signal for COOH was once again also not observed and is also likely to be due to an intermediate rate of exchange with other protons (Section 3.2.3, c) as well as the presence of other exchangeable protons (*i.e.* NH-9, NH-13 and NH-2').⁹⁷

HMQC correlations (Figure 3.16, Table 3.5) showed the methylene and the methine protons at δ 3.54 (H-1', q, 2H) and 3.61 (H-2', d, 1H) to be attached to carbons resonating at δ 47.7 and 56.4,

respectively. An HMBC correlation between H₂-1' and C-1 and to carbons resonating at δ 56.4 and 172.5 tentatively attached the methylene moiety to C-1. The carbon resonance C-3' (δ 172.5) implied a carboxylic acid functionality which would also fulfil the requirements of the molecular formula (which shows an additional two oxygen atoms as opposed to the usual two for discorhabdins). The carboxyl carbonyl is therefore placed at one end of the fragment *i.e.* CH₂-X-COOH. Finally, the carbon chemical shift of the methine carbon at δ 56.4 (C-2') implied an electron withdrawing substituent such as a hydroxyl or an amino group. An amino substituent, would satisfy the carbon chemical shift of C-2' as well as the requirements of the molecular formula. Due to the multiplicity of the methine proton at δ 3.61 (d), the only position available for H-2' was at position X (in the fragment CH₂-X-COOH). Following this construction of the fragment, the structure of the C-1 substituent is thus proposed as CH₂-CH(NH₂)-COOH. As established with compound **3.2**, a very large geminal coupling constant ($J = 17.9$ Hz) was once again observed for the H₂-1' protons.

The close proximity of the resonances for the H₂-1' protons and the H-2' and H-1 methine protons proved problematic in unequivocally establishing the contiguous coupling (H-1-H₂-1'-H-2') sequence from the COSY spectrum. The absence of the amino and carboxylic acid exchangeable protons in the ¹H NMR spectrum of **3.5** was also noted.

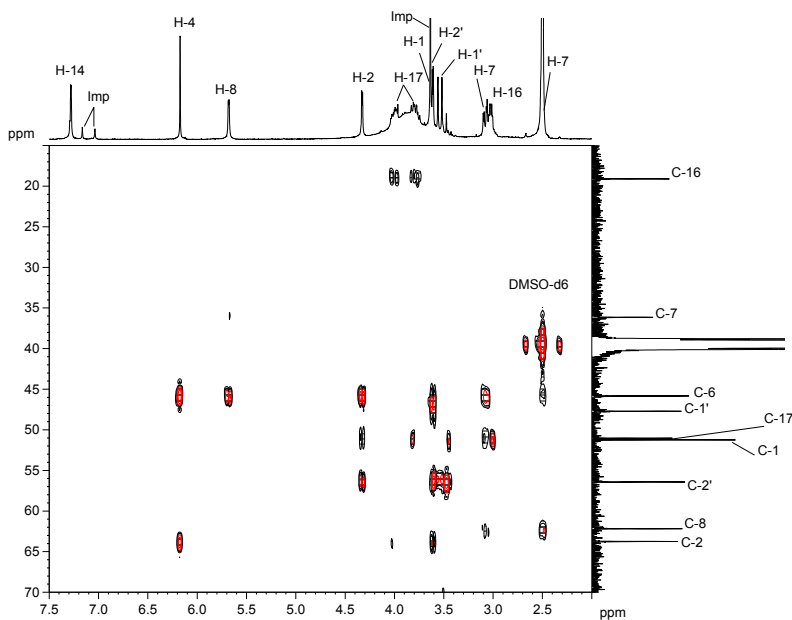


Figure 3.16 A section (F1 = δ 15 – 70 ppm, F2 = δ 2.0 – 7.5 ppm) of the HMBC spectrum of compound **3.5** (400/100 MHz, DMSO-d₆). (Imp = impurity).

The attachment of the α -amino acid substituent to the pyrroloiminoquinone structure *via* a carbon-carbon bond is, however, rather unusual in biosynthetic terms. Although the structure completely satisfied the molecular formula, confirmation of the proposed structure through various NMR

experiments and / or chemical degradation methods, especially in the absence of an unequivocal COSY correlation between H-1 and H₂-1', was necessary. An HSQC-TOCSY NMR experiment (Figure 3.17) was acquired (since the proton signals corresponding to H-1, H₂-1' and H-2' were better resolved in CD₃OD, Figure 3.15) in a further attempt to unambiguously establish the coupling between H-1, H₂-1' and H-2', since the experiment should be able to show the carbon atoms contiguously linked to H-1 proton. Regrettably, the ever elusive contiguous coupling was not observed.

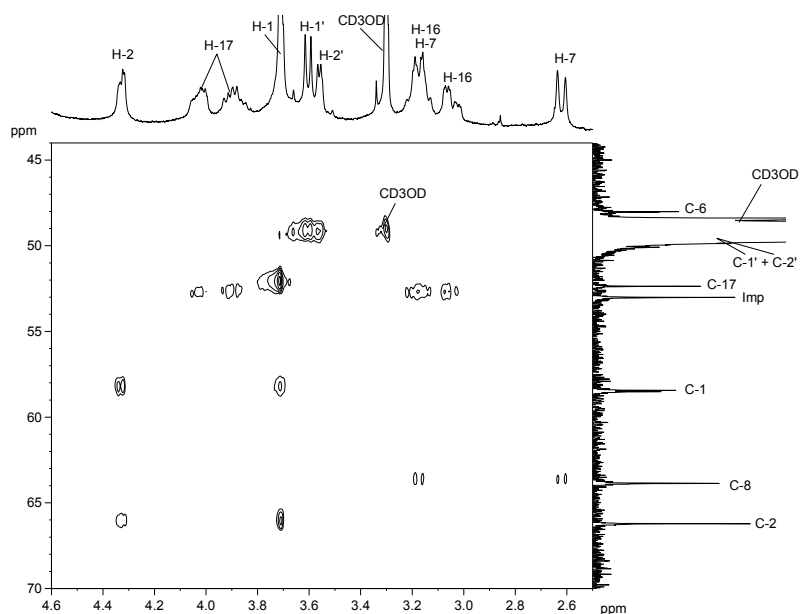


Figure 3.17 A section (F1 = δ 44 – 70 ppm, F2 = δ 2.5 – 4.6 ppm) of the HSQC-TOCSY spectrum of compound **3.5** (400/100 MHz, CD₃OD). (Imp = impurity).

A NOESY experiment provided additional evidence for the attachment of the H₂-1' methylene group to H-1 (Figure 3.18). Because the water signal in CD₃OD is further downfield than that in DMSO-d₆, we used CD₃OD since it offered less likelihood of the water resonance overlapping any relevant signals. In addition, the proton signals corresponding to H-1, H₂-1' and H-2' were better resolved in the ¹H spectrum of **3.5** acquired in CD₃OD (Figure 3.15). Due to the presence of a strong water signal in the deuterated solvent, transfer of magnetisation between the water and various proton signals were, however, observed which necessitated the use of a presaturated NOESY experiment. Long d₁ relaxation delays as well as mixing times (d₈) at 2.5 seconds (s) and 1.0 s, respectively, were found to be necessary, while the o1 value (solvent resonance to be irradiated) was set at 1924.05 Hz. Figures 3.18 and 3.19 and Table 3.6 show the NOESY correlations obtained for **3.5** at these settings. Figure 3.18 shows a NOESY correlation between H-1 and one of the H₂-1' protons providing some evidence in support of our assignment. The structure is thus tentatively proposed for **3.5**.

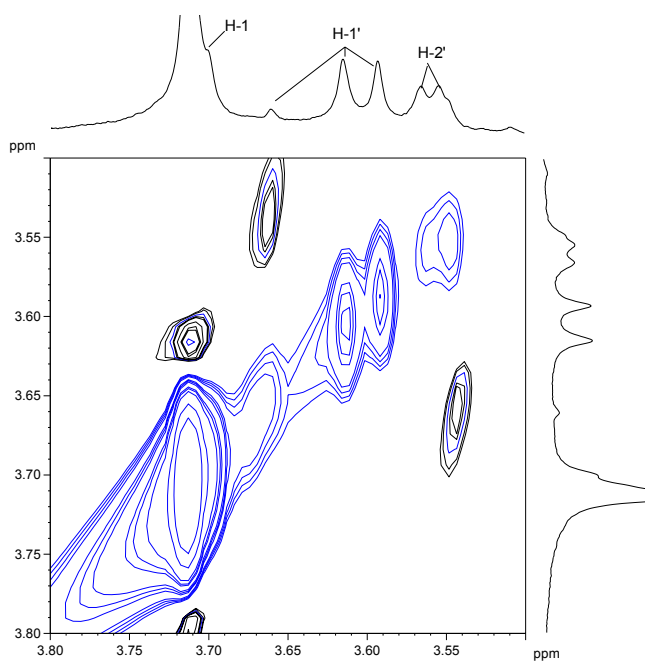


Figure 3.18 A section (F1, F2 = δ 3.50 – 3.80 ppm) of the NOESY spectrum of compound **3.5** (400 MHz, CD₃OD).

The nOe enhancements observed for **3.5** are given in Figure 3.19 in which the stereochemistry at C-1, C-2, C-6 and C-8 in **3.5** has been arbitrarily assigned based on the stereochemistry established for discorhabdin D.

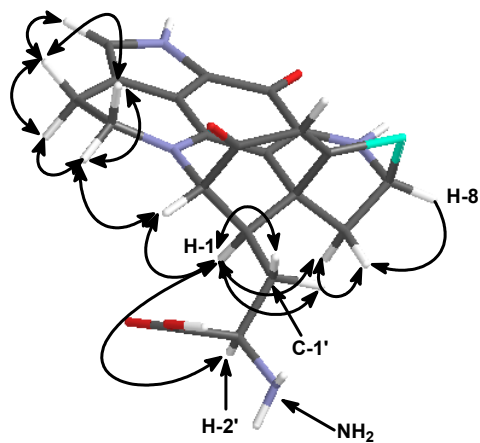


Figure 3.19 Enhancements observed in the NOESY spectra of **3.5** (400 MHz, CD₃OD). For the sake of clarity, weak enhancements have been omitted (please see Table 3.6).

Table 3.6 NMR (CD₃OD, 400 MHz for ¹H and 100 MHz for ¹³C) data for compound **3.5**.

Atom No.	δ_c	δ_H (mult, J, Hz)	COSY	HMBC	NOESY
C1	58.5 (d)	3.71, (s), 1H	H-2	C-2, C-3, C-5, C-6, C-3'	H-2; H-1'; H-2'; H-7a, H-7b (w)
C2	66.2 (d)	4.33 (m), 1H	H-1, H-4	C-1, C-3, C-6, C-19	H-1; H-17b, a (w)
C3	184.7 (s)				
C4	114.5 (d)	6.14 (s), 1H	H-2, H-7a	C-2, C-6, C-5, C-20	
C5	171.6 (s)				
C6	48.0 (s)				
C7	38.1 (t)	3.17 ^j (m), 1H 2.62 (d), 12.4 Hz, 1H	H-7a, H-8 H-4, H-7b, H-8	C-6, C-8, C-20 C-6, C-8, C-20	H-7a; H-1; H-7b
C8	63.9 (d)	5.59 (s), 1H	H-7	C-5, C-6, C-10	H-7b, a (w)
NH-9	-	-			
C10	148.1 (s)				
C11	167.5 (s)				
C12	125.5 (s)*				
NH-13	-	-			
C14	127.2 (d)	7.09 (s), 1H	H-16	C-11, C-12, C-15, C-21	H-16b, a (w)
C15	119.3 (s)				
C16	20.7 (t)	3.17 ^j (m) 3.05 (m)	H-17, H-16a H-17, H-16b, H-14	C-15	H-17; H-16
C17	53.0 (t)	4.01 (m), 1H 3.90 (m), 1H	H-17a, H-16 H-17b, H-16	C-19 C-19	H-16; H-17a; H-2 H-16; H-17b; H-2 (w)
C19	150.3 (s)				
C20	102.8 (s)				
C21	122.8 (s)*				
C1'	49.4 (t)	3.60 (q), 1H, 8.8 Hz		C-1, C-3'	-
C2'	49.4 (d)	3.56 (d), 1H, 4.4 Hz		C-1, C-3'	-
C3'	174.7 (s)				
NH-2'	-	-			

Note:

*C-12 and C-21 are interchangeable

(w) = weak enhancement (NOESY)

¹H-16 and H-7b protons are overlapped

C-1' and C-2' carbon signals are overlapped.

Interestingly, the large coupling constants observed for **3.5** in DMSO- d_6 were not observed when the same sample was run in CD_3OD .

3.3 Summary and Conclusion

The co-occurrence of makaluvamine C, damirone B and makaluvic acid A together with discorhabdins in the same latrunculid sponge is significant as it supports the proposed biosynthetic pathway outlined by Munro *et al.* (Chapter 1, Scheme 1.2).⁵⁹ Discorhabdins and makaluvamines (which are considered to be the probable biosynthetic precursors of the discorhabdins²⁶) have been isolated primarily from sponges of the genera *Latrunculia* (Family Latrunculidae) and *Zyzya*, respectively. Following taxonomic revisions, all the makaluvamines and damirones described thus far have been isolated from sponges of the genus *Zyzya*.²⁶ Discorhabdins A and P have, however, been isolated from the sponges of the genera *Zyzya fuliginosa*³⁰ and *Batzella*⁴⁰ respectively (Chapter 1, Section 1.2), while more recently, discorhabdin Q was isolated from sponges of the genera *Latrunculia* and *Zyzya*.⁴⁶ The previously unrecorded isolation of makaluvamine C, damirone B and makaluvic acid A (together with discorhabdins) from a latrunculid sponge is therefore noteworthy. It is indeed surprising that given the biosynthetic relationship between the damirones, makaluvamines and discorhabdins that these compounds have not been isolated from the same latrunculid sponge before.

Chapter 4: Pyrroloiminoquinone metabolites from *Tsitsikamma favus* and *Strongyloidesma* sp.

4.1 Introduction

Discorhabdin and *bis*-pyrroloiminoquinone type compounds predominated in the extract of the Latrunculid sponge *Tsitsikamma favus* (SAF 94-006) collected by SCUBA from the Tsitsikamma Marine Reserve. The sponge *T. favus* was the first species of a new genus of Latrunculid sponge to be discovered off the coast of South Africa.

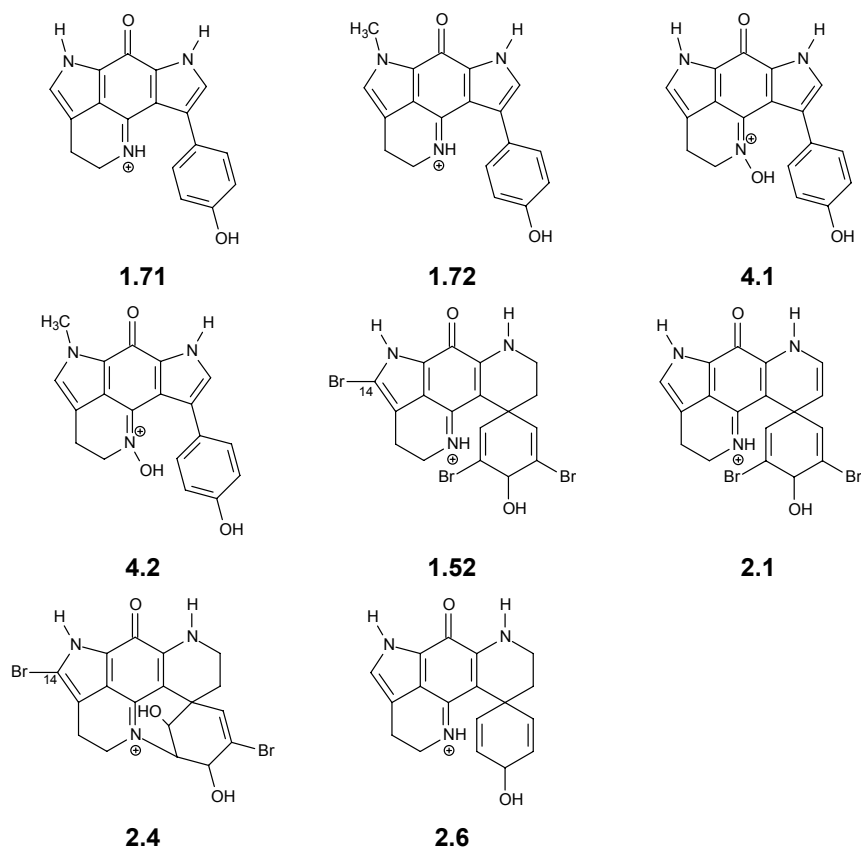


Figure 4.1 Summary of the compounds isolated from *T. favus*.

Although the major natural product constituents of this sponge had been examined previously by Hooper (as part of his PhD research),^{41,98} improvements in chromatographic and spectroscopic techniques warranted a re-investigation of the minor pyrroloiminoquinone metabolites of this sponge. Accordingly, the frozen sponge was soaked in methanol and the aqueous methanol extract partitioned between hexane, chloroform and *n*-butanol. Extensive chromatography of the concentrated chloroform and *n*-butanol partition fractions yielded three known (**1.71**, **1.72**, **1.52**) and five new pyrroloiminoquinones (**4.1**, **4.2**, **2.1**, **2.4** and **2.6**) (Figure 4.1). Discorhabdins **2.1**, **2.4**

and **2.6** were also isolated from *T. pedunculata* (Chapter 2). The co-occurrence of compounds **1.52**, **2.1**, **2.4** and **2.6** in *T. favus* and *T. pedunculata* provides some chemotaxonomic evidence in support of both species belonging to the same genus.⁵⁵ Of particular note is the bromination at C-14 in compounds **1.52** and **2.4** a structural feature that appears to be unique to pyrroloiminoquinone metabolites from the new genus *Tsitsikamma*. Another structural feature shared by the discorhabdin type metabolites (including the new discorhabdin S analogues) of the two species in this genus is the allylic secondary alcohol functionality at C-3. Interestingly, the bis-pyrroloiminoquinone metabolites, common in the extracts of *T. favus*, are absent in the abstracts of *T. pedunculata* and the tentative chemotaxonomic significance of this unusual skeleton, in defining species from the new genus *Tsitsikamma* alluded to by Hooper *et al.*,⁴¹ appears to be misplaced.

As described in previous chapters LC-MS was initially used to establish an approximate molecular mass and provide details of the degree of bromination within the molecule. The structures were solved using standard spectroanalytical techniques as well as by comparison of their spectroscopic data with those of known compounds in the series. Compounds **4.1**, **4.2** and particularly **2.1**, **2.4**, **2.6** were isolated from *T. favus* as minor metabolites. As discussed previously (Chapter 2) DMSO- d_6 was the preferred solvent used for the NMR analyses to maximize the information available from the exchangeable protons.

A fourth Latrunculid sponge belonging to the genus *Strongylodesma* and commonly known as Philip's Green sponge, also a new species, was collected from Algoa Bay in 1996. The ^1H NMR spectra showed primarily discorhabdin type pyrroloiminoquinones in its methanol extract. The frozen sponge was steeped in methanol and the concentrated extract partitioned between hexane, chloroform and *n*-butanol. Exhaustive chromatography carried out on the concentrated chloroform and *n*-butanol partition fractions yielded three known (**1.57**, **1.61**, **1.53**) and one new pyrroloiminoquinone (**3.3**) (Figure 4.2). The new discorhabdin **3.3** was also isolated from *L. lorii* (Chapter 3). The samples were routinely subjected to direct injection low resolution LC-MS following solid phase extraction (Section 4.3.2) and meticulous HPLC chromatography. The structures were also solved using standard spectroanalytical techniques as well as by comparison of their spectroscopic data with those of known compounds in the series. All NMR spectra were recorded in DMSO- d_6 .

The *Strongylodesma* sp. sponge contained the highly cytotoxic discorhabdin A as its major metabolite in addition to discorhabdin D. The *Strongylodesma* sp. metabolites were also characterised by a) either a reduced carbonyl and a ketone at C-3; b) bromination at C-2 and / or C-4; and c) a discorhabdin D and / or C type skeleton.

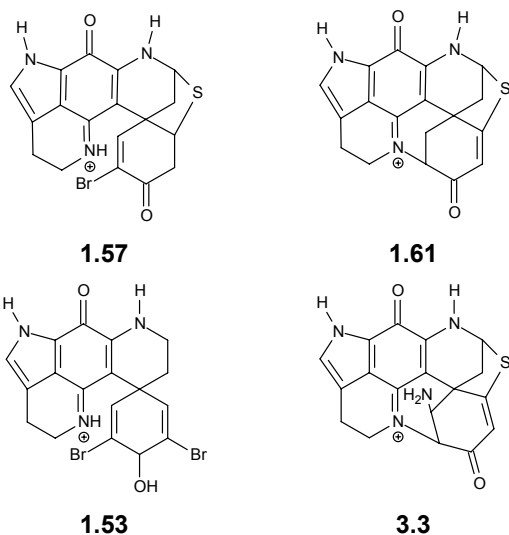


Figure 4.2 Summary of the compounds isolated from *Strongyloides* sp..

4.2 Results and Discussion

4.2.1 The taxonomy of the sponge *Tsitsikamma favus*



Figure 4.3 An underwater photograph of *T. favus*.

The brown nodular Latrunculid sponge *T. favus* (Figure 4.3) was collected by SCUBA at a depth of -20 m in the Tsitsikamma Marine Reserve, South Africa in 1994. Samaai and Kelly⁵⁵ described the sponge as follows: "Sponge is massive, ovo-spherical, sometimes thickly encrusting, 1 – 8 cm high and 10 – 15 cm wide. Texture is hard and only slightly compressible, resilient and leathery; surface smooth and crowded with large single to multichambered cylindrical lance-shaped oscules, 1 – 4 mm wide, 8 mm high and many pedunculate cauliform areolated porefields, 3 mm

wide, 5 – 6 mm high, with no membrane; colour in life is dark brown or liver brown and between cauliform structures dark turquoise, choanosome dark brown. The choanosome is divided into honeycomb-like chambers and convoluted layers by very thick reinforced tracts of anisostyles, these tracts range in width from 1000 – 1700 μm thick, forming meshes that are elliptical in shape and 5800 μm wide. These tracts are lined with microscleres, suggesting that they may represent an early ectosermal surface, and that the sponge grows in size and volume by putting on new chambers, as in many species of *Petrosia* and *Coelocarteria*. Within and between the chambers and convoluted layers the skeleton consists of an ill-formed, irregular reticulation of small anisostyles, these tracts range in width from 100 – 150 μm . Microscleres are isodischorhabds and these are abundant throughout the choanosome. The ectosome is composed of a thick dense feltwork of tangential and paratangential anisostyles approximately 900 μm wide. This layer is present in the fistulae with anisostyles disposed in a compact regular vertical to oblique arrangement supporting the cauliform areolate structures. A single layer of erect isochiadiscorhabds (48 μm wide) lines the surface of the ectosome. Megascleres in two categories of anisostyles, (1) slightly curved and thickened centrally, 621(537-700) x 14(14) μm , n = 20; (2) thinner slightly curved centrally: 530(480-566) x 9.6(9.6) μm . Microscleres are ischiadiscorhabds with three whorls of cylindrical, conical tubercles, the apex of each tubercular projection is acanthose: 48(41-60) x 9(7.2-9.6) μm . Reproduction: oocytes present in specimens but no further indication of reproductive mode yet corroborated. The huge spicule tracts that compartmentalize the body of *Tsitsikamma favus* are remarkable and clearly differentiate it from *Latrunculia*, *Strongylodesma* and *Sceptrella*, and other related demosponges. The characters that link the genera are the base pigmentation, chemistry, the surface palisade of microscleres and the soft skeletal parts.”

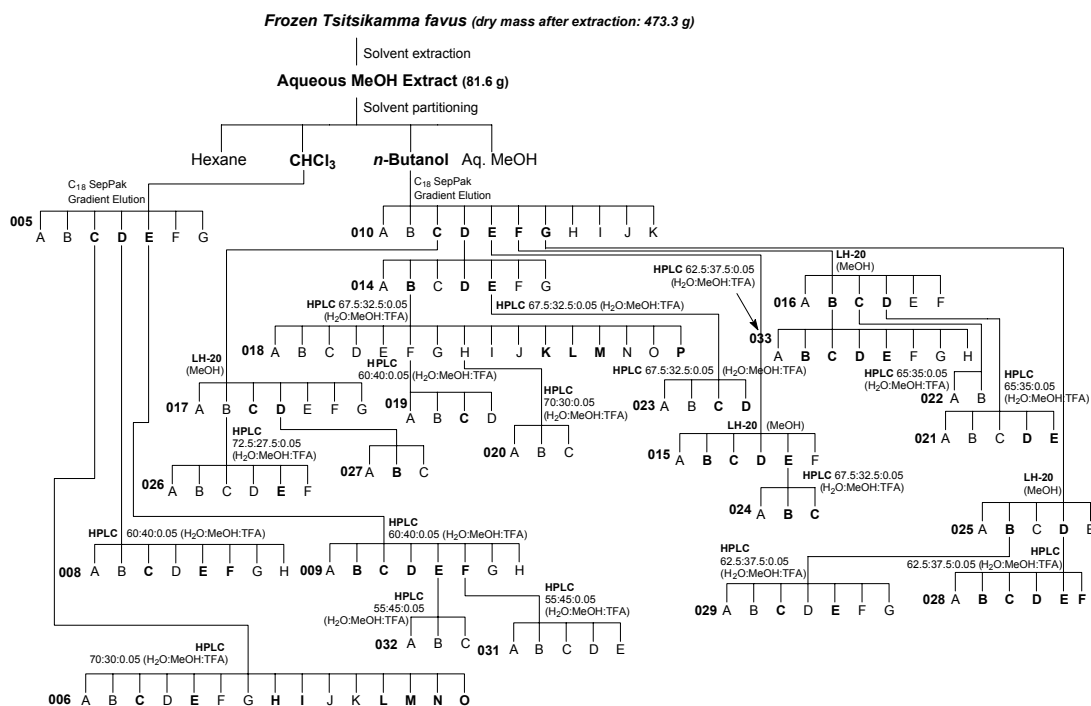
4.2.2 Extraction and isolation of pyrroloiminoquinone metabolites from *T. favus*

The frozen sponge (SAF 94-006) was steeped in methanol overnight and the aqueous methanol extract partitioned according to a modified Kupchan procedure (Scheme 4.1). The sponge was dried after the extractions to provide an approximate dry mass.

The known compounds tsitsikammamine A (**1.71**)^{41,98} and B (**1.72**)^{41,98} as well as 14-bromo-3-dihydro-discorhabdin C (**1.52**),^{41,98} together with the four new compounds, namely tsitsikammamine A N-oxime (**4.1**), tsitsikammamine B N-oxime (**4.2**), 7,8-dehydro-3-dihydro-discorhabdin C (**2.1**), 14-bromo-1-hydroxy-discorhabdin S (**2.4**), and 2,4-debromo-3-dihydro-discorhabdin C (**2.6**), were isolated from *T. favus*. Compounds **2.1**, **2.4** and **2.6** were previously isolated from *T. pedunculata* and their structure elucidation is described in Chapter 2.

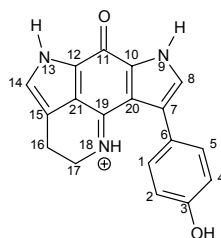
The tsitsikammamines (**1.71** and **1.72**) and compound **1.52** were isolated from the chloroform partition fraction of the sponge extract, while the new compounds (**4.1**, **4.2**, **2.1**, **2.4**, **2.6**) were obtained from the *n*-butanol partition fraction. The structures of the known compounds reported

here, were determined from a combination of 2D-NMR spectroscopy and spectral comparisons with known discorhabdins and *bis*-pyrroloiminoquinones, particularly discorhabdin C and D and tsitsikammamine A and B.



Scheme 4.1 Extraction and pyrroloiminoquinone isolation scheme for *T. favus*. The masses and yields (calculated relative to the dry mass of sponge) of the *T. favus* pyrroloiminoquinone metabolites are summarized below:

006-I, 008-C	1.71	10.3 mg	0.002 %
008-E, 009-B	1.72	36.8 mg	0.008 %
021-D	4.1	4.7 mg	0.001 %
021-E	4.2	2.9 mg	0.0006 %
009-D	1.52	9.6 mg	0.002 %
018-L	2.4	2.1 mg	0.0004 %
026-E	2.7	4.3 mg	0.001 %
018-M	2.9	2.0 mg	0.0004 %

4.2.3 Structure elucidation of pyrroloiminoquinone metabolites from *T. favus*a) *Tsitsikammamine A (1.71)***1.71**

HRFAB mass spectral analysis of the known compound *tsitsikammamine A (1.71)* (10.3 mg, 0.002 % yield) indicated an M^+ ion at m/z 304.1087 thus establishing the molecular formula of **1.71** as $C_{18}H_{14}N_3O_2$. Although the ^{13}C NMR spectrum of **1.71** revealed only sixteen distinct carbon resonances, the molecular formula, as well as the enhanced intensity of two of the ^{13}C signals (δ 116.2 and 128.9), implied that two resonance pairs were overlapped. The DEPT NMR experiment revealed two methylene and four methine signals (two of which were overlapped), supporting the presence of ten quaternary carbons. The characteristic 1H NMR spectrum of *tsitsikammamine A*, with its pair of exchangeable 1H NMR signals at approximately δ 13.1, is deceptively simple (Figure 4.4).

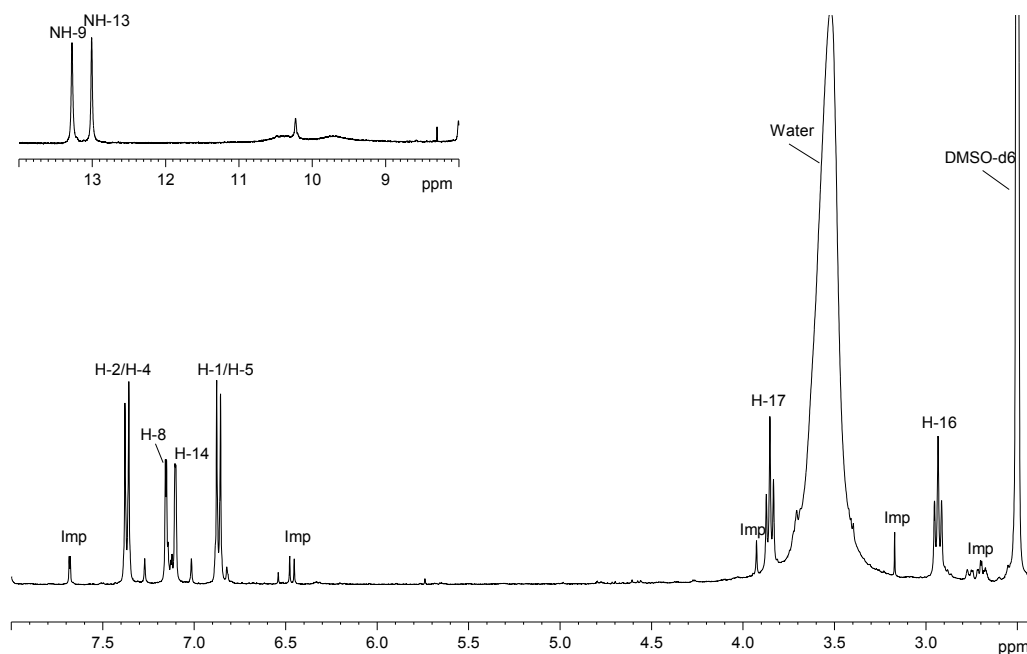
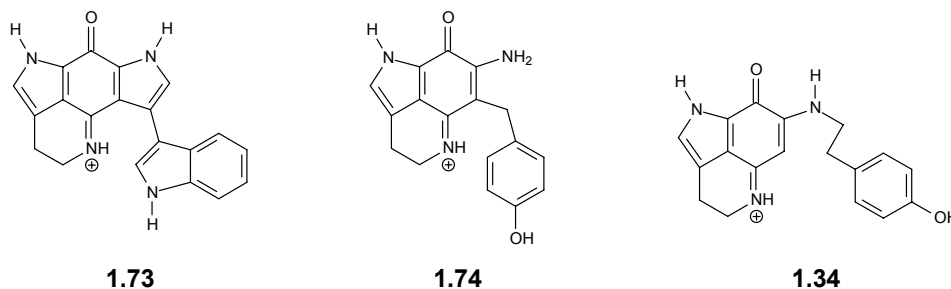


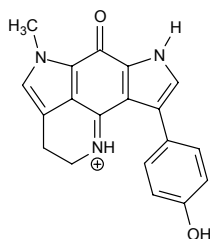
Figure 4.4 1H NMR spectrum of *tsitsikammamine A (1.71)* (400 MHz, $DMSO-d_6$) with NH-9 and NH-13 offset. (Imp = impurity).

The typical pyrroloiminoquinone substructure is evident from the mutually coupled methylene signals at δ 2.93 (2H, t, J = 8.0 Hz, H₂-16) and δ 3.85 (2H, t, J = 8.0 Hz, H₂-17) as well as the coupling of NH-13 (1H, br s) at δ 13.01 to δ 7.10 (1H, d, J = 1.6 Hz, H-14), observed in the COSY NMR spectrum. These spin systems, together with the pyrroloiminoquinone ¹³C resonances at δ 166.3 (C-11), 127.8 (C-12), 123.1 (C-14), 119.2 (C-15), 17.6 (C-16), 44.9 (C-17), 157.8 (C-19) and 120.7 (C-21), characteristic of the left hand hemisphere of a typical discorhabdin type substructure, accounted for eight of the fourteen degrees of unsaturation implied by the molecular formula. Evidence for the characteristic *para*-substituted phenol ring of the tsitsikammamines was provided by the mutually coupled two proton doublets at δ 7.37 (d, J = 8.4 Hz, H-2 and H-4) and δ 6.87 (d, J = 8.4 Hz, H-1 and H-5), as well as the distinctive ¹³C quaternary signals at δ 127.2 (C-6) and 157.5 (C-3). The remaining ¹³C signals at δ 122.4 and 125.0 were assigned to C-7 and C-8 in a trisubstituted pyrrole ring system. The ¹H and ¹³C NMR data of **1.71** was consistent with those published for tsitsikammamine A.^{1,2}

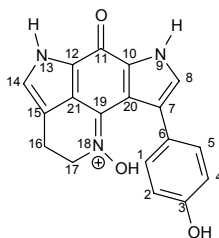
As mentioned previously, the related *bis*-pyrroloiminoquinone, wakayin (**1.73**) was isolated from a Fijian ascidian *Clavelina* sp. and is the first and only reported pyrroloiminoquinone metabolite to be isolated from a marine phylum other than Porifera.⁵³ The question of whether *bis*-pyrroloiminoquinones originate from the invertebrate organism alone or from associated microorganisms was therefore raised. Wakayin was initially reported to exhibit topoisomerase II inhibition (250 μ M) by Copp *et al.*⁵³ In contrast, a later report by Kokoshka *et al.* showed wakayin to exhibit topoisomerase I activity.⁹¹



An investigation of another Fijian marine invertebrate, *Zyzzya fuliginosa*, yielded the novel, related, pyrroloiminoquinone metabolite, veiutamine (**1.74**).⁵⁴ In common with wakayin (**1.73**), veiutamine, which also contains the *para*-phenol substituent characteristic of the tsitsikammamines, exhibited potent cytotoxicity and interestingly, was shown to be more active than its related analogue makaluvamine D (**1.34**).⁵⁴

b) *Tsitsikammamine B* (**1.72**)**7.2**

Tsitsikammamine B (**1.72**) (36.8 mg, 0.008 % yield) gave an M+1 ion at m/z 319.1321 upon analysis by HRFABMS, which is consistent with the molecular formula $C_{19}H_{17}N_3O_2$. The NMR data of *tsitsikammamine B* (**1.72**) *i.e.* the iminoquinone ^{13}C resonances at δ 166.7 (C-11), 126.3 (C-12), 118.7 (C-15), 17.5 (C-16), 44.6 (C-17), 156.2 (C-19) and 120.6 (C-21) and the phenolic ^{13}C signals at δ 116.2 (C-1/C-5), 128.9 (C-2/C-4) and 157.6 (C-3) were all consistent with a para-phenoxy *bis*-pyrroloiminoquinone structure. While the proton spectrum revealed the absence of the NH-13 signal and the presence of a single methyl singlet (δ 3.96), the ^{13}C spectrum with seventeen carbon signals (two overlapped), showed an additional methyl resonance at δ 35.7. This, together with the downfield carbon chemical shift of the C-14 resonance to δ 127.9, as well as the subsequent collapse of the H-14 resonance (δ 7.12) from a doublet ($J_{13,14} = 1.6$ Hz) to a singlet in the 1H spectrum, implied methylation at N-13. The NMR data for **1.72** was consistent with those of *tsitsikammamine B*.^{41,98}

c) *Tsitsikammamine A N-oxime* (**4.1**)**4.1**

The molecular formula of **4.1** (4.7 mg, 0.001 % yield) ascertained from HRFAB mass spectral analysis indicated a molecular ion at m/z 322.1192 ($\Delta +0.1$ mmu), corresponding to a molecular formula of $C_{18}H_{16}N_3O_3$. The difference between the molecular formula of **4.1** and **1.71** was therefore an oxygen atom.

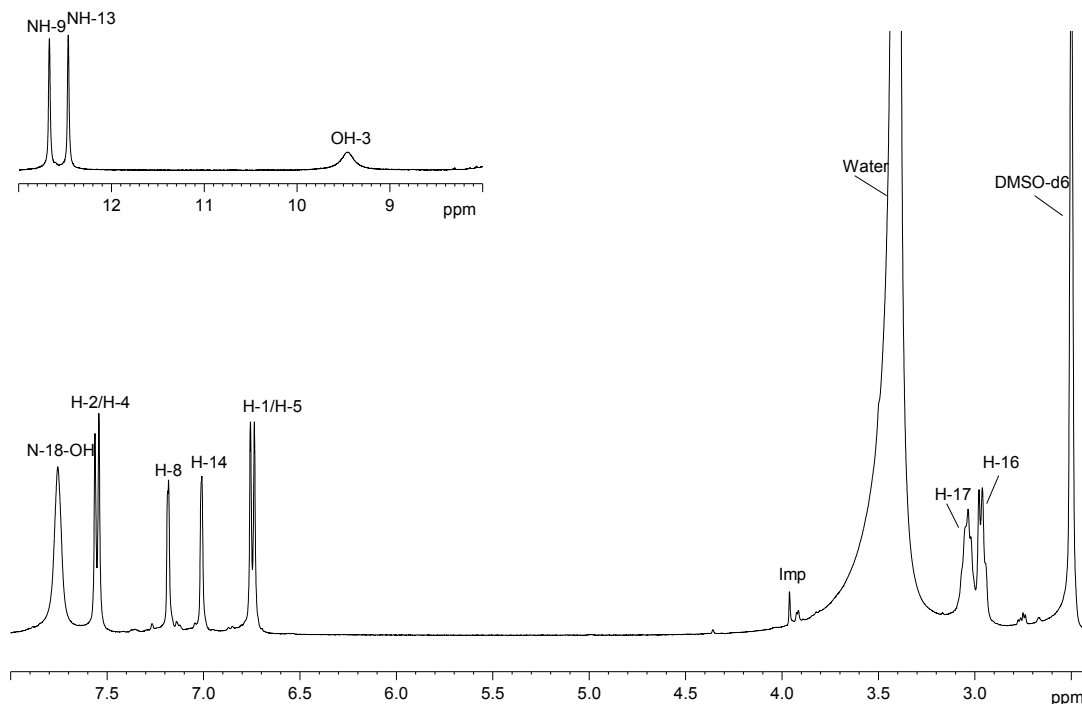


Figure 4.5 ^1H NMR spectrum of tsitsikammamine A N-oxime (**4.1**) (400 MHz, DMSO-d_6) with NH-9, NH-13 and OH-3 offset. (Imp = impurity).

The close similarities between the ^1H NMR spectra of **4.1** (Figure 4.5) and **1.71** (Figure 4.4) were immediately evident. The ^{13}C NMR spectrum (Figure 4.6) of **4.1** showed sixteen distinct carbon resonances, with two resonance pairs overlapped once again. The DEPT NMR experiment showed two methylene and four methine signals (two of which were overlapped), supporting the presence of ten quaternary carbons. The pyrroloiminoquinone substructure was evident from the mutually coupled methylene signals at δ 2.97 (2H, m, H_2 -16) and δ 3.04 (2H, m, H_2 -17) in addition to the small vicinal coupling of the NH-13 proton (1H, br s) at δ 12.47 to δ 7.01 (1H, br s, H-14), observed in the COSY NMR spectrum (Figure 4.7). These spin systems, together with the pyrroloiminoquinone ^{13}C resonances at δ 168.6 (C-11), 129.4 (C-12), 130.3 (C-14) and 119.8 (C-15) are characteristic of the tsitsikammamine compounds and accounted for eight of the fourteen degrees of unsaturation implied by the molecular formula. A careful evaluation of the differences between the ^1H NMR spectra of **4.1** and **1.71** revealed that the multiplet attributed to H_2 -17 was shifted upfield ($\Delta \delta$ 0.8 ppm) suggesting a change in substitution at the neighbouring N-18 atom. The significant carbon chemical shifts (Figure 4.6) of C-17 and C-19 to δ 38.7 and 180.4, respectively, as well as the less dramatic chemical shifts of C-16 and C-21 to δ 23.5 and 125.3, respectively, also suggested substitution at N-18.

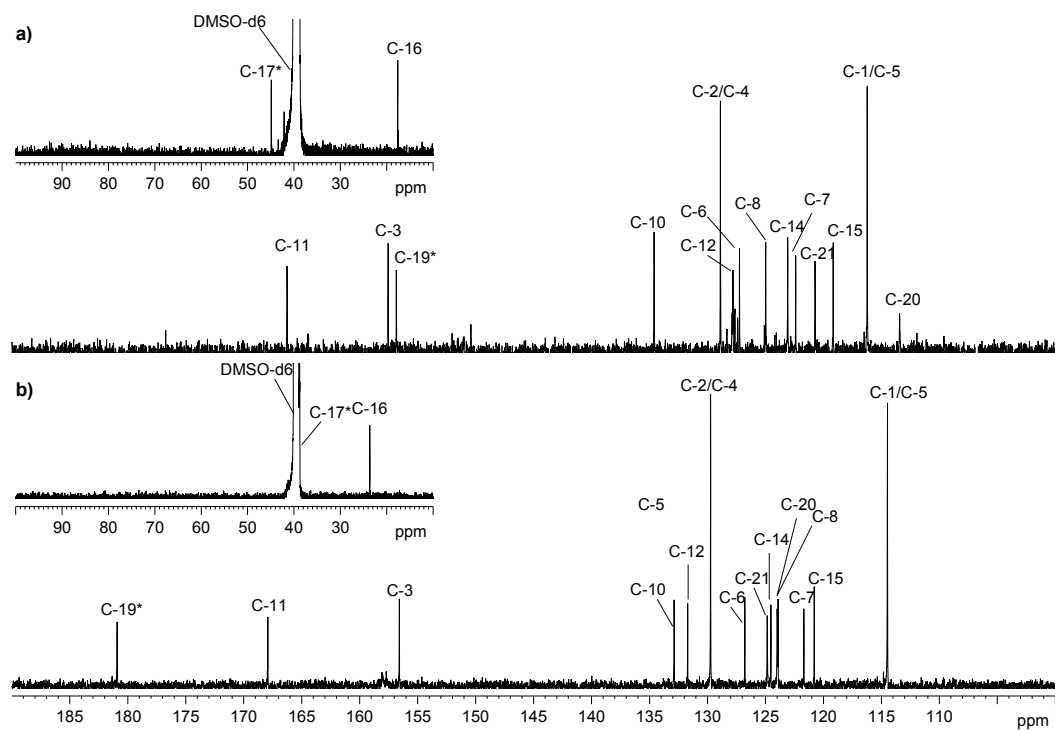


Figure 4.6 ^{13}C NMR spectrum (100 MHz, DMSO- d_6) of a) tsitsikammamine A (1.71) and b) tsitsikammamine A N-oxime (4.1) with C-16 and C-17 offset. Please note the chemical shifts of C-17* and C-19* in particular. (Imp = impurity).

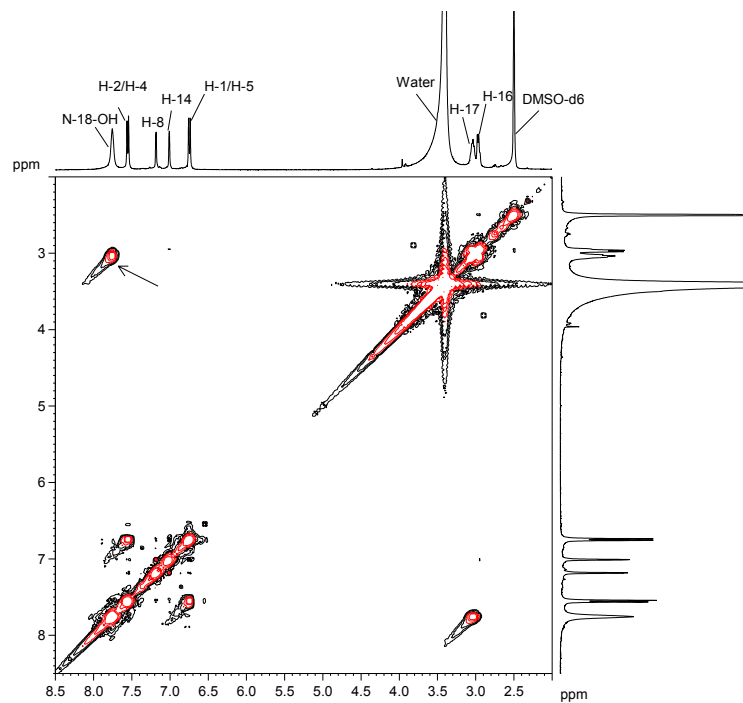


Figure 4.7 A section (F1, F2 = δ 2.0 – 8.5 ppm) of the COSY spectrum of compound 4.1 (400/100 MHz, DMSO- d_6) showing the 3J COSY coupling between N-18-OH and H₂-17.

Supporting evidence for the existence of an N-O band at N-18 was provided by infra red (IR) spectroscopy. The interpretation of the IR spectrum of fused ring compounds, such as **4.1**, is complicated by the greater vibrational coupling experienced compared to compounds with isolated ring systems.^{99,100} Significant shifts in IR absorption bands of the parent structure are expected in compounds possessing an N-oxygen band.⁹⁹⁻¹⁰² Five absorption bands, were identified as having undergone significant shifts in the IR spectrum of **4.1** (i.e. 438, 608, 908, 987 and 1487 cm^{-1}). Classic assignments of N-oxygen bands include the bands present at approximately 1250 cm^{-1} due to vibrational coupled $\nu\text{N-O}$ (e.g. 1252 and 1307 cm^{-1} for pyridine and pyrazine N-oxides respectively)⁹⁹ and approximately 470 cm^{-1} due to in plane bending ($\alpha\text{N-O}$) (468 and 475 cm^{-1} for pyridine and pyrazine N-oxides respectively).⁹⁹

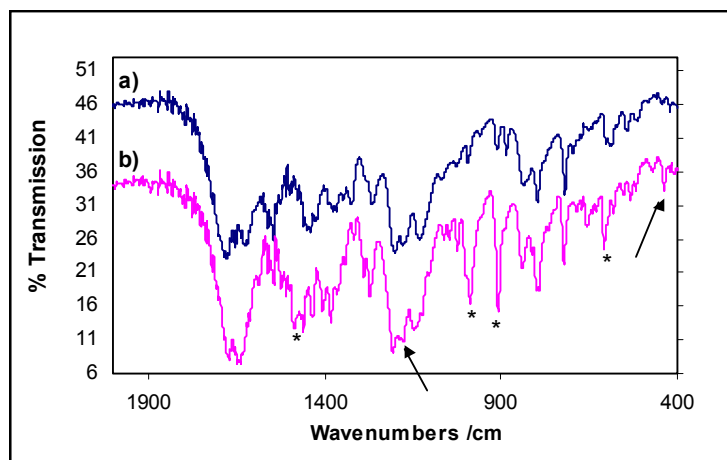


Figure 4.8 Overlaid IR spectra (2000 – 400 cm^{-1}) of a) tsitsikammamine A (**1.71**) and b) its N-oxime (**4.1**). The true N-oxide bands are indicated on the graph by means of an arrow while the bands which display the sensitivity typical of N-oxides and N-18 oximes are indicated by means of an asterisk (*).

Unfortunately compound **1.71** exhibited a strong band at 1207 cm^{-1} and it thus assumed that compound **4.1**'s N-oxygen band is buried underneath this peak (Figure 4.8). A true N-oxygen band (medium intensity), characteristic of an in plane bending for the N-oxygen band ($\alpha\text{N-O}$) was, however, observed at 438 cm^{-1} in the IR spectrum of **4.1**. The sensitivity of the bands at 608, 908, 987 and 1487 cm^{-1} together with the characteristic N-oxygen band at 438 cm^{-1} thus implies the presence of an N-oxygen type functionality. Substituent sensitivity was clearly observed upon comparison of naphthalene and quinoline N-oxide (Table 4.1), providing additional evidence for the existence of the N-oxygen type functionality.¹⁰⁰

Table 4.1 Substituent sensitivity of the planar ring modes in quinoline N-oxide compared to its homocyclic parent (naphthalene).¹⁰⁰

	Band (cm ⁻¹)	Band (cm ⁻¹)	Band (cm ⁻¹)	Band (cm ⁻¹)
Napthalene	1010	936	1458	618
Quinoline N-oxide	878	928	1447	628
Difference (shift)	-132	-8	-11	+10

The classic assignments for quinoline N-oxide have been given as 1233 (ν N-O, vibrational coupling) and 318 cm⁻¹ (α N-O).¹⁰⁰ This, together with the compounds ability to produce radicals upon irradiation, a feature characteristic of N-oxides and N-18 oximes^{103,104} (please refer to Chapter 5), also suggests the presence of an N-oxygen functionality.

It seems likely that **4.1** and **4.2** would exist as oximes instead of N-oxides since they were isolated at approximately pH 3.0 (0.05% TFA), which together with the N-18-OH signal at δ 7.76 obtained in the ¹H NMR spectrum, and the HRFAB MS data, resulted in the assignment of the oxime rather than an N-oxide functionality.

The distinctive ¹³C quaternary signals at δ 126.5 (C-6) and 156.6 (C-3) and the mutually coupled two proton pairs at δ 7.55 (d, J = 8.4 Hz, H-2 and H-4) and δ 6.75 (d, J = 8.4 Hz, H-1 and H-5), typical of the *para*-substituted phenol rings of tsitsikammamines were observed. The ¹³C signals at δ 121.2 and 123.9 of C-7 and C-8 of the trisubstituted pyrrole ring system complete the skeleton of a *bis*-pyrroloiminoquinone N-oxime, which is supported by two, three and four bond correlations observed in the HMBC NMR experiments (Figure 4.9) of **4.1** (Table 4.2).

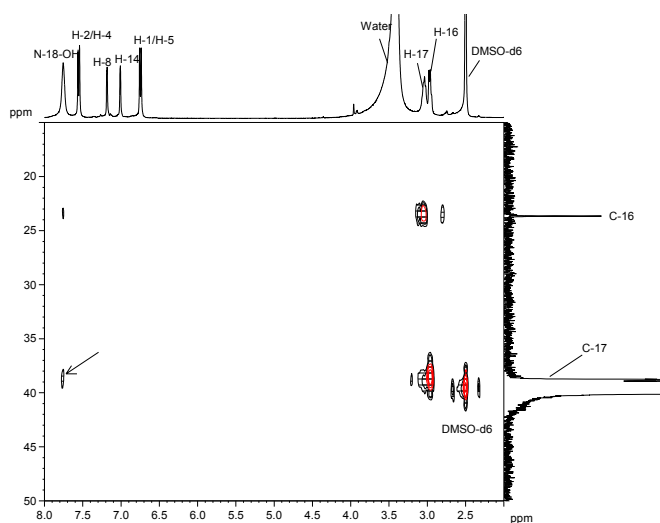
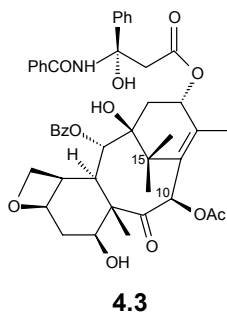
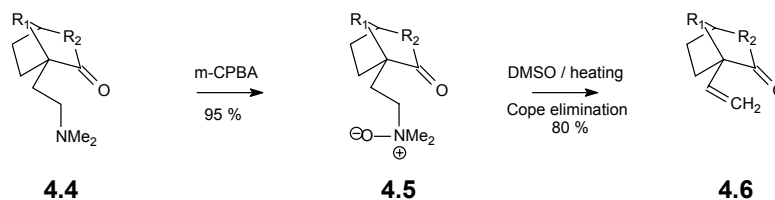
**Figure 4.9** A section (F1 = δ 10 – 50 ppm, F2 = δ 2.0 – 8.0 ppm) of the HMBC spectrum of compound **4.1** (400/100 MHz, DMSO-d₆).

Table 4.2 NMR (DMSO-d₆, 400 MHz for ¹H and 100 MHz for ¹³C) data for compound **4.1**.

Atom no.	δ _c	δ _H (mult, J, Hz)	COSY	HMBC
C1	114.5 (d)	6.75 (d), 2H, 8.4 Hz	H2 / H4	C2, C3, C4, C5, C8
C2	129.7 (d)	7.55 (d), 2H, 8.4 Hz	H1 / H5	C1, C3, C4, C5, C8
C3	156.6 (s)			
C4	129.7 (d)	7.55 (d), 2H, 8.4 Hz	H1 / H5	C1, C2, C3, C5, C8
C5	114.5 (d)	6.75 (d), 2H, 8.4 Hz	H2 / H4	C1, C2, C3, C4, C8
C6	126.5 (s)			
C7	121.2 (s)			
C8	123.9 (d)	7.18 (d), 1H, 2.8 Hz	NH-9	C6, C7, C10, C11
NH-9	-	12.67 (s), 1H	H-8	C6, C7, C10
C10	133.2 (s)			
C11	168.6 (s)			
C12	129.4 (s)			
NH-13	-	12.47 (s), 1H	H-14	C15
C14	130.3 (s)	7.01 (d), 1H, 2Hz	NH-13	C11, C12 / C21, C15
C15	119.8 (s)			
C16	23.5 (t)	2.97 (m), 2H	H-17	C15, C17
C17	38.7 (t)	3.04 (m), 3H	H-16, N-18-OH	C15, C16
N-18-OH	-	7.76 (s), 3H	H-17	C16, C17
C19	180.4 (s)			
C20	123.9 (s)			
C21	125.3 (s)			
C-3-OH		9.45 (br s), 1H		

In an effort to confirm the presence of the N-18-oxygen functionality, the conversion of tsitsikammamine A into **4.1** was attempted. Pyridine N-oxides, for example, are typically prepared by heating pyridine in glacial acetic acid at 80 °C with 30% hydrogen peroxide followed by neutralisation of the pyridine N-oxime and isolation of the pyridine N-oxide by distillation.¹⁰⁵ The preparation of (1S)-10-methylenecamphor, an intermediate in the synthesis of the natural product taxol (**4.3**, Scheme 4.2), by Martínez *et al.*¹⁰⁶ employed the use of *meta*-chloroperbenzoic acid (*m*-CPBA) to convert the amino ketone **4.4** via the N-oxide **4.5** to the taxane intermediate, enone **4.6** in Scheme 4.2.

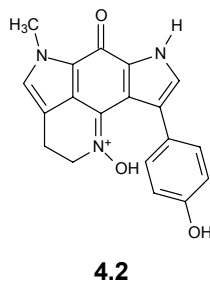




Scheme 4.2 Martínez *et al.*'s synthesis of the taxol intermediate 10-methylenecamphor.¹⁰⁶

Two attempted preparations of an N-oxide analogue of the TFA salt of tsitsikammamine A (**1.71**), using firstly hydrogen peroxide and glacial acetic acid and secondly *meta* chloroperbenzoic acid (*m*-CPBA), were unsuccessful. In a further effort to oxidise the N-18 of **1.71**, the free base of **1.71** was first prepared by neutralisation with 5 M sodium hydroxide but this neutralisation also proved difficult. These results may suggest that the N-oxime is not an artifact arising from the extraction and chromatography employed but rather that it might be of enzymatic origin.

d) *Tsitsikammamine B N-oxime* (**4.2**)



Compound **4.2** (2.9 mg, 0.0006 % yield) gave a M+1 ion at m/z 336.1348 (Δ +0.1 mmu) by HRFABMS analysis, consistent with the molecular formula $C_{19}H_{18}N_3O_3$.

The NMR data of tsitsikammamine B N-oxime (**4.2**) displayed the familiar iminoquinone ^{13}C resonances at δ 168.6 (C-11), 129.4 (C-12), 119.8 (C-15) and 125.3 (C-21), all consistent with the *para*-phenoxy *bis*-pyrroloiminoquinone structure. The proton NMR spectrum (Figure 4.10) revealed that the NH-13 signal had disappeared, while the ^{13}C spectrum revealed an additional methyl resonance at δ 35.8, which together with the carbon chemical shift of the C-14 resonance to δ 130.3, implied the presence of a methylated N-13. The additional oxygen given by the molecular formula coupled with the drastic chemical shifts of C-19 and C-17 to δ 180.4 and 38.7, respectively, implied that **4.2** was tsitsikammamine B N-oxime. Support for the tsitsikammamine B N-oxime structure is provided by the 2D NMR data (Figure 4.11 and Table 4.3).

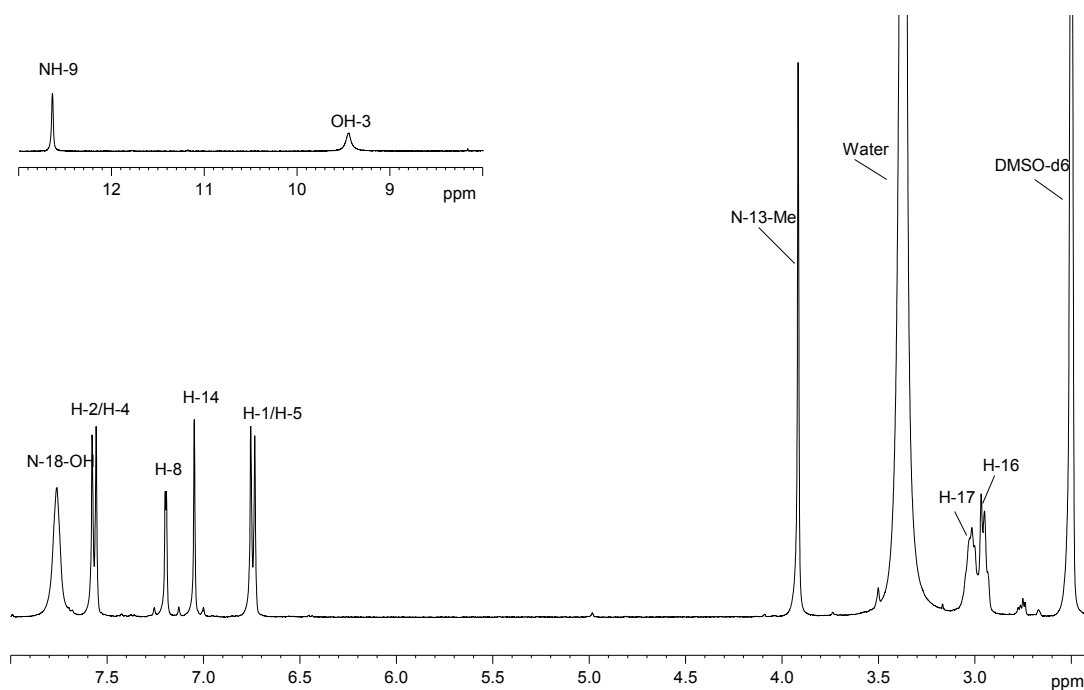


Figure 4.10 ^1H NMR of **4.2** (400 MHz, DMSO-d_6) with NH-9, NH-13 and OH-3 offset. (Imp = impurity).

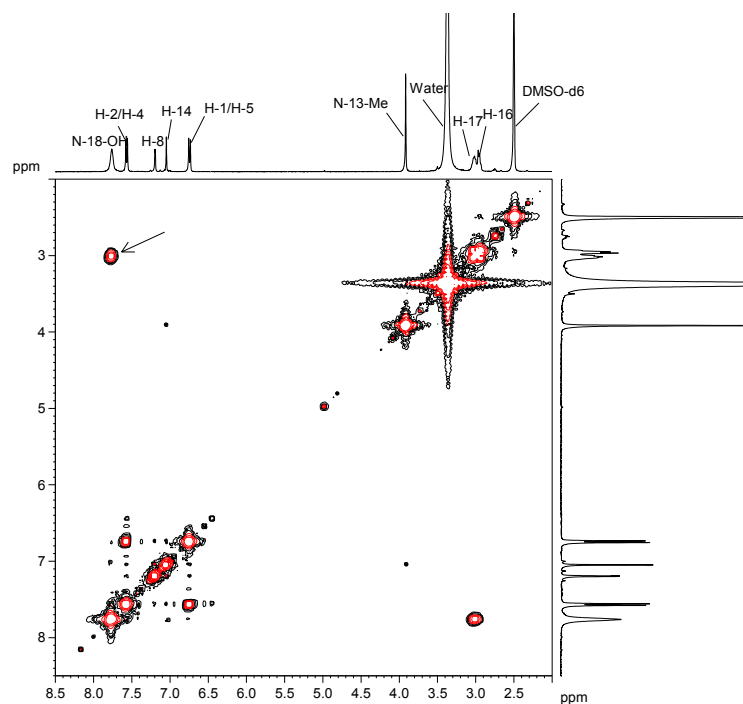
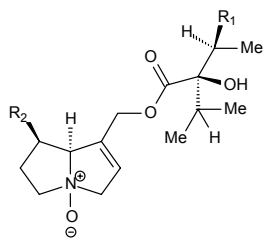


Figure 4.11 A section (F1, F2 = δ 2.0 – 8.5 ppm) of the COSY spectrum of compound **4.2** (400/100 MHz, DMSO-d_6). (Imp = impurity).

Table 4.3 NMR (DMSO-d₆, 400 MHz for ¹H and 100 MHz for ¹³C) data for compound **4.2**.

Atom no.	δ _c	δ _H (mult, J, Hz)	COSY	HMBC
C1	114.5 (d)	6.75 (d), 2H, 8.4 Hz	H2 / H4	C3, C5, C20
C2	129.7 (d)	7.57 (d), 2H, 8.4 Hz	H1 / H5	C1, C3, C4, C5, C6
C3	156.6 (s)			
C4	129.7 (d)	7.57 (d), 2H, 8.4 Hz	H1 / H5	C1, C2, C3, C5, C6
C5	114.5 (d)	6.75 (d), 2H, 8.4 Hz	H2 / H4	C1, C3, C20
C6	126.5 (s)			
C7	121.2 (s)			
C8	123.9 (d)	7.1 (d) 1H, 2.4 Hz	NH-9	C6, C7, C10
NH-9	-	12.63 (s), 1H	H-8	C6, C7, C10, C20
C10	133.2 (s)			
C11	168.6 (s)			
C12	129.4 (s)			
N-13	-	-		
C14	130.3 (s)	7.05 (s), 1H	N-13-Me	C12, N-13-Me, C15, C16, C11, C19, C21
C15	119.8 (s)			
C16	23.5 (t)	2.95 (m), 2H	H-17	C14, C15, C17, C21
C17	38.7 (t)	3.02 (m), 2H	H-16, N-18-OH	C16
N-18-OH	-	7.76 (s), 3H	H-17	
C19	180.4 (s)			
C20	123.9 (s)			
C21	125.3 (s)			
N-13-Me	35.8 (q)	3.19 (s), 3H	H-14	C14

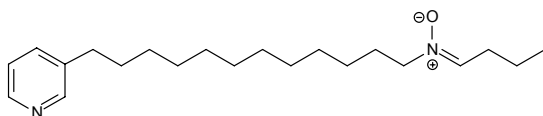
The isolation of N-oxides from a terrestrial source is fairly common e.g. pyrrolizidine alkaloid N-oxides from *Symphytum officinale* (comfrey), a plant from the *Boraginaceae* family. (To simplify interpretation of the spectroscopic data of these compounds, the N-oxides are usually reduced using zinc dust). The pyrrolizidine N-oxides are concentrated mainly in the fresh or dried root section of *S. officinale*. Long term administration of the roots of *S. officinale* to laboratory animals was observed to cause hepatotoxicity which led to the eventual development of tumours in laboratory animals.¹⁰⁷ Another investigation revealed the concentration of the N-oxides of indicine (**4.7**) and 12-acetyлиндicine (**4.8**) in the leaves and roots of the medicinal plant *Heliotropium arborescens*.¹⁰⁸



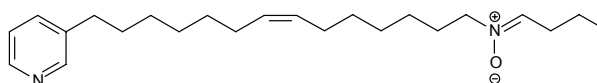
4.7 $R_1 = \text{OH}, R_2 = \text{OH}$

4.8 $R_1 = \text{OAc}, R_2 = \text{OH}$

Although the isolation of N-oxides from a marine source is still fairly uncommon, two antifungal 3-alkyl pyridine alkaloids Cribrochalinamines A (**4.9**) and B (**4.10**) have been isolated previously by Matsunaga *et al.*¹⁰⁹ from a Japanese sponge *Cribrochalina* sp. The aqueous methanol fraction was separated through a combination of chromatographies such as ODS flash (water : methanol), silica gel (chloroform : methanol) and reversed phase HPLC. Interestingly, at no point do the authors mention any use of TFA, or any other acid for that matter, to aid the separation of the two β -alkyl pyridine derivatives, which may be significant in defining the isolation of an N-oxide or an oxime metabolite.¹⁰⁹

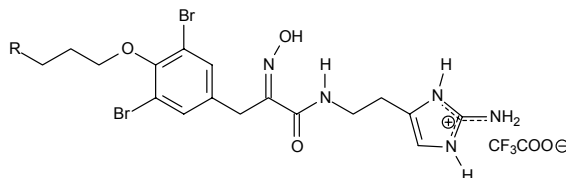


4.9



4.10

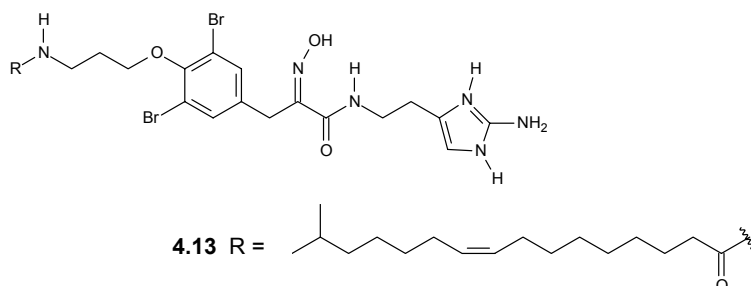
The bioactive bromotyrosine alkaloids purealidins A (**4.11**) and E (**4.12**), which have been shown to be useful in studying the regulatory mechanisms of myosin K^+ , EDTA-ATPase or Na^+ , K^+ - ATPase, were isolated from an Okinawan sponge *Psammaplysilla purea* Carter (family Verongidae). The *n*-butanol partition fraction was subjected to a combination of silica gel and molecular exclusion (LH-20) chromatography. The crude extract was then further purified using reversed phase HPLC with aqueous acetonitrile and trifluoroacetic acid.¹¹⁰



4.11 $R = \text{NMe}_3^+ \text{CF}_3\text{COO}^-$

4.12 $R = \text{NH}_3^+ \text{CF}_3\text{COO}^-$

Similarly, the bromotyrosine alkaloid lipopurealidin D (**4.13**), was also isolated from an Okinawan sponge *Psammaplysilla porea* Carter¹¹¹ and the ethyl acetate extract subjected to a combination of Si gel and LH-20 chromatography, where the eluent for the former chromatography contained either acetic acid or trifluoroacetic acid. Lipopurealidin D shows no cytotoxicity, however (> 10 µg/mL).¹¹¹



It thus appears that N-18 oximes are possibly formed during the purification procedures and are likely to exist in nature as N-oxides.

e) 14-bromo-3-dihydro-discorhabdin C (**1.52**)

Compound **1.52** (9.6 mg, 0.002 % yield) gave a M+1 ion at m/z 542.8792 by HRFABMS analysis, consistent with the molecular formula $C_{18}H_{16}N_3O_2Br_3$. 1H NMR data were consistent with those obtained for the compound isolated from *T. pedunculata*.

f) 7,8-dehydro-3-dihydro-discorhabdin C (**2.1**)

HRFABMS analysis gave a M+1 ion at m/z 462.9532 (Δ +0.1 mmu) for compound **2.1** (2.1 mg, 0.0004 % yield), consistent with the molecular formula $C_{18}H_{15}N_3O_2Br_2$. The 1H NMR spectra obtained were also consistent with those obtained for **2.1** isolated from *T. pedunculata*.

g) 14-bromo-1-hydroxy-discorhabdin S (**2.4**)

The 1H NMR spectrum obtained for **2.4** isolated from *T. favus* was identical to the 1H NMR spectrum obtained for the compound isolated from *T. pedunculata*. The molecular formula $C_{18}H_{17}N_3O_3Br_2$ was established for compound **2.4** (4.3 mg, 0.001 % yield) by HRFABMS analysis (M+1, m/z 480.9636, Δ -0.1 mmu).

h) 2,4-debromo-3-dihydro-discorhabdin C (**2.6**)

Matching 1H NMR spectra were obtained for compound **2.6** isolated from both *T. favus* and *T. pedunculata*. Compound **2.6** was also obtained in very low yields (2.0 mg, 0.0004 % yield).

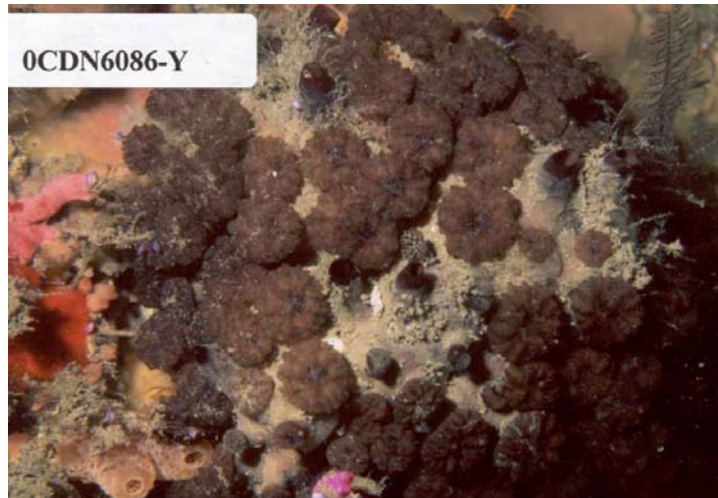
4.3.1 The taxonomy of the sponge *Strongylodesma* sp..

Figure 4.12 An underwater photograph of *Strongylodesma* sp..

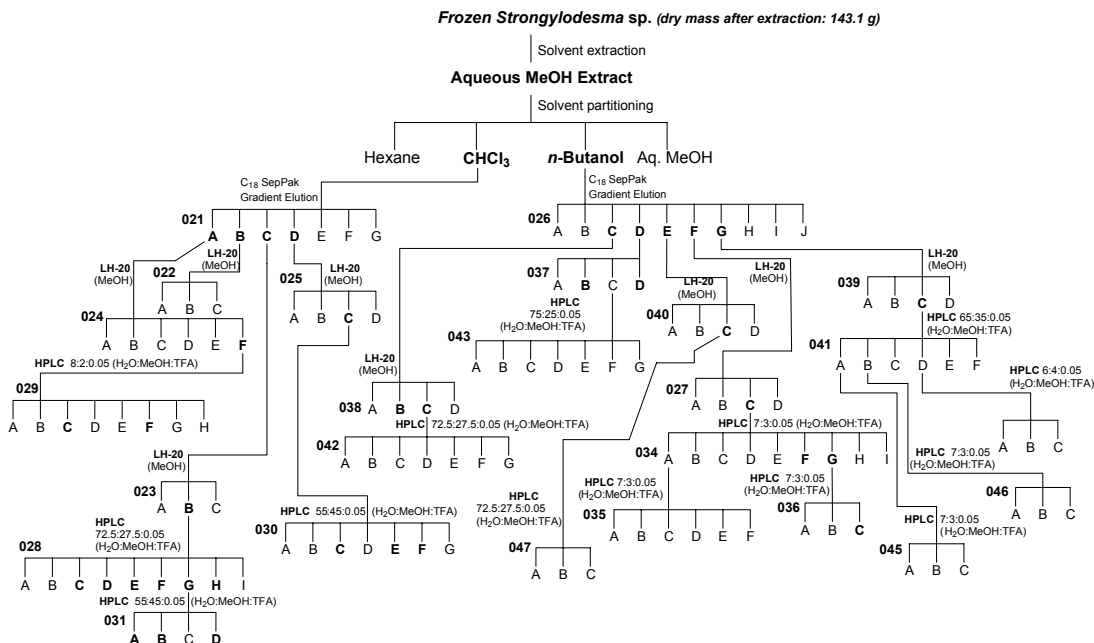
UPE-96-Philip's green sponge was collected in Algoa Bay, South Africa, in an intertidal rock pool at a depth of 2 m in 1996. "In life the sponge is semispherical, up to 5 cm high and 10 cm wide. The surface is smooth with volcano-shaped oscules and smooth mushroom-like areolate structures. The texture hard, compressible and the colour greenish-brown. The choanosomal skeleton consists of a dense irregular square to polygonal-meshed reticulation of strongyles (~ 80-100 μ m), with no distinction between the primary and secondary tracts. The ectosome is made up of a dense irregular interlocking layer of strongyles approximately 220 μ m deep above which is a layer of perpendicular strongyles, which pierce the surface. No microscleres are present. The sponge is most closely comparable to *Strongylodesma areolata* Lévi, 1969 (Family Latrunculiidae), but is here considered another specimen within a new species of *Strongylodesma*." ⁵⁸

4.3.2 Extraction and isolation of pyrroloiminoquinone metabolites from *Strongylodesma* sp..

The frozen sponge (UPE-96-Philip's Green sponge) was steeped in methanol and once again partitioned according to a modified Kupchan procedure (Scheme 4.3). The known compounds discorhabdins A (**1.57**),³⁶ D (**1.61**)⁴⁸ as well as 3-dihydro-disorhabdin C (**1.53**),⁴² together with one new compound, namely 1-amino-disorhabdin D (**3.3**) were isolated from *Strongylodesma* sp.. Compounds **1.53** and **3.3** have already been isolated from *T. pedunculata* and *L. lorii* respectively and are described in Chapters 2 and 3.

Discorhabdin A (**1.57**) and 3-dihydro-disorhabdin C (**1.53**) were isolated from the chloroform partition, while **1.57**, **1.61** as well as the new compound (**3.3**) were obtained from the *n*-butanol

partition. The structures of the known compounds reported here, are based on spectral comparisons with known discorhabdins.

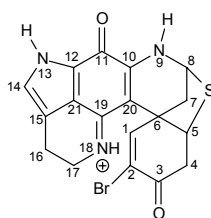


Scheme 4.3 Extraction and pyrroloiminoquinone isolation scheme for *Strongyloides* sp.. The masses and yields (calculated relative to the dry mass of sponge) of the *Strongyloides* sp. pyrroloiminoquinone metabolites are summarized below:

022B, 022C 029D, 029E,	1.57	208.8 mg	0.15 %
030A, 034G, 041A, 043F			
043D	1.61	6.7 mg	0.005 %
030E	1.53	6.9 mg	0.005 %
043B 042E 034E	3.3	19.2 mg	0.01 %

4.3.3 Structure elucidation of pyrroloiminoquinone metabolites from *Strongyloides* sp..

i) *Discorhabdin A* (**1.57**)



1.57

Discorhabdin A (**1.57**, 208.8 mg, 0.15 % yield) showed an M^+ ion peak at m/z 416.2 in the low resolution LC-MS analyses corresponding to a molecular formula of $C_{18}H_{15}N_3O_2S^{79}Br$. The 1H (Figure 4.13) and ^{13}C NMR spectra indicated a basic discorhabdin C type skeleton with the proton NMR spectra showing seven non-exchangeable and three exchangeable sets of protons. The 1H NMR spectrum (Figure 4.13) was rather simple showing two deshielded sp^2 methine signals corresponding to H-1 (δ 7.47) and H-14 (δ 7.38), together with two sp^3 methine signals at δ 5.33 and 4.58 corresponding to H-8 and H-5. The ^{13}C NMR spectrum showed well resolved signals corresponding to all eighteen carbons, while a DEPT experiment confirmed that the twelve non-exchangeable protons were attached to carbons which included four methylene carbons, four methine carbons and ten quaternary carbons. A deshielded carbon signal at δ 187.8 suggested an α,β -unsaturated ketone, while typical signals for the iminoquinone moiety were evident from the carbons resonating at δ 166.8 and 154.6. The NMR data obtained for this compound is consistent with the literature values.³⁶ The LC-MS spectrum of **1.57**, presented in Figure 4.14, shows the typical $M + 1$ 1:1 doublet isotope ion cluster indicative of a compound containing one bromine atom.

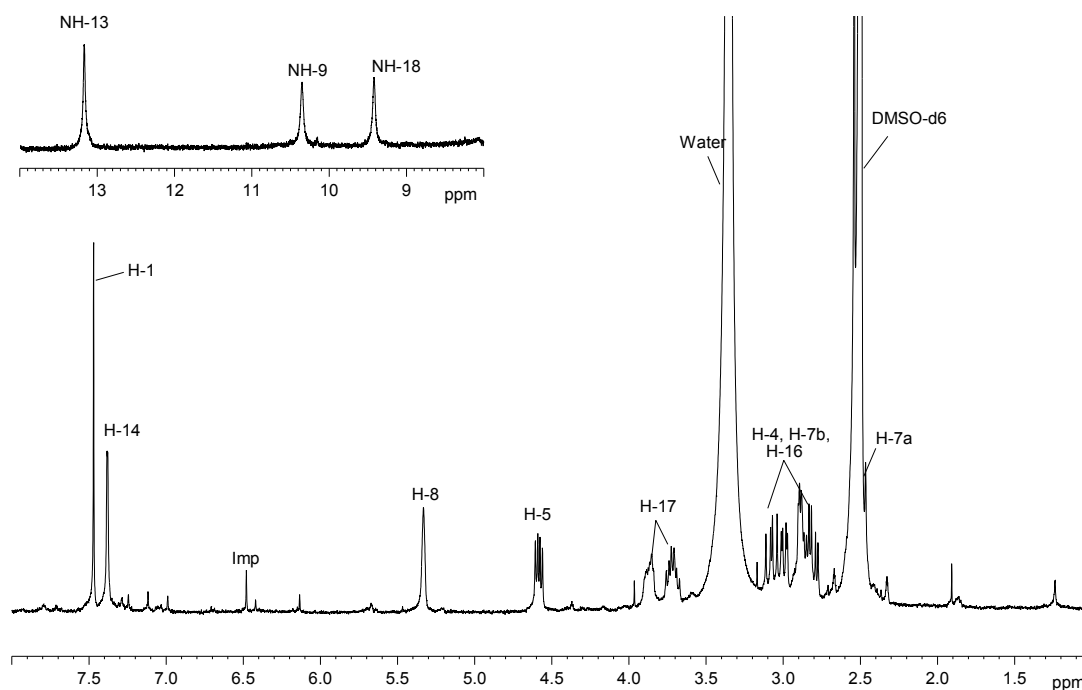


Figure 4.13 1H NMR spectrum of discorhabdin A (**1.57**) (400 MHz, $DMSO-d_6$) with NH-9 and NH-13 offset. (Imp = impurity).

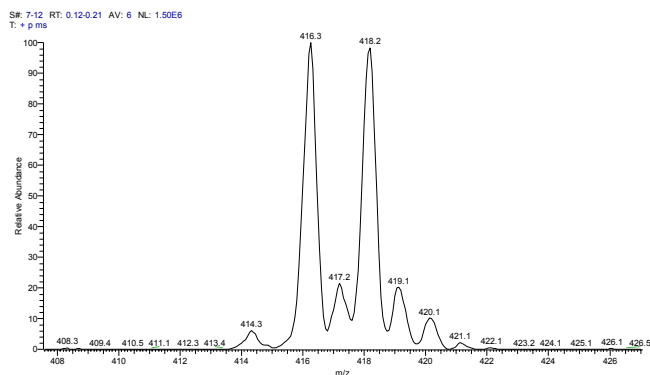
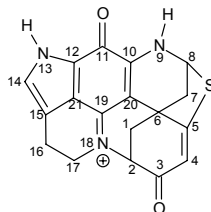


Figure 4.14 The LC-MS spectrum of **1.57** showing the typical $M + 1$ 1:1 doublet isotope ion cluster of a compound containing one bromine atom.

j) *Discorhabdin D* (**1.61**)



1.61

Discorhabdin D (6.7 mg, 0.005 % yield), isolated as a minor metabolite, showed an M^+ ion at m/z 336.4 in the low resolution LC-MS spectrum corresponding to a molecular formula of $C_{18}H_{14}N_3O_2S$. The 1H NMR spectra (Figure 4.15) showed eleven non-exchangeable and two exchangeable sets of protons. The ^{13}C NMR and DEPT 135 spectra revealed the presence of eighteen carbon resonances, including four methylene, two sp^2 and two sp^3 methine signals, together with ten quaternary carbon resonances. Two α,β -unsaturated carbons was evident from a carbon chemical shifts at δ 182.9 (C-3) and 166.4 (C-11). The 1H NMR spectrum, significantly different to that of *discorhabdin A* (**1.57**), lacked the proton chemical shifts of **1.57** at approximately δ 7.5 (H-1) and δ 8.1 (NH-18) suggesting substitution in the latter position. Methylene and methine signals at δ 2.44 (dd, H_2 -1), 2.91 (dd, H-1b) and 4.37 (s, H-2) were observed instead. The lack of an NH-18 proton signal together with the proton and carbon chemical shifts of C-2 (δ_C 62.1) suggested the presence of a bond between N-18 and C-2. Upon comparison of previously isolated *discorhabdins* (e.g. **3.2** – **3.5**), the carbon chemical shifts corresponding to C-5 (δ 172.9) and C-8 (δ 62.6) suggested the presence of a thioether functionality. The spectroscopic data were therefore consistent with those of *discorhabdin D* published by Perry *et al.*⁴⁸

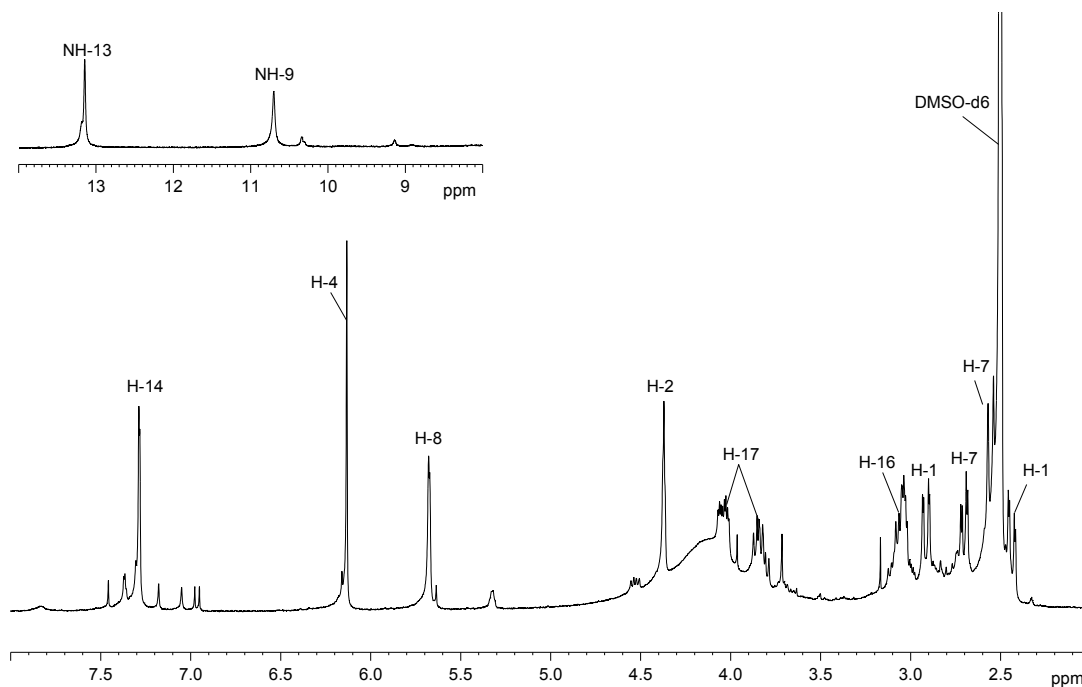


Figure 4.15 ^1H NMR spectrum of discorhabdin D (**1.61**) (400 MHz, DMSO-d_6) with NH-9 and NH-13 offset. (Imp = impurity).

k) **3-dihydro-discorhabdin C (1.53)**

The ^1H NMR spectra obtained for compound **1.53** (6.9 mg, 0.005 % yield) were also consistent with those obtained for **1.53** isolated from *T. pedunculata*.

l) **1-amino discorhabdin D (3.3)**

Compound **3.3** (19.2 mg, 0.01 % yield), also isolated from *L. lorii*, gave ^1H NMR data which were consistent with those obtained for compound **3.3**.

Chapter 5: Photochemistry

5.1 Introduction

The pyrroloamino-*ortho*-quinone, pyrroloiminoquinone and *bis*-pyrroloiminoquinone metabolites described in previous chapters have a dual purpose in the sponges that produce them. These metabolites potentially act as both cytotoxic chemical defence agents against predation and microbial infection and as pigments providing the characteristic brown, green and pink colours of the sponges from the family Latrunculiidae and Acarnidae. It is the role of pyrroloamino-*ortho*-quinone and pyrroloiminoquinone metabolites as pigments that we explore in this Chapter in particular the possible relationship between the interaction of these compounds with light and their resultant mechanism of action as cytotoxic agents. The potential of these compounds as photosensitive anti-cancer drugs suitable for use in photodynamic therapy is discussed.

Cancer is the uninhibited production of diseased cells that eventually develop into tumours. Therapy or management of cancer is dependent on the eradication of these diseased cells either through surgery; through chemical treatments that rely on the differences between cancerous and normal cells (with certain chemicals found to concentrate in cancerous cells rather than the unaffected cells); or through the effects of ionising radiation such as radiotherapy (a form of free radical therapy) or photodynamic therapy (the photosensitised production of singlet oxygen).^{104,112}

Free radicals are atoms, molecules or fragments of molecules with an unpaired electron, and are produced by a) a variety of metabolic processes in the body, such as the oxidants produced as byproducts of mitochondrial electron transport, various enzyme systems, and lipid peroxidation; b) as intermediates in the breakdown of drugs through metabolism; or c) through a variety of photosensitisation processes.¹⁰⁴ Superoxide ($O_2^{\cdot -}$) and the highly reactive hydroxyl (OH^{\cdot}) radicals are constantly produced in living organisms. Several non-radical oxygen derived species (hydrogen peroxide and hypochlorous acid) are also generated. The term reactive oxygen species (ROS) describes the oxygen radicals [$O_2^{\cdot -}$, OH^{\cdot} , peroxy (RO_2^{\cdot}) and alkoxy (RO^{\cdot}) radicals] and other non-radical derivatives [H_2O_2 , $HOCl$, singlet oxygen (1O_2), ozone]. As they are usually highly reactive and short-lived, any oxidants that escape the numerous antioxidant defences damage macromolecules such as DNA and proteins, leading ultimately to mutations and cancer. In the last decade a surge of interest in free radical chemistry and biology has led to great advances in understanding the role of reactive oxygen species (ROS) in DNA damage, ageing and the many diseases have been associated with ROS, among them cancer.^{104,113} But although free radicals are usually considered to be damaging to the body – some, such as nitric oxide and superoxide – are important in blood pressure control and destroying harmful bacteria. It is the damage inducing properties, however, that has led to the interest in exploiting ROS for cancer therapy e.g. radiotherapy and photodynamic therapy (PDT).

Radiotherapy involves the production of radicals through radiation. The radicals interact with DNA and adjacent molecules to cause breaks in the DNA strands, cell death and tumour necrosis. The necessity to produce compounds that have the potential to deliver damaging radicals to tumours is thus underlined. Similarly, the basis of PDT is a sensitised photooxidation process that destroys the fundamental components of the diseased cell. PDT involves the administration of a photosensitiser (which accumulates preferentially in the tumour cells) and its subsequent activation by laser light. In its activated form, the photosensitiser reacts with oxygen to produce highly toxic singlet oxygen which can itself damage DNA or lead to a variety of oxidation reactions involving important macromolecules in the cells, leading to cellular damage of the tumour tissue.^{104,112} The photosensitisers used in PDT are usually good oxidising agents in their excited state. Ironically, the cancer that is initiated mainly by mutations due to oxidative damage may be cured through oxidative free radical, or through the photosensitised production of singlet oxygen, damage to DNA in the cancer cells during radio- or photodynamic therapy.

During the past ten years, however, it has become evident that solid human tumours very often contain regions that are deficient in oxygen (hypoxic). The presence of hypoxia has been demonstrated in cervical cancer, squamous cell carcinoma of the head and neck, melanoma, breast, sarcoma and more recently prostate cancer.¹¹³

Because photochemical DNA damage mediated by organic molecules has important toxic and therapeutic consequences, the photochemical characterisation of potential antitumour agents should be undertaken. The aim of this study was thus to determine the singlet oxygen (photochemical processes) and fluorescence (photophysical processes) quantum yields of a suite of pyrroloamino-*ortho*-quinone and pyrroloiminoquinones isolated from four South African *Latrunculid* sponges (Chapters 2 - 4) and, since these metabolites have been shown to have significant cytotoxicity, perhaps propose a mechanism of cytotoxicity.

5.2 Photochemistry

Photosensitisation is the absorption of visible light by a coloured substance which initiates physical or chemical changes in a substrate.¹¹⁴ The chemical reaction, in which a photoexcited molecule M^* takes part, is termed photochemistry, and it may lead directly to the final products (e.g. isomerisation), or more frequently to an unstable or reactive chemical species (e.g. free radicals or radical ions). The reactive chemical species generated in this primary photochemical process may react further in secondary processes through a series of dark reactions that lead ultimately to the final photoproducts.¹¹²

The sequence of a photochemical reaction may be followed through a succession of steps (also Figure 5.1):

- i) Absorption of light $M + h\nu \rightarrow M^*$ (5.1 a)
- ii) Fluorescence $M^* \rightarrow M + h\nu_f$ (5.1 b)
- iii) Non-radiative deactivation $M^* \rightsquigarrow M (+ \text{heat})$ (5.1 c)
- iv) Intersystem crossing $M^* \rightsquigarrow {}^3M^*$ (5.1 d)
- v) Primary reaction:
- unimolecular $M^* \xrightarrow{\text{Light reaction}} P$ (5.1 e)
- bimolecular $M^* \xrightarrow{\text{Light reaction}} P$ (5.1 f)
- P is the primary photochemical product(s), these can then react further in a variety of dark reactions.
- vi) Secondary processes $P \xrightarrow{\text{Dark reaction}} F$ (final products) (5.1 g)
- In organic molecules, M^* can either be an excited singlet or triplet state and may react on its own in unimolecular reactions (dissociations, isomerisations) or with another ground state molecule N, in bimolecular processes (additions, substitutions, etc.).
- ii a) Phosphorescence ${}^3M^* \rightarrow M + h\nu_p$ (5.1 h)
- iii a) Non-radiative deactivation ${}^3M^* \rightsquigarrow M (+ \text{heat})$ (5.1 i)

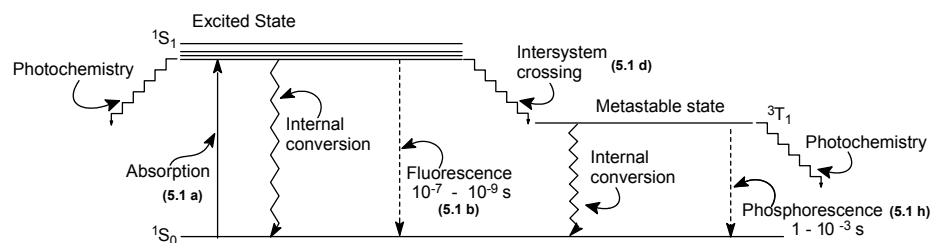
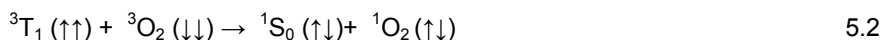


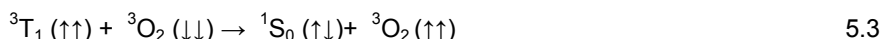
Figure 5.1 Jablonski diagram.¹¹⁷

Upon the absorption of light (5.1a) one electron is excited without a change in spin direction from the ground singlet state (1S_0) to an excited level, 1S_1 , *i.e.* an excited singlet state.¹¹⁴ For the sake of simplicity, only the first excited state is shown. Depending on the molecular structure and environment, the excitation energy of the 1S_1 state may be released by one of several processes: a) The unexcited sensitizer may be restored by emission of a photon as fluorescence (5.1b) and by radiationless energy transfer to the medium as heat (5.1c); b) alternatively, the transfer of the 1S_1 excitation energy to an unexcited molecule may result in relaxation (efficient energy transfer from a donor to an acceptor requires that the acceptor be a lower energy 'state' or system); c) intersystem crossing (ISC, 5.1d) to the lowest energy triplet state (3T_1) requires a spin flip (this conversion from the triplet to the singlet ground state would require another spin flip - a 'forbidden' transition, accounting for the long lifetimes inherent in triplet states; and d) the radiative decay of a triplet state leads to phosphorescence (5.1h). Molecules with heavy atoms or a medium with heavy atoms promote ISC.¹¹⁴

Due to their long decay lifetimes and the presence of unpaired valence electrons, dye (as sensitiser) triplet states are chemically reactive. Type I photosensitisation, where fast electron transfer reactions between an unstable complex of an excited singlet state and other substrates have been identified. Whereas Type I photosensitisation initiated by excited singlet states are uncommon, initiation by a metastable triplet state is favoured because of long decay lifetimes and the separated, unpaired electrons in different molecular orbitals. In a Type II pathway, energy transfer from the sensitiser triplet state to molecular oxygen generates $^1\text{O}_2$ in the following manner:¹¹⁴



The energy of the sensitiser in the triplet state relative to the energy in the $^1\text{S}_0$ ground state must be greater than the 0.98 eV (22.5 kcal/mol) needed to excite the triplet O_2 to the singlet O_2 ($^1\Delta_g^+$). Triplet states of many organic molecules are capable of generating $^1\text{O}_2$. Quenching of a sensitiser triplet state by molecular oxygen is a competing process, given by:



where $^3\text{O}_2$ denotes ground state O_2 ($^3\Sigma_g^-$). Competition between electron transfer and $^1\text{O}_2$ production by energy transfer occurs as shown by:



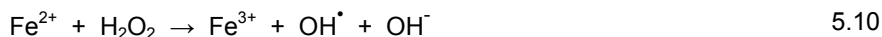
where S^+ is the oxidised photosensitiser free radical and $\text{O}_2^{\cdot-}$ is the anion radical superoxide. This is also classified as a Type I reaction process. Superoxide is the anion of the hydroperoxy (perhydroxyl) radical HO_2^{\cdot} with $\text{pK}_a = 4.4$, an important form of active oxygen. Its function and reactions differ from those of $^1\text{O}_2$. The enzyme superoxide dismutase catalyses the conversion of superoxide to hydrogen peroxide in many cells. Some photosensitisers are capable of generating both $^1\text{O}_2$ (by energy transfer from the triplet state) and superoxide (by electron transfer). When sensitiser triplet states react with substrates other than oxygen, the process may either return the sensitiser to its ground state (which is known as physical quenching) or initiate a chemical reaction (known as chemical quenching):¹¹⁴



where R_{red} and R_{ox} are quencher free radicals and S^- is the reduced sensitiser free radical. In quinoid sensitiser S^- is usually a semiquinone. Reduced sensitiser is another source of superoxide as indicated by the following reactions:



The Fenton reaction, in which a metal ion is oxidised by hydrogen peroxide, has also been found to generate hydroxyl radicals (OH^\bullet) upon photosensitisation:



5.2.1 Singlet Oxygen

Because many photochemical reactions involve the attack of excited singlet oxygen 1O_2 on a ground state reactant molecule, the photophysical properties of the oxygen molecule are important.¹¹²

a) Electronic structure and lifetime of singlet oxygen

Molecular oxygen has two unpaired electrons in its lowest energy state. The existence of unpaired valence electrons in a stable molecule is very rare in nature resulting in a highly reactive chemical system.¹¹⁴ The electronic structure of singlet oxygen is ably described by the molecular orbital theory. The oxygen molecule is unique in that its lowest electronic state is the triplet ground state ($^3\Sigma_g^-$) and, with two unpaired electrons distributed in the highest orbitals (Figure 5.2), two possible singlet excited states result upon the rearrangement of the electron spins within the degenerate orbitals. Oxygen is thus capable of having both triplet and singlet excited states. The first excited state ($^1\Delta_g^+$), *i.e.* both electrons paired in the same orbital (Figure 5.2), has the lowest energy and is expected to undergo two electron reactions. The excitation energy of this form is 0.98 eV or 22.5 kcal/mol (Figure 5.3). Alternatively, the higher energy singlet state ($^1\Sigma_g^+$) is expected to undergo one electron free radical reactions due to its spin-paired electrons occurring in different molecular orbitals (Figure 5.3). The more reactive $^1\Sigma_g^+$, with an excitation energy of 1.63 eV (35.7 kcal/mol⁻¹), has a much shorter lifetime than the $^1\Delta_g^+$ state and decays to the lower energy state before any chemical reactions can occur. Neither form ($^1\Delta_g^+$ nor $^1\Sigma_g^+$) is a radical, given that there are no unpaired electrons, nor are there any spin restrictions. The lifetime of the singlet oxygen has been found to be dependent on the solvent.^{114,115}

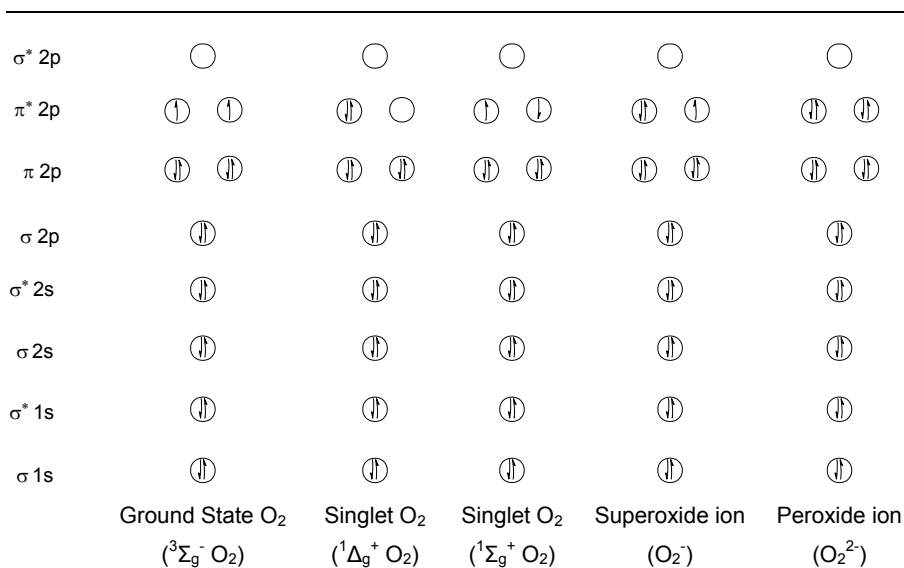


Figure 5.2 Bonding in the diatomic oxygen molecule.¹¹⁶

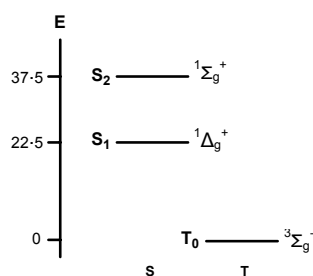


Figure 5.3 Jablonski diagram for an oxygen molecule. (Energy in kcal/mol).¹¹²

Figure 5.3 shows the Jablonski diagram for the oxygen molecule. Only the first few states relevant to photooxidation processes are shown.

b) Production of singlet oxygen

Singlet oxygen may be generated by either a) chemical methods, *e.g.*, the biologically important reaction of hydrogen peroxide with sodium hypochlorite to produce singlet oxygen b) enzymatic reactions *e.g.* by the myeloperoxidase enzyme during phagocytosis; c) gaseous discharge (produced by passing an electric current through a gas or vapour) or d) by physical methods such as photosensitisation (used in PDT).

The pathway in which a photosensitiser triplet state reacts first with a substrate other than molecular oxygen is termed Type I, and reactions involving O_2^- also occur. The alternative Type II pathway involves the photosensitiser triplet state reacting first with molecular oxygen (Figure 5.4). Type II photosensitisation of a biological system is known as photodynamic action.

Type I reactions are characterised by the excitation of a sensitiser (S) followed by electron transfer between the sensitiser and the substrate (RH) or solvent to give radicals or radical ions. These radicals then react with surrounding oxygen molecules ($^3\text{O}_2$) to form the superoxide radical anion that may be protonated at low pH to form the reactive HO_2^\cdot radical. The mechanism for a Type II reaction involves the transfer of energy from the excited sensitiser (S^*) (as a result of the absorption of light) to adjacent $^3\text{O}_2$ molecules to form singlet oxygen ($^1\text{O}_2$). Singlet oxygen and superoxide thus formed can cause the oxidative destruction of tissue, forming the basis for photodynamic therapy (please see Section f) for more detail).

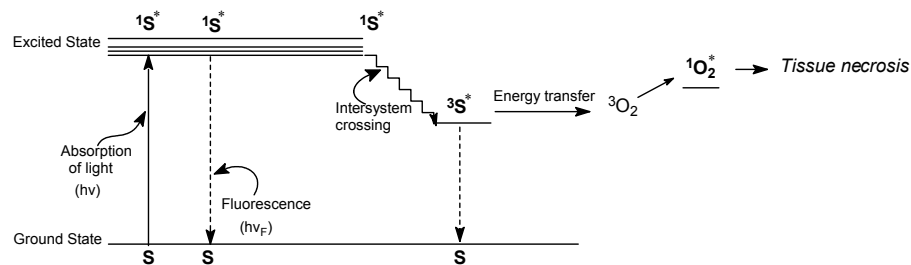


Figure 5.4 A modified Jablonski diagram showing the relevant reactions for a Type II mechanism, emphasising the basis of PDT. (S = sensitiser).

c) *Detection and measurement of singlet oxygen*

Several methods may be used to detect singlet oxygen including the use of:

- i. the protective effects of additives such as scavengers which inhibit the rate of a $^1\text{O}_2$ or photochemical reaction *e.g.* histidine, tryptophan, melatonin, 1,4-diazobicyclo-[2,2,2]octane (DABCO), thiols, azides, ascorbates (*e.g.* vitamin C), cholesterol and the carotenes;
- ii. deuterated solvents, an unambiguous test for $^1\text{O}_2$, which prolong the lifetime of the $^1\text{O}_2$ *e.g.* D_2O , DMSO-d_6 , etc.; and
- iii. luminescence, termed the 'gold standard of singlet oxygen identification', which is the result of the energy given off during the transition from the excited $^1\text{O}_2$ back to the ground state, and corresponds to an absorption in the near infra-red (NIR) region at 1268 nm;
- iv. electron paramagnetic resonance (EPR), a non optical technique in which the energy transfer between the magnetism of unpaired electrons and an external magnetic field is measured with a sensitive microwave detection system. The magnetic interaction between an electron and the magnetic field corresponds to the energy difference between the spin up and spin down states. Singlet oxygen, however, is a non magnetic molecule (Figure 5.2) and cannot be detected directly by EPR. The reaction of singlet oxygen with a spin label whose structure, as determined by EPR, provides an unambiguous identification *e.g.* 2,2,6,6-tetramethyl-4-piperidone (TEMP) is often used.¹¹⁴

d) Reactions involving singlet oxygen

Singlet oxygen reacts with many compounds including: olefins, dienes, sulfides, aromatics, hetero-aromatics, terpenes, steroids, fatty acids, flavones, tetracyclines, vitamins, amino acids, proteins nucleic acids, blood and bile pigments and synthetic polymers.^{114,115}

Reactions fall into three general classes:

- i. the 'ene' reaction, which involves hydrogen abstraction and oxygen addition
- ii. cycloaddition, which includes the formation of a typical product 1,2-dioxetane and endoperoxides of e.g. anthracene, and
- iii. oxygenation as illustrated by:

*e) Quenching of singlet oxygen*

Deactivation of the ${}^1\text{O}_2$ back to its ground state is known as quenching and may be accomplished by either physical or chemical methods (please see Section 5.3.1). Physical deactivation is simply the reversion of the singlet oxygen to its ground state without any product formation or oxygen consumption. Chemical quenching, consisting of energy transfer and electron transfer mechanisms, incorporates the use of a quencher (Q) that reacts with the singlet oxygen to produce RO_2 . Energy transfer involves the generation of a triplet state quencher together with the subsequent formation of ground state oxygen, while electron transfer quenching entails the interaction between the electron deficient ${}^1\text{O}_2$ molecule and the electron donors to form a charge transfer complex.

f) Photodynamic therapy

A number of factors are important in PDT and a good photosensitiser should have:

- i. sufficient triplet energy (more than 94 kJ/mol), for adequate interaction with ground state oxygen;
- ii. a high triplet yield;
- iii. a long triplet lifetime;
- iv. a high singlet oxygen quantum yield; and
- v. a strong absorption in the red region of the spectrum (owing to the light absorption and scattering properties of human tissue).¹¹⁸

The singlet oxygen quantum yield is a key property of a photosensitising agent since the ability of a compound to produce singlet oxygen determines its potency in photodynamic therapy (PDT). The production of singlet oxygen is measured as the singlet oxygen quantum yield (Φ_Δ).¹¹⁷ The

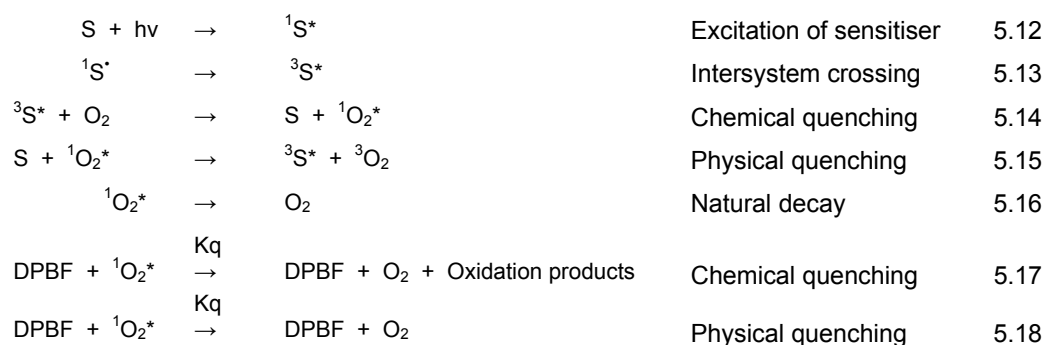
quantum yield gives an indication of the overall efficiency of a photochemical process and may be described as the number of molecules of $^1\text{O}_2$ generated for every photon absorbed by the photosensitiser. The production of $^1\text{O}_2$ by photosensitisation involves 4 steps (Figure 5.4): 1) the absorption of light by the sensitiser, 2) the formation of the sensitiser triplet state, the quantum yield of this process is the ISC efficiency or triplet yield (Φ_T), 3) trapping of the triplet state by molecular oxygen within its lifetime (the fraction of trapped triplet state is given by f_T), 4) Energy transfer from the triplet state to molecular oxygen. Virtually all measurements of the quantum yield (Φ_Δ) are scaled to a reference substance, e.g. rose bengal (Φ_Δ 0.79) in aqueous media.

5.3 Photochemical techniques

5.3.1 Singlet oxygen quantum yield determinations

The efficiency of a photochemical process is recognised as the quantum yield, defined as the number of reactive species formed for every photon of light absorbed.¹¹² The effectiveness or ability of a molecule or sensitiser in the excited (triplet) state to react with ground state oxygen thus forms the basis of singlet oxygen quantum yield determinations.

The foundation for the analysis was based on the production of singlet oxygen upon irradiation by a sensitiser and a quencher, and the quencher subsequently allowed to react with the singlet oxygen accordingly produced.¹¹⁷ 1,3-Diphenylisobenzofuran (DPBF), with its absorption maximum at 417 nm, was used as the quencher and its disappearance was easily monitored. Only the first 20% decrease is applicable in order to obtain reliable or accurate first order kinetics data. The disappearance of the DPBF quencher is related to the production of singlet oxygen and the following processes may take place:



The physical quenching processes (Eqn. 5.15 and 5.18) noted above may be ignored because the quantum yield of singlet oxygen is not dependent on the concentration of the sensitiser present and the DPBF is known to act as a chemical quencher only in organic solvents, respectively. Also, compared to the potential sensitiser, DPBF is highly reactive to singlet oxygen, making equation 5.14 invalid.¹¹⁷ Thus, the only equations of relevance are 5.16 and 5.17 (while

equations 5.12 and 5.13 are mentioned only for the sake of clarity). The rate of disappearance of DPBF as a result of singlet oxygen is given by:¹¹⁷

$$-\frac{[\text{DPBF}]}{dt} = Kq[\text{DPBF}][^1\text{O}_2] \quad 5.19$$

Following rearrangement and substitution the following equation is derived:¹¹⁷

$$\Phi_{\Delta}^{\text{S}} = \Phi_{\Delta}^{\text{Std}} \times \frac{(C_o - C_t)^{\text{S}}}{(C_o - C_t)^{\text{Std}}} \times \frac{(\alpha t)^{\text{Std}}}{(\alpha t)^{\text{S}}} \times \frac{[\text{DPBF}]^{\text{Std}}}{[\text{DPBF}]^{\text{S}}} \quad 5.20$$

where:

S	=	sample
Std	=	standard
(C _o - C _t)	=	change in DPBF concentration (C _o = initial and C _t = final)
α	=	1 (for the monochromatic laser light, previously determined by Maree ¹¹⁷)
t	=	photolysis time-span in seconds

It is important, though, to clarify the use of low concentrations of DPBF since first order kinetics are observed, while at high concentrations the reaction rate would become independent of the DPBF concentration and a zero order rate law would be observed.

5.3.2 Fluorescence quantum yield determinations

The number of photons emitted relative to the number of photons absorbed is known as the fluorescence quantum yield. The quantum yield is determined by using a suitable reference material (of a known quantum yield) in a specific solvent such as benzene in cyclohexane (Φ_F). Absorption spectra are recorded prior to plotting emission spectra, while quenching necessitates the use of low concentrations. Fluorescence quantum yields are determined using the following equation:¹¹⁷

$$\Phi_{\text{F}} = \Phi_{\text{F}(\text{std})} \times \frac{\text{Area}_{(\text{S})} \times A_{(\text{Std})} \times \eta_{(\text{S})}^2}{\text{Area}_{(\text{Std})} \times A_{(\text{S})} \times \eta_{(\text{Std})}^2} \quad 5.21$$

where:

S	=	sample
Std	=	standard
Area	=	area of the relative emission and absorbance bands together
A	=	absorbance
η	=	refractive indices of the solvents used

5.4 Experimental

5.4.1 Instrumentation and techniques for singlet oxygen determination

The excitation pulse source for the singlet oxygen studies was provided by an Nd-Yag laser (providing 47 mW, 9 ns pulses of laser light at 532 nm) and the basic setup is shown in Figure 5.5. An energy meter was used to measure the pulse energy of the laser light.

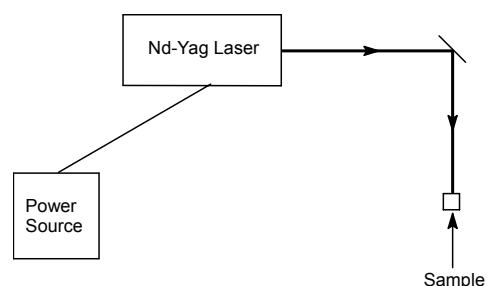


Figure 5.5 Set-up for singlet oxygen quantum yield determinations.

Absorbance spectra were recorded on a Varian UV-Vis-NIR spectrophotometer. The photochemical experiments were carried out in a 4 mL UV cell with an optical pathlength of 1 cm. The absorbances of the quencher (DPBF) and the sample sensitizer solutions were set to approximately 1 by dilution. Care was taken to ensure that the absorbance peak of the DPBF (at 417 nm) was observed, thus the volume of DPBF used was dependent on the UV bands observed for a particular sample. Both the DPBF and pyrroloiminoquinone solutions were made up in DMSO. Air saturated solutions were used for all experiments except where stated and the measurements carried out at room temperature. The decrease in the DPBF band was monitored while ensuring that the bands belonging to the pyrroloiminoquinone samples remained unchanged (the light intensity was kept low enough to avoid this decrease, as any change would indicate photobleaching or photodegradation of the sample). The absorbance of a reference solution (porphine in benzene, $\Phi_{\Delta} = 0.66$),¹¹⁸ was used to calculate the Φ_{Δ} of porphine in DMSO, which was found to be 0.658, *i.e.* ~ 0.66 .

5.4.2 Instrumentation and techniques for fluorescence quantum yield determinations

Absorbance and fluorescence spectra were recorded in MeOH on a Cary Varian 500 UV-Vis-NIR spectrophotometer and a Varian Eclipse spectrofluorimeter. Slit widths for the spectrofluorimeter were kept at 10 nm and the excitation wavelengths used were between 260 and 483 nm. Fluorescence of the MeOH solvent occurs at excitation wavelengths lower than 240 nm. The experiments were carried out in a cell with an optical pathlength of 1 cm at room temperature. The absorbance spectra of the sample solutions were recorded and set to between 0.2 and 0.4 by

dilution (in order to minimise quenching), and the fluorescence emission spectra subsequently run. The reference material used was benzene in cyclohexane ($\Phi_F = 0.05 \pm 0.02$).¹¹⁹

5.5 Results and Discussion

5.5.1 Singlet oxygen quantum yield determinations

Upon irradiation of the DPBF quencher, in the presence of a select group of pyrroloiminoquinones, the absorbance of DPBF was observed to decrease. The UV absorption bands of the samples remained unchanged (Figure 5.6), indicating the suitability of the light intensity chosen. The singlet oxygen quantum yields (Φ_Δ), calculated using Eqn. 5.20, is presented graphically in Figure 5.7 and listed in Table 5.1.

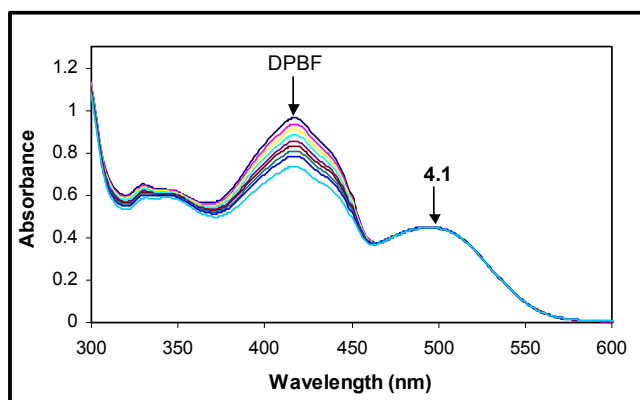


Figure 5.6 A typical UV / Visible absorbance spectrum obtained during singlet oxygen production of compound **4.1** in the presence of the DPBF quencher.

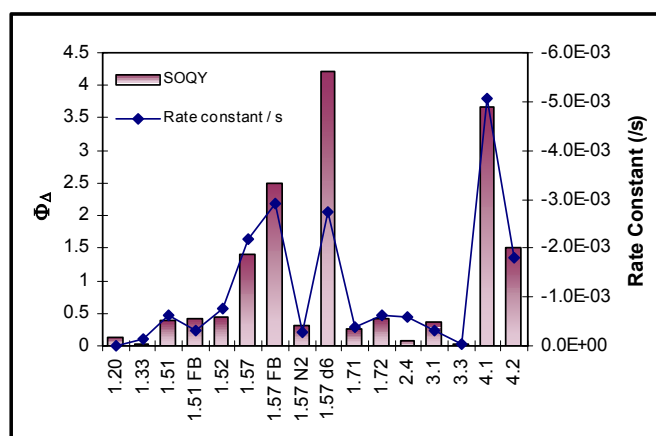


Figure 5.7 Comparison of the singlet oxygen quantum yields and rate constants obtained for the pyrroloamino-*ortho*-quinone, pyrroloiminoquinones and *bis*-pyrroloiminoquinones.

Moderate values ($0.36 \leq \Phi_{\Delta} < 0.43$) were obtained for **3.1**, **1.52**, **1.51** and **1.51 FB**. Upon comparison of the results, the brominated compounds were shown to have slightly higher values. These observations may be due to a combination of effects including the heavy atom effect^{114,117} and the fact that these compounds are slightly more electron donating. The free base of **1.51** showed only a marginal increase in singlet oxygen production, though the rate of production was slightly slower. Conversely, compounds with stronger electron withdrawing groups (such as **3.3**, **2.4**, **1.33** and **1.20**) were found to have particularly low quantum yields ($0.01 \leq \Phi_{\Delta} \leq 0.1$). It is possible that these low values may in part be due to the quenching abilities of the amino groups (**3.3**, **1.33**), or due to the extra hydroxyl and carbonyl group (**2.4**, **1.20**) functionalities, which are also able to act as quenchers.

The *bis*-pyrroloiminoquinones also demonstrated moderate, though lower, Φ_{Δ} values than the discorhabdin type compounds, with the methylated **1.72** compound exhibiting a slightly higher value than its counterpart **1.71**. A possible explanation, here again, could be the presence of the extra inductively electron donating group (a methyl group). Following excitation of these pyrroloiminoquinones (PIQ), the following mechanism may have been observed:



Surprisingly, three compounds, **1.57** and the N-18 oximes (**4.1** and **4.2**), consistently produced singlet oxygen quantum yields above 1. The free base of **1.57** showed a marked increase in its singlet oxygen quantum yield. A quantum yield value greater than 1 is often observed when photolysed compounds generate radicals. Bearing in mind that a quantum yield of a primary process is a value between 0 and 1 (since it represents the probability that an excited state will undergo a reaction), the quantum yield of an overall reaction (primary and secondary processes) can, however, be greater than 1, depending on the secondary processes taking place (please see Eqn. 5.1 g, Section 5.2.1). These yields can be quite large when chain reactions occur.¹¹²

Some photosensitisers have been shown to generate both ${}^1\text{O}_2$ and superoxide (by electron transfer), which may also explain our observations. As discussed previously, quinoid-type sensitisers can form semiquinone radicals and these reduced sensitisers may then produce superoxide by electron transfer as shown in Section 5.2. Although a great deal of work still needs to be done, the following is a tentative proposal for the production singlet oxygen by pyrroloiminoquinone metabolites:

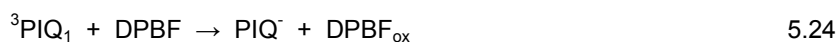


Table 5.1 Singlet oxygen quantum yields (Φ_{Δ}), rate constants and R^2 data obtained for the various pyrroloamino-*ortho*-quinone, pyrroloiminoquinones and *bis*-pyrroloiminoquinones in DMSO.

Compound	Φ_{Δ}	Rate constant (/s)	R^2
1.20	0.14	-1.56×10^{-5}	0.997
1.33	0.03	-1.56×10^{-4}	0.997
1.51	0.38	-6.20×10^{-4}	0.992
1.51 FB	0.41	-3.10×10^{-4}	0.991
1.52	0.43	-7.70×10^{-4}	0.992
1.57	1.39	-2.18×10^{-3}	0.996
1.57 FB	2.50	-2.90×10^{-3}	0.995
1.57 (N ₂)	0.31	-2.92×10^{-4}	0.990
1.57 DMSO-d ₆	4.23	-2.74×10^{-3}	0.993
1.71	0.25	-3.75×10^{-4}	0.997
1.72	0.41	-6.26×10^{-4}	0.992
2.4	0.07	-6.06×10^{-4}	0.995
3.1	0.36	-3.26×10^{-4}	0.993
3.3	0.01	-2.75×10^{-5}	0.981
4.1	3.68	-5.05×10^{-3}	0.999
4.2	1.51	-1.79×10^{-3}	0.998

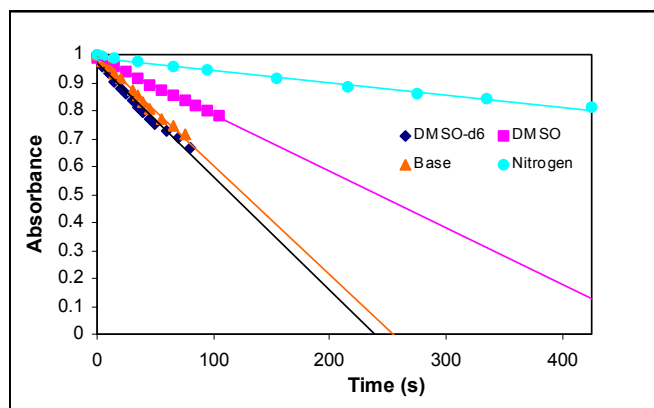


Figure 5.8 The effects of deuterated, air saturated and 'nitrogen saturated' DMSO on the singlet oxygen (Φ_{Δ}) production of discorhabdin A (**1.57**). The difference between **1.57** (TFA salt) and its free base (marked base on the graph) on Φ_{Δ} production is also shown.

As discussed in Section 5.2 c), evidence for the presence or involvement of singlet oxygen in the study may be confirmed by performing the photolysis in deuterated solvents (in this instance DMSO-d₆) or by bubbling an inert gas such as argon or nitrogen to de-aerate the system. The former was found to increase the rate of disappearance of DPBF (Figure 5.8), which is typical since singlet oxygen has a much longer lifetime in deuterated solvents and the singlet oxygen is

thus able to interact with the photo excited molecule to a larger degree. On removal of oxygen from the system, on the other hand, the expected substantial decrease in the rate of reaction was observed (Table 5.1 and Figure 5.8). Both experiments thus provided the evidence for the presence of singlet oxygen. It may therefore be concluded that the pyrroloiminoquinones tested produced singlet oxygen.

5.5.2 Fluorescence quantum yield determinations

For the most part, the fluorescence quantum yields (Φ_F) obtained for the select group of pyrroloiminoquinones were found to be low (Figure 5.9). Amino groups are known to quench singlet excited states, which may account for the low values obtained for **3.3** and **3.2**, but not **1.33**. Comparison of the values obtained for **3.3** and **3.2** with the moderately high Φ_F value obtained for the desulfurated **2.4**, which has an additional hydroxyl group, may indicate that a thioether, *i.e.* heavy atom effect,¹¹⁷ may account for a decrease in the quantum yield, as seen with **1.57**. Compound **1.33** (Figure 5.9) had a relatively high Φ_F , whereas compound **1.20** had one of the lowest Φ_F values, along with **1.57**, and so perhaps the complexity of the ring system is unimportant. Comparison of **1.57** with **1.51**, **1.52** and **1.53** which have slightly higher quantum yields, also indicated that a thioether led to a decrease in Φ_F , while an additional hydroxyl group led to a slightly higher value (**1.51** and **1.52**). On the other hand, the effect of an additional bromine on the quantum yields of **1.52** and **1.53** was found to lead to a slightly lower quantum yield, since molecules with heavy atoms promote ISC (Section 5.2). The N-13-methylated *bis*-pyrroloiminoquinone **1.72**, had a slightly higher quantum yield than **1.71**. On the contrary, a higher quantum yield was observed for **1.71**'s N-oxime (*i.e.* **4.1**). In retrospect, taking into consideration the satisfactory results obtained for the singlet oxygen quantum yield study, the low values arrived at for the fluorescence studies are not unusual (please refer to Figures 5.1 and 5.4). As a rule of thumb, a low value obtained for the fluorescence may imply a higher value for phosphorescence.

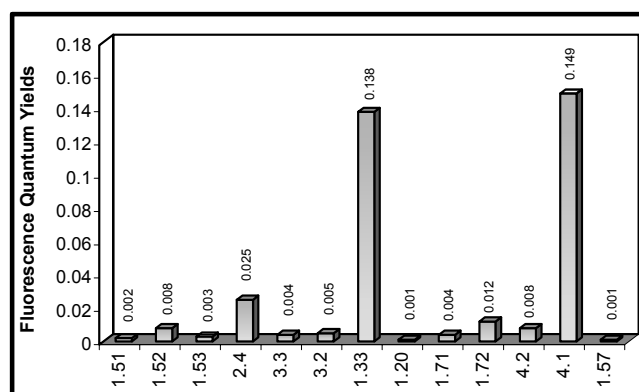


Figure 5.9 Fluorescence quantum yield (Φ_F) data obtained for selected pyrroloiminoquinones (values given in the graph).

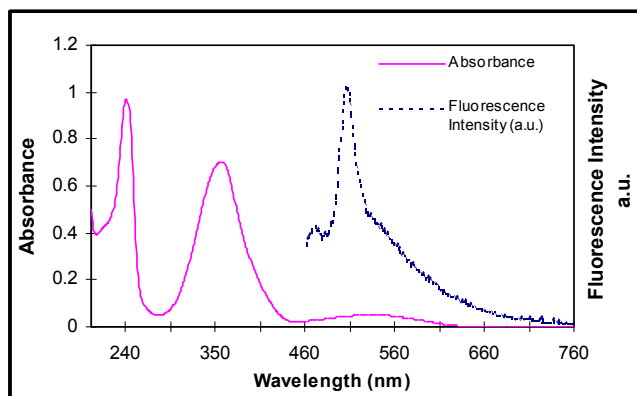


Figure 5.10 Fluorescence and absorbance spectra of **1.33**.

Figure 5.10 shows the absorbance and fluorescence spectra obtained for a representative sample **1.33**. The spectra are distinctly different, perhaps indicating that the nuclear configurations of the ground and excited states are not the same and that the system may have undergone geometrical and structural alterations upon excitation.¹¹⁷

5.6 Conclusion

Most of the pyrroloiminoquinones were shown to produce singlet oxygen which could be effective in cell destruction. In general, those compounds with stronger electron withdrawing groups, such as amino, or extra carbonyl or hydroxyl group functionalities, were found to have low singlet oxygen quantum yields. These functional groups are, however, known to quench singlet oxygen production thus explaining the low singlet oxygen quantum yields observed. Alternatively, those compounds with thioethers and additional bromines, or inductively electron donating groups such as a methyl group, were found to have higher quantum yields. These compounds may follow a Type II reaction mechanism. The quantum yields obtained for the N-18 oximes (**4.1** and **4.2**) and **1.57** are likely to indicate the production of radicals, perhaps with some contribution from singlet oxygen, suggesting that a Type I, or a Type I and II, reaction mechanism is involved.

PDT relies on the presence of oxygen to destroy cancerous cells. Hypoxic tumours, however, present a drawback for such an aerobic process. The N-18 oximes, having been shown to produce radicals, may still find use in cancer therapy since they could have the dual purpose of acting as an oxygen surrogate (thus enabling the production of singlet oxygen) in oxygen poor tumours (hypoxic) as well as being responsible for the generation of DNA damaging radicals. Quinoxaline di-N-oxide¹⁰³ has been found to be highly selective in killing hypoxic cells found in tumours. Upon irradiation, the lesions under both aerobic and anaerobic conditions were believed to occur *via* electron transfer from the nucleobase to the photoexcited quinoxaline di-N-oxide, although under aerobic conditions, some contribution from $^1\text{O}_2$ was thought to have taken place.

In the past, pyrroloiminoquinones have demonstrated significant anticancer activity and were originally considered as potential candidates for development as antitumour drugs. These compounds interact with DNA in the following manner:

- by intercalation,
- through DNA strand breakage,
- by topoisomerase I / II inhibition, and
- through semiquinone radical intermediates (which would lead to DNA single strand breaks)

Ireland and Barrows³⁰ proposed the *in vivo* activation of the iminoquinone moiety to the semiquinone intermediates and these photochemical investigations conducted have confirmed that pyrroloiminoquinones (**1.57** and the N-18 oximes) are indeed capable of producing radicals that could lead to single strand breakages the study has therefore shown that the pyrroloiminoquinones are capable of mediating DNA damage through the production of singlet oxygen upon photosensitisation.

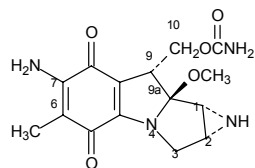
The fluorescence quantum yields were found to be low for all compounds except **1.33** and **4.1**. These two compounds may still find use in PDT in terms of imaging where the compounds ability to fluoresce is used to image the tumour by fluorescence detection and its biodistribution is therefore followed. Since the basis of PDT is the fact that the sensitiser is harmless until activated by light, light may thus be selectively shone on the tumour (the sensitiser located through its ability to fluoresce) through an optical fibre. The molecule will therefore be activated and cell death will only occur in the predetermined area. In view of the singlet oxygen quantum yield production for these compounds the low Φ_F yields could be expected (Figure 5.1).

Chapter 6: Electrochemistry

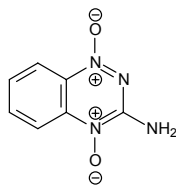
6.1 Introduction

Electrochemistry has often been used to describe and understand certain biological processes which are known to have an electrochemical foundation. Electron transfer is well known in the biological realm, and, ironically, in addition to being responsible for the progressive replication of cancerous cells, molecular electron transfer has been proposed to be crucial in an organism's biological defence.¹²⁰ Common physiological and biochemical processes associated with electrochemical reactions include photosynthesis, nerve excitation, blood coagulation, vision, smell and many enzymatic reactions, as well as the bioreductive activation of pro-drugs to a more toxic constituent.^{120,121} A biological cell has a rich source of transferable electrons in its compounds containing nitrogen, sulfur and oxygen atoms, all of which have non-bonding pairs of electrons, *i.e.* electrons which are available for transfer. However, the cell is poor in electron acceptors, with only carbonyls and keto-aldehydes, for example, readily available. A large amount of research has thus been carried out over the years in evaluating the electrochemical properties of proteins, enzymes and various cellular components,¹²⁰ and with particular relevance to the work described in this thesis in investigating the interaction of various molecules with DNA.¹²²

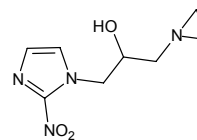
The concept of bioreductive activation of pro-drugs in hypoxic tumour cells, first observed *in vitro* with metronidazole, to produce the more toxic active compound, has been extensively reviewed¹²¹ and three general classes of such agents are now known. The first class comprises the quinone antibiotics of which mitomycin C (**6.1**) was the prototype drug. The second class of bioreductive cytotoxins are benzotriazine di-N-oxides of which tirapazamine (**6.2**) is the prototype compound. Tirapazamine is the first drug to be introduced into clinical trials as a bioreductive cytotoxic agent. The nitroimidazoles which were initially developed as radiation sensitisers but also show preferential toxicity to hypoxic cells as dual function agents, *e.g.* RSU 1069 (**6.3**) form part of the third class.¹²¹



6.1



6.2

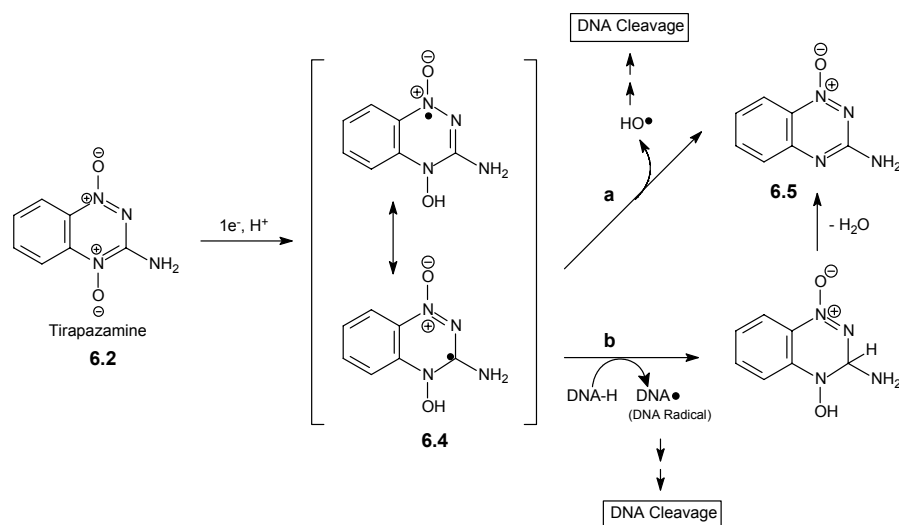


6.3

The first two classes contain compounds which exhibit some structural homology with the pyrroloiminoquinones discussed in previous Chapters and a brief overview of their electrochemical properties is therefore deemed necessary.

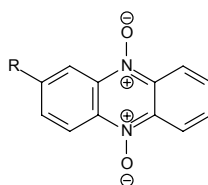
As mentioned previously, mitomycin C is an example of a pro-drug that is metabolically activated by reduction or acidification. Chemical and enzymatic one electron reduction of mitomycin, followed by the removal of the C-9a methoxy substituent, with the assistance of the non-bonding electrons on the neighbouring aziridine nitrogen atom, a reduced mitosene is obtained. This intermediate is a bifunctional alkylating agent capable of cross-linking DNA. Upon oxidation, the activated, reduced form of mitomycin C, which produces adducts with the nucleophiles present, covalently linked at C-1 or both C-1 and C-10. Reduced mitosenes are therefore the active intermediates in the bioreductive activation process.^{123,124} Studies on the relationship between structural modifications in mitosenes and their antitumour activity have included variations of the 6- and 7- substituent of the quinone ring, the carbamate function and the aziridine ring and results indicate that the reductive activation of mitosenes proceeds *via* a quinone methide and/or iminium ion intermediate.¹²³

The 1,2,4-benzotriazine 1,4-di-oxides, after several groups investigated the mechanism for the selective toxicity of tirapazamine on hypoxic cells found in solid tumours, are thought to derive their antitumour properties from DNA cleavage.^{123,125} The importance of the N-oxide group for the selective activity of **6.2** led to the design of new heterocyclic N,N-dioxides and the exploration of their activity in hypoxic cells.¹²³ An enzymatic one electron reduction of the heterocycle was proposed to lead to the production of radical species and ultimately to DNA damage. The redox activated DNA cleavage by tirapazamine is markedly inhibited by molecular oxygen and, in the absence of reducing systems, **6.2** alone does not damage DNA. Workers have suggested that the more negative the reduction potential displayed by a particular compound, *i.e.* to the point at which enzymes can no longer reduce the compound, the greater the hypoxia selectivity.¹²¹ Monge *et al.* included electrochemical data in their research paper to demonstrate whether the reduction potentials can be related to oxidic or hypoxic selectivity.¹²¹



Scheme 6.1 The two possible mechanisms for DNA Cleavage by tirapazamine (**6.2**).¹²⁴

Two possible mechanisms for DNA cleavage in mammalian cells by tirapazamine are shown in Scheme 6.1. The highly cytotoxic **6.4** is produced on reduction of **6.2** and the rates of reduction parallel cytotoxicity in several different cell lines. The specific toxicity of **6.2** toward hypoxic cells is thought to occur *via* the activated form of the drug radical (**6.4**) being destroyed by molecular oxygen (*i.e.* **6.4** is oxidised back to the parent drug in the presence of oxygen). Such back oxygenation regenerates the drug and leads to the production of a superoxide radical, a species whose *in vivo* toxicity is diminished by the cellular enzymes superoxide dismutase and catalase. Daniels and Gates¹²⁵ provide evidence in support of the notion that a hydroxyl radical species, rather than the radical form of **6.2**, is involved in the cleavage of DNA by the reductively activated **6.2**. This supposition, realised through the use of radical scavengers that react specifically with oxygen radicals *versus* other radical species and through monitoring of the low sequence selectivity observed in the DNA cleavage by the tirapazamine, is consistent with the involvement of a highly reactive, nonselective cleaving agent such as a hydroxyl radical. The ability of **6.2** to cleave DNA was also found to depend on the enzymatic reduction.¹²⁵ The drug radical **6.4** when produced *in vivo* could, however, perhaps react with non-nucleic acid cellular components, resulting in DNA cleavage. A weak reduction dependent DNA cleavage was observed with the two electron reduced form of tirapazamine (**6.5**) upon incubation with an enzyme system, which alone is not a DNA-cleaving agent. Reducing agents such as sodium dithionite, sodium ascorbate and thiols were found to be incapable of effecting the reductive activation of **6.2**. It thus appeared that **6.2**, together with reductive cellular enzymes, may serve as an agent to provide hydroxyl radicals, which are known DNA cleaving agents in radiotherapy, specifically to hypoxic tumour cells *in vivo*.¹²⁵ Hecht and co-workers obtained similar results upon describing the redox-activated DNA cleavage by phenazine N-oxides **6.6**.^{125,126}

**6.6**

Radisky *et al.*³⁰ showed that the DNA reductive cleavage activity of certain pyrroloiminoquinones is mediated by redox chemistry. The results demonstrated that makaluvamine-mediated reductive cleavage of DNA (determined using a supercoiled pBR322 DNA assay) is dependent on the capacity of the compound to intercalate into DNA as well as on its ability to produce a (semi-quinone) radical. In addition, the makaluvamines (as well as discorhabdin A) were also shown to cause significant DNA single-stranded scission, *i.e.* no double-stranded cleavage was observed in the reductive cleavage assay.

The photochemistry study (Chapter 5) showed that a suite of fourteen pyrroloiminoquinones isolated from South African Latrunculid sponges are proficient singlet oxygen producers, three of which were shown to be capable of producing radicals upon irradiation. Electrochemistry may therefore a) give insight as to whether these pyrroloiminoquinones undergo one or two electron reductions (one electron reductions have been shown to initiate radical-mediated DNA strand damage¹⁰³ and this information may therefore be important in understanding the compound's mechanism of action *in vitro*), b) give an indication of the compounds' stability and susceptibility to reduction (and thereby characterise these compounds electrochemically), and c) confirm or resolve the results obtained using other techniques such as photochemistry. With the expectation that a more detailed understanding of the redox chemistry of selected compounds may ultimately help facilitate the design of new improved antitumour agents, and since many drugs have been shown to be activated *in vivo* through enzymatic reduction processes, the ability of the pyrroloiminoquinone compounds to undergo redox reactions has therefore been investigated. It is thus anticipated that the photophysical and electrochemical studies carried out may ultimately lead to a deeper understanding of the mechanism of DNA damage induced by these compounds. The literature available on the electrochemistry of pyrroloiminoquinones in particular is limited³⁰ and the properties of sixteen structurally related pyrroloiminoquinones, in pH-varied experiments, were characterised using cyclic and square wave voltammetry.

6.2 Electrochemical techniques

6.2.1 Cyclic voltammetry

One of the techniques used to obtain mechanistic information in redox systems is cyclic voltammetry (CV). CV enables the electrode potential to be scanned rapidly in search of redox couples. Once located, a couple can then be characterised from the potentials of peaks on the cyclic voltammogram and from changes caused by variation of scan rate.¹²⁷ CV is an enormously popular technique and the acquisition of a cyclic voltammogram of a new electrochemical system is often the predecessor to other less- straightforward techniques that furnish more detailed information.¹²⁸

In CV, a potential is applied and swept back and forth (where the sweep direction is inverted at a chosen potential) linearly with time. By measuring the resultant current, which is monitored continuously, the subsequent oxidation or reduction of the surface species may then be examined. Invaluable, necessary, information as to the presence of an electroactive species (*i.e.* the species adsorbed onto the surface of the electrode) in solution or at the electrode surface is easily obtained with CV. Cyclic voltammograms are, however, often ambiguous and thus great care is taken in the interpretation.¹²⁸

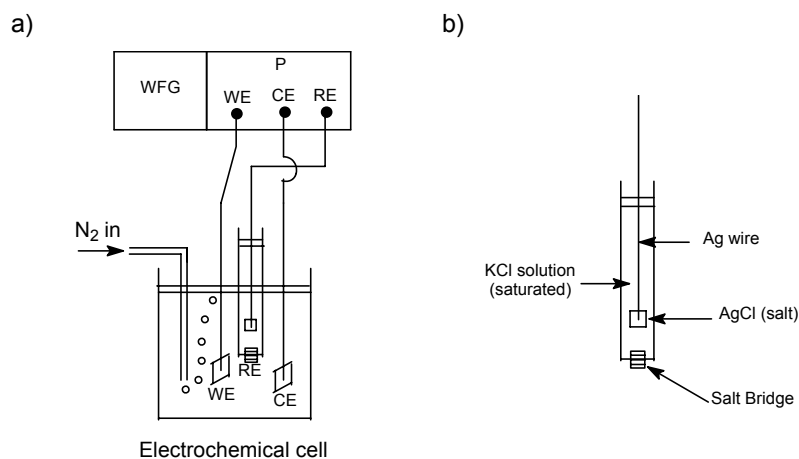


Figure 6.1 Schematic representation of a) the basic setup for a cyclic and square wave voltammetric system and b) enlarged schematic of the reference electrode (Ag|AgCl). (WFG = waveform generator, P = potentiostat, WE = working electrode, CE = counter electrode, RE = reference electrode).¹²⁸

The equipment used to carry out CV is illustrated in Figure 6.1. The electrochemical cell consists of a vessel with an inlet port to allow the saturation of a solution with an inert gas, such as N₂ or Ar. The removal of O₂ is a necessary step to prevent interfering currents that are due to the reduction of O₂. A standard cell consists of three electrodes immersed in the electrolyte solution: a) a working electrode (WE), b) a reference electrode (RE) and c) a counter electrode (CE). A potentiostat monitors and controls the WE potential with respect to the RE. The current flowing between the WE and CE (also connected in series) is measured as the potential drop V across a resistor R ($I = V/R$). The I/V data thus obtained is stored, allowing for further manipulation.¹²⁸

Figure 6.2 shows a typical cyclic voltammogram that would be obtained from an electroactive adsorbed species provided that:

- the electrode has the maximum coverage of an oxidised form (O);
- the electrochemical reaction can be represented by: $O_{\text{ads}} + ne^- \leftrightarrow R_{\text{ads}}$ and is kinetically fast enough to maintain Nernstian (*i.e.* reversible) behaviour at each point in the CV scan such that the concentrations of O and R near the electrode obey the Nernst equation;
- the oxidised and reduced species are both strongly adsorbed and have the same enthalpy of adsorption.¹²⁸

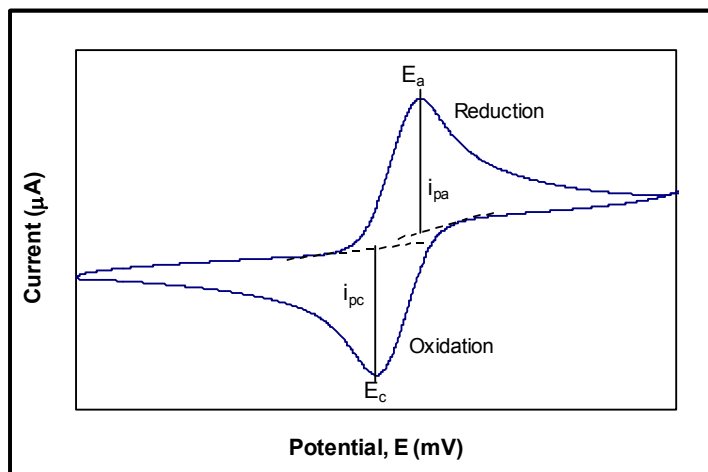


Figure 6.2 The current / potential (I / V) curves expected from an electroactive adsorbed species in a reversible redox reaction: $O_{ads} + ne^- \rightleftharpoons R_{ads}$. E is the potential at which the maxima (E_a) and minima (E_c) in the current are observed.¹²⁸

a) *Reversible processes*

In reversible systems, the species formed in the forward direction is regenerated in the reverse sweep (Figure 6.2), *i.e.*



Information obtained from a reversible system includes:¹²⁹

- i. the $E_{1/2}$, the half-wave potential, which is characteristic of a particular species, *i.e.* where

$$E^{\circ} = E_{1/2} = (E_a + E_c) / 2 \quad 6.2$$

E° is the formal potential, which is corrected to the reference electrode used.

- ii. the number of moles of electrons involved in a particular process where:

$$\Delta E = E_a - E_c \quad 6.3$$

$$\Delta E = 2.3 RT / nF \quad 6.4$$

where:

- R = Gas constant
 T = Temperature
 F = Faraday's constant
 n = moles of electrons

which at 25 °C becomes

$$\Delta E = 0.0592 / n \quad 6.5$$

where n = moles of electrons involved

- iii. stability of a compound (starting compound remains unchanged) and true reversibility of a particular species *i.e.* where

$$i_a / i_c = 1 \quad 6.6$$

i_p is described by the Randles – Sevcik equation:

$$i_p = 2.69 \times 10^5 n^{3/2} A D^{1/2} C V^{1/2} \quad 6.7$$

where:

i_p = peak current (amperes)

A = area of electrode (cm²)

n = moles of electrons

D = diffusion coefficient (cm²/s)

C = concentration (mol/cm³)

V = scan rate (V/s)

According to the Randles-Sevcik equation, an increase in i_p is directly proportional to an increase in $V^{1/2}$, which is related to concentration. A linear plot of $V^{1/2}$ versus i_c or i_a indicates a diffusion-controlled mass transfer and is therefore of importance in analytical applications or during determinations concerning electrode mechanisms.

CV may thus be used to a) characterise the electroactive system by $E_{1/2}$; b) to determine whether oxidation is occurring; and c) to verify the stability of a complex once oxidation or reduction has taken place.

b) Irreversible processes

In an irreversible reaction of the type $O_{ads} + ne^- \rightarrow R_{ads}$, the voltammogram (Figure 6.3) shows no inverse peak on reversing the scan direction, *i.e.* the compound is unstable. With respect to reversible systems the waves are broader and lower, *i.e.* they are less intense.¹²⁰ Irreversible systems are capable of producing both anodic and cathodic waves but the peaks exhibit very large separations *i.e.* > 200 mV.

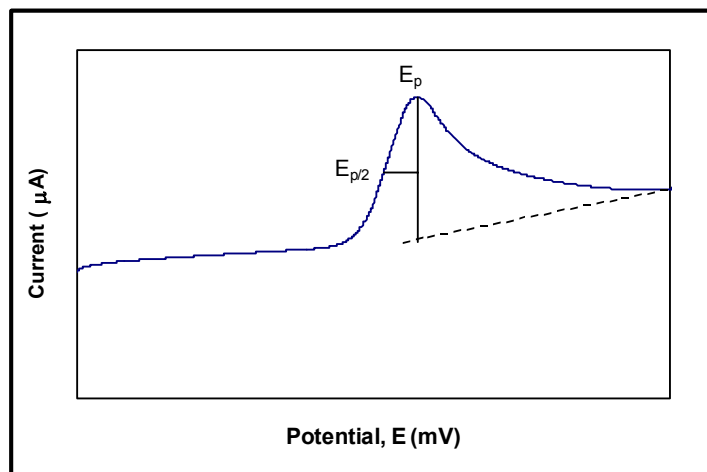


Figure 6.3 The current / potential (I / V) curves expected from an electroactive adsorbed species in an irreversible reaction.

$E_{p/2}$ (where $E_{p/2}$ = peak at $\frac{1}{2}$ current) is related to $E_{1/2}$ and may be used in the identification of a compound.¹²⁹

c) *Quasi-reversible processes*¹²⁹

In a quasi-reversible system, the peaks appear to be reversible but

i. at 25 °C

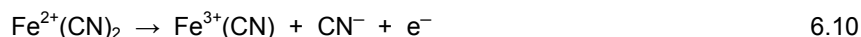
$$\Delta E \neq 0.0592 / n \quad 6.8$$

and

ii. if

$$\Delta E > 60 \text{ Mv} \quad 6.9$$

the system is characterised as a quasi-reversible process. In essence, molecules undergo an appreciable but not a severe change, e.g.



6.2.2 Osteryoung square wave voltammetry

Square wave voltammetry (SWV), in this case Osteryoung Square Wave Voltammetry (OSWV), is a pulse technique that compliments CV. A predetermined pulse, e.g. 100 mV, is applied for a certain time period e.g. 2.5 ms (Figure 6.4). The current (i) obtained before (i_1) and after (i_2) the application of a pulse is recorded simultaneously. The base potential increases by a certain amount (dE) for each full cycle of the square wave (e.g. E_1 or E_2 etc.). All i_1 are recorded, as are

i_2 , and subtracted at the end of a run, rather than at the end of each cycle.¹²⁹ Since only the difference in current is recorded, any current recorded due to impurities or the electrolyte solution is eliminated. The charging current, *i.e.* the surplus current which is used to neutralise the electrode in CV, is also removed.¹²⁹

Overall, these factors lead to an increase in sensitivity observed in pulse techniques. SWV is thus a rapid method which may be used to monitor transient processes, it is extremely sensitive to the electrochemical reversibility of a couple as well as the chemical stability of a product in a forward step (Figure 6.5).¹³⁰ OSWV, which is more sensitive than CV, provides greater resolution of any overlapped peaks obtained previously in CV and the $E_{1/2}$ is thus accurately determined. The number of moles of electrons involved may also be determined from the width of a peak at half height.¹²⁹

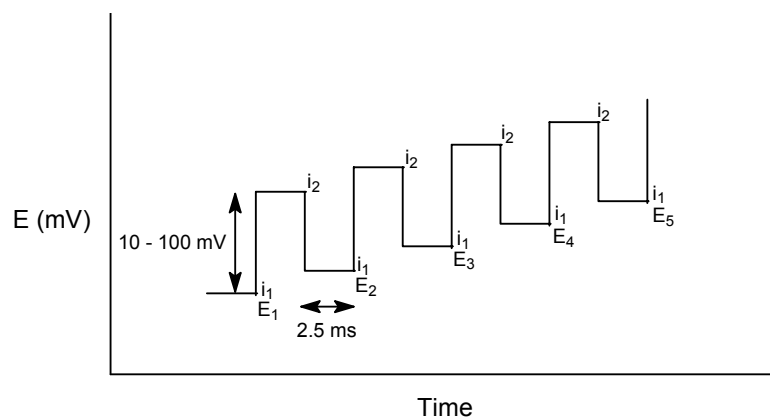


Figure 6.4 Excitation signals observed in square wave voltammetry.^{129,130}

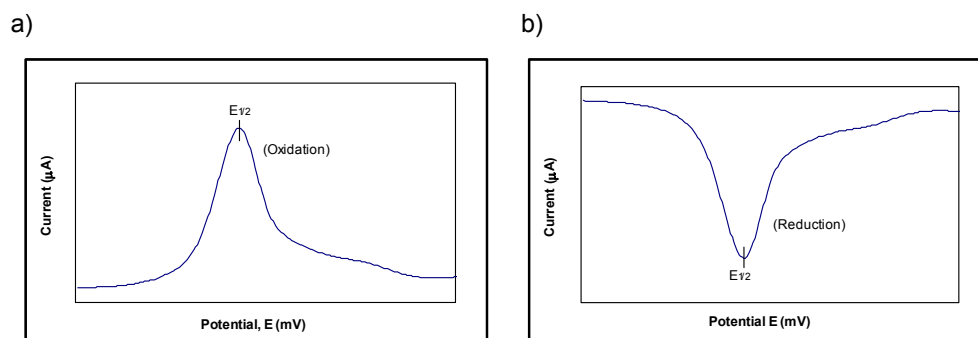


Figure 6.5 The current *versus* potential (I / V) curves from a) an oxidised and b) a reduced electroactive adsorbed species in OSWV, which is often dependent on the scan direction.

The current *versus* potential (I / V) curves expected from a) an oxidised and b) a reduced electroactive adsorbed species using OSWV, shown in Figure 6.5, where $E_{1/2} = (E_a + E_c) / 2$ as

determined in CV. The peak at half height, $W_{1/2}$ is related to the electron stoichiometry by the equation 6.9:

$$W_{1/2} = \frac{3.52 RT}{nF} \quad 6.9$$

where:

- R = Gas constant
 T = Temperature
 F = Faraday's constant
 n = moles of electrons

Thus for:

- n = 1, $W_{1/2}$ is 90.4 mV and
 n = 2, $W_{1/2}$ is 45.2 mV at 25°C.

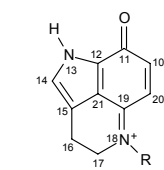
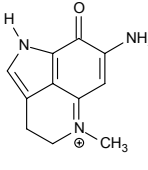
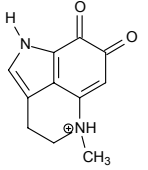
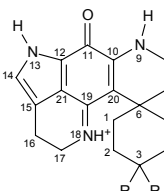
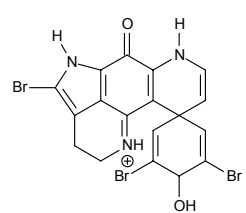
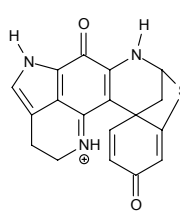
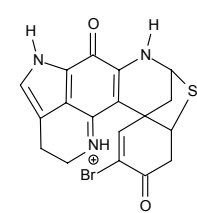
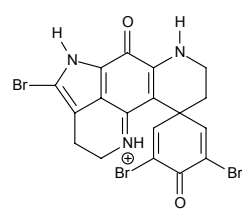
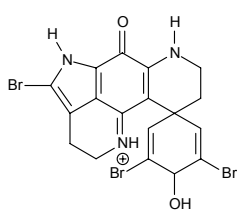
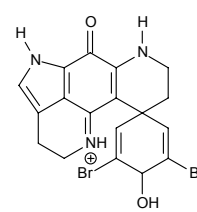
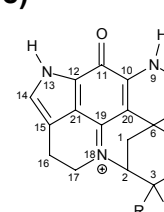
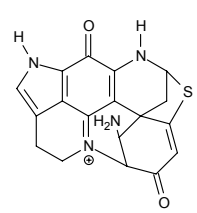
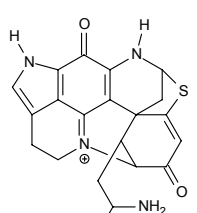
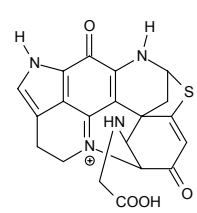
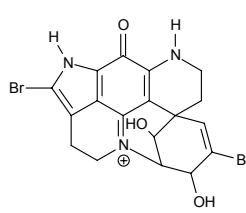
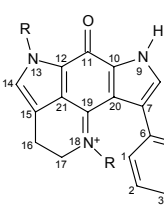
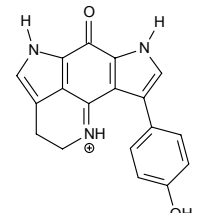
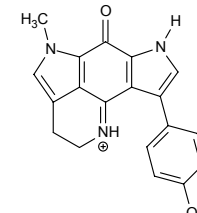
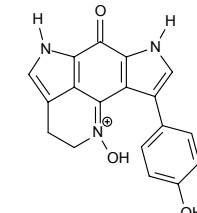
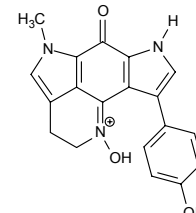
Sensitivity and resolution involved is dependent on pulse amplitude, frequency and scan rates, with larger pulse amplitudes resulting in larger and broader peaks. Because sensitivity and resolution is compromised in irreversible processes, these systems show lower and broader peaks. Like CV, peak currents are proportional to concentration.

6.3 Results and Discussion

6.3.1 Voltammetric characterisation of pyrroloiminoquinones

For most of the pyrroloiminoquinone metabolites, cyclic voltammetry revealed one clear reduction process. Occasionally, only the anodic peak potentials are listed when only the anodic component of the reduction process was observed. The main reduction process was assigned as Couple I and any additional reduction couples as Couple II, Couple III, etc. Only the main reduction process, *i.e.* Couple I, was studied as a function of voltage sweep rate and switching potential, and the tabulated data (Tables 6.2 - 6.5) summarises the main reduction process (Couple I) for each of the pyrroloiminoquinones studied. The $E_{1/2}$ potentials were generally observed to be independent of voltage sweep rate and the anodic to cathodic peak separation (ΔE), *i.e.* the ΔE values increased with an increase in sweep rates but the $E_{1/2}$ values remained roughly the same. Where there was some uncertainty as to the presence of additional peaks in the data obtained from CV, OSWV was used. The buffer solutions (pH 5.5 and 7.5), made up as described in the experimental section (Section 8.6), were used as the solvent and the potential swept between -800 and 0 mV for all experiments. For the sake of simplicity, the data has been arranged into structural classes *i.e.* a) tricyclic pyrroloiminoquinones, b) discorhabdin C type skeleton, c) the discorhabdin D / S type skeleton and d) the *bis*-pyrroloiminoquinones (Table 6.1).

Table 6.1 The grouping of the sixteen pyrroloiminoquinone metabolites into four structural classes.

Structural Class	Pyrroloiminoquinone metabolites			
a)				
		1.33	1.20	
b)				
		2.2	3.1	1.57
				
		1.51	1.52	1.53
c)				
		3.3	3.5	3.2
				
				2.4
d)				
		1.71	1.72	4.1
				
				4.2

In general, the pH was observed to influence the number of moles of electrons transferred and, as expected, the ease of reduction decreased with an increase in pH for all compounds (Figure 6.6). The discorhabdin D type compounds, *i.e.* those with sulfur, were found to be the easiest to

reduce, while the most difficult were the *bis*-pyrroloiminoquinones. ΔE values were found to be closer to 60 mV implying a one electron reduction process for the pH 7.5 buffered solutions, except for **1.52**, **1.53** and **1.72**. These three compounds were, however, found to have i_a / i_c (*i.e.* unity, equation 6.6) values indicating reversible electron transfer processes. No relationship between ΔE and i_a / i_c was found. The calculations performed to demonstrate unity for i_a / i_c indicated greater deviation from unity for experiments conducted at pH 7.5 (36 % within the range of 0.9 and 1.1) which may be due to the lower solubility of these compounds at a higher pH. Except for the *bis*-pyrroloiminoquinones (and their N-18 oximes), the compounds were shown to maintain a greater stability at a lower pH (64 % within the same range).

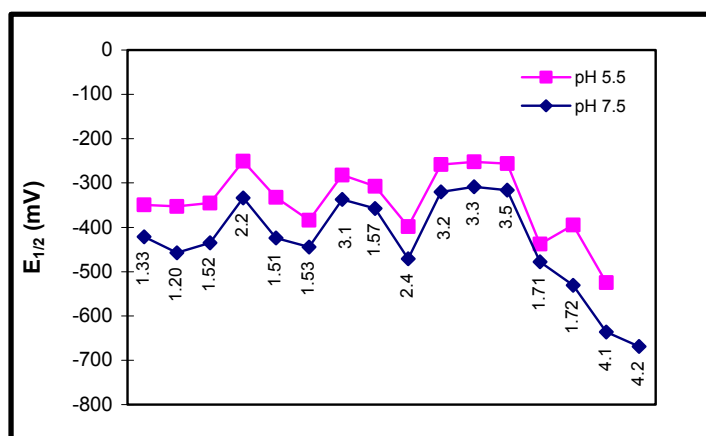


Figure 6.6 Comparison of the $E_{1/2}$ values obtained for the pyrroloiminoquinone metabolites.

The mode of transport (*i.e.* the affinity of a particular species for the electrode surface rather than the bulk solution) in an electrochemical cell may take place in one of three ways a) migration, where the movement is due to charge; b) diffusion, where the movement is due to the difference in concentration of the electroactive species near the electrode and that of the bulk solution; and c) stir-convection processes where the electroactive species is forced to move to the desired site. Only one mode is operational at any one time provided that the solution is not stirred and that a large amount of inert electrolyte is added. Diffusion controlled processes make up the largest proportion of all electrochemical analyses.¹²⁹ In order to verify whether a diffusion-controlled process dominated the reactions taking place, a plot of the current (i_a) versus the square root of the scan rate was evaluated. A diffusion controlled mechanism was found to be the dominant process for the pyrroloiminoquinones except for **1.52** and **2.2**. From the results obtained, the rate constants showed a decrease with an increase in pH, except for the N-18 oximes. The lower solubility of these compounds at pH 7.5 may account for the slower rate of electron transfer (the observed decrease in the rate constants). No relationship between unity and rate was found *e.g.* upon comparing **1.33**, which has a high rate constant and greater deviation from unity (i_a / i_c) and

1.71, which exhibits greater deviation from unity for i_a / i_c as well as a low rate constant. On the whole, the rates and ease of reduction increased with a decrease in pH.

a) *Makaluvamine C (1.33) and Damirone B (1.20)*

Figure 6.7 shows a typical voltammogram obtained for **1.33**. From the ΔE and i_a / i_c data presented in Table 6.2, it is clear that these compounds exhibit mainly reversible, stable behaviour, with the exception of **1.33** at pH 7.5 which could be classified as quasi-reversible.

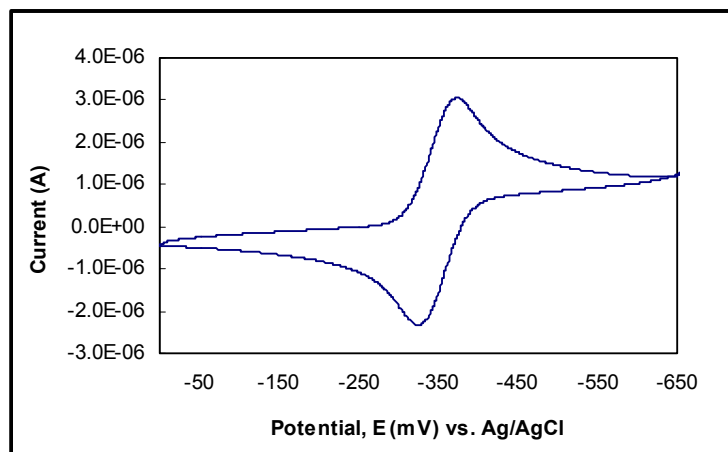


Figure 6.7 Cyclic voltammogram of **1.33** (pH 5.5). Scan rate: 25 mV/s.

The ΔE calculations inferred a two electron reduction process (except for **1.33** at pH 7.5) according to equation 6.5, while the $E_{1/2}$ values (Table 6.2 and Figure 6.6) showed that both **1.33** and **1.20** were quite difficult to reduce, with the more highly oxygenated compound (**1.20**) exhibiting the higher $E_{1/2}$ value. Both damirone B and makaluvamine C have a methylated, charged N-18, though damirone B also has an acidic proton on N-18, which may therefore reflect the relative ease of reduction of iminoquinone *versus* amino-*ortho*-quinone functionalities.

Table 6.2 Electrochemical CV data for the tricyclic pyrroloiminoquinones *versus* pH Scan rate: 25 mV/s.

Compound	E_a (mV)	$E_{1/2}$ (mV)	ΔE (mV)	i_a / i_c
1.33				
pH 5.5:	-326	-350	47	1.00
pH 7.5:	-384	-422	75	0.97
1.20				
pH 5.5:	-327	-353	51	0.94
pH 7.5:	-428	-458	59	0.92

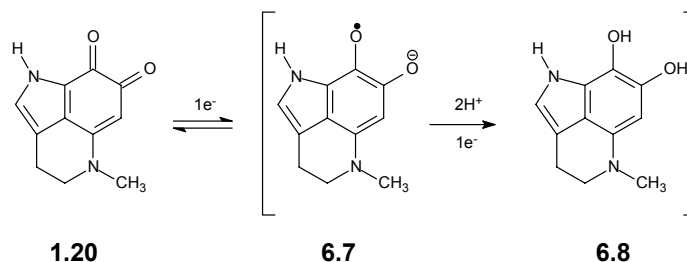


Figure 6.8 Proposed mechanism for the redox reaction of damirone B (**1.20**).

Proposed mechanisms for the reduction-oxidation processes taking place in damirone B and makaluvamine C are given in Figures 6.8 and 6.9, respectively. The initial product of oxidation in damirone B is an electron deficient species, giving rise to a semiquinone radical (**6.7**, Figure 6.8), which can therefore react with H_2O and OH^- to give rise to the product (**6.8**, Figure 6.8).

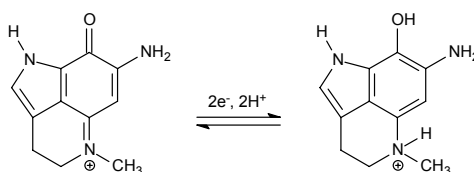


Figure 6.9 Proposed mechanism for the redox reaction of makaluvamine C (**1.33**).

b) Discorhabdin C type compounds

Table 6.3 presents the data obtained for the discorhabdin C type pyrroloiminoquinones. The compounds are listed according to the ease of reduction of these compounds at pH 5.5 (*i.e.* from lower to higher reduction potentials). One redox couple was typically observed, with the exception of **1.52** and **1.53**. The ΔE and i_a / i_c data indicate that these compounds exhibit mainly reversible behaviour at pH 5.5, while at pH 7.5 the processes may be classified as quasi-reversible (in that i_a / i_c deviated slightly from unity), with the exception of **1.53**. At a higher pH, these compounds experience a lower solubility, which may account for the decrease in stability of the compound reactions at the electrode surface. The ΔE values also show that a two electron reduction process (with the exception of **2.2** at pH 7.5) predominates at pH 5.5 and 7.5. The ease of reduction at both pH 5.5 and 7.5 was observed as follows: **2.2** > **3.1** > **1.57** > **1.51** > **1.52** > **1.53** (Figure 6.6, Table 6.3).

On comparison of **1.52** with **2.2**, where only a Δ^7 olefin distinguishes the two, the ease of reduction is observed to increase with increased conjugation. Both compounds have three bromine atoms and **2.2** was found to be the easiest of the discorhabdin C type compounds to reduce. The oxidised form of **1.52** (*i.e.* compound **1.51**) leads only to a slight decrease in the $E_{1/2}$ value, suggesting perhaps that the reduction process is not centred around C-3. In order to

investigate the effect of removing a bromine atom on the $E_{1/2}$ value, **1.52** and **1.53** were compared and an increase (from **1.52** to **1.53**) in reduction potential observed, *i.e.* removal of the C-14-Br led to an increase in $E_{1/2}$ and the compound (**1.53**) was therefore more difficult to reduce. Bromine has a high electronegativity and could draw electrons away from the ring, which should make the compound easier to reduce (**1.52** with three bromine atoms is easier to reduce than **1.53** which has only two). However, upon comparison of **1.53** and **3.1**, which has only a thioether moiety (no bromine groups), a large decrease in the reduction potential is observed with **3.1**. The lower electronegativity of the sulfur, or perhaps the formation of the extra ring through the sulfur, may account for the decrease. A decrease in conjugation (removal of the Δ^4 olefin) as well as bromination at position 2 led to the expected increase in the reduction potential of discorhabdin A on comparison with **3.1**. Interestingly, a plot of the ^{13}C NMR shifts for the C-19 carbon of the pyrroloiminoquinone skeleton, shown in Figure 6.10, certainly gives an indication of the relationship between lack of electron density at C-19 and the ease of reduction *i.e.* the more deshielded the carbon (*e.g.* **2.2**) the easier it is to reduce. The graph also shows a better correlation at a lower pH, most likely due to improved solubility.

Table 6.3 Electrochemical CV data for discorhabdin C type pyrroloiminoquinones *versus* pH. Scan Rate: 25 mV/s.

Compound	E_a (mV)		$E_{1/2}$ (mV)		ΔE (mV)		i_a / i_c	
	Couple I	Couple II	Couple I	Couple II	Couple I	Couple II	Couple I	Couple II
2.2								
pH 5.5:	-223	-450 [†]	-251	-*	56	-*	0.95	-*
pH 7.5:	-297	-469 [†]	-334	-*	73	-*	0.89	-*
3.1								
pH 5.5:	-263	-	-282	-	38	-	0.95	-
pH 7.5:	-315	-	-337	-	44	-	0.89	-
1.57								
pH 5.5:	-289	-	-307	-	36	-	0.95	-
pH 7.5:	-340	-	-358	-	35	-	1.67	-
1.51								
pH 5.5:	-311	-261 [†]	-333	-*	43	-*	0.94	-*
pH 7.5:	-401	-233	-424	-266.5	46	67	0.44	0.09
1.52								
pH 5.5:	-326	-204	-346	-222.2	39	36	1.12	0.05
pH 7.5:	-417	-594 [†]	-435	-*	36	-*	0.84	-*
1.53								
pH 5.5:	-356	-295	-384	-*	56	-*	0.96	-*
pH 7.5:	-423	-	-445	-	43	-	0.99	-

* Note:

-*: No return wave

†: Reduced peak potential (*i.e.* E_a)

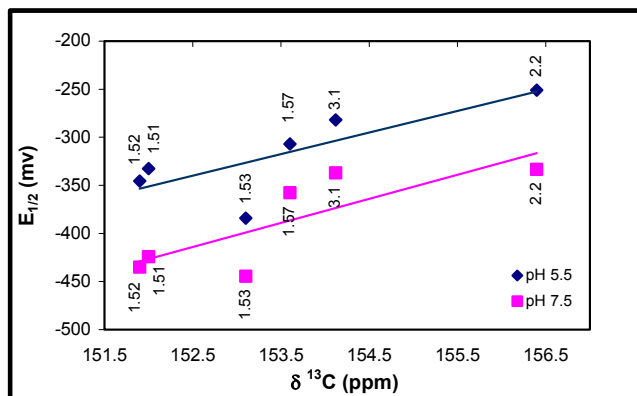


Figure 6.10 A plot of the C-19 ^{13}C NMR shifts for the discorhabdin C type pyrroloiminoquinones.

A proposed mechanism for the reduction process of **1.52** is given below in Figure 6.11. Once again the electron deficient species formed upon oxidation gives rise to a semiquinone radical, which may react with H_2O and OH^- .

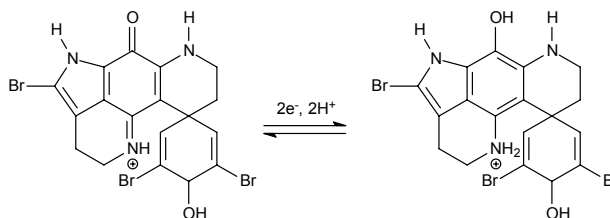


Figure 6.11 Proposed mechanism for the redox reaction of **1.52** at pH 5.5 and 7.5.

c) *Discorhabdin D / S type compounds*

Table 6.4 lists the electrochemical data obtained for the discorhabdin D type pyrroloiminoquinones. Generally, only one redox couple was observed, with the exception of **2.4**. Once again the ΔE and i_a / i_c data indicate that these compounds exhibit mainly reversible behaviour at pH 5.5, while at pH 7.5 the processes may be classified as quasi-reversible (due to the larger deviation in the i_a / i_c values). The ΔE values show that two electron reduction processes predominate at both pH 5.5 and 7.5. A proposed mechanism for **3.3** (similarly for the other discorhabdin C type compounds) at pH 5.5 is given in Figure 6.12.

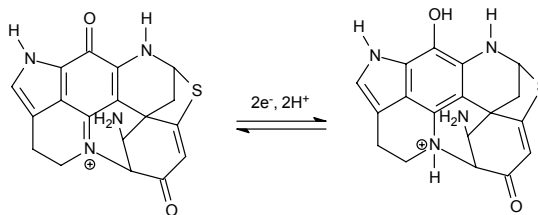


Figure 6.12 Proposed mechanism for the redox reaction of **3.3** at both pH 5.5 and 7.5.

The order in the ease of reduction of the discorhabdin D type compounds at pH 5.5 and 7.5 is as follows: **3.3** > **3.5** > **3.2** > **2.4** (Figure 6.6).

Table 6.4 Electrochemical CV data for discorhabdin D type pyrroloiminoquinones versus pH. Scan Rate: 25 mV/s.

Compound	E_a		$E_{1/2}$		ΔE		i_a / i_c	
	Couple I	Couple II	Couple I	Couple II	Couple I	Couple II	Couple I	Couple II
3.3								
pH 5.5:	-236	†	-253		-33		-0.91	
pH 7.5:	-284	-	-309	-	-49	-	-0.90	-
3.5								
pH 5.5:	-236	-	-257	-	-41	-	-0.99	-
pH 7.5:	-294	-	-316	-	-44	-	-0.78	-
3.2								
pH 5.5:	-238		-259		-41		-0.91	
pH 7.5:	-297		-320		-46		-0.79	
2.4								
pH 5.5:	-380	-267†	-398	-*	-36	-*	-1.19	-*
pH 7.5:	-449	-650†	-471	-*	-44	-*	-0.62	-*

*Note:

-*: No return wave

†: Reduced peak potential (*i.e.* E_a)

Compound **2.4** (with bromines at C-4 and C-14 and no thioether functionality) was found to be the most difficult to reduce of the discorhabdin D type compounds. Drawing on earlier observations this may be expected since the remaining discorhabdin D type compounds have a thioether and no halogenated groups, which should make them easier to reduce. Compound **1.51** which also has no thioether functionality, has three bromine groups and the increase in the $E_{1/2}$ value is therefore expected when compared to the sulfur containing discorhabdin D type compounds. Upon comparison of compound **2.4** and **1.53**, $E_{1/2}$ is less negative for the latter compound (*i.e.* **2.4** is more difficult to reduce), which may be due to the lack of a Δ^1 olefin or because of the presence of a strong electron withdrawing group at C-1, since electron donating groups are generally considered to make the reduction of a particular compound easier. Neither have a thioether functionality and both compounds have two bromine atoms albeit in different positions. In order to

assess the effect of a substituent at C-1 on the discorhabdin D types, the $E_{1/2}$ values of **3.2**, **3.3** and **3.5** were compared. Those compounds with primary amines (**3.3** and **3.5**) were recognised as being easier to reduce than those with secondary amines, regardless of the complexity of the substituent at C-1. Compound **3.5** with its carboxylic acid side-chain led to a slight increase in the $E_{1/2}$ value and was consequently found to be slightly harder to reduce. The extra ring formed through the formation of a N-18 to C-2 bond, does not seem to have an unfavourable influence on the $E_{1/2}$ values especially if an additional ring is also formed through a thioether functionality. Comparison of **1.57** with **3.2**, **3.3**, and **3.5** showed that the more complex systems were easier to reduce. Discorhabdin A has a Δ^1 olefin and a thioether which should increase the ease of reduction, but the presence of a single bromine group on position 2 may lead to an increase in $E_{1/2}$ and discorhabdin A is therefore more difficult to reduce. Finally, in order to evaluate the influence of the extra ring of discorhabdin D types on $E_{1/2}$, **3.3** was compared to **3.1**. These compounds have no bromine atoms, both have a ketone at position 3 and both contain sulfur. Compound **3.1** has a Δ^1 olefin while **3.3** has N-18 to C-2 bond and a substituent at position 1. Even though **3.3** lacks the Δ^1 olefin, it underwent reduction at the lowest potential in this group, which may be due to the extra ring or the strong electron withdrawing substituent at position 1.

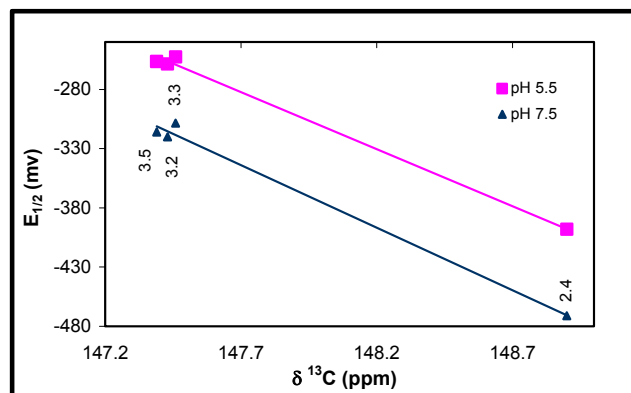


Figure 6.13 A plot of the C-19 ^{13}C NMR shifts for the discorhabdin D type pyrroloiminoquinones. Although the data points are few, this graph is intended to show the general trend for the tricyclic pyrroloiminoquinones (a), the discorhabdin D / S types (c) and the *bis*-pyrroloiminoquinone (d) classes in contrast to that obtained for the discorhabdin C types (b) (Figure 6.10).

At a higher pH, protons are generally more easily stripped from primary amines than secondary amines. However, the same ΔE values are observed for the secondary amine substituent (**3.2**) and **2.4**, indicating perhaps that the reduction processes observed are not taking place at the spiro ring. The discorhabdin D type compounds were therefore acknowledged as being far easier to reduce than most of the discorhabdin C type compounds e.g. **1.51**.

Figure 6.13 shows a plot of the ^{13}C NMR shifts for the C-19 carbon of the (c) class pyrroloiminoquinone skeleton. The opposite was found to be true for the discorhabdin D type compounds and a negative slope obtained was in this instance *i.e.* the relationship between the lower electron density at carbon 19 and an increase in reduction potential was observed *i.e.* the more deshielded the carbon (*e.g.* **2.4**) the harder it was to reduce. Once again, the plot shows better correlations at a lower pH, most likely due to solubility.

d) *Bis-pyrroloiminoquinones*

The data obtained for the *bis-pyrroloiminoquinone* compounds is presented in Table 6.5.

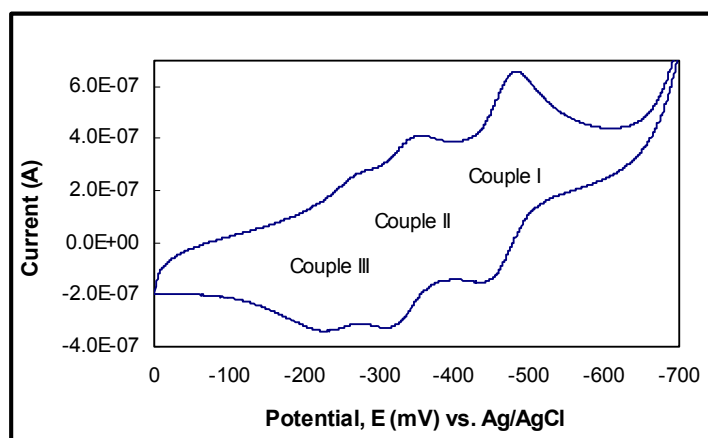


Figure 6.14 Cyclic voltammogram of **1.72**. Scan rate: 25 mV/s.

The potentials of the redox couples for the *bis-pyrroloiminoquinones* range from -349 to -567 mV for Couple I, from -310 to -414 mV for Couple II and -224 mV for Couple III at pH 5.5. The peak potentials become increasingly negative with an increase in pH. The ΔE values were found to be too large for a reversible system and the i_a / i_c data was generally found to deviate from unity. The results indicate that these compounds exhibit mainly quasi-reversible to irreversible behaviour at both pHs. Slow electron transfer, or irreversible structural change, between the compound of interest and the working electrode is often to blame for an observation deemed irreversible. Hydrogen bonding may also be responsible for inefficient or slow electron transfer.¹¹⁷ The cyclic voltammogram obtained for **1.72**, shown in Figure 6.14, is the most complex of the pyrroloiminoquinones. The cyclic voltammogram shows two reversible systems of approximately the same height, and therefore the same number of electrons are transferred, while the demethylated compound **1.71** shows only two reduction couples, implicating the involvement of the N-13 methyl group. The increasingly negative peak potentials of the N-18 oximes (**4.1** and **4.2**) make these pyrroloiminoquinones the most difficult to reduce and perhaps the ionic character of the N^+-OH bond could be responsible for the additional increase in peak reduction potential and stability. A plot of the C-19 ^{13}C NMR shifts revealed that the electron density at C-19 is far

less relevant for the *bis*-pyrroloiminoquinone compounds than for the discorhabdin type compounds.

The ease of reduction at pH 5.5 was observed as follows: **1.72** > **1.71** > **4.1** > **4.2**, while at pH 7.5 the sequence obtained was: **1.71** > **1.72** > **4.1** > **4.2** (Figure 6.6, Table 6.5).

Table 6.5 Potential assignments (CV) of the *bis*-pyrroloiminoquinones *versus* pH. Scan Rate: 25 mV/s.

Compound	E _a			E _{1/2}			ΔE			i _a / i _c		
	Couple			Couple			Couple			Couple		
	I	II	III	I	II	III	I	II	III	I	II	III
1.72												
pH 5.5:	-349	-310	-224	-395	-396	-248	92	172	48	1.25	0.69	1.25
pH 7.5:	-505	-414	-297	-531	-425	-318	52	22	43	0.85	0.58	0.06
1.71												
pH 5.5:	-417	-310	-	-438	-333	-	41	46	-	1.33	0.75	-
pH 7.5:	-425	-	-	-478	-	-	105	-	-	0.001	-	-
4.1												
pH 5.5:	-508	-	-	-525	-	-	33	-	-	0.48	-	-
pH 7.5:	-620	-	-	-637	-	-	33	-	-	0.38	-	-
4.2												
pH 5.5:	-567 [†]	-	-	-*	-	-	-*	-	-	-*	-	-
pH 7.5:	-690	-	-	-669	-	-	42	-	-	0.65	-	-

*Note:

-*: No return wave

†: Reduced peak potential (*i.e.* E_a)

The electron donating group of **1.72** led to a decrease in E_{1/2} at pH 5.5, while the opposite is true for pH 7.5. The presence of an N-oxime at N-18 signified a large increase in the reduction potential for these compounds, implicating the iminoquinone moiety in the reduction processes. The strong electron withdrawing group or the ionic character of the bond present on N-18, may be responsible for the E_{1/2} observed.

A large difference in the E_{1/2} values was also realised upon comparison of **1.71** and **3.1**. The compounds possess the same number of carbons and both are not halogenated. Compound **3.1** differs in that it has sulfur, a spiro ring and is comparatively less conjugated. **1.71**, on the other hand, has a hydroxyl group at position 3. Compound **1.71** was found to be far harder to reduce and this may be due to the absence of the sulfur group or the lack of a spiro ring. This is unexpected since sulfur, with its electron rich nature, is expected to lead to a decrease in ease of reduction. Comparison of compounds **1.71** and **1.53**, both of which lack a thioether and have a hydroxyl group at position 3 and where the latter is brominated at positions 2 and 4 and is less conjugated, showed that **1.71** is far more difficult to reduce than **1.53**. Again, the lack of a spiro ring and electron withdrawing groups on positions 2 and 4 (where bromine is, in fact, expected to

lead to an ease in reduction due to its electron withdrawing nature) may account for the variation. These observations may therefore indicate that the site of the reduction process is not likely to be taking place at the spiro ring, but rather on the 'left hand side' of the molecule, *i.e.* the iminoquinone portion.

A proposed mechanism for the observed reduction-oxidation process is given below in Figure 6.15.

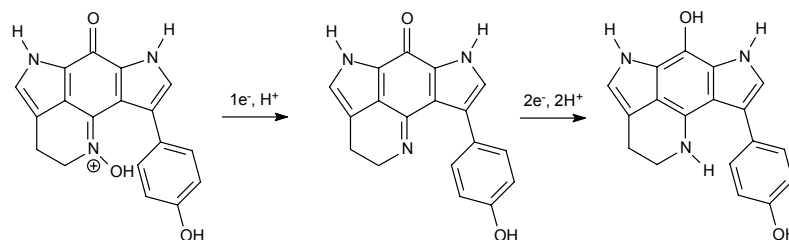


Figure 6.15 Proposed mechanism for the redox reaction of 4.1.

6.3.2 Stability study

Upon variation of the sweep rates, electroactive intermediates of widely varying stabilities may be observed and, in order to determine whether a diffusion-controlled process is the dominant mechanism at the electrode surface, the peak current (i_a) versus the square root of the scan rate is monitored (Table 6.6 and Figure 6.16).

Figure 6.16 shows a sample plot of the variation of the catalytic currents with an increase in square root of the scan rate, for scan rates ranging from 25 to 800 mV/s, confirming the diffusion-controlled movement of the species to the electrode at these scan rates during the reduction of the pyrroloiminoquinones. The linear plots obtained for most of the pyrroloiminoquinones (Table 6.6) indicate that a diffusion-controlled process prevails with the exception of, as shown by the R^2 values, **1.52** and **2.2**, both at pH 7.5. The dynamics involved could include the lower solubility of the compounds at the higher pH, adsorption onto the electrode surface between scans, or slow electron transfer between the compound and the electrode surface. The i_a / i_c values obtained (Table 6.3) were also observed to be quite low for these two compounds at pH 7.5.

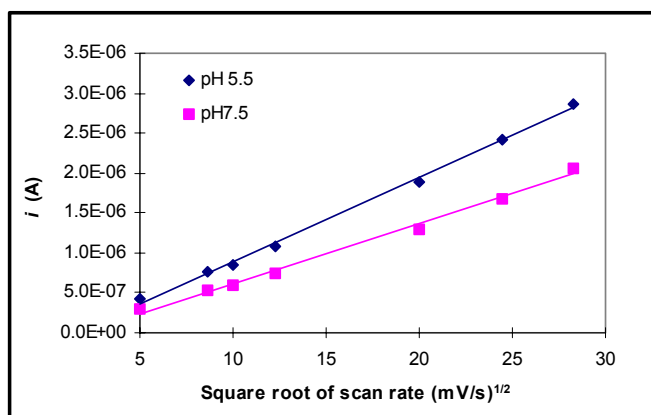


Figure 6.16 Plot of i_a versus the square root of the scan rate for **3.2**.

Table 6.6 Data (rate constants and R^2 values) obtained for the plot of peak current (i_a) versus square root of the scan rate at pH 5.5 and 7.5.

Compound	pH 5.5		pH 7.5	
	Rate constant / (mV/s) ^{1/2}	R ²	Rate constant / (mV/s) ^{1/2}	R ²
1.52	-1.986 × 10 ⁻⁷	0.994	-1.086 × 10 ⁻⁷	0.875
2.2	-1.647 × 10 ⁻⁷	0.987	-7.588 × 10 ⁻⁸	0.868
1.51	-1.947 × 10 ⁻⁷	0.995	-6.482 × 10 ⁻⁸	0.987
1.53	-2.779 × 10 ⁻⁷	0.946	-1.970 × 10 ⁻⁷	0.995
1.33	-5.600 × 10 ⁻⁷	0.999	-4.736 × 10 ⁻⁷	0.974
3.2	-1.055 × 10 ⁻⁷	0.997	-7.544 × 10 ⁻⁸	0.994
3.3	-1.341 × 10 ⁻⁷	0.998	-1.102 × 10 ⁻⁷	0.999
1.20	-2.907 × 10 ⁻⁷	0.986	-2.695 × 10 ⁻⁷	0.989
3.5	-1.656 × 10 ⁻⁷	0.991	-1.013 × 10 ⁻⁷	0.991
3.1	-1.667 × 10 ⁻⁷	0.999	-8.177 × 10 ⁻⁸	0.999
1.71	-1.448 × 10 ⁻⁷	0.993	-1.444 × 10 ⁻⁷	0.991
1.72	-6.991 × 10 ⁻⁸	0.998	-9.261 × 10 ⁻⁸	0.982
4.1	-9.745 × 10 ⁻⁸	0.997	-1.276 × 10 ⁻⁷	0.988
4.2	1.657 × 10 ⁻⁸	0.967	8.224 × 10 ⁻⁸	0.996
2.4	-9.287 × 10 ⁻⁸	0.918	-8.271 × 10 ⁻⁸	0.999
1.57	-3.543 × 10 ⁻⁷	0.905	-5.902 × 10 ⁻⁸	0.930

Comparison of the simpler pyrroloiminoquinones indicated that the oxidised compound (**1.20**) showed a decrease in rate (Figure 6.17 and Table 6.6) when compared to **1.33** which has a primary amine. On the whole, the more complex systems showed lower rate constants, while **1.33** underwent the fastest process.

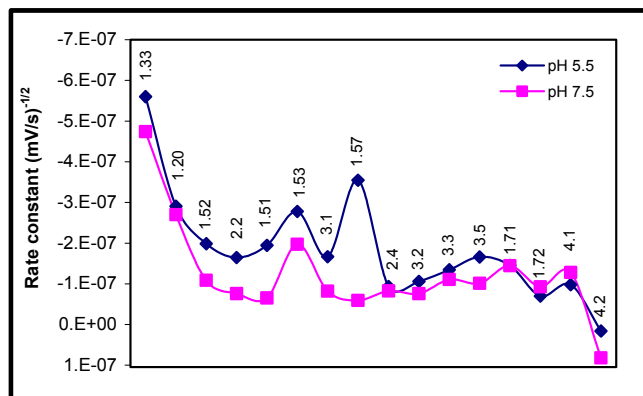


Figure 6.17 Comparison of the rate constants obtained for the pyrroloamino-*ortho*-quinones, pyrroloiminoquinones and *bis*-pyrroloiminoquinones.

An increase in conjugation was found to lead to a decrease in the rate constants obtained. This was observed upon comparison of **1.52** and **2.2**. Oxidation of **1.52** at C-3 (**1.51**) was found to lead to a slight decrease in rate, which may indicate that perhaps reduction is not taking place at C-3 (drawn from the comparisons between **1.51** and **1.52** as well as **1.53** and **1.57**). An increase in rate, upon sulfuration and reduction or elimination in the number bromine groups present (upon comparison of **1.53** and **3.1**, **1.52** and **1.53**, as well as **1.53** and **1.57**) was observed. Discorhabdin A, with its bromine at C-2 and the lack of a Δ^4 olefin, has a higher rate constant than **3.1**, perhaps due to a decrease in conjugation.

Compound **2.4** was found to have the slowest rate among the discorhabdin D types. A substantial decrease in rate, due either to the formation of N-18 to C-2 bond (extra ring), substitution at C-1 or the lack of $\Delta^{1,2}$, is observed upon comparison of **1.53** and **2.4**. An increase in conjugation has, however, previously been found to lead to a decrease in rate. Upon comparison of **3.3** with **3.1** substitution at C-1, the lack of a Δ^1 olefin, or the presence of an extra ring were found to decrease the rate constants. Of the discorhabdin D type compounds, all of which have a substituent at position 1, those with primary amines at C-1 were faster than **3.2** (which has a secondary amine). The presence of the more complex side-chain (as found in **3.5**) led to a slight increase in rate when compared to a simple amino group (**3.3**). A thioether functionality was found to lead to an increase in rate upon comparison of **2.4** with **3.2**, **3.3** as well as **3.5**. Compounds **3.2** and **2.4** with their less acidic substituents, may account for the slower rates.

The occurrence of an electron donating group on N-13 of the *bis*-pyrroloiminoquinone skeleton, led to a decrease in rate, while the presence of an electron withdrawing group on N-18 also led to a decrease. A decrease in rate, perhaps due to the lack of a spiro ring or a thioether was also observed upon comparison of **1.71** with **3.1**. Overall, lower rate constants were observed at pH 7.5 except for the N-18 oximes.

6.4 Conclusion

The electrochemical behaviour of sixteen pyrroloiminoquinones was studied using cyclic voltammetry and square wave voltammetry. All compounds had negative reduction potentials within biologically relevant ranges and the pH-varied experiments demonstrated that the reduction potentials are pH dependent. Generally, it was found that the reduction potentials increased with an increase in pH for all compounds, that the moles of electrons transferred were dependent on the pH, and that the rates increased with a decrease in pH, except for the N-18 oximes. The following list is drawn from observation:

Lower reduction potentials were observed with:

- a) increased conjugation,
- b) oxidation at C-3 (slight increase in the ease of reduction)
- c) the introduction of a primary amine at C-10
- d) the introduction of a sulfur group, which should in fact lead to a higher reduction potential
- e) the introduction of an extra rings through the formation of the N-18 to C-2 bond or through a thioether
- f) the introduction of electron withdrawing groups at position 1

Higher reduction potentials were observed upon:

- a) oxidation at C-10
- b) removal of bromine at C-14
- c) the introduction of bromines at position 2 and 4, which is unexpected
- d) substitution at N-18 with a strong electron withdrawing group
- e) removal or replacement of the spiro ring, which may or may not be associated with the reduction process

A discorhabdin D type skeleton was found to render the compounds more susceptible to reductive activation. The number of bromine atoms was unexpectedly observed to lead to increasingly negative reduction potentials for some compounds (discorhabdin C types) and, since most of the bromines are located on the spiro ring (with only one bromine ever present on the pyrrole ring), it is likely therefore that the reduction is taking place at the iminoquinone moiety. The pyrrole bromine atoms may, however, affect the ease of reduction. The *bis*-pyrroloiminoquinones and the N-18 oximes in particular, were found to have largely negative reduction peak potentials. In a study of the quinoxaline di-N-oxides, it was found that as the electron withdrawing nature of the substituents increased, the potential for the first reduction became less negative and the compound more easily reduced.¹²¹ This is in contrast to what has been observed with some of the pyrroloiminoquinones. Bromine is known to be strongly electron withdrawing and should therefore be expected to lead to an increase in the ease of reduction. This was observed and expected with

compounds **1.53** and **1.52** (where **1.52** has three bromine atoms while **1.53** has two), but upon comparison of **3.1** and **1.57** (where **1.57** has a bromine group), the opposite was true. This may, however be accounted for if the site of the reduction process is far removed from the spiro ring, *i.e.* if the reduction process is taking place rather at the iminoquinone moiety. A plot of the $E_{1/2}$ values *versus* C-19 ^{13}C NMR shifts showed negative slopes for all of the pyrroloiminoquinone classes except for the discorhabdin C type pyrroloiminoquinones. Thus the more deshielded the carbon at position 19, the easier the compound was to reduce, except for the discorhabdin C types. This may, however, suggest that either an alternate mechanism is in operation for the C type pyrroloiminoquinones or that the reduction process is taking place only at the iminoquinone moiety. Further evidence could be provided by the fact that a sulfur group is expected to lead to a decrease in the ease of reduction of these compounds, where more often than not, the opposite was true, *e.g.* the discorhabdin D / S type compounds, discorhabdin A, etc.

A decrease in the rate was recognised upon oxidation, an increase in conjugation and the elimination of all bromines from the pyrroloiminoquinone skeleton. An increase in rate constant was observed upon removal of the C-14-Br and sulfuration. Thus, with a decrease in pH, the rates and ease of reduction of the pyrroloiminoquinones were therefore increased.

As expected, greater deviation from $i_a / i_c = 1$ (36 % within the range of 0.9 and 1.1) was found for experiments conducted at pH 7.5 which may be due to the lower solubility of these compounds at the higher pH. The pyrroloiminoquinones were found to have greater stability at pH 5.5 (64 % within the same range) except for the *bis*-pyrroloiminoquinones and their N-18 oximes. No relationship was found between i_a / i_c and rate *e.g.* compound **1.33** has a high rate and i_a / i_c , while the opposite is true for **1.71** (which has low unity, and therefore stability, and a low rate constant. ΔE and i_a / i_c values indicated that most of the reactions taking place, with a few exceptions (*i.e.* the *bis*-pyrroloiminoquinone types), were reversible at pH 5.5 and quasi-reversible at pH 7.5 and that no relationship existed between i_a / i_c and ΔE .

In conclusion, in addition to the possibility of $^1\text{O}_2$ and radical-mediated DNA strand damage, these observations may provide an additional mechanism for cell destruction *i.e.* electron transfer mechanisms, especially the one electron reduction mechanisms, may also be at play. The data obtained by Monge *et al.*¹²¹ for anthraquinone ($\Delta E = 80$ mV, $i_{pa} / i_{pc} \approx 1$), was found to be consistent with a reversible one electron reduction to its semiquinone (in DMF, using a platinum working electrode and measured against a standard calomel electrode (SCE)).¹²¹ Examples of the types of compounds containing an anthraquinone nucleus includes the anthracyclines, where the nucleus is attached to an amino sugar, which are used as broad-spectrum antineoplastic drugs. Because these drugs contain a quinone-hydroquinone functionality, they participate in biological oxidation-reduction reactions and are able to chelate divalent cations such as Ca^{2+} and Fe^{2+} and this leads to a lower cardiac toxicity. More importantly, just like the pyrroloiminoquinones, they are able to intercalate between the base pairs in a DNA double helix. Anthracyclines such as

doxorubicin are also known to cause single stranded DNA breaks and impair DNA repair. Results of *in vitro* studies have confirmed that doxorubicin radicals participate in oxygen mediated single strand breakage, which is, unfortunately also the cause of their high cardiac toxicity.¹²⁴

Since quinones have been observed to produce semiquinones^{30, 116, 121, 124} it may be assumed, for those pyrroloiminoquinones that undergo a one electron reduction at least, that they are, in fact, also producing semiquinone radicals. The compounds that were observed to produce radicals upon photosensitisation (discorhabdin A and the tsitsikammamine N-18 oximes) were resolved to undergo two electron reduction processes. These compounds are, however, still likely to produce a semiquinone radical, since they also possess the quinone moiety. In the case of the N-18 oximes, this may be accounted for by the simultaneous production of a radical on N-18 and as well as the semiquinone. Because of the inherent highly negative peak potentials displayed by **4.1** and **4.2** at pH 5.5 and, especially, biological pH, and because these N-18 oximes have been shown to produce radicals (Chapter 5), these compounds could show some, perhaps even selective, toxicity towards hypoxia tumour cells, albeit at perhaps a slightly lower toxicity level; since the two electron reduced mono-N-oxide (**6.5**) has been shown by Daniels and Gates¹²⁵ (Scheme 6.1) to have a weaker reduction-dependent DNA cleavage activity. The authors¹²⁵ did, however, state that the poor cleavage by the mono-N-oxide (**6.5**) could be due to the fact that the enzyme system employed in the study was not effectively reducing the compound and that the compound is likely to produce hydroxyl radicals in a similar approach to that outlined in Scheme 6.1. An investigation of the type of radicals produced and the mechanism of toxicity of the highly cytotoxic discorhabdin A, however, remains an intriguing experimental opportunity.

Chapter 7: Bioactivity

7.1 Human colon tumour (HCT-116), Oesophageal (WHC01) and ovarian (ME180) cytotoxicity assays

HCT-116 has often been used as an initial screen for evaluating the cytotoxicity of pyrroloamino-*ortho*-quinone and pyrroloiminoquinone natural products, e.g. the makaluvamines.^{30,70} It was therefore an ideal cell line model for studying our suite of compounds since it provided a basis from which to compare the cytotoxicity of pyrroloamino-*ortho*-quinone and the pyrroloiminoquinone metabolites.

In addition to the HCT-116 cell line model used to test twenty four of our compounds, the cytotoxicity of two pyrroloiminoquinones, i.e. discorhabdin A and tsitsikammamine B, towards oesophageal (WHC01) and cervical (ME180) cancer cell lines was also studied. Black populations in certain regions of Southern Africa and the central and eastern seaboard of Africa experience an abnormally high incidence of oesophageal cancer.¹³¹ The high incidence of this disease is associated with a range of environmental factors including smoking, woodsmoke, alcohol, the inadvertent consumption of carcinogenic mycotoxins produced by the *Fusarium* fungus that thrives on grain stored under damp conditions and a diet poor in fresh fruit and vegetables.¹³¹ The identification of novel agents with significant cytotoxic activity against oesophageal cancer cells would substantially enhance our ability to treat this debilitating disease in Africa.

The HCT-116 cytotoxicity assays were performed by Catherine Sincich (Scripps Institution of Oceanography) and the oesophageal and cervical cancer screens by Catherine Arendse (Department of Medical Biochemistry, University of Cape Town). Details of the protocols used are provided in Chapter 8 (Section 8.7).

The results of the HCT-116 cytotoxicity screening of twenty four pyrroloamino-*ortho*-quinones and the pyrroloiminoquinones isolated from four species of Latrunculid sponge are presented in Table 7.1. Discorhabdin A (**1.57**) displayed the highest toxicity at 0.007 μ M, followed by the free base of discorhabdin A (**1.57 FB**), **1.51**, **3.3**, **2.1**, **2.2**, **3.4**, **1.53**, **3.5**. Curiously, three discorhabdin D type compounds (**3.3**, **3.4** and **3.5**) displayed relatively high toxicities, which is unexpected based on Blunt *et al.*'s observation that discorhabdin D (**1.61**) had a much lower *in vitro* cytotoxicity than its *in vivo* toxicity.³⁶ It would therefore be interesting to obtain the *in vivo* activity of these three compounds. The presence of a Δ^7 olefin also appeared to improve the cytotoxicity of the discorhabdins as observed with **2.1** and **2.2** compared to **1.52** and **1.53** respectively. The presence of a tetrahydrothiophene bridge also appeared to be important (e.g. **3.1**). In accordance with the literature available,^{30,70} the importance of a pyrroloiminoquinone core as a prerequisite for cytotoxicity was also demonstrated upon comparison of the IC₅₀ values obtained for

makaluvamine C (**1.33**) with those of damirone B (**1.20**) and makaluvic acid A (**1.47**). The fact that discorhabdin A is present in vast quantities in the shallow water *Strongyloidesma* sp. sponge and that it has such potent activity together with its ability to produce free radicals in the presence of light (Chapter 5) may be significant in terms of the organism's defence mechanisms. The inactivity of the tsitsikammamine A and B N-18 oximes in the HCT-116 assay was also of interest.

Table 7.1 Human colon tumour (HCT-116) cytotoxicity data for the pyrroloamino-*ortho*-quinone, pyrroloiminoquinone and *bis*-pyrroloiminoquinone metabolites.

Compound	HCT-116 (IC ₅₀ μM)	Compound	HCT-116 (IC ₅₀ μM)
1.20	3.102	2.2	0.222
1.33	1.089	2.3	1.266
1.47	28.399	2.4	12.496
1.51	0.077	2.5	0.298
1.52	0.645	2.6	1.655
1.53	0.323	3.1	0.327
1.57	0.007	3.2	2.249
1.57 FB*	0.058	3.3	0.119
1.61	0.595	3.4	0.232
1.71	1.414	3.5	0.355
1.72	2.382	4.1	128.213
2.1	0.197	4.2	16.541

* FB = free base

The 'cut-off' established by Bristol-Myers for determining if a compound is worth pursuing as a clinical drug are those with IC₅₀ values below 3 μM.¹³² With three quarters of the compounds tested exhibiting possibly exploitable cytotoxic activity, the question of selectivity still remains (See Table 7.2).

Tsitsikammamine B (**1.72**) and discorhabdin A (**1.57**) both showed strong activity¹³³ (Table 7.2) against oesophageal (WHC01) and cervical (ME180) cancer cell lines. The non-selectivity of discorhabdin A and tsitsikammamine B for cancer cells is clearly shown by the toxicity of these compounds to normal cells *viz* breast epithelial (MCF12F) and fibroblasts (DMB).

Table 7.2 Oesophageal (WHC01) and ovarian (ME180) cancer inhibition of discorhabdin A and tsitsikammamine B.

Compound	WHC01 (IC ₅₀ μM)	ME180 (IC ₅₀ μM)	MCF12F (IC ₅₀ μM)	DMB (IC ₅₀ μM)
1.57	0.0168	0.0205	0.0216	0.0284
1.72	2.8918	-	-	5.0786

7.2 Topoisomerase I activity

Prior to DNA replication, the supercoiled DNA must be relaxed (untwisted). The topoisomerase I enzyme relieves the torsional strain in supercoiled DNA by binding to the DNA molecule, cleaving one strand and at the same time inducing a covalent bond between the released phosphodiester bond and a tyrosine residue in the enzyme to form a phosphotyrosine bond. The unbroken DNA strand then passes through this single strand break and the single strand break is subsequently resealed. Type I topoisomerase enzymes are therefore important in the transcription and repair of damaged DNA and are thought to be positioned just ahead of the DNA replication fork (Figure 7.1).¹³⁴

During the initial stage of replication, the two DNA strands are prepared for this process and a number of proteins are also involved. As illustrated in Figure 7.1, a helicase is required for the unwinding of the DNA at the replication fork. DNA binding protein molecules, which fix themselves to the two DNA strands, stabilise the unwound DNA. The function of these proteins is to open a region on the DNA strand that will allow an enzyme to begin the synthesis of an RNA primer. This is followed by chain elongation, a process catalysed by a DNA polymerase III holoenzyme. The completion of the transcription of a DNA strand follows the removal of the RNA primers by the DNA polymerase I enzyme and the establishment of a phosphodiester bond between the two strands which is catalysed by the DNA ligase enzyme.¹³⁵

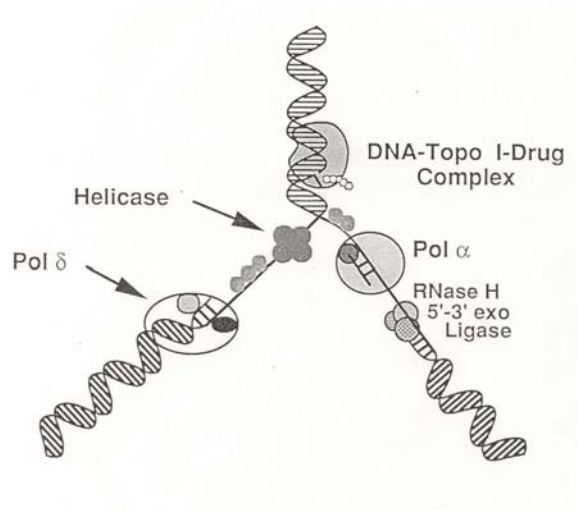
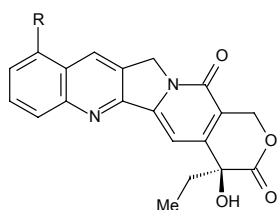
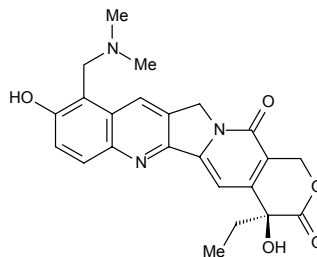
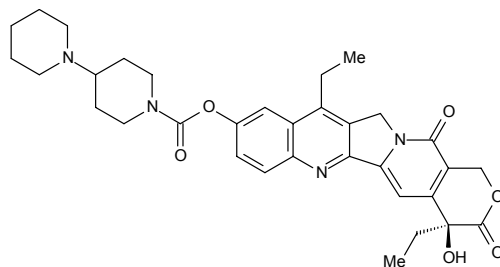


Figure 7.1 DNA topoisomerase I – a unique target for anti-tumour drugs (reproduced with permission from Dr. Brad Carte).

Camptothecin (**7.1**), one of the few natural products displaying significant topoisomerase I inhibition, was isolated from the Chinese ornamental tree *Camptotheca acuminata*.¹³⁶ Camptothecin is thought to stabilise the crucial step of the topoisomerase I catalysis when the enzyme induces a single strand break in the DNA and is covalently bound to the DNA molecule

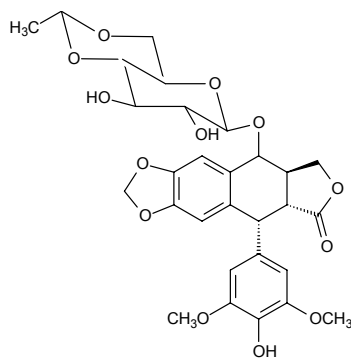
(Figure 7.1).⁹¹ The camptothecin – topoisomerase I – DNA complex is therefore stabilised, preventing the passage of the helicases and other replication enzymes down the DNA strand. Although **7.1** was in clinical trials in the 1970's, the severe bladder toxicity exhibited by camptothecin precluded its use as an anticancer agent, and this in turn led to the development of camptothecin analogues topotecan (**7.2**, Hycamptin[®]), irinotecan (**7.3** Camptosar[®]), 9-amino- (**7.4**) and 9-nitro-camptothecin (**7.5**). The latter two compounds are awaiting approval, while the former two agents have been approved for use in the USA.²

**7.1** R = H**7.4** R = NH₂**7.5** R = NO₂**7.2****7.3**

Like camptothecin (**7.1**), wakayin (**1.73**) was found by Kokoshka *et al.*⁹¹ to inhibit topoisomerase I catalysed relaxation of DNA, and both camptothecin and wakayin were found to enhance the cleavage at DNA sites normally attributed to topoisomerase I attack. However, unlike camptothecin, wakayin was also found to be a strong intercalator (K_s 20 μ M, for the displacement of 50 % EtBr (5 μ M) from DNA (25 μ g/mL)), suggesting a different cleavage complex nature.⁹¹

Topoisomerase II enzymes are ATP dependent and are able to cleave both strands of a DNA molecule, subsequently allowing another portion of the DNA molecule to pass through this cut. These enzymes thus catalyse the linking (catenation) and unlinking (decatenation) of two different DNA molecules. The conformational changes induced by these processes causes topological changes which are vital to the cellular functions such as replication, transcription and chromosomal segregation.^{134,137} The importance of the topoisomerase II enzyme thus becomes an obvious target for a wide variety of anticancer drugs in which the interruption of the enzyme's function would inevitably lead to cell death. Examples of such anticancer agents include the epipodophyllotoxins, such as etoposide (**7.6**) and teniposide. These drugs are thought to block

the catalytic activity of DNA topoisomerase II by stabilising an enzyme-DNA complex in which the DNA is subsequently cleaved and covalently linked to the enzyme.^{134,137}



7.6

In a paper describing the cytotoxicity of the pyrroloiminoquinones, the makaluvamines, Barrows *et al.*⁷⁰ demonstrated the ability of makaluvamines to act through inhibition of topoisomerase II, in contrast to the topoisomerase I inhibitory properties of the apparently structurally related wakayin. The makaluvamines showed enhanced activity towards topoisomerase II cleavable complex-sensitive cell lines (Chinese hamster ovarian (CHO) cell line, xrs-6, where positive control drugs include bleomycin and etoposide (**7.6**) and negative controls such as camptothecin (**7.1**) and melphalan) were used). Makaluvamine C (**1.33**) was shown to produce protein linked DNA double strand breaks while makaluvamine A (**1.31**) induced double strand breaks in a neutral filter elution assay in a manner similar to the standard amsacrine (*m*-AMSA). Makaluvone and damirone B displayed insignificant toxicity and, interestingly, while discorhabdin A did show some toxicity in the CHO cell line model, **1.57** did not show enhanced activity toward the DNA mutant repair cell line xrs-6.⁷⁰ The details of the topoisomerase I inhibition assays performed by Katherine Marshall at the University of Utah are presented in Chapter 8 (Section 8.7).

An example of the type of data obtained from a topoisomerase inhibition assay is given in Figure 7.2. The activities of tsitsikammamines A and B and their respective N-18 oximes were compared with 9-amino-camptothecin (**7.1**) in the topoisomerase I inhibition assay. Neither the tsitsikammamines nor their N-18 oxime analogues showed any activity in the topoisomerase II inhibition assays.¹³⁸

Figure 7.2 shows an agarose containing gel and topoisomerase I – cleaved DNA. DNA can be seen to migrate from top to bottom of the gel in three bands. The top band is nicked (n) circular DNA. The next band down is supercoiled (sc) DNA and the fastest migrating band is relaxed but intact circular DNA (at the bottom of the lanes except for lanes 4 and 5 in a)). In the assay, the percent of DNA cleavage varied greatly amongst the *bis*-pyrroloiminoquinones from a high of 59 % for tsitsikammamine A at 500 μ M to rather low levels for tsitsikammamine B N-18 oxime. Although the *bis*-pyrroloiminoquinones did display some topoisomerase I inhibition from

comparison with the activity displayed by 9-amino-camptothecin (**7.4**, 87 % cleavage at a concentration of 9 μM), the activity of the tsitsikammamines is lower by a factor of approximately 100.

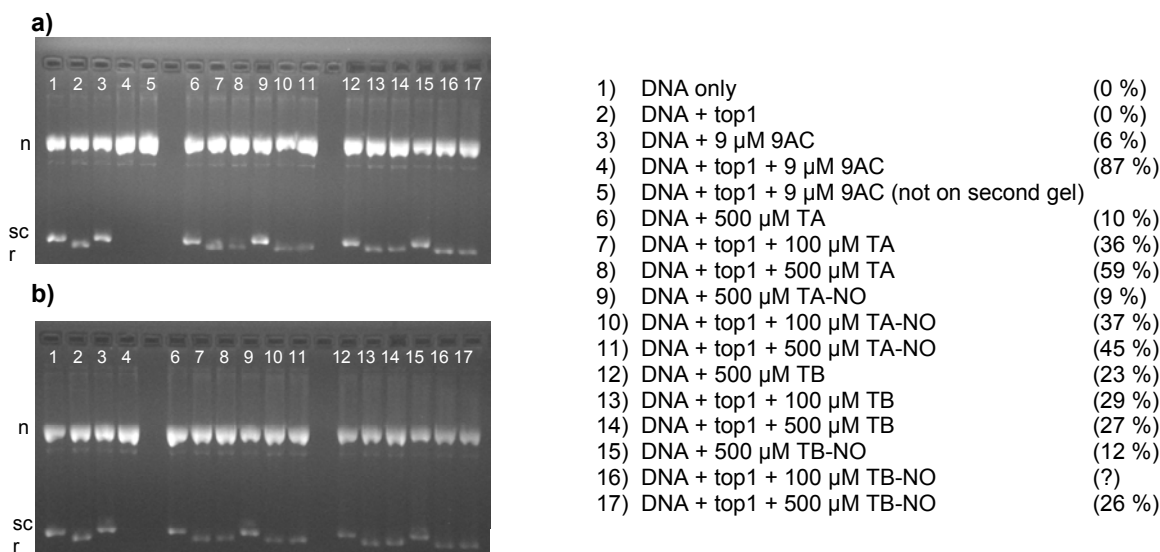


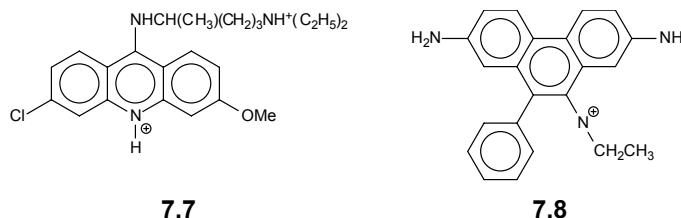
Figure 7.2 DNA cleavage assayed by agarose gel electrophoresis. Electrophoresis was carried out in the presence of 9-amino-camptothecin (**7.4**). (Reproduced with permission from Katherine Marshall, University of Utah, USA.).¹³⁸ (r = relaxed, sc = supercoiled, n = nicked, top1 = topoisomerase I, 9AC = 9-amino-camptothecin, TA = tsitsikammamine A, TA-NO = tsitsikammamine A N-18 oxime, TB = tsitsikammamine B, TB-NO = tsitsikammamine B N-18 oxime).

Lane 1, substrate DNA only. Lane 2, a reaction of substrate and DNA topoisomerase I. Lanes 3 and 4, reaction of DNA substrate and 9-AC without (lane 3) and with (lane 4) topoisomerase I. Lanes 6, 8, 9 and 11 reaction of DNA substrate with 500 μM TA and TA-NO without (lanes 6 and 9) and with (lanes 8 and 11) topoisomerase I. Lanes 7 and 10 DNA substrate with topoisomerase I and 100 μM TA and TA-NO respectively. Similarly, lanes 12, 14, 15 and 17 reaction of DNA substrate with 500 μM TB and TB-NO without (lanes 12 and 15) and with (lanes 14 and 17 respectively) topoisomerase I. Lanes 13 and 16 reaction of DNA substrate with 100 μM TA and TA-NO, respectively, with topoisomerase I.

7.3 Intercalation studies

Intercalation is the process whereby compounds which possess a planar aromatic ring system may be inserted between base pairs of DNA. This interaction leads to inhibition of DNA and or RNA polymerase reactions, causing metabolic changes and cell death.^{124,139} There is evidence that many of the known intercalating compounds, such as quinacrine (**7.7**) and ethidium (**7.8**), which also have activity against microbial organisms and neoplastic cells, exert their effect through a binding process of this type with DNA.¹³⁹

Factors not related to intercalation, such as transport through membranes and the metabolic transformation of drugs, also influence the activity of a potential drug. Intercalation and medicinal activity are influenced by factors such as binding constants, kinetics, and structural effects and activity. Specific drugs that have been found to bind to DNA by intercalation include the antimalarial drugs and antitumour drugs.¹³⁹



DNA intercalators typically cause viscosity increases in low-molecular weight sonicated DNA, unwinding of superhelical DNA, *i.e.* a characteristic 3.4 Å length increase for sonicated DNA, as well as an unwinding angle similar to that of the standard intercalator example ethidium (**7.8**), which has an arbitrarily assigned unwinding angle of 26°. ¹³⁹ NMR spectroscopy as well as X-ray crystallographic data can also be used to confirm the binding mode of potential intercalators. When compounds intercalate into DNA, the planar ring structure is inserted approximately perpendicularly to the long axis of the DNA double helix.^{124,139}

The ability of a compound to displace ethidium bromide (EtBr) from DNA is generally used as a measure of DNA intercalation. The flat planar pyrroloiminoquinone core of the tsitsikammamines implied that these compounds could be capable of intercalating into DNA. An EtBr displacement assay confirmed this activity. Figure 7.3 presents the results of the ethidium bromide displacement assay for the tsitsikammamines and their respective N-18 oximes. The tsitsikammamines together with their N-18 oximes were thus found to intercalate DNA.¹³⁸

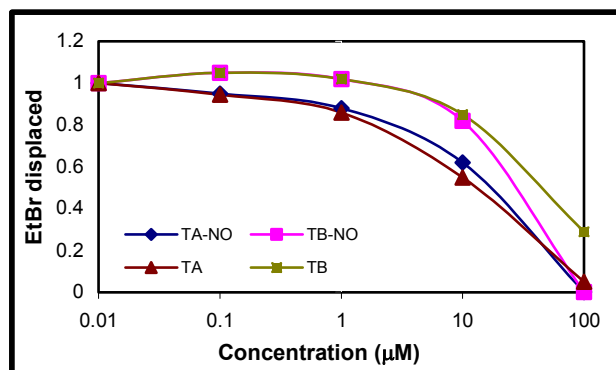


Figure 7.3 Results obtained for the ethidium bromide displacement assay for the tsitsikammamines and their respective oximes (reproduced with permission from Katherine Marshall, University of Utah).¹³⁸ EtBr displacement was determined by

subtracting the amount of background EtBr fluorescence from all samples and then dividing by the amount of fluorescence in the DNA and EtBr control. 0 is complete displacement, >1 no displacement.

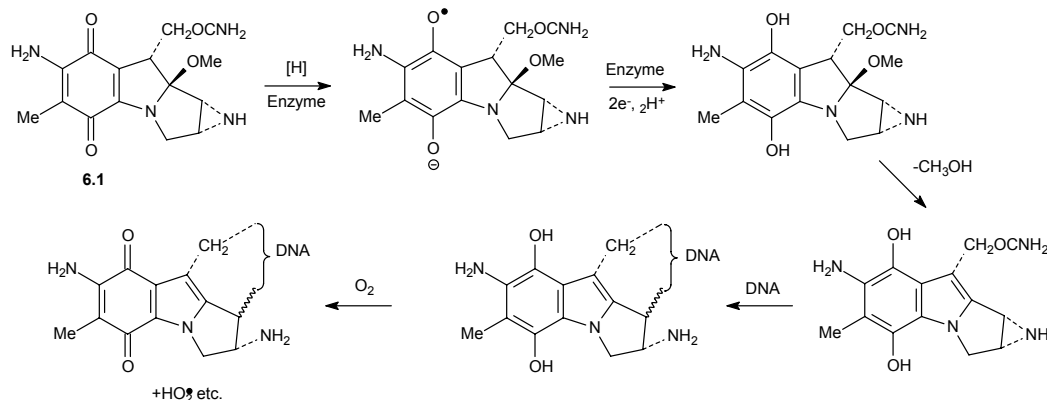
Wakayin was found to be a strong intercalator with a K_s value of 20 μM for displacement of 50 % EtBr (5 μM) from DNA (25 $\mu\text{g/mL}$).⁹¹ It appears that the tsitsikammamines and their respective N-18 oximes were found to be strong intercalators with **1.71** and its N-18 oxime **4.1** having the stronger activity ($K_s \sim 10 \mu\text{M}$ for both **1.71** and **4.1**). Interestingly discorhabdin A is regarded as a poor intercalator (K_s 89 μM).⁷⁰

7.4 Bioreductive activation as a basis for selective cytotoxicity?

Since the existence of certain processes in biological systems are known to have an electrochemical foundation, electrochemistry has often been used to describe and understand these processes.¹²⁰ Lin *et al.*¹⁴⁰ suggested in 1972 that the reductive reactions of hypoxic cells (oxygen deficient) outside of the vascular supply of a tumour mass could be more likely than that for the normal well-oxygenated equivalent.¹⁴⁰ Experiments conducted previously on anaerobic cultures of microbes had demonstrated the possibility that certain biological systems may be conducive to reductive processes and this property could therefore, similarly, be exploited in oxygen deficient tumours to develop chemotherapeutic agents which became cytotoxic after reductive activation.^{103,125,126,141} Hypoxic cells are resistant to radiation therapy and a number of common chemotherapeutic agents, and therefore tumour cell hypoxia is often a problem rather than an advantage in cancer treatment. However, several promising or clinically useful antitumour agents are thought to obtain some therapeutic advantage by causing DNA damage more efficiently in hypoxic tumour cells as compared to normally oxygenated cancer cells.^{125,141} The activation of certain pro-drugs such as nitroimidazole, mitomycin C and other quinones, and benzotriazine di-N-oxides in hypoxic cells to a more toxic compound upon reduction has been shown by a number of workers.^{126,141-143}

As discussed previously in Chapter 6, the natural product mitomycin C (**6.1**), a pro-drug, that is an alkylating agent and is activated *in vivo* to a bifunctional or trifunctional DNA-acting agent.^{124,141,144} After activation **6.1** binds preferentially to the guanine and cytosine moieties of DNA, leading to cross linking of DNA, thus inhibiting DNA synthesis and function. Mitomycin C contains three groups that can damage cells, the quinone moiety that can participate in free radical reactions generating superoxides,^{123,124,144} and aziridinyl and urethane functions that can take part in DNA alkylation. Studies have shown that the carbamate and aziridinyl moieties are not essential for activation and that the anticancer activity was linked to the low redox potential displayed by mitomycin molecules.¹⁴¹ Activation of mitomycin is known to proceed by means of a one electron reduction of the quinone and loss of a methoxy group (Scheme 7.1). This is followed by alkylation of DNA with the formation of interstrand cross links, resulting in inhibition of DNA synthesis, DNA

fragmentation and cell death.^{123,124,141,144} Reduced mitosenes are therefore the active intermediates in the bioreductive activation process.

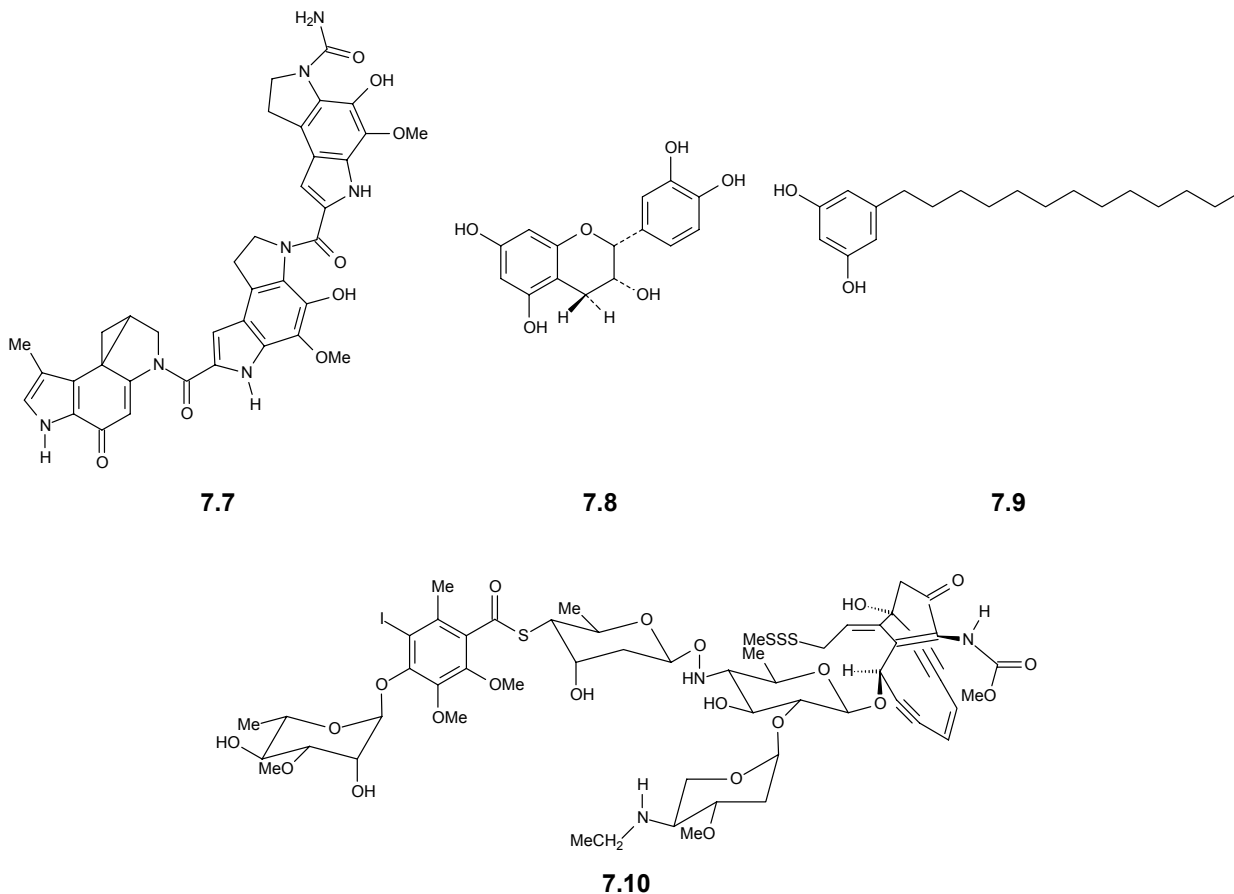


Scheme 7.1 Bioreductive alkylation pathway for mitomycin C (**6.1**).¹²⁴

The nitroimidazoles, initially developed as radiation sensitisers, also show preferential toxicity to hypoxic cells, e.g. RSU 1069 (**6.3**).¹⁴² Benzotriazine di-N-oxides e.g. tirapazamine are also examples of bioreductive cytotoxic agents. It has been suggested that the more negative the reduction potential, the greater the hypoxia selectivity, *i.e.* to the point at which enzymes can no longer reduce the compound.¹²¹ The antitumour properties of these compounds are thought to stem from their selective toxicity toward hypoxic cells found in solid tumours, and are thought to derive their biological activity from the cleavage of DNA. It is believed that an enzymatic one-electron reduction of the antitumour heterocycle leads to the production of radical species (thought to be a hydroxyl radical species). The redox activated DNA cleavage of e.g. tirapazamine is found to be markedly inhibited by molecular oxygen. In the absence of reducing systems, tirapazamine alone does not damage DNA. It thus appears that tirapazamine, together with reductive cellular enzymes, may serve as a vehicle to deliver the known DNA cleaving agent of radiotherapy, the hydroxyl radical, specifically to hypoxic tumour cells *in vivo*.¹²⁵ Evidence obtained from these studies suggested that a hydroxyl radical rather than a radical form of the potential drug was responsible for the DNA cleavage activity, which had no sequence specificity, and this is typical of the involvement of hydroxyl radicals. In addition, workers^{103,125,126} suggested that the hydroxyl radical was formed in a reaction triggered by a one electron enzymatic reduction of the potential drug.

DNA sequencing and conformation studies have been assisted by the availability of molecules that mediate strand scission. New DNA cleaving agents are also of substantial practical interest in the development of potential anti tumour agents, especially those that may be able to damage a target sequence selectively. However, the DNA cleavage induced by potential drugs must occur proficiently under physiological conditions.¹²⁶ Relatively few molecules meet this requirement and

interestingly most are natural products, such as the antibiotic CC-1065 (**7.7**),¹⁴⁵ (-)-epicatechin (**7.8**),¹⁴⁶ 5-alkylresorcinol (**7.9**)¹⁴⁷ and calicheamicin γ_1^I (**7.10**).¹⁴⁸



Since many drugs are activated *in vivo* through enzymatic reduction processes and then become active, the electrochemical data was included to demonstrate whether the reduction potentials can be related to selectivity. Figure 7.4 which shows graphs of the $E_{1/2}$ reduction potentials *versus* HCT-116 appears to demonstrate generally the lower the reduction potential (*i.e.* the easier a compound is to reduce), the greater the cytotoxicity (at both pH 5.5 and 7.5).

The discorhabdin C type compounds *i.e.* **1.51** - **1.53** and discorhabdin A, were found to deviate the most from the trends emerging from the graphs displayed in Figure 7.4, which may indicate that the cytotoxicity displayed by these compounds is unlikely to be related to their reduction potentials. Interestingly, the more elaborate the discorhabdin skeleton (heptacyclic *versus* pentacyclic), the lower the reduction potentials observed.

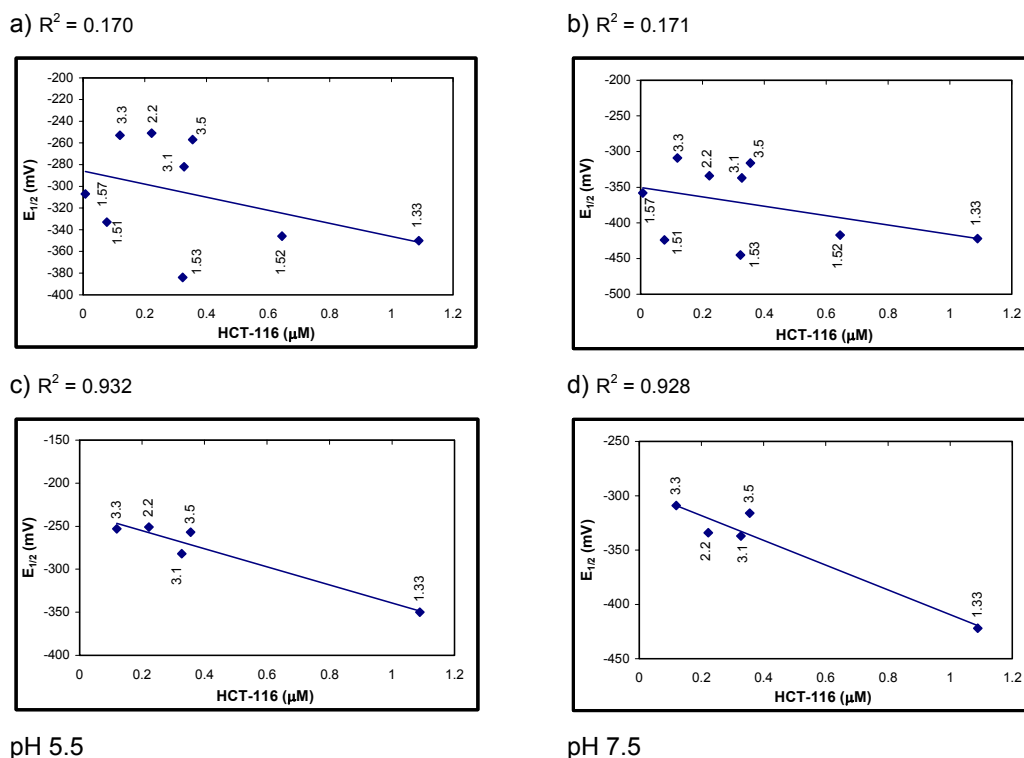


Figure 7.4 Plot of the $E_{1/2}$ (mV) reductive potentials at both pH 5.5 (a) and (c); and 7.5 (b) and (d) versus IC_{50} HCT-116 values obtained for a select group of nine pyrroloiminoquinone compounds. Plots a) and b) investigated the correlation between HCT-116 cytotoxicity and reduction potential of all nine compounds tested ($R^2 = 0.17$). Selective removal of discorhabdin A and three compounds with a discorhabdin C skeleton (1.51 - 1.53) suggested a possible correlation ($R^2 = 0.93$) between HCT-116 cytotoxicity and reduction potentials for the remaining six compounds.

While the makaluvamines have been shown to possess topoisomerase inhibition in several papers, discorhabdin A was shown by Radisky *et al.*³⁰ and Barrows *et al.*⁷⁰ to be a poor inhibitor of topoisomerase II. In the same paper, the makaluvamines were shown to be DNA-active compounds which under some conditions could react chemically to cleave DNA (*e.g.* reductive conditions).³⁰ Their potential as anticancer agents was suggested from their cytotoxicity to HCT-116 and their ability to inhibit topoisomerase II. In addition the makaluvamines were observed to intercalate into DNA and were shown to cause DNA strand breakage like the mitosenes (*e.g.* mitomycin C) but only under reductive conditions. In euoxic conditions, the makaluvamines did not damage DNA *in vitro* unless a topoisomerase II enzyme extract was added. Consistent with this, the makaluvamines did not show enhanced toxicity in other repair deficient lines. These lines were the DNA excision repair deficient and mitomycin C-sensitive UV-20 line and the single strand break repair deficient and X-ray sensitive EM9 line. Barrows *et al.*⁷⁰ showed that the most active (toxic) makaluvamines were those that intercalate well into DNA and also those that displayed the highest reductive potentials. Makaluvone and damirone B, which were shown to be

poor intercalators, and makaluvamine B, which showed no reductive potential versus -180 to -250 mV for the other makaluvamines, were neither cytotoxic nor inhibitors of topoisomerase II. Discorhabdin A was found to be one of the poorer intercalators (K_s value of $85 \mu\text{M}$) and had the second smallest reduction potential (after makaluvamine B), which was consistent with its inactivity against topoisomerase II.^{30,70}

7.5 Singlet oxygen production as a basis for selective cytotoxicity?

No correlation between singlet oxygen production and HCT-116 cytotoxicity (Figure 7.5) was observed, which was expected since the two experiments are unlikely to be related. The compounds were observed to produce radicals only upon activation with laser light at a wavelength of 532 nm and, since the cell cytotoxicity assays are not done specifically at these light conditions, a correlation between the two sets of data is not expected.

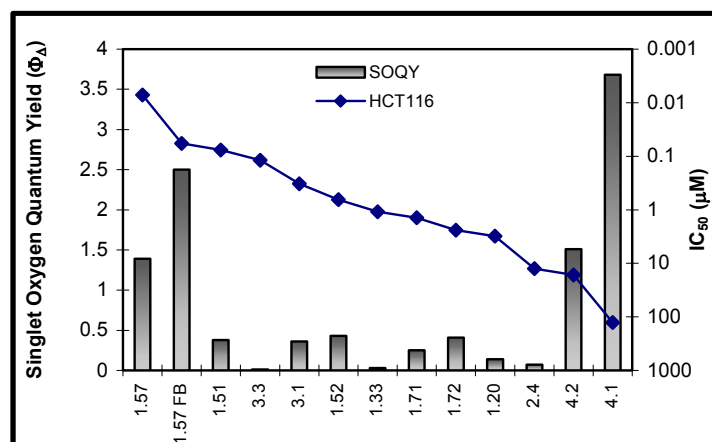


Figure 7.5 Comparison of the singlet oxygen quantum yields (Φ_{Δ}) performed at $\lambda = 532$ nm versus IC_{50} HCT-116 values obtained for a select group of thirteen pyrroloamino-*ortho*-quinone, pyrroloiminoquinones and *bis*-pyrroloiminoquinones. (SOQY = singlet oxygen quantum yield).

Interestingly, the most cytotoxic compound (for all three cancer cell line models), discorhabdin A (**1.57**), exhibited a singlet oxygen quantum yield value greater than 1, which implies the production of radicals (Chapter 5). Similarly, the N-18 oximes (**4.1** and **4.2**) were also observed to produce radicals, though the IC_{50} values obtained in the cytotoxicity assays resulted in the cytotoxicity of these compounds being regarded as insignificant, which could in fact turn out to be an advantage (since the general toxicity of discorhabdin A would preclude its use as a drug, please see Table 7.2). The low cytotoxicity of the N-18 oximes may therefore be advantageous since they could only be induced to produce radicals upon irradiation and may therefore be competent beneficial PDT candidates.

7.6 Conclusion

Discorhabdin A (**1.57**) showed extremely strong cytotoxic activity and our results were in agreement with the available literature. Interestingly, discorhabdin D and its analogues (**3.2**, **3.3**, **3.4** and **3.5**) all displayed significant cytotoxicity in the HCT-116 cell line model. Our results also agreed with available literature in that the pyrroloiminoquinone core structure is essential to the cytotoxic activity displayed by the pyrroloiminoquinones and pyrroloamino-*ortho*-quinones.

In addition to the strong activity displayed by discorhabdin A, the compound also demonstrated the ability to produce radicals upon photo activation. The tsitsikammamine N-18 oximes, which were also found to produce radicals and singlet oxygen, did not display any significant bioactivity. This relative non-toxicity of the tsitsikammamine oximes, unless activated by light, may prove to make them suitable for PDT. In addition, compound **4.1** displayed the ability to fluoresce upon excitation at longer wavelengths, which means that tsitsikammamine A N-18 oxime could also be used in imaging, another requirement of PDT.¹¹⁷ All four tsitsikammamines were also shown to intercalate into DNA and to inhibit topoisomerase activity to some extent. Interestingly, discorhabdin A, unlike the makaluvamines,⁷⁰ does not inhibit topoisomerase II activity, while the tsitsikammamines¹³⁸ and the related alkaloid wakayin⁹¹ inhibit topoisomerase I. Comparison of these apparently related structures may therefore give some idea as to the structural requirements for specific inhibition of topoisomerase I and II. Since most antimalarials are known DNA intercalators, it would be interesting to see whether the pyrroloiminoquinones would also show some antimalarial activity, but their general cytotoxicity would probably preclude their use as antimalarials (Table 7.1).

Chapter 8: Experimental Section

8.1 General experimental section

Unless otherwise stated, the experimental procedures followed were carried out as follows. The ^1H (400 MHz), ^{13}C (100 MHz), Dept 135, COSY, HMQC, HMBC, NOESY and HSQC-TOCSY NMR spectra were recorded on an Avance Bruker 400 MHz spectrometer using standard pulse sequences. Chemical shifts are reported in ppm and referenced to the residual undeuterated solvent resonances (DMSO δ_{H} 2.50, δ_{C} 39.43; CH_3OH δ_{H} 3.30, δ_{C} 49.05) and coupling constants are reported in Hz. Infra-red spectra were recorded as KBr discs on a Perkin-Elmer Spectrum 2000 FT-IR spectrometer. Since the discorhabdins isolated display such close structural similarities, IR spectra were obtained for only a select few compounds. The low resolution mass spectra were obtained using a Finnigan Mat LCQ mass spectrometer, while the high resolution spectra were obtained by Prof. L. Fourie of the Mass Spectrometry Unit at the Universiteit vir Hoër Christelike Onderwys in Potchefstroom on a Micromass 70-70E spectrometer. Separation of the pyrroloiminoquinones was achieved on a reverse phase high performance liquid chromatographic system using a Phenomenex C_{18} column (10 mm i.d., 15 cm, flow rate 3 mL/min) using a Spectra-Physics liquid chromatography pump, Waters R401 differential refractometer and a Rheodyne injector. Analysis of pyrroloiminoquinones by LC-MS (ESI) conditions employed: positive ion mode, capillary temperature 200 °C, capillary voltage 7.0 V, discharge voltage 4.5 kV, tube lens offset -60.0 V, discharge current 50 μA , octapole 1 offset -5.8 V, octapole 2 offset -7.5 V, interoctapole lens -58.0 V, with the sheath and auxiliary gases set to 30 and 0 arbitrary units.

All solvents were distilled prior to use. Reverse phase TLC was done on Merck RP-18 $\text{F}_{254\text{s}}$ glass plates and viewed under UV light (254 nm). Solid phase extractions of the crude extracts were carried out on Waters 10 cm^3 C_{18} Sep-Paks[®].

8.2 Chapter 2: Experimental information

Collection and extraction of *Tsitsikamma pedunculata* (OCDN 6451-V):

Tsitsikamma pedunculata (OCDN 6451-V) was collected in Algoa Bay, South Africa in 1999 at a depth of -40 m and frozen immediately after collection (dry mass 105.5 g). The methanol / dichloromethane (2 : 1) organic extract was partitioned to give the hexane (2.51 g), chloroform (3.20 g), *n*-butanol (2.41 g) and aqueous methanol (8.90 g) fractions. A sequence of C_{18} solid phase extractions using a step gradient (100 % H_2O to 100 % MeOH / TFA) and reversed phase HPLC (using 0.05 % TFA in various H_2O / MeOH eluents) of the chloroform and *n*-butanol partition fractions afforded compounds **1.51** – **1.53**, and **1.52**, **1.53** and **2.1** - **2.6** respectively. See Scheme 2.1 for chromatographic details.

14-bromo-disorhabdin C (1.51): a reddish-brown solid (22.7 mg, 0.02 % yield), was characterised as its TFA salt. ^1H (DMSO- d_6 , 400 MHz) δ 2.02 (2H, t, J = 5.6 Hz, H-7); 2.70 (2H, t, J = 7.3 Hz, H-16); 3.63 (1H, m, H-8); 3.70 (2H, t, J = 7.1 Hz, H-17); 7.70 (1H, s, H-1); 7.70 (1H, s, H-5); 8.20 (1H, br s, NH-18); 10.30 (1H, br s, NH-9); 14.15 (1H, br s, NH-13). ^{13}C (DMSO- d_6 , 100 MHz) δ 17.5 (C-16, t); 33.4 (C-7, t); 38.3 (C-8, t); 43.4 (C-17, t); 44.5 (C-6, s); 91.7 (C-20, s); 112.4 (C-14, s); 119.8 (C-15, s); 122.6 (C-2, s); 122.6 (C-4, s); 124.1 (C-12, s); 124.2 (C-21, s); 150.9 (C-1, d); 150.9 (C-5, d); 151.5 (C-10, s); 152.0 (C-19, s); 164.3 (C-11, s); 171.2 (C-3, s). HRFABMS m/z [M+1] 540.8636 (calcd for $\text{C}_{18}\text{H}_{14}\text{N}_3\text{O}_2^{79}\text{Br}_3$, 540.8636).

14-bromo-3-dihydro-disorhabdin C (1.52): an olive green solid (18.7 mg, 0.02 % yield), was characterised as its TFA salt. ^1H (DMSO- d_6 , 400 MHz) δ 6.37 (1H, s, H-1); 1.89 (2H, t, J = 5.3 Hz, H-7); 2.74 (2H, t, J = 7.2 Hz, H-16); 3.53 (1H, m, H-8); 3.81 (2H, t, J = 7.1 Hz, H-17); 4.68 (1H, s, H-3); 6.37 (1H, s, H-5); 7.80 (1H, br s, NH-18); 10.10 (1H, br s, NH-9); 14.00 (1H, br s, NH-13). ^{13}C (DMSO- d_6 , 100 MHz) δ 17.6 (C-16, t); 34.7 (C-7, t); 38.2 (C-8, t); 41.9 (C-6, s); 43.6 (C-17, t); 70.8 (C-3, d); 96.1 (C-20, s); 112.1 (C-14, s); 119.7 (C-15, s); 124.1 (C-2, s); 124.1 (C-4, s); 124.1 (C-12, s); 124.4 (C-21, s); 133.9 (C-1, d); 133.9 (C-5, d); 151.2 (C-10, s); 151.9 (C-19, s); 164.6 (C-11, s). HRFABMS m/z [M+1] 542.8792 (calcd for $\text{C}_{18}\text{H}_{16}\text{N}_3\text{O}_2^{79}\text{Br}_3$, 542.8793).

3-dihydro-disorhabdin C (1.53): a red solid (90.4 mg, 0.09 % yield), was characterised as its TFA salt. ^1H (DMSO- d_6 , 400 MHz) δ 1.85 (2H, t, J = 7.3 Hz, H-16); 2.80 (2H, t, J = 5.6 Hz, H-7); 3.60 (1H, t, J = 5.6 Hz, H-8); 3.70 (2H, t, J = 7.6 Hz, H-17); 4.60 (1H, s, H-3); 6.50 (1H, s, H-1); 6.50 (1H, s, H-5); 7.40 (1H, s, H-14); 7.80 (1H, br s, NH-18); 10.20 (1H, br s, NH-9); 13.20 (1H, br s, NH-13). ^{13}C (DMSO- d_6 , 100 MHz) δ 17.7 (C-16, t); 33.4 (C-7, t); 37.2 (C-8, t); 42.1 (C-6, s); 42.6 (C-17, t); 69.2 (C-3, d); 92.9 (C-20, s); 119.7 (C-15, s); 122.7 (C-2, s); 122.7 (C-4, s); 122.9 (C-21, s); 123.1 (C-12, s); 127.4 (C-14, d); 133.5 (C-1, d); 133.5 (C-5, d); 152.4 (C-10, s); 153.1 (C-19, s); 165.5 (C-11, s). HRFABMS m/z [M+1] 464.9688 (calcd for $\text{C}_{18}\text{H}_{17}\text{N}_3\text{O}_2^{79}\text{Br}_2$, 464.9688).

7,8-dehydro-3-dihydro-disorhabdin C (2.1): an olive green solid (1.2 mg, 0.001 % yield), was characterised as its TFA salt. For ^1H and ^{13}C NMR data (400/100 MHz, DMSO- d_6) see Table 2.1. HRFABMS m/z [M+1] 462.9532 (calcd. for $\text{C}_{18}\text{H}_{15}\text{N}_3\text{O}_2^{79}\text{Br}_2$, 462.9531).

14-bromo-7,8-dehydro-3-dihydro-disorhabdin C (2.2): a green solid (7.7 mg, 0.007 % yield), was characterised as its TFA salt. For ^1H and ^{13}C NMR data (400/100 MHz, DMSO- d_6) see Table 2.2. HRFABM m/z [M+1] 540.8635 (calcd for $\text{C}_{18}\text{H}_{14}\text{N}_3\text{O}_2^{79}\text{Br}_3$, 540.8636).

Disorhabdin S (2.3): a dark green solid (4.4 mg, 0.004 % yield), was characterised as its TFA salt. For ^1H and ^{13}C NMR data (400/100 MHz, DMSO- d_6) see Table 2.3. HRFABMS m/z [M+1] 387.0582 (calcd for $\text{C}_{18}\text{H}_{18}\text{N}_3\text{O}_2^{79}\text{Br}$, 387.0582).

14-bromo-1-hydroxy-disorhabdin S (2.4): a brown solid (4.2 mg, 0.004 % yield), was characterised as its TFA salt. For ^1H and ^{13}C NMR data (400/100 MHz, DMSO- d_6) see Table 2.4. HRFABMS m/z $[M+1]$ 480.9638 (calcd for $\text{C}_{18}\text{H}_{17}\text{N}_3\text{O}_3^{79}\text{Br}_2$, 480.9637).

1-bromo-4-debromo-2-hydroxy-disorhabdin S (2.5): a golden brown solid (2.6 mg, 0.003 % yield), was characterised as its TFA salt. For ^1H and ^{13}C NMR data (400/100 MHz, DMSO- d_6) see Table 2.5. HRFABMS m/z $[M+1]$ 403.0532 (calcd for $\text{C}_{18}\text{H}_{18}\text{N}_3\text{O}_3^{79}\text{Br}$, 403.0532).

2,4-debromo-3-dihydro-disorhabdin C (2.6): a reddish-brown solid (1.2 mg, 0.001 % yield), was characterised as its TFA salt. For ^1H and ^{13}C NMR data (400/100 MHz, DMSO- d_6) see Table 2.6. HRFABMS m/z $[M^+]$ 308.1400 (calcd for $\text{C}_{18}\text{H}_{18}\text{N}_3\text{O}_2$, 308.1399).

8.3 Chapter 3: Experimental information

Collection and extraction of *Latrunculia lorii* (OCDN 6428-V):

Latrunculia lorii (OCDN 6428-V) was collected in Riy Banks, Algoa Bay, South Africa in 1999 at a depth of -24 m and frozen immediately after collection (dry mass 138.2 g). The methanol / dichloromethane organic extract was partitioned to give the hexane (4.17 g), chloroform (0.99 g), *n*-butanol (6.27 g) and aqueous methanol (9.60 g) fractions. A sequence of C_{18} solid phase extractions using a step gradient (100 % H_2O to 100 % MeOH / TFA) and reversed phase HPLC (using 0.05 % TFA in various H_2O / MeOH eluents) of the chloroform and *n*-butanol partition fractions afforded compounds **1.33**, **1.20**, **1.47**, **3.1 - 3.4**, and **1.33**, **1.20**, **3.1 - 3.3** and **3.5** (in larger quantities) respectively. See Scheme 3.1 for chromatographic details.

Makaluvamine C (1.33): a reddish brown solid (22.6 mg, 0.02 % yield), was characterised as its TFA salt. ^1H (DMSO- d_6 , 400 MHz) δ 2.91 (2H, t, $J_{3,4} = 7.6$ Hz, H-3); 3.31 (3H, s, H-5'); 3.89 (2H, t, $J_{3,4} = 7.6$ Hz, H-4); 5.73 (1H, s, H-6); 7.26 (2H, s, H-2); 8.61 (1H, br s, H-9a); 9.43 (1H, br s, NH-9b); 13.07 (1H, br s, NH-1). ^{13}C (DMSO- d_6 , 100 MHz) δ 18.8 (C-3, t); 38.9 (C-5', q); 52.5 (C-4, t); 85.4 (C-6, d); 117.7 (C-8b, s); 123.2 (C-8a, s); 123.3 (C-2a, s); 126.5 (C-2, d); 155.6 (C-5a, s); 156.5 (C-7, s); 167.3 (C-8, s). HRFABMS m/z $[M^+]$ 202.0980 (calcd for $\text{C}_{11}\text{H}_{12}\text{N}_3\text{O}$, 202.0980).

Damirone B (1.20): a reddish brown solid (70.2 mg, 0.05 % yield), was characterised as its TFA salt. ^1H (DMSO- d_6 , 400 MHz) δ 2.81 (2H, t, $J_{3,4} = 6.6$ Hz, H-3); 3.05 (3H, s, H-5'); 3.61 (2H, t, $J_{3,4} = 6.6$ Hz, H-4); 5.20 (1H, s, H-6); 6.66 (1H, br s, NH-5); 7.06 (1H, s, H-2); 12.42 (1H, br s, NH-1). ^{13}C (DMSO- d_6 , 100 MHz) δ 19.6 (C-3, t); 37.8 (C-5', q); 51.3 (C-4, t); 92.6 (C-6, d); 116.4 (C-8b, s); 124.0 (C-2, d); 124.2 (C-8a, s); 124.7 (C-2a, s); 153.8 (C-5a, s); 170.2 (C-7, s); 177.5 (C-8, s). HRFABMS m/z $[M^+]$ 203.0821 (calcd for $\text{C}_{11}\text{H}_{11}\text{N}_2\text{O}_2$, 203.0821).

Makaluvic Acid (1.47): a brown solid (2.7 mg, 0.002 % yield), was characterised as its TFA salt. ^1H (DMSO- d_6 , 400 MHz) δ 2.81 (2H, t, $J_{3,4} = 7.1$ Hz, H-3); 3.06 (3H, s, H-5'); 3.63 (2H, t, $J_{3,4} = 7.1$

Hz, H-4); 6.89 (1H, d, $J_{\text{NH}1,2} = 2.8$ Hz, H-2); 12.29 (1H, br s, NH-1); 16.05 (1H, s, H-8a). ^{13}C (DMSO- d_6 , 100 MHz) δ 19.6 (C-3, t); 34.0 (C-5', q); 49.9 (C-4, t); 115.1 (C-8b, s); 118.2 (C-2, d); 122.1 (C-2a, s); 123.2 (C-8a, s); 159.8 (C-8, s); 165.0 (C-5a, s). HRFABMS m/z [M+1] 195.0760 (calcd for $\text{C}_9\text{H}_{11}\text{N}_2\text{O}_3$, 195.0770).

Discorhabdin G* (3.1): a dark golden brown solid (18.2 mg, 0.01 % yield), was characterised as its TFA salt. ^1H and ^{13}C NMR data (400/100 MHz, DMSO- d_6) see Table 3.1. HRFABMS m/z [M $^+$] 336.0807 (calcd for $\text{C}_{18}\text{H}_{14}\text{N}_3\text{SO}_2$, 336.0807).

Discorhabdin M (3.2): a reddish-brown solid (35.1 mg, 0.03 % yield), was characterised as its TFA salt. For ^1H and ^{13}C NMR data (400/100 MHz, DMSO- d_6) see Table 3.2. HRFABMS m/z [M $^+$] 409.0971 (calcd for $\text{C}_{20}\text{H}_{17}\text{N}_4\text{SO}_4$, 409.0971).

1-amino discorhabdin D (3.3): a dark green solid (56.9 mg, 0.04 % yield), was characterised as its TFA salt. For ^1H and ^{13}C NMR data (400/100 MHz, DMSO- d_6) see Table 3.3. HRFABMS m/z [M $^+$] 352.0995 (calcd for $\text{C}_{18}\text{H}_{15}\text{N}_4\text{SO}_2$, 352.0994).

1-methoxy discorhabdin D (3.4): a brown solid (4.1 mg, 0.003 % yield), was characterised as its TFA salt. For ^1H and ^{13}C NMR data (400/100 MHz, DMSO- d_6) see Table 3.4. HRFABMS m/z [M $^+$] 366.0912 (calcd for $\text{C}_{19}\text{H}_{16}\text{N}_3\text{SO}_3$, 366.0912).

1-alanyl discorhabdin D (3.5): a dark green solid (16.3 mg, 0.01 % yield), was characterised as its TFA salt. For ^1H and ^{13}C NMR data (400/100 MHz, DMSO- d_6) see Table 3.5. HRFABMS m/z [M $^+$] 423.1127 (calcd for $\text{C}_{21}\text{H}_{19}\text{N}_4\text{SO}_4$, 423.1127).

8.4 Chapter 4: Experimental information

Collection and extraction of *Tsitsikamma favus* (SAF 94-006):

Tsitsikamma favus was collected in Tsitsikamma Marine Reserve, South Africa in 1994 at a depth of -20 m and frozen immediately after collection (dry mass 473.3 g). The methanol organic extract was partitioned to give the hexane (17.50 g), chloroform (3.85 g), *n*-butanol (4.64 g) and aqueous methanol (28.65 g) fractions. A sequence of C_{18} solid phase extractions using a step gradient (100% H_2O to 100% MeOH/TFA) and reversed phase HPLC (using 0.05% TFA in $\text{H}_2\text{O}/\text{MeOH}$) of the chloroform and *n*-butanol partition fractions afforded compounds **1.71**, **1.72**, **1.52** and **4.1**, **4.2**, **2.1**, **2.4**, **2.6**, respectively. See Scheme 4.1 for chromatographic details.

Tsitsikammamine A (1.71): a reddish brown solid (10.3 mg, 0.002 % yield), was characterised as its TFA salt. IR (KBr disk) ν_{max} 3154, 1680, 1626, 1447, 1372, 1324, 1266, 1201, 1131, 836, 796, 719, 592 cm^{-1} . ^1H (DMSO- d_6 , 400 MHz) δ 2.93 (2H, t, $J = 8.0$ Hz, H-16); 3.85 (2H, $J = 8.0$ Hz, t, H-17); 6.87 (2H, d, $J = 8.4$ Hz, H-1); 6.87 (2H, d, $J = 8.4$ Hz, H-5); 7.10 (1H, d, $J = 1.6$ Hz, H-14); 7.15 (1H, m, H-8); 7.37 (2H, d, $J = 8.4$ Hz, H-2); 7.37 (2H, d, $J = 8.4$ Hz, H-4); 13.01 (1H,

br s, NH-13); 13.28 (1H, br s, NH-9). ^{13}C (DMSO- d_6 , 100 MHz) δ 17.6 (C-16, t); 44.9 (C-17, t); 113.4 (C-20, s); 116.2 (C-1, d); 116.2 (C-5, d); 119.2 (C-15, s); 120.7 (C-21, s); 122.4 (C-7, s); 123.1 (C-14, d); 125.0 (C-8, d); 127.2 (C-6, s); 127.8 (C-12, s); 128.9 (C-2, d); 128.9 (C-4, d); 134.6 (C-10, s); 156.8 (C-19, s); 157.5 (C-3, s); 166.3 (C-11, s). HRFABMS m/z [M^+] 304.1087 (calcd for $\text{C}_{18}\text{H}_{14}\text{N}_3\text{O}_2$, 304.1086).

Tsitsikammamine B (1.72): a dark red solid (36.8 mg, 0.008 % yield), was characterised as its TFA salt. ^1H (DMSO- d_6 , 400 MHz) δ 2.91 (2H, t, $J = 8.0$ Hz, H-16); 3.83 (2H, $J = 8.0$ Hz, t, H-17); 3.96 (3H, s, N-Me); 6.87 (2H, d, $J = 8.4$ Hz, H-1); 6.87 (2H, d, $J = 8.4$ Hz, H-5); 7.12 (1H, s, H-14); 7.17 (1H, d, $J = 2.4$ Hz, H-8); 7.36 (2H, d, $J = 8.4$ Hz, H-2); 7.36 (2H, d, $J = 8.4$ Hz, H-4); 13.28 (1H, br s, NH-9). ^{13}C (DMSO- d_6 , 100 MHz) δ 17.5 (C-16, t); 35.7 (N- CH_3 , q); 44.6 (C-17, t); 113.3 (C-20, s); 116.2 (C-1, d); 116.2 (C-5, d); 118.7 (C-15, s); 120.6 (C-21, s); 122.4 (C-7, s); 125.1 (C-8, d); 126.3 (C-12, s); 127.1 (C-6, s); 127.9 (C-14, d); 128.9 (C-2, d); 128.9 (C-4, d); 134.5 (C-10, s); 156.2 (C-19, s); 157.6 (C-3, s); 166.7 (C-11, s). HRFABMS m/z [$M+1$] 319.1321 (calcd for $\text{C}_{19}\text{H}_{17}\text{N}_3\text{O}_2$, 319.1321).

Tsitsikammamine A N-oxime (4.1): a bright orange red solid (4.7 mg, 0.001 % yield), was characterised as its TFA salt. IR (KBr disk) ν_{max} 3066, 1674, 1646, 1487, 1434, 1405, 1381, 1271, 1207, 1147, 987, 908, 841, 792, 721, 608, 438 cm^{-1} . For ^1H and ^{13}C NMR data (400/100 MHz, DMSO- d_6) see Table 4.1. HRFABMS m/z [$M+2$] 322.1192 (calcd for $\text{C}_{18}\text{H}_{16}\text{N}_3\text{O}_3$, 322.1192).

Tsitsikammamine B N-oxime (4.2): a bright orange red solid (2.9 mg, 0.0006 % yield), was characterised as its TFA salt. For ^1H and ^{13}C NMR data (400/100 MHz, DMSO- d_6) see Table 4.2. HRFABMS m/z [$M+1$] 336.1348 (calcd for $\text{C}_{19}\text{H}_{18}\text{N}_3\text{O}_3$, 336.1348).

14-bromo-3-dihydro-disorhabdin C (1.52): an olive green solid (9.6 mg, 0.002 % yield), was characterised as its TFA salt. For ^1H and ^{13}C NMR data (400/100 MHz, DMSO- d_6) see Section 9.2 above. HRFABMS m/z [$M+1$] 542.8792 (calcd for $\text{C}_{18}\text{H}_{16}\text{N}_3\text{O}_2$ $^{79}\text{Br}_3$, 542.8793).

7,8-dehydro-3-dihydro-7,8-dehydro-disorhabdin C (2.1): an olive green solid (2.1 mg, 0.0004 % yield), was characterised as its TFA salt. For ^1H and ^{13}C NMR data (400/100 MHz, DMSO- d_6) see Table 2.1. HRFABMS m/z [$M+1$] 462.9532 (calcd. for $\text{C}_{18}\text{H}_{15}\text{N}_3\text{O}_2$ $^{79}\text{Br}_2$, 462.9531).

14-bromo-1-hydroxy-disorhabdin S (2.4): a brown solid (4.3 mg, 0.001 % yield) was characterised as its TFA salt. For ^1H and ^{13}C NMR data (400/100 MHz, DMSO- d_6) see Table 2.4. HRFABMS m/z [$M+1$] 480.9636 (calcd for $\text{C}_{18}\text{H}_{17}\text{N}_3\text{O}_3$ $^{79}\text{Br}_2$, 480.9637).

2,4-debromo-3-dihydro-disorhabdin C (2.6): a reddish-brown solid (2.0 mg, 0.0004 % yield), was characterised as its TFA salt. For ^1H and ^{13}C NMR data (400/100 MHz, DMSO- d_6) see Table 2.6.

Attempted oxidation of 1.71:

Compound **1.71** (3.0 mg) was dissolved in glacial acetic acid (0.5 mL) and treated with an excess 30 % solution of H₂O₂ (1.0 mL) at 80 °C for 24 hrs with stirring. No colour change was observed and only starting material was recovered.

Compound **1.71** (2.5 mg) was dissolved in MeOH (1 mL) and treated with an excess *m*-CPBA (1.5 mg) with stirring for 24 hrs. No colour change was observed and only starting material was recovered.

Collection and extraction of *Strongylodesma* sp.:

The *Strongylodesma* sp. sponge was collected in Algoa Bay, South Africa in 1996 at a depth of – 2 m and frozen immediately after collection (dry mass 143.1 g). The methanol organic extract was partitioned to give the hexane (16.69 g), chloroform (1.17 g), *n*-butanol (4.65 g) and aqueous methanol (5.45 g) fractions. A sequence of C₁₈ solid phase extractions using a step gradient (100% H₂O to 100% MeOH/TFA) and reversed phase HPLC (using 0.05% TFA in H₂O/MeOH) of the chloroform and *n*-butanol partition fractions afforded compounds **1.57**, **1.53** and **1.61**, and **3.3** respectively. See Scheme 4.3 for chromatographic details.

Discorhabdin A (1.57): a dark green solid (208.8 mg, 0.15 % yield) was characterised as its TFA salt. ¹H (DMSO-d₆, 400 MHz) δ 2.48 (1H, m, H-7a); 2.67-3.17 (5H, m, H-4, H-7b, H-16); 3.70 (1H, m, H-17a); 3.93 (1H, m, H-17b); 4.58 (2H, dd, *J* = 6.0, 11.6 Hz, H-5); 5.33 (1H, s, H-8); 7.38 (1H, d, *J* = 1.6 Hz, H-14); 7.47 (1H, s, H-1); 9.42 (1H, br s, NH-18); 10.35 (1H, br s, NH-9); 13.18 (1H, br s, NH-13). ¹³C (DMSO-d₆, 100 MHz) δ 18.8 (C-16, t); 41.3 (C-7, t); 44.6 (C-17, t); 45.2 (C-4, t); 50.3 (C-6, s); 54.6 (C-5, d); 59.6 (C-8, d); ~105 (C-20, s); 120.7 (C-15, s); 124.0 (C-21, s); 124.2 (C-12, s); 128.1 (C-14, s); 148.8 (C-10, s); 154.6 (C-19, s); 166.8 (C-11, s); 187.8 (C-3, s). Low resolution MS *m/z* [M⁺] 416.2.

Discorhabdin D (1.61): a green solid (6.7 mg, 0.005 % yield) was characterised as its TFA salt. ¹H (DMSO-d₆, 400 MHz) δ 2.44 (1H, dd, *J* = 2.8, 13.4 Hz, H-1a); 2.55 (1H, d, *J* = 12.1 Hz, H-7a); 2.70 (1H, dd, *J* = 3.5, 12.1 Hz, H-7b); 2.91 (1H, dd, *J* = 2.8, 13.4 Hz, H-1b); 3.03 (1H, m, H-16); 3.84 (1H, m, H-17a); 4.03 (1H, m, H-17b); 4.37 (1H, s, H-2); 5.68 (1H, m, H-8); 6.13 (1H, s, H-4); 7.29 (1H, d, *J* = 2.3 Hz, H-14); 10.70 (1H, br s, NH-9) 13.15 (1H, br s, NH-13). ¹³C (DMSO-d₆, 100 MHz) δ 19.3 (C-16, t); 30.1 (C-1, t); 38.5 (C-7, t); 41.0 (C-6, s); 51.1 (C-17, t); 62.1 (C-2, d); 62.6 (C-8, d); 99.5 (C-20, s); 112.3 (C-4, d); 117.6 (C-15, s); 121.4 (C-12, s); 123.6 (C-21, s); 126.8 (C-14, d); 145.8 (C-10, s); 147.7 (C-19, s); 166.4 (C-11, s); 172.9 (C-5, s); 182.9 (C-3, s). Low resolution MS *m/z* [M⁺] 436.4.

3-dihydro-disorhabdin C (1.53): a red solid (6.9, 0.005 % yield), was characterised as its TFA salt. For ^1H and ^{13}C NMR data (400/100 MHz, DMSO- d_6) see Section 8.2.

1-amino discorhabdin D (3.3): a dark green solid (19.2 mg, 0.01 % yield), was characterised as its TFA salt. For ^1H and ^{13}C NMR data (400/100 MHz, DMSO- d_6) see Table 3.3.

8.5 Chapter 5: Experimental information

Materials:

A select group of pyrroloiminoquinones, previously isolated from various *latrunculid* sponges, were used to determine the singlet oxygen quantum yields. DMSO, 5,10,15,20-tetraphenyl-21*H*,23*H*-porphine (porphine) and 1,3-diphenylisobenzofuran (DPBF) were purchased from Sigma-Aldrich.

Preparation of the free base of compounds 1.51 and 1.57:

Compounds **1.51** (2.5 mg) and **1.57** was dissolved in 5 M NaOH. A change of colour (to yellow) was observed and the compounds subsequently extracted with chloroform. The chloroform fractions containing the compounds were dried and the solvent removed *in vacuo*. The compounds were then subjected to reversed phase fractionation on a rapid sample preparation SepPak[®] (Part No. 51910) using a gradient elution and dried.

8.6 Chapter 6: Experimental information

Methods:

Voltammetric measurements were done in a conventional three-electrode system. Both CV and OSWV data were collected using a CV-50W Bio-Analytical System (BAS) voltammetric analyser. A gold electrode (0.8 mm in diameter) and a platinum electrode were used as the working and auxiliary electrodes, respectively. Before use in the electrochemical experiments, the surface of the gold electrode was hand polished on fine chamois leather containing $\gamma\text{-Al}_2\text{O}_3$ slurry. A Ag|AgCl (3 mol/dm³ KCl) reference electrode was used for the aqueous solutions studied. The electrolyte buffer solutions were made up prior to data collection and the solutions saturated with nitrogen before running the experiment. Nitrogen was supplied by MG Fed gas and purified by passing through a Drierite self-indicating mesh 8 (anhydrous CaSO₄) from SAAR Chemicals. All experiments were carried out at ambient temperature. The buffer solutions were made up as follows:

pH 5.5: (NaH₂PO₄·H₂O 6.22 mg/mL, Na₂HPO₄ (anhydrous) 0.232 mg/mL, Na₂EDTA 0.375 mg/mL);

pH 7.5: (NaH₂PO₄·H₂O 0.575 mg/mL, Na₂HPO₄ (anhydrous) 2.17 mg/mL, Na₂EDTA 0.375 mg/mL).³⁰

8.7 Chapter 7: Experimental information

HCT-116, WHC01 and ME180 cytotoxicity assays:

a) Cell culture

The human colon tumour cell line (HCT-116) was purchased from ATCC. The HCT-116 cells were maintained in McCoy's medium similarly enriched with 2 % foetal bovine serum, 8 % newborn serum, 8 % newborn bovine serum with penicillin (100 µg/mL), streptomycin (100 µg/mL). Cells were grown at 37 °C as monolayers in culture flasks (75 cm²) and detached with trypsin before seeding into microtiter culture plates.

The WHC01 (oesophageal) and ME180 (ovarian) cell lines (MTT assay) were similarly maintained and prepared by Catherine Arendse, Department of Medical Biochemistry, University of Cape Town, South Africa. IC₅₀ determinations were carried out using the MTT kit from Roche (Cat # 1465007), according to manufacturer's instructions. Briefly, 1500 cells were seeded per well in 90 µL in Cellstar 96-well plates. Cells were incubated for 24 hours then the pyrroloiminoquinones plated at various concentrations in 10 µL (constant final concentration of DMSO = 0.1 %). After 48 hours incubation, observations were made, and 10 µL MTT solution added to each well. After a further 4 hours incubation, 100 µL of solubilisation solution was added to each well and the plates incubated again overnight. The following morning, plates were read at 595 nm on an Anthos microplate reader 2001.

b) Cell cytotoxicity

Cytotoxicity was established in a 3-(4,5-dimethylthiazol-2-yl)-2,5-diphenyltetrazolium bromide (MTT) assay as performed by Mossmann¹⁴⁹ and modified by others.^{91,150,151} Drugs were dissolved in 100 % DMSO at initial concentrations of 10 mM and serially diluted. The final concentration of DMSO in the cell culture wells was 1 % or less. 20000 Cells were seeded in growth media in 200 µL in 96-well plates. 4 hours after seeding, cells were treated, each dose in quadruplicate, with serially diluted drug (1 µL). After 72 hrs, all cultures were re-fed with McCoy's medium (100 µL) and an aliquot of MTT solution (11 µL, 5 mg/mL in PBS, pH 7.4) was added to each well. The plates were incubated for 4 hrs at 37 °C. Viable cells reduced MTT to a purple formazan product that was solubilised by the addition of DMSO (100 µL) to aspirated culture wells. The absorbance at 540 nm was measure for each well using a Bio-Rad MP450 plate reader. Average absorbance for each set of drug treated wells was compared to the average absorbance of the control wells to determine the fractional survival at any particular drug concentration. The IC₅₀ was defined as the

drug concentration that yielded a fraction survival of 50 %. IC₅₀ values reported were the average of three to five independent experiments.

Quantitation of DNA catenation and cleavage:

DNA cleavage assays were performed as described by Matsumoto *et al.*¹⁵² Aliquot (20 µL) volumes containing Tris-HCl (50 mM, pH 7.5), KCl (85 mM), MgCl₂ (10 mM), EDTA (0.5 mM), bovine serum albumin (30 µg/mL), DTT (2 mM), radiolabelled (500 ng) and supercoiled rf M13 mp 19 DNA and purified top2 or top1 (80 – 120 ng) were treated with the drug made up in DMSO and incubated at 30 °C for 30 min. The reactions were stopped by the addition of 1.5 mg/mL proteinase K (2 µL) in 0.5 % SDS and incubated at 37 °C for 60 min. The DNA was fractionated by electrophoresis in 0.8 % agarose (containing 50 ng ethidium bromide/mL TAE) to separate nicked (n), linear – only on top2 gel and runs just below the nicked band (l), relaxed (r) and supercoiled (sc) DNA. DNA was visualised under UV light and sliced out of the gel. Gel slices were placed in scintillation vials with water (1 mL), melted in a microwave oven and mixed with Opti-Fluor (10 mL, Packer Co.) while molten, and radioactivity determined by standard scintillation counting. The percentage of cleaved DNA, represented by radioactivity in the combined nicked and linear bands) was determined relative to the total radioactivity in the reactions, following subtraction of radioactivity due to endogenously cleaved DNA. The percentage of catenated DNA was determined similarly.

Ethidium bromide (EtBr) displacement assays:

The K_s value is defined as the concentration of compound required to decrease DNA bound EtBr fluorescence by 50 % and the assay has been described by Kokoshka *et al.*⁹¹ and modified by Barrows *et al.*⁷⁰ Salmon testes sperm DNA (25 µg/mL) and EtBr (0.5 µg/mL) were put in a 96-well plate in TE (100 µL). Controls consisted of EtBr in TE only, DNA in TE only and EtBr + DNA in TE. Final concentrations in the wells ranged from 100, 1, 0.1 to 0.01µM for each compound. Each plate consisted of an n = 4 for each drug dose tested and n = 8 for the controls. The 96-well plates were read by a fluorescent plate reader. EtBr displacement was determined by subtracting the amount of background EtBr fluorescence from all samples and then dividing by the amount of fluorescence in the DNA and EtBr control. All four compounds were found to intercalate into DNA.

REFERENCES:

1. Carte, B.K. *Bioscience* **1996**, *46*, 271.
2. Newman, D.J.; Cragg, G.M.; Snader, K.M. *Nat. Prod. Rep.* **2000**, *17*, 215 - 234.
3. Munro, M.H.G.; Blunt, J.W.; Dumdei, E.J.; Dickford, S.J.H.; Lill, R.E.; Li, S. Battershill, C.N.; Duckworth, A.R. *J. Biotechnology* **1999**, *70*, 15 - 25.
4. Pomponi, S.A. *J. Biotechnology* **1999**, *70*, 5 - 13.
5. Andersen, R.J.; Williams, D.E. in *Issues in Environmental Science and Technology 13: Chemistry in the Marine Environment*; Hester, R.E.; Harrison, R.M. Eds. Royal Society of Chemistry: Cambridge, **2000** pp. 55 - 79.
6. Faulkner, D.J. *Nat. Prod. Rep.* **2000**, *17*, 7 - 55.
7. Faulkner, D.J. *Nat. Prod. Rep.* **1990**, 269 - 309.
8. Faulkner, D.J. *Nat. Prod. Rep.* **1997**, 259 - 302.
9. Faulkner, D.J. *Nat. Prod. Rep.* **1998**, 113 - 158.
10. Faulkner, D.J. *Nat. Prod. Rep.* **1999**, *16*, 155 - 198.
11. Bewley, C.; Faulkner, D.J. *Angew. Chem. Int. Ed.* **1998**, *37*, 2162 - 2178.
12. Gunawardana, G.P.; Kohmoto, S.; Gunasekera, S.P.; McConnell, O.J.; Koehn, F.E. *J. Am. Chem. Soc.* **1988**, *110*, 4856-4858.
13. Litaudon, M.; Hickford, S.J.H.; Lill, R.E.; Lake, R.J.; Blunt, J.W.; Munro, M.H.G. *J. Org. Chem.* **1997**, *62*, 1868 - 1871.
14. Hirata, Y. Uemura, D. *Pure Appl. Chem.* **1986**, *58*, 701 - 710.
15. Gunasekera, S.P.; Gunasekera, M.; Longley, R.E.; Schulte, G.K. *J. Org. Chem.* **1990**, *55*, 4512 - 4515.
16. Chan, G.W.; Mong, S.; Hemling, M.E.; Freyer, A.J.; Offen, P.H.; de Brosse, C.W.; Saran, H.M.; Westley, J.W. *J. Nat. Prod.* **1993**, *56*, 116 - 121.
17. Burgoyne, D.L.; Andersen, R.J.; Allen, T.M. *J. Org. Chem.* **1992**, *57*, 525 - 528.
18. Jaspers, M. *Chem. and Ind.* **1999**, 51 - 55.
19. Pettit, G.R.; Collins, J.C.; Herald, D.L.; Doubek, D.L.; Boyd, M.R.; Schmidt J.M.; Hopper, J.N.A.; Tackett, L.P. *Can. J. Chem.* **1992**, *70*, 1170 - 1175.
20. De Silva, E.D.; Scheuer, P.J. *Tetrahedron Letters* **1980**, *21*, 1611 - 1614.
21. Patil, A.D.; Kumar, N.V.; Kokke, W.C.; Bean, M.F.; Freyer, A.J.; De Brosse, C.; Mai, S.; Truneh, A.; Faulkner, D.J.; Carte, B.; Breen, A.L.; Hertzberg, R.P.; Johnson, R.K.; Westley, J.W.; Potts, B.C.M. *J. Org. Chem.* **1995**, *60*, 1182 - 1188.
22. Urban, S.; Hickford, S. J. H.; Blunt, J. W.; Munro, M. H. G. *Curr. Org. Chem.* **2000**, *4*, 765 - 807.
23. Märki, F.; Robertson, A.V. Witkop, B. *J. Am. Chem. Soc.* **1961**, *83*, 3341 - 3342.
24. Baumann, C.; Brockelmann, M.; Fugmann, B.; Steffan, B.; Steglich, W.; Sheldrick, W. S. *Angew. Chem. Int. Ed. Engl.* **1993**, *32*, 1087 - 1089.
25. Stierle, D.B.; Faulkner, D.J. *J. Nat. Prod.* **1991**, *54*, 1131 - 1133.
26. Schmidt, E. W.; Harper, M. K.; Faulkner, D. J. *J. Nat. Prod.* **1995**, *58*, 1861 - 1867.

27. Sakemi, S.; Sun, H.H.; Jefford, C.W.; Bernardinelli, G. *Tetrahedron Letters* **1989**, *30*, 2517 - 2520.
28. Sun, H.H.; Sakemi, S.; Burren, N.; McCarthy, P. *J. Org. Chem.* **1990**, *55*, 4964 - 4966.
29. Gunasekera, S. P.; McCarthy, P. J.; Longley, R. E.; Pomponi, S. A.; Wright, A. E. *J. Nat. Prod.* **1999**, *62*, 1208 - 1211.
30. Radisky, D. C.; Radisky, E. S.; Barrows, L. R.; Copp, B. R.; Kramer, R. A.; Ireland, C. M. *J. Am. Chem. Soc.* **1993**, *115*, 1632 - 1638.
31. Carney, J. R.; Scheuer, P. J.; Kelly-Borges, M. *J. Nat. Prod.* **1993**, *49*, 8483 - 8486.
32. Venables, D.A.; Concepción, G.P.; Matsumoto, S.S.; Barrows, L.R.; Ireland, C.M. *J. Nat. Prod.* **1997**, *60*, 408 - 410.
33. Casapullo, A.; Cutignano, A.; Bruno, I. Bifulco, G.; Debitus, C.; Gomez-Paloma, L.; Riccio, R. *J. Nat. Prod.* **2001**, *64*, 1354 - 1356.
34. Fu, X.; Ng, P.; Schmitz, F. J.; Hossain M. B.; van der Helm, D.; Kelly-Borges, M. *J. Nat. Prod.* **1996**, *59*, 1104 - 1106.
35. Perry, N. B.; Blunt, J. W.; McCombs J. D.; Munro, M. H. G. *J. Org. Chem.* **1986**, *51*, 5476 - 5478.
36. Perry, N. B.; Blunt, J. W.; Munro, M. H. G. *Tetrahedron* **1988**, *58*, 1727 - 1734.
37. New Zealand Institute of Chemistry Conference (7-10 December 1993)
38. 37th Annual Meeting of the American Society of Pharmacognosy (1996)
39. The structures and ¹H NMR spectra of discorhabdins E-M were kindly supplied to us by Professor Munro.
40. Gunasekera, S. P.; McCarthy, P. J.; Longley, R. E.; Pomponi, S. A.; Wright, A. E.; Lobkovsky, E.; Clardy J. *J. Nat. Prod.* **1999**, *62*, 173 - 175.
41. Hooper, G. J.; Davies-Coleman, M. T.; Kelly-Borges, M.; Coetzee, P. S. *Tetrahedron Letters* **1996**, *37*, 7135 - 7138.
42. Beukes, D.R. PhD Thesis, Rhodes University, **2000**, pp. 71 - 117.
43. Copp, B. R.; Fulton, K. F.; Perry, N. B.; Blunt, J. W.; Munro, M. H. G. *J. Org. Chem.* **1994**, *59*, 8233 - 8238.
44. Blunt, J.W.; Munro, M.H.G.; Battershill, C.N.; Copp, B.R.; McCombs, J.D.; Perry, N.B.; Prinsep, M.; Thompson, A.M. *New J. Chem.* **1990**, *14*, 761.
45. Yang, A.; Baker, B. J. *J. Nat. Prod.* **1995**, *58*, 1596 - 1599.
46. Dijoux, M.; Gamble, W. R.; Hallock, Y. F.; Cardellina, J. H.; van Soest, R.; Boyd, M. R. *J. Nat. Prod.* **1999**, *62*, 636 - 637.
47. Ford, J.; Capon, R. J. *J. Nat. Prod.* **2000**, *63*, 1527 - 1528.
48. Perry, N. B.; Blunt, J. W.; Munro, M. H. G. *J. Org. Chem.* **1988**, *53*, 4127 - 4128.
49. Kobayashi, J.; Cheng, J.; Ishibashi, M.; Nakamura, H.; Ohizumi, Y.; Hirata, Y.; Sasaki, T.; Lu, H.; Clardy, J. *Tetrahedron Letters* **1987**, *28*, 4939 - 4942.
50. Cheng, J.; Ohizumi, Y.; Wälchli, M. R.; Nakamura, H.; Hirata, Y.; Sasaki, T.; Kobayashi, J. *J. Org. Chem.* **1988**, *53*, 4621 - 4624.
51. Kobayashi, J.; Cheng, J.-F.; Yamamura, S.; Ishibashi, M. *Tetrahedron Letters* **1991**, *32*,

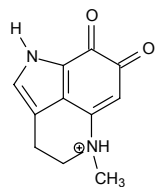
- 1227 - 1228.
52. D'Ambrosio, M.; Guerriero, A.; Chiasera, G.; Pietra, F. *Tetrahedron* **1996**, *52*, 8899 - 8906.
53. Copp, B.R.; Barrows, L.R.; Ireland, C.M. *J. Org. Chem.* **1991**, *56*, 4596 - 4597.
54. Venables, D. A.; Barrows, L. R.; Lassota, P.; Ireland, C. M. *Tetrahedron Letters* **1997**, *38*, 721 - 722.
55. Samaai, T.; Kelly, M. *Systema Porifera: A Guide to the Classification of Sponges* Eds. Hooper, J. N. A.; Van Soest, R. W. M.; Kluwer Academic Publishers, New York, **2002**, pp. 708 - 719.
56. Miller, K.; Alvarez, B.; Battershill, C.; Northcote, P.; Parthasarathy, H. *Marine Biology* **2001**, *139*, 235 - 250.
57. van Soest, R.W.M.; Braekman, J.C. *Mem. Qld. Mus.* **1999**, *44*, 569 - 589.
58. Samaai, T. PhD Thesis, University of the Western Cape, **2001**, pp. 683 - 721.
59. Lill, R.E.; Major, D.A.; Blunt, J.W.; Munro, M.H.G.; Battershill, C.N.; McLean, M.G.; Baxter, R.L. *J. Nat. Prod.* **1995**, *58*, 306 - 311.
60. Beukes, D.R.; Davies-Coleman, M.T.; Kelly-Borges, M.; Harper M.K.; Faulkner, D.J. *J. Nat. Prod.* **1998**, *61*, 699 - 701.
61. MarinLit, Marine Literature Database, vpc 11.1, **2002**, Munro, M.H.G.; Blunt, J.W.; University of Canterbury, Christchurch, New Zealand.
62. Kashman, Y.; Groweiss, A.; Shmueli, U. *Tetrahedron Letters* **1980**, *21*, 3629 - 3632.
63. Capon, R.J.; MacLeod, J.K.; Willis, A.C. *J. Org. Chem.* **1987**, *52*, 339 - 342.
64. Tymiak, A.A.; Rinehart, K.L.; *J. Am. Chem. Soc.* **1981**, *103*, 6763 - 6765.
65. Minale, L.; Cimino, G.; de Stefano, S.; Sodano, G. *Fortschr. Chem. Org. Naturst.* **1976**, *33*, 1 - 72.
66. Ishibashi, M.; Iwasaki, T.; Imai, S.; Sakamoto, S.; Yamaguchi, K.; Ito, A. *J. Nat. Prod.* **2001**, *64*, 108 - 110.
67. Ishibashi, M.; Mitamura, M.; Ito, A. *Nat. Med.* **1999**, *53*, 316 - 318.
68. Erdman, T.R.; Thomson, R.H. *Tetrahedron* **1972**, *28*, 5163 - 5173.
69. Patterson, G.W. *Phytochemistry* **1972**, *11*, 3481 - 3483.
70. Barrows, L.R.; Radisky, D.C.; Copp, B.R.; Swaffar, D.S.; Kramer, R.A.; Warters, R.L.; Ireland, C.M. *Anti-Cancer Drug Design* **1993**, *8*, 333 - 347.
71. Sadandan, E. V.; Cava, M. P. *Tetrahedron Letters* **1993**, *34*, 2405 - 2408.
72. Roberts, D.; Venemalm, L.; Alvarez, M.; Joule, J. A. *Tetrahedron Letters* **1994**, *35*, 7857 - 7860.
73. Tao, X. L.; Cheng, J. F.; Nishiyama, S.; Yamamura, S. *Tetrahedron* **1994**, *50*, 2017 - 2028.
74. Alvarez, M.; Bros, M. A.; Joule, J. A. *Tetrahedron Letters* **1998**, *39*, 679 - 680
75. Alvarez, M.; Bros, M. A.; Gras, G.; Ajana, W.; Joule, J. A. *Eur. J. Org. Chem.* **1999**, *5*, 1173 - 1183.
76. Kraus, G. A.; Selvakumar, N. *J. Org. Chem.* **1998**, *63*, 9846 - 9849.
77. Iwao, M.; Motoi, O.; Fukuda, T.; Ishibashi, F. *Tetrahedron* **1998**, *54*, 8999 - 9010.
78. White, J. D.; Yager, K. M.; Yakura, T. *J. Am. Chem. Soc.* **1994**, *116*, 1831 - 1838.

79. Roberts, D.; Alvarez, M.; Joule, J. A. *Tetrahedron Letters* **1996**, *37*, 1509 - 1512.
80. Izawa, T.; Nishiyama, S.; Yamamura, S. *Tetrahedron* **1994**, *50*, 13593 - 13600.
81. Nishiyama, S.; Cheng, J. F.; Tao, X. L.; Yamamura, S. *Tetrahedron Letters* **1991**, *32*, 4151 - 4154.
82. Wang, H.; Al-Said, N. H.; Lown, J. W. *Tetrahedron Letters*. **1994**, *35*, 4085 - 4086.
83. Kita, Y.; Egi, M.; Takada, T.; Tohma, H. *Synthesis* **1999**, *5*, 885 - 897.
84. Kita, Y.; Egi, M.; Tohma, H. *Chem. Comm.* **1999**, *2*, 143 - 144.
85. Kita, Y.; Tohma, H.; Inagaki, M.; Hatanaka, K.; Yakura, T. *J. Am. Chem. Soc.* **1992**, *114*, 2175 - 2180.
86. Kita, Y.; Tohma, H.; Inagaki, M.; Hatanaka, K.; Kikuchi, K.; Yakura, T. *Tetrahedron Letters* **1991**, *32*, 2035 - 2038.
87. Kita, Y.; Yakura, T.; Tohma, H.; Kikuchi, K.; Tamura, Y. *Tetrahedron Letters* **1989**, *30*, 1119 - 1120.
88. Aubart, K. M.; Heathcock, C. H. *J. Org. Chem.* **1999**, *64*, 16 - 22.
89. Tohma, H., Harayam, Y., Hashizume, M., Iwata, M., Ergi, M., Kita, Y. *Angew. Chem. Int. Ed.* **2002**, *41*, 348 - 350.
90. Moro-oka, Y.; Fukuda, T.; Iwao, M. *Tetrahedron Letters* **1999**, *40*, 1713 - 1716.
91. Kokoshka, J.M.; Capson, T.L.; Holden, J.A.; Ireland, C.M.; Barrows, L.R. *Anticancer Drugs* **1996**, *7*, 758 - 765.
92. Samaai, T.; Kelly, M.; Gibbons, M. *J. Zoology*, **2002**, (in press).
93. Mc Cloud T.G.; Sheffield H.G.; Nemeč, J.; Muschik, G.; Suffness, M.; Cragg, G.; Thompson, J.; Snader, K. *Presentation at the 30th Meeting of the American Society of Pharmacognosy*, San Juan, Puerto Rico, August 6-10, **1989**.
94. Mano, N., Oda, Y., Ohe, H., Asakawa, N., Yoshida, Y. and Sato, T. *J. Pharm. Biomed. Anal.* **1994**, *12*, 557 - 567.
95. Finnigan Mat LCQ Manual, Eds. Mason, F.P.; Pettijohn, R.R. Technical Publications, Finnigan Corporation, San Jose, CA, U.S.A, **1996**.
96. Crews, P.; Rodriguez, J.; Jaspers, M. *Organic Structure Analysis*, Oxford University Press, Oxford, **1998**, pp. 141.
97. Pretsch, E.; Bühlmann, P.; Affolter, C. *Structure Determination of Organic Compounds: Tables of Spectral Data*; Third completely revised and enlarged English Edition, Springer-Verlag, Berlin Heidelberg, Germany, **2000**, pp. 207, 220, 223, 234 - 235.
98. Hooper, G.J. PhD Thesis, Rhodes University, **1997**, pp. 52 - 59.
99. Thornton, D.A.; Watkins, G.M. *Spec. Letters* **1992**, *25*, 1023 - 1036.
100. Thornton, D.A.; Watkins, G.M. *Bull. Soc. Chim. Belg.* **1991**, *100*, 235 - 245.
101. Dega-Szafran, Z. *Roczniki Chemii Ann. Soc. Chim. Polonorum* **1972**, *46*, 827 - 836.
102. Dega-Szafran, Z. *Roczniki Chemii Ann. Soc. Chim. Polonorum* **1970**, *44*, 2371 - 2385.
103. Fuchs, T.; Gates, K.S.; Hwang, J-T.; Greenberg, M.M. *Chem. Res. Toxicol.* **1999**, *12*, 1190 - 1194.
104. Wardman, P. *Scientific Yearbook*, **2001-2002**, 36 - 39.

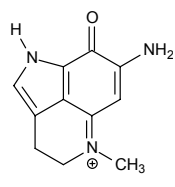
105. Katritzky, A.R.; Pozharskii, A.F. *Handbook of Heterocyclic Chemistry* **2000**, 2nd Edition, Pergamon, Elsevier Science Ltd., Oxford, pp. 183.
106. Martínez, A.G. Vilar, E.T.; Fraile, A.G.; Cerero, S.d.M.; Maroto, B.L. *Tetrahedron: Asymmetry* **2002**, *13*, 17 - 19.
107. Committee for veterinary medicinal products *Symphyti Radix Summary Report* **1999**
<http://www.eudra.org/emea.html>
108. Röder, E. *Medicinal plants in Europe containing pyrrolizidine alkaloids*, *Pharmazie*, **1995**
<http://www.ibiblio.org/herbmed/PAs>.
109. Matsunaga, S.; Shinoda, K.; Fusetani, N. *Tetrahedron Letters* **1993**, *34*, 5953 - 5954.
110. Tsuda, M.; Shigemori, H.; Ishibashi, M.; Kobayashi, J. *J. Nat. Prod.* **1992**, *55*, 1325 - 1327.
111. Kobayashi, J.; Honma, K.; Tsuda, M.; Kosaka, T. *J. Nat. Prod.* **1995**, *58*, 467 - 470.
112. Suppan, P. *Chemistry and Light* Royal Society of Chemistry, **1994**, pp. 93, 138, 184.
113. Lambin, P. Inaugural address, Maastricht University, September **2001**.
114. Grossweiner, L.I. Singlet Oxygen: Generation and Properties; <http://www.photobiology.com/educational/len2/singox.html>
115. Jenny, T.A.; Turro, N.J. *Tetrahedron Letters* **1982**, *23*, 2923 - 2926.
116. Halliwell, B.; Gutteridge, J. M. C. *Free Radicals in Biology and Medicine* 2nd Edition, Oxford University Press, Oxford, **1989**, pp.12.
117. Maree, S. PhD Thesis, Rhodes University, **2002** 78 - 84, 92 - 93,109.
118. Katona, Z.; Grofcsik, A.; Baranyai, P.; Bitter, I.; Grabner, G.; Kubinyi, M.; Vidóczy, T. *J. Mol. Struc.* **1998**, *450*, 41 - 45.
119. Dawson, W.R.; Windsor, M.W. *J. Phys. Chem.* **1968**, *72*, 3251 - 3260.
120. Brett, C. M. A.; Brett, A. M. O. *Electrochemistry: Principles, Methods, Applications*, Oxford University Press, Oxford, **1993**, pp 181 - 183
121. Monge, A.; Palop, J.A.; López de Cerain, A.; Senador, V.; Martínez-Crespo, F.J.; Sainz, Y.; Narro, S.; García, E.; de Miguel, C.; González, M.; Hamilton, E.; Barker, A.J.; Clarke, E.D; Greenhow, D.T. *J. Med. Chem.* **1995**, *38*, 1786 - 1792.
122. Zhu, Z.; Li, C.; Li, N-Q. *Microchem. J.* **2002**, *71*, 57 - 63.
123. Orlemans, E.O.M; Verboom, W.; Scheltinga, M.W.; Reinhoudt, D.N.; Lelieveld, P.; Fiebig, H.H.; Winterhalter, B.R.; Double, J.A.; Bibby, M.C. *J. Med. Chem.* **1989**, *32*, 1612 - 1620.
124. Foye, W.O.; Lemke, T.L.; Williams, D.A. *Principles of Medicinal Chemistry*, 4th Edition, Lippincott Williams and Wilkins, London, U.K. **1995**, pp. 822 - 845.
125. Daniels, J.S.; Gates, K.S. *J. Am. Chem. Soc.* **1996**, *118*, 3380 - 3385.
126. Nagai, K.; Carter, B.J.; Xu, J.; Hecht, S.M. *J. Am. Chem. Soc.* **1991**, *113*, 5099 - 5100.
127. Heineman W.R.; Kissinger P.T. *Laboratory Techniques in Electroanalytical Chemistry*, 2nd Edition, Marcel Dekker, Inc., New York, Eds. Kissinger, P.T.; Heineman W.R. **1996**, Chapter 3: *Large-Amplitude Controlled-Potential Techniques*, pp. 84
128. Christensen, P.A.; Hamnett, A. *Techniques and Mechanisms in Electrochemistry* Blackie Academic and Professional, London, **1994**, pp. 33, 35, 56 - 57, 67
129. Nyokong, T. Honours Electrochemistry lecture course, Rhodes University, **2002**.

130. Kissinger, P.T.; Ridgway; *Laboratory Techniques in Electroanalytical Chemistry*, 2nd Edition, Marcel Dekker, Inc., New York, Eds. Kissinger, P.T.; Heineman W.R. **1996**, Chapter 4: *Small-Amplitude Controlled-Potential Techniques*, pp. 158.
131. Hendricks, D.; Parker, M.I. Oesophageal cancer in Africa. International Union of Biochemistry and Molecular Biology (IUBMB) *Life* **2002**, *53*, 263 - 268.
132. Sincich, C. Scripps Institution of Oceanography, San Diego, U.S.A., Personal Communication.
133. Hendricks, D. University of Cape Town, South Africa, Personal Communication.
134. Lodish, H.; Berk, A.; Zipursky, S.L.; Matsudaira, P.; Baltimore, D.; Darnell, J. *Molecular Cell Biology* 4th Edition, **2000**, W.H. Freeman and Company and Sumanas, Media Connected, pp. 468 - 470.
135. Armstrong, F.B. *Biochemistry* 2nd Edition, **1983**, Oxford University Press, pp. 444.
136. Wall, M.E.; Wani, M. *Alkaloids* **1998**, *50*, 509 - 536.
137. Lee, K-H.; Imakura, Y.; Haruna, M.; Beers, S.A.; Thurston, L.S.; Dai, H-J.; Chen, C-H. *J. Nat. Prod.* **1989**, *52*, 606 - 613.
138. Marshall, K. University of Utah, U.S.A. Personal Communication.
139. Wilson, W.D.; Jones, R.L. *Adv. Pharmacol.* **1982**, *18*, 177 - 222.
140. Lin, A.J.; Cosby, L.A.; Shansky, C.W.; Sartorelli, A.C. *J. Med. Chem.* **1972**, *15*, 1247 - 1252.
141. Kennedy, K.A.; Teicher, B.A.; Rockwell, S.; Sartorelli, A.C. *Biochem. Pharmacol.* **1980**, *29*, 1 - 8.
142. Stratford, I.J.; O'Neill, P.; Sheldon, P.W.; Silver, A.R.J.; Walling, J.M.; Adams, G.E. *Biochem. Pharmacol.* **1986**, *35*, 105 - 109.
143. Laderoute, K.R.; Rauth, A.M. *Biochem. Pharmacol.* **1986**, *35*, 3417 - 3420.
144. Ueda, K.; Morita, J.; Komano, T. *Biochemistry* **1984**, *23*, 1634 - 1640.
145. Hurley, L.H.; Reynolds, V.L.; Swenson, D.H.; Petzold, G.L.; Scahill, T.A. *Science* **1984**, *226*, 843 - 844.
146. Chrisey, L.A.; Shahidi Bonjar, G.H.; Hecht, S.M. *J. Am. Chem. Soc.* **1988**, *110*, 644 - 646.
147. Scannel, R.T.; Barr, J.R.; Murty, V.S.; Sambhi Reddy, K.; Hecht, S.M. *J. Am. Chem. Soc.* **1988**, *110*, 3650 - 3651.
148. Lee, M.D.; Dunne, T.S.; Chang, C.C.; Ellestad, G.A.; Siegel, M.M.; Morton, G.O.; McGahren, W.J.; Borders, D.B. *J. Am. Chem. Soc.* **1987**, *109*, 3466 - 3468.
149. Mosmann T. *J Immunol. Methods* **1983**, *65*, 55 - 63.
150. Denizot, F.; Lang R. *J Immunol. Methods* **1986**, *89*, 271 - 277.
151. Jeggo, P.A.; Caldecott, K.; Pidsley, S.; Banks, G.R. *Cancer Res.* **1989**, *49*, 7057 - 7063.
152. Matsumoto, S.S.; Haughey, H.M.; Schmehl, D.M.; Venables, D.A.; Ireland, C.M.; Holden, J.A.; Barrows, L.R. *Anticancer Drugs* **1999**, *10*, 39 - 45.

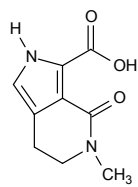
The structures of the twenty three metabolites isolated from South African Latrunculid sponges.



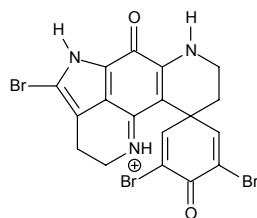
1.20 pp. 6, 73



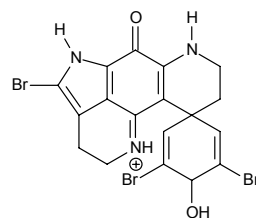
1.33 pp. 8, 72



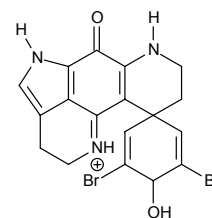
1.47 pp. 10, 73



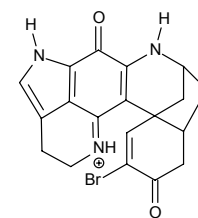
1.51 pp. 11, 48



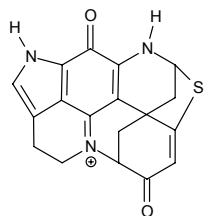
1.52 pp. 11, 48



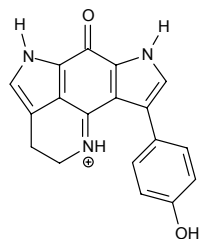
1.53 pp. 11, 51



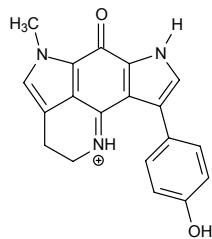
1.57 pp. 14, 115



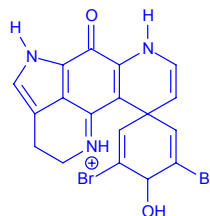
1.61 pp. 15, 117



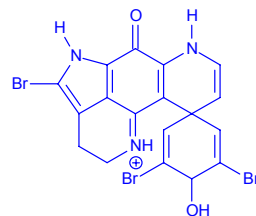
1.71 pp. 17, 101



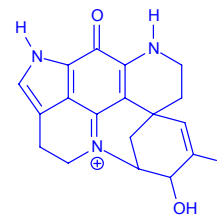
1.72 pp. 17, 103



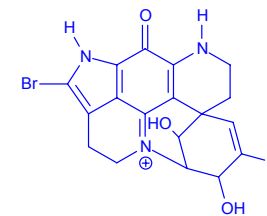
2.1 p. 52



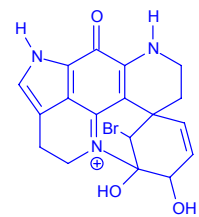
2.2 p. 54



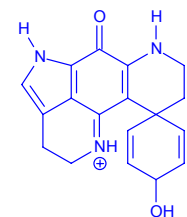
2.3 p. 55



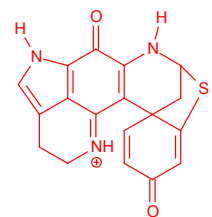
2.4 p. 60



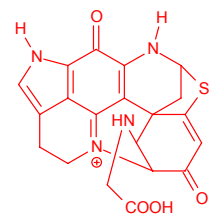
2.5 p. 62



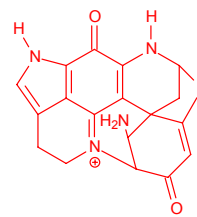
2.6 p. 66



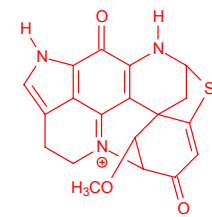
3.1 p. 74



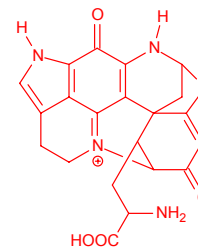
3.2 p. 78



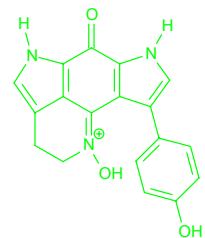
3.3 p. 82



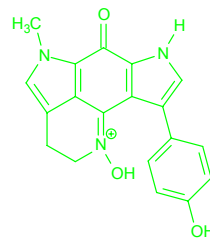
3.4 p. 85



3.5 p. 88



4.1 p. 103



4.2 p. 109